THE ROLE OF FEATURE-TRACKING CARDIOVASCULAR MAGNETIC RESONANCE IN OPTIMISING RESPONSE TO CARDIAC RESYNCHRONISATION THERAPY

ROBIN JAMES TAYLOR

A thesis submitted to the University of Birmingham for the degree of

DOCTORATE OF MEDICINE

The Institute of Cardiovascular Sciences

School of Clinical and Experimental Medicine

College of Medical and Dental Sciences

University of Birmingham

January 2017

ABSTRACT

Cardiac resynchronisation therapy (CRT) forms part of the established treatment for heart failure, but individual response is variable. Deformation imaging permits assessment of myocardial mechanics. Echocardiography-based techniques are unable to refine patient selection for CRT, although can identify preferential late mechanically activated (LMA) targets for lead placement. Feature-tracking (FT) is a rapid cardiac magnetic resonance (CMR) deformation technique performed on standard acquisition, overcoming the limitations of myocardial tagging (MT). This work aims to validate FT-CMR against MT and establish its role in patient selection and left ventricular (LV) lead deployment in the context of CRT.

A validation study performed on healthy volunteers and cardiomyopathy patients demonstrated good intra- and inter-observer variability, and reasonable agreement compared with MT. In a retrospective observational study of CRT recipients, greater baseline dyssynchrony did not predict LV reverse remodelling (LVRR) or symptomatic response at 6 months, but low strain was associated with a high risk of cardiovascular mortality. Furthermore, lead deployment over non-scarred, LMA myocardium, assessed using late gadolinium enhancement (LGE) and FT-CMR was associated with better LVRR and long term survival.

FT-CMR showed no ability to enhance patient selection for CRT but, coupled with LGE CMR, has a role in guiding LV lead deployment.

DEDICATION

To Mum and Dad

ACKNOWLEDGEMENTS

I would like to express my gratitude to the many people who have supported me in this work. First and foremost, to Prof Francisco Leyva, not only for the considerable time he has invested providing expert mentorship, but also his ongoing support and friendship. I am also extremely grateful for the valuable advice provided by both Dr Richard Steeds and Dr Berthold Stegemann.

Dr Fraz Umar deserves special mention, as my fellow researcher, who proactively assisted with patient recruitment and contributed so richly to my overall research experience, who was like a brother throughout my research period. My thanks is also extended to my other fellow researchers Dr William Moody and Nicola Edwards, for their erudite support and for training me in the acquisition of cardiac magnetic resonance images.

I am grateful to Wojciech Mazur and Kan Hor, Paediatric Cardiologists from the Christ Hospital, Ohio, who were instrumental in the development of FT-CMR algorithm, and who shared their invaluable experience. I am grateful to the software writers, Tomtec, for making technical and scientific support so readily available. Thank you to Dr Peter Nightingale at University of Birmingham for providing valuable statistical advice.

Finally, I would like to thank my wife, Alison, for her incredible patience and support during this undertaking, and my children Emily and Joshua for providing me with the best incentive to complete it.

EXTENT OF PERSONAL CONTRIBUTION

The work carried out in this thesis is my own, with the following notable support:

Professor Francisco Leyva provided considerable input into the conception and design of all study investigations.

The healthy controls were identified from an ongoing research study examining the effects of living kidney donation on cardiovascular structure and function which was the focus of Dr William Moody's Ph.D. and he was responsible for subject recruitment. Scans were performed together, and these formed my training in CMR acquitions.

The historical CRT population was recruited prospectively by the staff of Good Hope Hospital between 2000-2009. They were responsible for baseline and follow-up echocardiography, and the prospective recording of cardiac events. I performed a retrospective analysis of all subjects notes to enhance the accuracy of outcome data (supplemented by the interviewing of other healthcare providers where required). The CMR analyses on these patients, including volumetric analyses, scar quantification and feature tracking were conducted personally (except in chapter 5 where Dr Paul Foley's original analyses were used).

In Chapter 2 W.M. performed the tagging analyses and I performed the feature tracking analyses with this interchanging for inter-observer variability analyses. We worked collaboratively on the published manuscript, in which he is listed first, but we are credited as joint first authors. This study also features as a chapter in his thesis.

The CURE and RURE dyssynchrony analyses in chapters 4 & 7 were performed using custom Matlab software written by Dr Berthold Stegemann.

In chapter 6 the presence or absence of midwall fibrosis, and the LV lead position in chapter 9, were assessed by F.L. as he was blinded to all other study data.

Chapters 3, 4, 6, & 9 relate to published scientific manuscripts that I am first author on. Other authors (and the reviewers) offered critical appraisal which is reflected in my final work. Chapter 5 relates to work conducted around the time of commencing my research, on which I am the second author, having been responsible for data analysis and writing the initial manuscript.

TABLE OF CONTENTS

LIST OF TABLES

LIST OF FIGURES

LIST OF ABBREVIATIONS

2DE	two dimensional echocardiography
3DE	three dimensional echocardiography
6MWT	Six minute walk test
ACE-I	angiotensin converting enzyme inhibitor
ARB	angiotensin receptor blockers.
AUC	area under curve
AV	atrio-ventricular
CMR	cardiovascular magnetic resonance
CO	cardiac output
CRT	cardiac resynchronisation therapy
CURE	circumferential uniformity ratio estimate
DSR	diastolic strain rate
eGFR	estimated glomerular filtration rate
Ɛ	strain
FT	feature-tracking
HARP	harmonic phase analysis
HF	heart failure
HFpEF	heart failure with preserved ejection fraction
HFrEF	heart failure with reduced ejection fraction
HR	hazard ratio
ICC	interclass correlation coefficient
ICM	ischaemic cardiomyopathy
IDCM	Idiopathic dilated cardiomyopathy
LBBB	left bundle branch block
LGE	late gadolinium enhancement
LMA	latest mechanical activation/activated
LV	left ventricle or left ventricular
LVEDP	left ventricular end diastolic pressure
LVEDV	left ventricular end-diastolic volume

LVEF	left ventricular ejection fraction
LVESV	left ventricular end-systolic volume
LVRR	left ventricular reverse remodelling
MAP	mean arterial pressure
MDRD	modification of diet in renal disease
MLWHF	Minnesota living with heart failure questionnaire
MRA	mineralocorticoid receptor antagonists
MWF	midwall fibrosis
NHYA	New York heart association
NICD	nonspecific intraventricular conduction delay
NICE	National Institute for Health and Care Excellence
NICM	non-ischaemic cardiomyopathy
PCWP	pulmonary capillary wedge pressure
RAAS	renin angiotensin aldosterone system
RAAS	renin-angiotensin-aldosterone system
RBBB	right bundle branch block
ROC	receiver operating characteristic
RURE	radial uniformity ratio estimate
SD	standard deviation
SNS	sympathetic nervous system
SPAMM	spatial modulation of magnetization
SR	strain rate
SSFP	steady state free precession
SSR	systolic strain rate
STE	speckle tracking echocardiography
SV	stroke volume
TDI	tissue Doppler imaging
VLA	vertical long axis
VO_2	oxygen consumption

1 INTRODUCTION: CARDIAC RESYNCHRONISATION THERAPY – A REVOLUTION IN HEART FAILURE THERAPY

1.1 Heart failure

Heart failure is a complex syndrome of symptoms and signs resulting from any impairment of the function of the myocardial pump. This impairment can be secondary to any abnormality of the structure, mechanical function or electrical activation of the heart.

1.1.1 The heart failure epidemic

The burden of heart failure on healthcare systems is increasing in developed countries as a consequence of the ageing population and the improving management and survival from myocardial infarction. The prevalence of heart failure within the United Kingdom is 550,000 (Townsend N et al., 2014) and even larger numbers of patients have discernible impairment of left ventricular function on imaging examination, but are at a pre-symptomatic stage (Redfield et al., 2003). The prevalence of heart failure rises from 0.7% in the 45-54 years age group to 8.4% in those aged 75 years or greater (Redfield et al., 2003). Heart failure currently accounts for 2% of inpatient bed days, 5% of emergency admissions, and the National Institute for Health and Care Excellence (NICE) projects a 50% increase in heart failure admissions over the next quarter of a century (NICE, 2010).

The devastating effects on quality of life are not restricted to exercise intolerance. Further physical symptoms, social consequences and the detrimental effect on mental health lead to a comparable decrease in quality of life to that associated with stroke or chronic

haemodialysis (Juenger et al., 2002). Survival following an index admission for heart failure is shorter than that observed following a new diagnosis of a colon, breast, bladder, ovarian or prostate malignancy (Stewart et al., 2001).

1.1.2 Systolic versus diastolic dysfunction

Central to the management of the patient with heart failure is categorisation according to left ventricular ejection fraction (LVEF). This dichotomises patients into distinct cohorts with different demographics, aetiologies, pathophysiology, evidence based management strategies and disease trajectories.

For patients with a LVEF <40% the term heart failure with reduced ejection fraction (HFrEF) is widely agreed and the underlying problem is predominantly one of impaired LV systolic pump function. The underlying pathophysiology of this group is well understood **(1.1.4**) which has facilitated the development of targeted treatments.

The management of patients with heart failure despite a normal LVEF is more problematic, and there is even deliberation over the most suitable name for this syndrome (Sanderson, 2014). Impairment of diastolic relaxation and filling are key components, with left atrial dilatation, LV hypertrophy and elevated filling pressures seen on imaging (Ponikowski et al., 2016). The term heart failure with reduced ejection fraction (HFpEF) is preferred to diastolic heart failure as reductions in systolic long axis function, strain, LV twist and reserve have been demonstrated (Borlaug et al., 2010; Tan et al., 2009). Variance in the diagnosis of

HFpEF has obstructed large scale study of this syndrome, and its treatment base lags that of HFrEF.

1.1.3 Aetiology of HFrEF

The list of aetiologies of heart failure is diverse, and the prevalence of these is geographically dependant. Within the United Kingdom coronary artery disease is the major cause of heart failure, with many patients having had a previous myocardial infarction (Petersen et al., 2002), and such patients are labelled as having an ischaemic cardiomyopathy (ICM). Primary cardiomyopathies, hypertension, valvular disease, metabolic and infiltrative diseases, conduction disease and congenital heart disease are other aetiologies and are occasionally categorised together as non-ischaemic cardiomyopathies (NICM), but due to their heterogeneity this is often counter-productive.

Idiopathic dilated cardiomyopathy (IDCM) is a primary heart muscle disorder with LV systolic dysfunction in the absence of abnormal loading conditions (Elliott, 2000). After coronary artery disease it is the most prevalent cause of heart failure in the developed world. It accounts for 50% of heart failure cases where the diagnosis is not clear at presentation (Felker et al., 2000). Rather than being a single disease, it is the consequence of a number of environmental and genetic processes which present with a similar phenotype. At present over 60 causal genes have been identified (Japp et al., 2016).

1.1.4 Pathophysiology of HFrEF

Myocardial injury from any cause leads to reductions in cardiac stroke volume (SV), cardiac output (CO), and their product: mean arterial pressure (MAP). This triggers a number of compensatory mechanisms and, despite being initially beneficial, these interrelated processes sustain a number of deleterious vicious cycles.

Frank-Starling mechanism. As CO decreases, LV end diastolic volume and pressure (LVEDP) rise, and the extra myocardial stretch (pre-load) increases myocardial contractility via a process known as homeometric autoregulation (Sarnoff et al., 1960). Whilst this initially maintains performance, further increases in LVEDP result in successively smaller contractile rewards, and as systolic function falls further so does the benefit of this compensatory mechanism. Yet the increasing LVEDP leads to elevated pulmonary capillary pressures and dyspnoea, cough and wheeze attributable to pulmonary congestion.

Ventricular remodelling. The haemodynamic overload leads to myocyte and ventricular hypertrophy and dilatation in an attempt to negate increasing wall stress (Cohn et al., 2000; Sandler et al., 1963). This remodelling process leads to changes in ventricular size, shape and function. Ventricular dilatation interferes with the sophisticated geometrical construct of the ventricle; not only is pump efficiency reduced, but atrioventricular valve ring stretch leads to valvular incompetence which exacerbates volume overload. Eventually, elevated wall tension promotes myocyte apoptosis and myocardial fibrosis (Cohn et al., 2000).

Neurohumoral adaptations. A number of systemic processes, which are probable evolutional responses to shock, leads to increased arterial vasoconstriction and sodium and water retention (Camm et al., 2009). Expanding the intravascular volume initially improves cardiac output by exploiting the Frank Starling mechanism. Reduced stimulation of arterial baroreceptors augments sympathetic nervous system (SNS) drive, which directly increases heart rate, myocardial contractility and arterial vasoconstriction. Sympathetic overdrive is also a determinant in cardiac rhythm instability in heart failure. Direct sympathetic flow to Beta-1 adrenergic receptors is partly responsible for increased Renin release from the juxtaglomerular apparatus of the kidney, alongside reduced MAP at the renal afferent arterioles. Activation of the renin-angiotensin–aldosterone system (RAAS) promotes volume retention, vasoconstriction, further activation of the SNS and myocardial fibrosis (Lijnen et al., 2000). Angiotensin II mediated Vasopressin release from the hypothalamus further contributes to fluid retention.

1.1.5 Pharmacological treatment of HFrEF

Clinical trials have focused on patients with LVEF<40%. It is only in HFrEF that there are proven therapies that improve symptoms and prognosis. Beta-blockers (CIBIS-II Investigators and Committees, 1999; Flather et al., 2005; 1999; Packer et al., 2002) and Angiotensin Converting Enzyme (ACE) inhibitors (The Consensus Trial Study Group, 1987; The SOLVD Investigators, 1991) have a strong evidence base and, in combination with diuretics, form the foundation of heart failure pharmacotherapy.

ACE inhibitors diminish the activity of the RAAS by preventing the conversion of inactive Angiotensin I to active Angiotensin II within the pulmonary and renal endothelium. In those patients in whom the resultant accumulation of bradykinin restricts use due to cough or angio-oedema, they can be substituted for an Angiotensin receptor blocker (ARB), which inhibits the RAAS at a later stage but provides similar benefits (Cohn et al., 2001; Granger et al., 2003; McMurray et al., 2003). The prognostic benefits of beta-blockade are additional to those bestowed from ACE inhibition, and are due to protection from the harmful effects of excessive sympathetic activation.

Diuretics ameliorate the signs and symptoms of heart failure by blocking reabsorption of sodium and water from the renal tubule. Their widespread use pre-dates the era of the randomised controlled trial but, despite no evidence base, their role is unquestionable. Whilst loop diuretics are most widely used, mineralocorticoid receptor antagonists also have a diuretic effect, further impede the RAAS, and their addition to above therapies provides further measurable benefit in selected populations (Pitt et al., 2003; Pitt et al., 1999; Zannad et al., 2011).

The above drugs all target the counter-productive neurohumoral responses. Neprilysin inhibitors offer the potential for further advances in management by enhancing advantageous systemic responses. Neprilysin degregates biologically active natriuretic peptides and its inhibition causes vasodilation, natriuresis, and diuresis. When combined with an ARB this compound has been shown to provide a further survival advantage compared to ACE inhibition in selected patients (McMurray et al., 2014).

1.2 Cardiac resynchronisation therapy

1.2.1 Dyssynchrony and wasted work

The temporal sequence of events within the cardiac cycle is commonly disrupted in heart failure. This phenomenon, dyssynchrony, exists at the atrioventricular, inter-ventricular and intra-ventricular levels and leads to multiple inefficiencies that negatively impact cardiac function. The paradigm of cardiac resynchronisation therapy (CRT) is that correction of these abnormal electrical and mechanical abnormalities improves cardiac function.

AV dyssynchrony, readily identified by prolongation of the PR interval on the electrocardiogram, is common place in heart failure and can be a factor limiting optimal beta-blockade. With prolonged AV delay, atrial priming occurs too early in diastole, reducing both the passive LV filling time and the contribution of the atrial 'kick' towards cardiac output. Furthermore, the delay in ventricular activation after atrial emptying retards papillary muscle contraction and mitral valve closure and, as the left atrium relaxes, a ventricular-atrial pressure gradient is generated driving pre-systolic mitral regurgitation (Nishimura et al., 1995). These disturbances elevate left atrial pressure whilst reducing LV preload at the onset of systole.

Inter-ventricular dyssynchrony disturbs the harmonic functional relationship between both ventricles. With left bundle branch block (LBBB), the pressure generated in the right ventricle (RV) during isovolumic contraction is greater than the simultaneous end-diastolic pressure within the LV (Grines et al., 1989). This pressure gradient produces an early abnormal inward LV septal motion. During LV ejection there is a subsequent paradoxical

outward anteroseptal movement due to the low pressure within the now comparatively volume deplete RV. This reduces local septal (and thus global) ejection fraction and increases the LV end systolic volume (LVEDV).

Disruption of normal activation leads to dis-coordinate contraction of segments within the LV itself. With LBBB, rather than contribute to LV ejection, the forces generated by earlier contracting septal regions are dissipated as pre-stretch of the LV free wall. As the postero-lateral papillary muscle will be yet to contract, further cardiac output will be lost due to sub-optimal mitral valve closure and mitral regurgitation. Later activated segments contract under a higher wall stress, and energy is wasted stretching the now relaxing opposite walls. Although the converse is true in right bundle branch block (RBBB), the deleterious effects of intra-ventricular dyssynchrony are not as pronounced (Byrne et al., 2007). The septum is still loaded from its right ventricular aspect, which to some extent protects from pre-stretch during early contraction of the lateral free wall.

1.2.2 The theoretical basis of CRT

The first attempts to resynchronise the heart targeted AV dyssynchrony in isolation with conventional dual chamber pacing. The hypothesis was that in patients with first degree heart block, dual chamber pacing programmed with a short AV delay would beneficially prolong LV filling time and reduce pre-systolic mitral regurgitation. Despite proof of principle studies showing an immediate improvement in LV filling time and cardiac output (Auricchio et al., 1993; Brecker et al., 1992), this augmentation was seldom maintained and this strategy at best provided no benefit (Gold et al., 1995; Linde et al., 1995), but was probably

detrimental (Nagele et al., 2002). In hindsight the failure of dual chamber pacing is not surprising now that the deleterious consequences of right ventricular pacing are appreciated (Sweeney et al., 2003; Wilkoff et al., 2002).

More complete resynchronisation was demonstrated by Cazeau et al. in 1994, when they performed four chamber (bi-atrial and bi-ventricular) pacing in a 54 year old man with heart failure refractory to medical therapy, and electro- and echocardiographic evidence of dyssynchrony (Cazeau et al., 1994). The haemodynamic response to this was so considerable (cardiac output increased from 3.9L to 5.7L and pulmonary capillary wedge pressure [PCWP] decreased from 36mmHg to 25mmHg) that they implanted the first permanent CRT device using an epicardial LV lead; the recipient improved from New York Heart Association (NYHA) class IV to II and lost 17kg of fluid in less than 2 months.

A number of case series demonstrated the acute haemodynamic benefits of cardiac resynchronisation. The first studied 8 patients with end stage heart failure refractory to optimal medical therapy and wide QRS complexes (Cazeau et al., 1996). Compared to baseline, temporary biventricular pacing improved mean cardiac index by 25% and decreased PWCP by 17%. These results were duplicated in two similar, but larger (41 patients in aggregate) case series (Blanc et al., 1997; Leclercq et al., 1998b). Interestingly, in all three studies, despite a group improvement in haemodynamics, one third of patients had no response to resynchronisation.

In these preliminary studies temporary LV pacing was accomplished via trans-aortic arterial electrodes with temporary systems. The earliest permanent systems required surgical thoracoscopic placed epicardial LV electrodes. This was not suitable for widespread use, but before the turn of the century two French centres described the use of specially designed pacing leads that could be implanted transvenously to pace the LV epicardially via branches of the coronary sinus (Daubert et al., 1998), and this remains the conventional approach to CRT implantation.

1.2.3 Early landmark studies

The MUSTIC (multisite stimulation in cardiomyopathies) study confirmed that CRT could be delivered safely and effectively, producing improvements in patients' symptoms and exercise tolerance (Cazeau et al., 2001). In this single-blinded, randomised, cross-over study, active CRT improved performance in the six minute walk test (6MWT) by 23% ($p<0.001$), quality of life scores by 32% ($p<0.001$), and peak oxygen consumption (VO_2) by 8% ($p<0.03$). 85% of blinded patients selected active therapy as their preferred modality ($p<0.001$).

The MIRACLE (multisite Insync randomised clinical evaluation) study was a double blinded randomised controlled trial that confirmed these benefits and showed that CRT reduced heart failure admission rates and hospitalisation time, but the study was underpowered to detect any difference in mortality (Abraham et al., 2002).

The COMPANION (comparison of medical therapy, pacing and defibrillation in heart failure) study demonstrated that in patients with advanced symptoms (NHYA class III-IV), compared

to medical treatment, CRT-D provided a survival benefit at one year (RRR 36%; p=0.003), but the study narrowly failed to confirm a similar advantage for CRT-P (RRR 24%; p=0.059) (Bristow et al., 2004). The CARE-HF (Cardiac Resynchronisation in Heart Failure) study did confirm that CRT can provide a mortality benefit independent of a defibrillator (Cleland et al., 2005). Over a mean follow up of 29.4 months, as compared to medical therapy, CRT-P reduced the risk of mortality by 36% (p< 0.002).

1.2.4 CRT and mild symptoms

These early studies proved the benefit of CRT in populations with advanced symptoms, broad QRS and LV systolic dysfunction, and led to guideline driven allocation of CRT to this population. These studies did not examine whether CRT modifies disease course when provided at an earlier time point.

The REVERSE (Resynchronization Reverses Remodeling in Systolic Left Ventricular Dysfunction) trial (Linde et al., 2008), MADIT-CRT (Multicenter Automatic Defibrillator Implantation Trial with Cardiac Resynchronization Therapy) (Moss et al., 2009) and RAFT (Resynchronization Defibrillation for Ambulatory Heart Failure Trial) (Tang et al., 2010) addressed this and compared CRT-D to ICD in populations with an indication for a primary prevention defibrillator. To date, almost 5000 patients with asymptomatic or mild HF have been investigated in randomised controlled studies.

REVERSE randomised 610 patients with NHYA Class I-II to CRT-D on or off in a 2:1 fashion. Over 12 months it demonstrated improved LV remodelling (p<0.0001) and delayed time to

first HF hospitalisation (p= 0.03). MADIT-CRT compared CRT-D with ICD therapy in 1820 patients with NHYA Class I-II symptoms. Over a mean of 2.4 years CRT reduced LV volumes, improved LVEF, and delayed the composite of death or a non-fatal heart failure event ($p<0.001$ for all). There was a 34% reduction in the composite end-point, but this was driven by a 41% reduction in heart failure events and mortality was similar between cohorts.

RAFT was the sole study to demonstrate a mortality benefit for CRT (25% RRR); whilst this was partly attributable to the longer follow-up (mean 40 months), RAFT studied a sicker population. NHYA class III patients were included and overall the mortality rate in the control population was 26% compared to 7% in MADIT-CRT, and 2% in REVERSE.

The recently published long term follow ups of these trials show CRT provides striking benefits over the longer term. Mortality in the MADIT-CRT population was 18% in patients assigned to CRT-D, compared to 29% among controls ($P<0.001$) (Goldenberg et al., 2014). Annualised and 5-year mortality of the REVERSE cohort were 2.9% and 13.5% which compares favourably with historical populations (Linde et al., 2013). LV remodelling benefits are sustained over this time frame.

1.2.5 The role of CRT in contemporary heart failure management

Following recent evidence of the benefit of CRT in milder heart failure the various major societies updated their guidelines to aid clinicians' allocation of CRT. The European Society of Cardiology's latest device guidelines were published in 2013 (Brignole et al., 2013) and the UK NICE guidance was updated in 2014 (**Figure 1-1a**) (NICE, 2014). Both recommend CRT for

	NYHA Class			
QRS Interval	I	II	III	IV
<120 miliseconds	ICD if there is a high risk of sudden cardiac death			ICD and CRT not clinically indicated
120-149 milliseconds without LBBB	ICD	ICD	ICD	CRT-P
120–149 milliseconds with LBBB	ICD	CRT-D	CRT-P OR CRT-D	CRT-P
≥150 milliseconds with or without LBBB	CRT-D	CRT-D	CRT-P OR CRT-D	CRT-P
LBBB, left bundle branch block; NYHA, New York Heart Association				

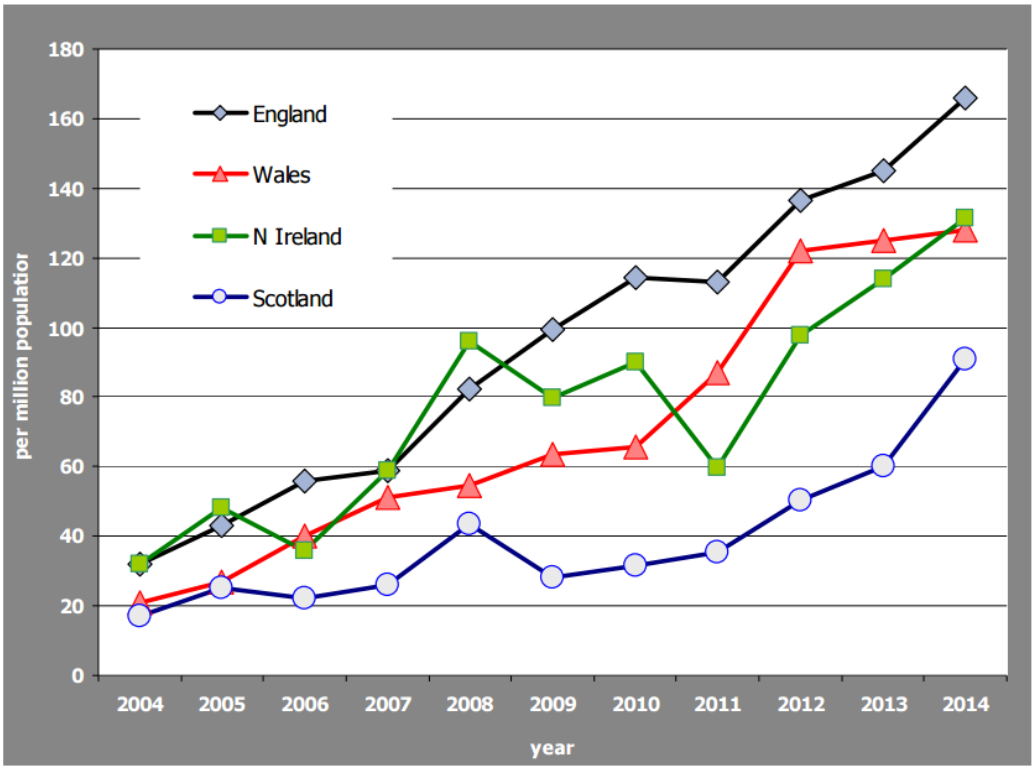

Figure 1-1. Contemporary CRT implantation in the United Kingdom

a) Latest NICE guidelines for device allocation for people with heart failure who have left ventricular dysfunction with an LVEF of 35% or less (adapted from NICE guidelines 2014) b) UK CRT implant rate trend 2004-2014. (Murgatroyd et al., 2016)

symptomatic patients with LVEF <35%, and either LBBB >120ms or any QRS ≥150ms. They differ in their recommendations for patients with NHYA class I symptoms. Whilst such patients should receive a CRT under NICE guidance, they are excluded from ESC recommendations. NHYA I recipients made up a very small proportion of REVERSE (15%) and MADIT-CRT (18%) and subgroup analysis of these patients did not show a reduced event rate.

Figure 1-1**b** shows CRT implantation rates within the UK increasing year on year currently at a rate of 15% (Murgatroyd et al., 2016). The latest guidelines will lead to a further dramatic rise in recommended recipients, with implant rates retarded by the volume of implanters and implant centres.

1.2.6 Response to CRT on an individual level

Although CRT improves symptoms, exercise capacity, quality of life and LV reverse remodelling, whilst reducing heart failure admissions and death on a population level, the individual benefit from CRT shows considerable inter-patient variation. 20-40% of recipients fail to meet the various 'response' criteria set out in land mark studies (Daubert et al., 2012).

Defining response or non-response in a dichotomous fashion is an oversimplification. The multiple potential gains from CRT can each be measured as a continuous variable. An individual's benefit is the aggregate of these; this is unmeasurable in simple binary fashion. Moreover, as with all continuous spectrums, zero is a mid-point on the scale and overlooks

the possibility that CRT may have negative impact, as seen when delivered to patients with a QRS duration < 120ms (Thibault et al., 2013).

The original notion of 'responders' was born from the early haemodynamic studies (Leclercq et al., 1995). Problematically, most post implant metrics act as poor surrogates of another. An example is the notable disconnect between symptomatic response and LV reverse remodelling (Yu et al., 2005), with the former being more susceptible to the placebo effect.

Our concept of response is likely to change alongside the implanted population. As with any new therapy it was originally trialled in the sickest patients in whom an immediate improvement in well-being is a priority. The high event rates in early trials confirm that these patients were reaching end-stage disease. As latest guidance dictates we implant CRT into patients at an earlier time point in their disease, CRT becomes a disease modifying agent. A more valuable metric is prolongation of symptom free (or minimal symptom) survival.

The benefits of any therapy need to be weighed against the potential for harm and cost. CRT implantation is an evolving field and, as operator experience develops and delivery tools evolve, complication rates are falling (Forleo et al., 2015). Health economics must be viewed in the context that most of these patients warrant primary prevention ICDs, and the addition of a LV lead only increases upfront costs by around 25% (from £9,692 to £12,293) (NICE, 2014).

Whilst developing our ability to select patients is prudent so that implantation can be avoided in populations where benefit is unlikely, a more important focus should be on maximising gains from CRT on an individual basis. Strategies include improved post-operative device optimisation and optimal LV lead positioning at implant.

1.3 Electrical dyssynchrony and CRT

1.3.1 QRS morphology

In clinical practice the electrocardiographic QRS complex provides the most readily available indicator of ventricular synchrony. In keeping with the concept of CRT, early studies mandated a wide QRS duration, but never differentiated between LBBB, RBBB and nonspecific intraventricular conduction delay (NICD). However, important differences in terms of underlying electrical and mechanical activation exist. In keeping with these, pulsed Doppler study of 200 conventional CRT recipients pre-implant, showed significantly greater interventricular mechanical delay with LBBB than pure RBBB (Haghjoo et al., 2008). Similarly, Intra-ventricular dyssynchrony was more frequently observed with tissue Doppler (63% vs. 31%) in LBBB. Patients with RBBB and left hemi block (LAHF) had intermediate values.

A retrospective analysis of 632 consecutive CRT recipients over 7 years from a United States university hospital showed reduced survival in those with RBBB pre-implant after controlling for baseline differences (p=0.006) (Adelstein et al., 2009). Improvements in echocardiographic parameters and NHYA class were less probable.

A pooled analysis of the Contak CD and MIRACLE trials identified 61 patients with RBBB (34 randomised to CRT, 27 controls) (Egoavil et al., 2005). At 6 months there was no significant improvement in 6MWT, peak VO_2 or quality of life scores in CRT recipients. There was a significant improvement in NHYA class, although this was also seen in the control population.

In MADIT-CRT, 228 and 308 patients had baseline RBBB and NICD respectively prior to randomisation. CRT reduced the likelihood of the primary composite end-point of death or heart failure in patients with LBBB morphology (Hazard ratio [HR]: 0.47, $p<0.001$), but not in the non-LBBB population (1.24, $p=0.257$) (Zareba et al., 2011). There were greater absolute reductions in LV end-systolic volume (LVESV) in both sub-groups compared to controls, but this reduction was significantly greater in the LBBB sub-group (LBBB: -62mls; Non-LBBB: -45mls; Controls: -18mls; $p<0.001$ for LBBB vs. non-LBBB), with the same trend for other volumetric parameters. Sub-group analysis of CARE-HF also showed higher event rates in the RBBB population (Gervais et al., 2009).

RBBB morphology only accounts for 9-13% of subjects throughout all studies, and this limits the conclusions that can be drawn from these sub-group analyses. Furthermore, invasive 3D electro-anatomical mapping comparisons of heart failure patients showed greater electrical abnormalities in RBBB than LBBB (Fantoni et al., 2005). As anticipated, RBBB was associated with more delayed RV breakthrough, RV anterior and lateral activation and total activation times. Although LV break through was more delayed in LBBB, regional and total activation

times were similar. Seemingly, RBBB can conceal electrocardiographic evidence of LV activation delay, so it is difficult to argue that there is no premise for CRT without LBBB.

1.3.2 QRS duration

Whilst landmark studies such as COMPANION and CARE-HF required a QRS duration of >120-130ms for enrolment, mean QRS duration was around 160ms in these studies with few patients just above the inclusion cut-off.

In MADIT-CRT pre-specified sub group analysis found CRT was associated with event reduction in patients with QRS ≥150m (HR: 0.37-0.64), but not if QRS <150ms (HR: 0.74-1.52). An almost identical association in terms of direction and size was observed in RAFT and REVERSE: the other 2 trials of CRT in patients with mild symptoms.

A meta-analysis of major studies dichotomised 6502 patients according to a threshold QRS duration pre-implant of 150ms (4437 with QRS ≥150ms) (Stavrakis et al., 2012). CRT reduced the hazard of HF hospitalisation or death in patients with QRS ≥150ms (HR: 0.58, p<0.00001) but not in those with QRS <150ms (HR: 0.95, p=0.51). This effect was consistent across NHYA classes.

However, the positive findings in these studies were largely driven by a reduction in heart failure admissions. The aforementioned long term survival results from MADIT-CRT found that over 5.6 years the survival advantage was irrespective of baseline QRS (HR for death: QRS ≥150m: 0.46-0.90, p=0.01; QRS <150m: 0.31-0.97, p=0.04) (Goldenberg et al., 2014). It

stands to reason that in this setting an extended time frame is likely to be necessary to realise the potential for CRT.

A recent Italian analysis of 243 patients challenged the concept that the relationship between QRS duration and response is linear, and they report a more parabolic effect (Sassone et al., 2015). In LBBB there were clusters of non-responders with QRS duration below 130ms and above 180ms. LBBB with more marked QRS prolongation also heralded poorer event-free survival at 2 years. This is the first electrocardiographic report of an upper limit of dyssynchrony at which the benefit from CRT diminishes, although this concurs with previous mechanical studies (Chalil et al., 2007b).

1.3.3 CRT and narrow QRS duration

The disconnect between electrical and mechanical dyssynchrony led to the theory that there may be a sub-group of patients with narrow QRS duration who would benefit from CRT (Yu et al., 2003a). On this premise a number of randomised controlled trials have explored CRT in this population. The LESSER-EARTH (Evaluation of Resynchronization Therapy for Heart failure) trial was terminated prematurely as there was no evidence of benefit, a significant reduction in 6MWT, and a trend torwards an increase in heart failure admissions (Thibault et al., 2013).

A shortcoming of the LESSER-EARTH trial was that mechanical dyssynchrony was not a pre-requisite for enrolment. The earlier RethinQ (Resynchronization therapy in narrow QRS) Study did mandate echocardiographic evidence of mechanical dyssynchrony, but this study's

negative findings are potentially attributable to the dyssynchrony parameters utilised and the choice of peak VO_2 as a primary endpoint (Beshai et al., 2007). The EchoCRT (Echocardiography Guided Cardiac Resynchronization Therapy) trial, which required echocardiographic dyssynchrony in patients with a pre-implant QRS duration <130ms, was stopped due to futility (Ruschitzka et al., 2013). However, an 81% relative risk increase was seen for all-cause mortality in the CRT-On arm. This excess mortality was seen late after implant and was primarily due to arrhythmias and heart failure, providing the clearest signal that CRT pacing in narrow QRS is hazardous (Sohaib et al., 2015). Sub-group analysis failed to show evidence of benefit from CRT in the QRS 120-130ms population (Steffel et al., 2015).

1.3.4 Other ECG methodologies

The sum absolute QRST integral (SAI QRST) was initially trialled as a marker of risk from tachyarrythmias, but its recent evaluation in CRT populations has shown promise (Tereshchenko et al., 2011). A standard digital pre-implant 12 lead ECG is converted into 3 orthogonal leads (x, y and z), and SAI QRST is calculated as the sum magnitude of the QRS and T integrals (above and below the baseline) from all 3 leads. Validation of this measure has shown it to correlate closely with the SD of activation times recorded by non-invasive epicardial electrocardiographic mapping using 291 surface electrodes ($r=0.96$, $p= 0.045$). In contrast, QRS duration correlated poorly, and SAI QRST is a superior surrogate quantitative marker of late activated LV myocardium (Tereshchenko et al., 2015b).

In the SMART-AV (SmartDelay determined AV optimization: a comparison to other AV delay methods used in cardiac resynchronization therapy) trial, those with the highest tertile for

SAI QRST had a 2.5 times greater chance of LV remodelling than those in the lowest (OR: 1.3-5.0, p=0.01) (Tereshchenko et al., 2015a). In a retrospective study of a cohort of 496 CRT recipients a SAI QRST <302mV ms was associated with a 60-70% higher relative risk of mortality or HF hospitalisation at 2 years (Jacobsson et al., 2016). It remained a predictor of outcome even after adjustment for known predictors including QRS duration and morphology.

1.3.5 QLV

Delivering the LV pacing stimulus at a late activating site will have the greatest potential to correct the total myocardial activation time. The aforementioned metrics all prove an association between delayed LV activation and response, and it is plausible that this is due to the greater probability of LV stimulation being delivered at a region of late activated myocardium. Consequently, QLV, a measure of electrical delay at the left ventricular pacing site, should be a more specific predictor of response.

QLV is measured from intracardiac electrograms at CRT implant, and as shown in **Figure 1-2,** is the time delay between initial intrinsic activation at the septum (the onset of the Q wave on the standard ECG) and the spread of this wavefront to the site of the LV stimulating electrode. It thus quantifies the amount of electrical resynchronisation that pacing at a particular site can generate. The degree of electrical delay was shown in a pilot study of 71 CRT recipients to correlate with the acute haemodynamic benefit, particularly in the absence of previous myocardial infarction (Singh et al., 2006). Regardless of aetiology, less electrical delay was associated with poorer response.

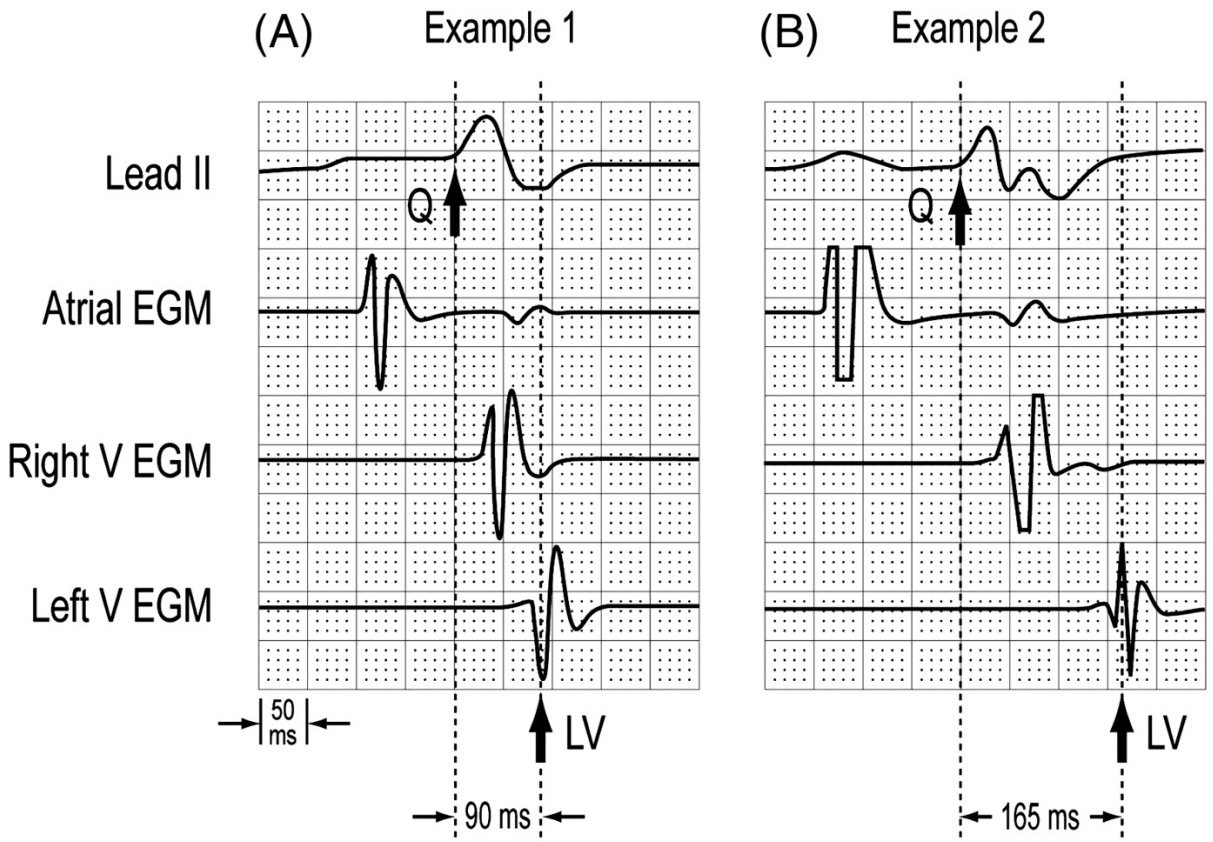

Figure 1-2. Examples of QLV measurements

The calipers are aligned with the onset of QRS and peak of the left venticular electrogram. The QLV was calculated as 90 ms for the patient in (A) and 165 ms for the patient in (B).

(Gold et al., 2011)

QLV was prospectively recorded in a sub-group of the multicentre SMART-AV trial and was shown to correlate with QRS duration and morphology. Whilst all three parameters predicted the primary end-point of LV reverse remodelling (LVRR), only QLV remained statistically important in multivariate analyses, supporting electrical delay at the pacing site being the integral determinant of benefit (Gold et al., 2011). The majority of patients had posterolateral LV lead positions, preventing assumptions on the utility of QLV to direct the implanter to less conventional sites such as the anterior wall or the apex. In a single centre observation of 329 patients a shorter QLV as a proportion of the total QRS duration was associated with greater cardiac mortality (HR: 1.8, p= 0.01), heart failure mortality (HR: 2.9, p= 0.001) and sudden cardiac death (HR: 2.1, p= 0.01) over a 9 year follow up period (Roubicek et al., 2015).

1.4 Assessment of LV systolic function

1.4.1 Assessment of LV systolic function by LV volumetric analysis

Quantitative assessment of LV volumes and function underpins the diagnosis of HFrEF and guides prognosis and the allocation of therapies including CRT.

1.4.1.1 Echocardiography and LV volumetric analysis

Two dimensional trans-thoracic echocardiography (2DE) is a cardiac ultrasonographic technique that remains the cornerstone of diagnostic imaging, not least because of its wide availability, speed, portability and non-reliance on ionising radiation. LV function is most widely calculated using ‘Simpson’s method’ or the ‘method of disks’ which is a volumetric

measure (Leeson et al., 2008). The LV is imaged from an apical window along its long axis from 2 orthogonal views. The volume of the LV is calculated by segregating the chamber into a series of equal height discs from the apex to the mitral valve annulus. Summation of the volume of each disc gives the total LV volume and subtraction of the LVESV from the LVEDV provides the LV stroke volume (LVSV). LVEF is an expression of the LVSV as a percentage of the LVEDV. Whilst this can be calculated manually, modern day processing software calculates this automatically following operator contouring of the LV endocardium.

As with all 2DE techniques the major limitation is image quality; the main barriers being chronic lung disease, obesity and chest wall deformities (Yong et al., 2002). LV foreshortening will lead to underestimation of volumes and sub-optimal LV endocardial definition will lead to an overestimation. Harmonic imaging in preference to fundamental imaging can improve endocardial definition by reducing reverberation artefact (Spencer et al., 1998). LV opacification, using microbubbles that consist of a gas contained in an outershell, improves backscatter and enhances differentiation of the endocardial border from the blood pool to an even greater extent (Chahal et al., 2010). Nonetheless, Simpson's method still requires certain assumptions regarding the uniformity of the LV which are less valid in the diseased ventricle. Three-dimensional echocardiography (3DE) overcomes these geometric assumptions by providing absolute chamber volumes and, in experienced hands, has close accuracy with radionuclide angiography (Nosir et al., 1996) and cardiac magnetic resonance (CMR) (Kuhl et al., 2004). However, image quality remains a factor and current availability is limited.

Core lab re-evaluation of 2DE volumetrics from many of the enrolees in the landmark studies highlights the deficiencies of this as an inclusion criterion for studies and a means for allocating CRT. In MADIT-CRT 38% had a LVEF outside the inclusion criteria (<30%). In some cases a massive discrepancy saw LVEF being re-calculated as high as 45% (Kutyifa et al., 2013). 24% of participants in PROSPECT had a LVEF adjudged to be greater than the 35% cut-off when reassessed (Chung et al., 2010).

1.4.1.2 CMR and LV volumetric analysis

Cardiac magnetic resonance (CMR) is the reference standard for ventricular volumetric and functional assessment with robust accuracy and reproducibility (Grothues et al., 2002). A series of contiguous cines ('a stack') is acquired, during breath-holds, providing full coverage of both ventricles so that there are no limitations due to geometric assumptions. This process is supported by the unlimited imaging planes that CMR offers, so the stack is acquired entirely in plane, running parallel to the AV valve annuli and perpendicular to the long axis (using previously acquired orthogonal long axis views as a guide).

Cine acquisition typically takes a few minutes using steady state free precession (SSFP) imaging: a gradient echo sequence, which produces images with a high signal to noise ratio and sharp contrast between the blood pool and myocardium. Along with unparalleled spatial resolution this makes subsequent volumetric assessment highly reproducible (typically conducted remotely and taking an experienced operator around 15 minutes). Simultaneously, RV volumetric analysis and LV mass can be obtained (Maceira et al., 2006).

As with any modality CMR is not without limitations. Acquisition requires ECG gated segmented imaging. Poor breath-holding or arrhythmias, both potentially problematic in heart failure patients, will degrade image quality.

1.4.2 Assessment of LV systolic function by myocardial strain analysis

In routine clinical practice the assessment of LV function consists of assessments of global systolic and diastolic function. It is well recognised, however, that global measures such as LVEF, may not be sensitive enough to detect subtle changes in LV function, as is the case with incipient disease (Nagueh et al., 2001; Sutherland et al., 1994).

Cardiac strain, a sensitive measure of deformation, is defined as the relative change in fibre length from end-diastole; strain rate being a measure of the velocity at which this change occurs (**Figure 1-3**). Whilst measuring this in vivo would require a precise knowledge of the local fibre direction, clinical imaging modalities circumnavigate this by measuring strain in three principle directions (radial, circumferential and longitudinal), relative to the central axis of the ventricle. Longitudinal strain is deformation relative to the long axis of the myocardium; circumferential and radial strains are orthogonal measures both relative to the myocardial short axis (**Figure 1-4**). By convention cardiac strains are dimensionless, but they are expressed as a percentage change from end-diastolic state, with myocardial contraction or shortening assigned a negative value and thickening or elongation a positive value. As strain rate records the change in strain over time it is typically expressed as the reciprocal of time in seconds (S^{-1}).

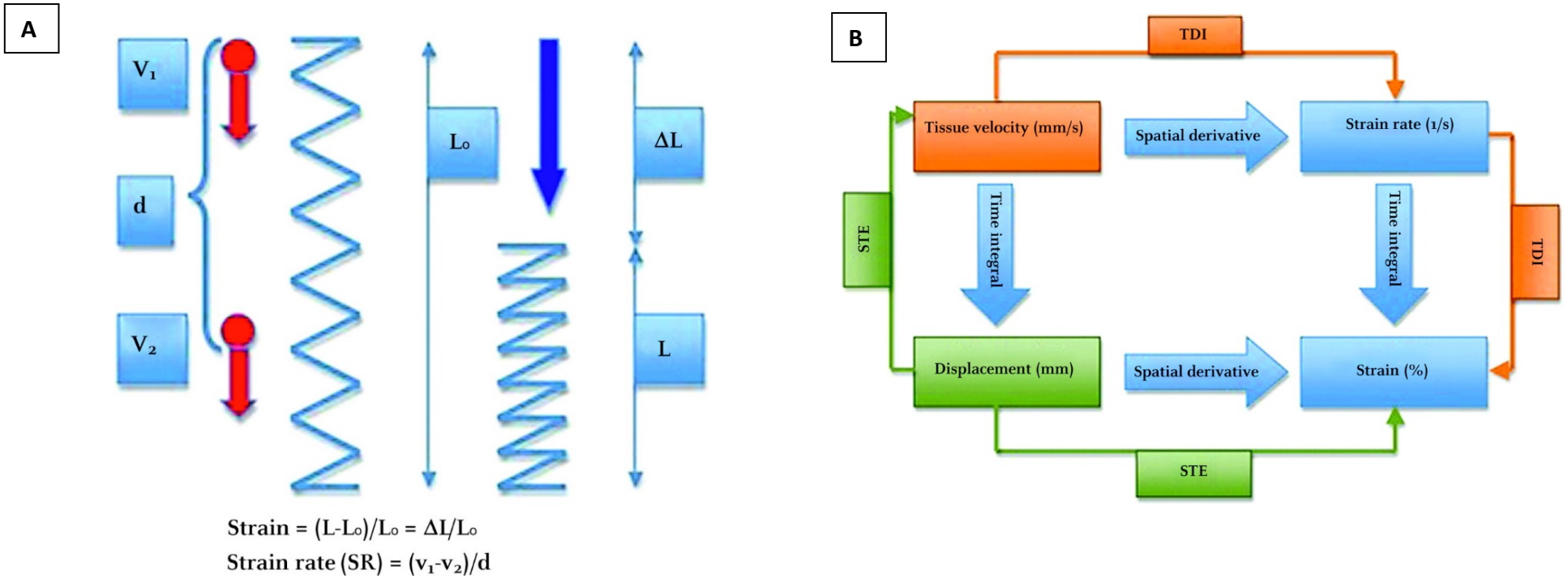

Figure 1-3. Displacement, velocity, strain and strain rate.

(A) shows how to calculate strain and strain rate. Strain= change of fibre length compared to original length, strain rate= difference of tissue velocities at two distinctive points related to their distance. ΔL, change of length; Lo, unstressed original length; L, length at the end of contraction; blue arrow, direction of contraction; v1, velocity point 1; v2, velocity point 2; d, distance.

(B) The mathematical relationship between different deformation parameters. Using conventional echocardiographic techniques speckle (STE) primarily assesses myocardial displacement, whereas tissue Doppler imaging (TDI) primarily assesses tissue velocity.

Adapted from (Blessberger et al., 2010)

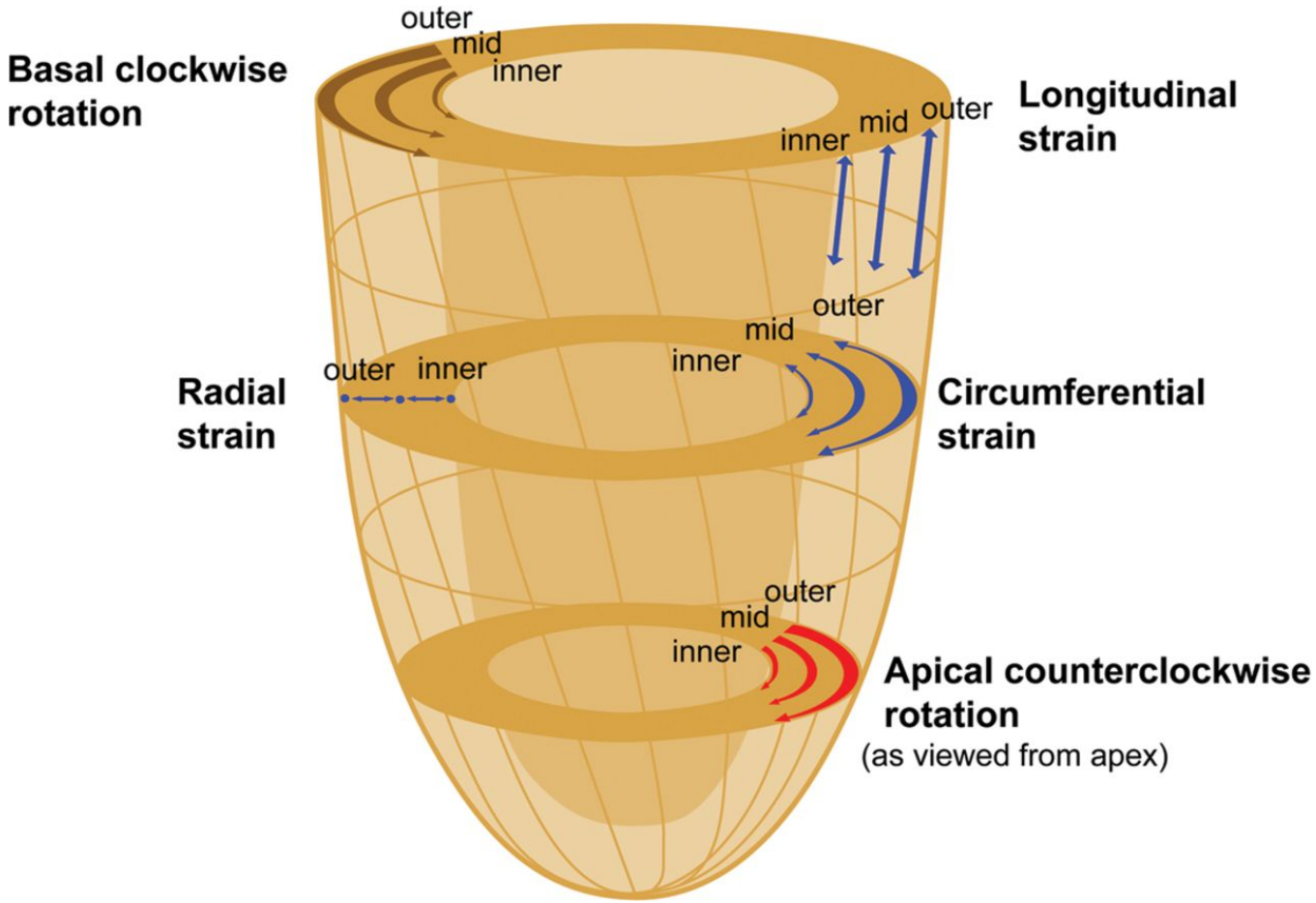

Figure 1-4. The layer-specific left ventricular myocardial wall strains and cardiac rotation.

(Yu et al., 2013)

The myocardium can be theoretically sub-divided into any number of smaller units and each strain can be calculated at any spatial or temporal point. The peak strains or strain rates are the most clinically useful as these relate to maximal function. This allows both regional and global measures to be derived.

LVEF is load dependant; it incorporates the net result of the neurohumoral compensatory mechanisms described in **1.1.4**, with an increased LVEDV preventing any discernible change in LVEF in early disease. In contrast, myocardial strain is a purer gauge of the myocardium's contractile function. In this respect global strain measures are affected by the degree of myocardial scarring (Becker et al., 2006b). In keeping with these intrinsic differences between LVEF and strain parameters, whilst they correlate in healthy controls, there is disconnect between them in the failing heart (Delgado et al., 2008). Strain rate measures the rate at which deformation occurs, it is the least load dependent parameter and a surrogate for dP/dt (Weidemann et al., 2002). **Figure 1-3** shows the mathematical relationship between the key parameters of myocardial motion.

1.4.2.1 Invasive measures of myocardial strain

The earliest in vivo assessments of cardiac strain and motion used the surgical implantation of markers within the myocardium. The location of implanted radio-opaque markers can be monitored fluroscopically (Ingels et al., 1980), and sonomicrometry makes use of tranducers comprising piezoelectric crystals that have dual ultrasound transmitting and receiving capabilities, so that their relative distance can be identified (Chitwood et al., 1980). The

number of regions that can be assessed is limited by the number of placed tags, and whether the implants themselves alter cardiac motion is unknown. Regardless, invasive techniques are more suited to animal studies and have limited application in the human field, although they remain a useful tool by which to validate new non-invasive methods.

1.4.2.2 Tissue Doppler measures of myocardial strain

Echocardiography based tissue Doppler imaging (TDI) facilitates the calculation of regional tissue velocities relative to the transducer probe. The use of TDI is limited by the inability to differentiate true velocity from that of passive stretch that occurs when scarred myocardium is tethered to adjacent contractile tissue. However, TDI based strain measures overcome this limitation; velocity is calculated at two adjacent myocardial points, and velocity-regression allows the computation of the strain rate between the points (Marwick, 2006).

The technical complexity of this modality limits its accuracy and use. Underlying velocity signals are prone to noise such as that from reverberation artifact (e.g. from ribs) or the blood pool (Edvardsen et al., 2002; Miyatake et al., 1995). The necessary high frame rates limit spatial resolution. The optimal distance between areas of interest is 12mm, greater than the usual thickness of the myocardium, rendering the technique only apt to measure longitudinal strain. The technique is angle dependent, and any loss of alignment reduces accuracy so images are best obtained in held expiration to prevent respiratory drift (Castro et al., 2000).

1.4.2.3 Speckle tracking echocardiography measures of myocardial strain

Speckle tracking echocardiography (STE) has facilitated strain measures from standard 2DE images, thus largely overcoming noise interference and angle dependency. The tracking algorithm follows collections of natural acoustic markers and interference patterns (speckles) that remain constant throughout the imaged cycle. It has been validated against sonomicrometry (Amundsen et al., 2006), and is reproducible by experienced operators (Belghitia et al., 2008). As expected with a 2DE technique, image quality is the limiting factor (Amundsen et al., 2006). There is a difficult trade-off balancing temporal resolution, as at high levels noise impairs image quality, but at lower resolutions the analysis software loses speckles between frames. Feasibility of obtaining utilisable images is reported as 94% in healthy populations (Hurlburt et al., 2007), but is considerably less in diseased populations, especially IDCM when wider sector widths limit frame rate.

1.4.2.4 Myocardial tagging measures of myocardial strain

CMR combined with myocardial tagging is the reference standard technique for the assessment of myocardial motion. Myocardial tags, created by manipulating magnetisation, act as fiducial markers that conform to the region of interest (Axel et al., 1989). Additional radiofrequency impulses are delivered in time with the R wave, perpendicular to the imaging plane to saturate the magnetic properties of the tissues. This has the effect of producing sets of parallel dark bands within the image creating a tagged pattern. This grid is intrinsic to the tissues, so motion of the tags depicts myocardial motion.

A variety of techniques exists: a recent review reports 25 different algorithms each requiring specific pulsed sequences for acquisition and specific post processing software (Ibrahim el, 2011), such as harmonic phase analysis (HARP) or spatial modulation of magnetisation (SPAMM). These techniques have been validated for the assessment of regional wall motion in animals and humans (Kraitchman et al., 2003).

The acquisition sequences are additional to routine protocols and require lengthy breath holds, and requisite post-processing is time consuming and laborious. Whilst successive generations of this modality address these shortcomings, they have largely confined its use to the research environment. Research applications have focused on systolic assessment as tag loss at temporal distances from the R wave, due to T1 relaxation, has constrained diastolic assessment with cines acquired using 1.5T scanners (Edvardsen et al., 2006).

1.5 CRT and mild-moderate systolic dysfunction

An LVEF <35% is an arbitrary cut-off for allocating CRT and corresponds to the echocardiographic definition of severe LV impairment. The natural evolution of any therapy sees it initially trialled in the sickest patients and it is easiest to demonstrate value in patients with high event rates. However, a single centre registry using conventional implantation guidelines retrospectively re-analysed LVEF on the basis of baseline CMR, and found that the 27 patients identified as having LVEF >35% had at least similar clinical response rates to other recipients (Foley et al., 2009c).

Re-analysis of the landmark trials, using core laboratory revised LVEFs provides the richest insight into the potential benefits of CRT in more moderate LV systolic dysfunction. In PROSPECT 86 patients had an LVEF >35% and broadly similar improvements in the clinical composite score and remodelling were seen in this group (Chung et al., 2010). In MADIT-CRT 696 patients had LVEF >30% (Range: 30.1%-45.3%), and despite the smallest event rate in this cohort, the greatest protection from hospitalisation and death was observed (HR: 0.56, 95% CI: 0.39 - 0.82, p= 0.003) (Kutyifa et al., 2013). Furthermore, the best remodelling response was also seen in the least impaired ventricles. The ultimate goal of heart failure treatment is to provide complete heart failure remission, i.e. minimal or no symptoms with complete recovery of systolic function. An observational study of 520 patients has shown that least impaired LVEF at baseline is a predictor of this (Gasparini et al., 2008). When normalisation of LVEF is achieved the risk of arrhythmic death becomes minimal (Ruwald et al., 2014).

There is a compelling argument for trialling CRT at an earlier time point in the natural history of heart failure, and assessing its utility as a preventative disease modifying therapy rather than a last resort therapy. However, designing such a study is challenging and MIRACLE EF, which addressed this, was abandoned due to poor recruitment (Linde et al., 2016). The long follow-up required to show benefit in a population with low anticipated event rates proved unacceptable to potential enrolees, particularly in the face of the possibility of being randomised to the inactive device arm for this period. As strain measures are more sensitive to impaired contractility, it is plausible that they could be used to select a sub-population of

patients with mild-moderate LV systolic dysfunction who are more suitable for study and thus would require shorter follow up.

The management of patients with a co-existing indication for bradycardia is more resolved. Right ventricular (RV) pacing has detrimental effects in heart failure. In the DAVID (Dual Chamber and VVI Implantable Defibrillator) trial, rather than prove the hypothesis that continuous pacing would facilitate more aggressive medical therapy and improve outcomes, dual chamber pacing increased the rate of death and hospitalisation (Wilkoff et al., 2002). Echocardiographic studies have shown that the deleterious effects of RV apical pacing are, at least in part, due to the induction of mechanical dyssynchrony (Cojoc et al., 2006). The BLOCK-HF (Biventricular versus Right Ventricular Pacing in Heart Failure) study demonstrated the advantages of CRT over conventional bradycardia pacing in patients with mild to moderate LV systolic dysfunction and AV nodal disease (Curtis et al., 2007). CRT resulted in a significant delay in time to the primary composite endpoint (HR: 0.74, 95% CI: 0.60 - 0.90).

1.6 Mechanical dyssynchrony assessment and CRT

1.6.1 Doppler based dyssynchrony assessment

The assessment of cardiac dyssynchrony has been the focus of increasing attention with the advent of CRT. The concept that pre-implant dyssynchrony is prerequisite for a benefit from CRT has driven the search for imaging markers of dyssynchrony that can refine patient selection beyond the use of QRS duration. This expectation was fuelled by a series of promising M-mode (Pitzalis et al., 2002), pulsed Doppler (Achilli et al., 2006) and TDI (Bax et

al., 2004; Notabartolo et al., 2004; Yu et al., 2004; Yu et al., 2003b) techniques tested in single centre studies.

The observational PROSPECT (Predictors of response to CRT) study did not support earlier findings. 498 patients with conventional CRT indications (LVEF ≤35%, NYHA III or IV, QRS duration ≥130 ms) underwent CRT implant at 53 centres from 3 continents (Chung et al., 2008). Similarly to other trials 69% patients had a symptomatic improvement and 56% showed reverse remodelling. Not one of the tested dyssynchrony markers had an AUROC curve > 0.62 for its ability to predict either a symptomatic or echocardiographic response. Despite each centre having undergone prior training in dyssynchrony assessment, and requiring regional accreditation prior to enrolling, yield, intra-, and inter-observer reproducibility were all poor. This variability may have been exacerbated by the use of different echocardiographic platforms, but this reflects the 'real-world' situation.

1.6.2 Strain based dyssynchrony assessment utilising echocardiography

In general, strain based methods involve analysing the timing of peak strain regionally and the calculations of various parameters based on these. STE based parameters overcome the angle dependence of Doppler. The initial study experience used segmental peak radial strains obtained from speckle tracking mid ventricular short axis images to evaluate baseline dyssynchrony in 64 patients.

The earliest studies classed dyssynchrony as a > 130ms delay between peak radial strain being reached in the anteroseptal and posterior walls in the mid-ventricle; this parameter

was a predictor of an acute haemodynamic response and subsequent remodelling (Suffoletto et al., 2006). In a follow-up study of 176 patients the same group combined this STE parameter with a TDI derived longitudinal dyssynchrony marker. Patients with both radial and longitudinal dyssynchrony pre-implant had a 95% likelihood of reverse remodelling, compared to only 59% or 10% if 1 or neither parameter was positive (Gorcsan et al., 2007). This interplay of different dyssynchrony patterns highlights the complexity of dyssynchrony assessment and provides insight into the difficulties of utilising any single dyssynchrony index.

The STAR (speckle tracking and resynchronisation) study provides the strongest signal that dyssynchrony assessment may be of value. STAR provides a prospective, multi-centre comparison of the predictive value of radial, circumferential, longitudinal and transverse (radial strain viewed from the long axis) strain derived dyssynchrony indexes (all adjudged by > 130ms opposing wall delay) (Tanaka et al., 2010). Patients without pre-implant radial dyssynchrony were three times more likely to die or require heart transplantation or LV assist device (LVAD) over 3.5 years follow-up. Circumferential and longitudinal measures were not significant predictors. An independent study reiterated these findings and showed that a lack of pre-implant radial dyssynchrony was associated with reduced event free survival in patients with QRS durations of 120-150ms (Gorcsan et al., 2010). However, the EchoCRT study tested whether such radial dyssynchrony could identify patients with a QRS duration <130ms who would benefit from CRT; the study was stopped early due to futility (Ruschitzka et al., 2013).

A shortcoming in current methodology has been the focus on markers of temporal dispersion. This is a particular flaw when late mechanically activated regions have extensive scar, so offer minimal contribution to overall contractility. Summations of the difference between peak strain and strain at end systole for each segment provide measures of wasted work caused by dyssynchrony (**Figure 1-5**). Such a concept has been tested using speckle tracking, proved superior to traditional temporal dispersion based measures (Lim et al., 2008; Tatsumi et al., 2011), and has recently been shown to predict survival in a single centre study (Kydd et al., 2013).

3DE allows complete assessment of the LV geometry and facilitates dyssynchrony to be based on the entire ventricle; offering another scope for investigation. Commercially available packages (TomTec Imaging Systems, Munich, Germany) facilitate the tracking of the entire endocardial border which, once segmented into a traditional 16 segment model, allows computation of the SD of time to minimal volume (a surrogate for contraction). A dual centre study of 187 patients found that this was reproducible with an inter-hospital agreement of 7.6%. It had an area under curve (AUC) of 0.66 and 0.86 for predicting LVRR, and a 20% improvement in LVEF respectively (Kapetanakis et al., 2011). Whether 3D STE offers superiority to 2D parameters needs investigating.

1.6.3 CMR based dyssynchrony assessment

At the time when dyssynchrony assessment was a major research theme CMR was comparatively less prevalent, and this is reflected in its literature base. The CMR tissue synchronisation index (CMR-TSI) index utilised radial wall motion from each cine of the short

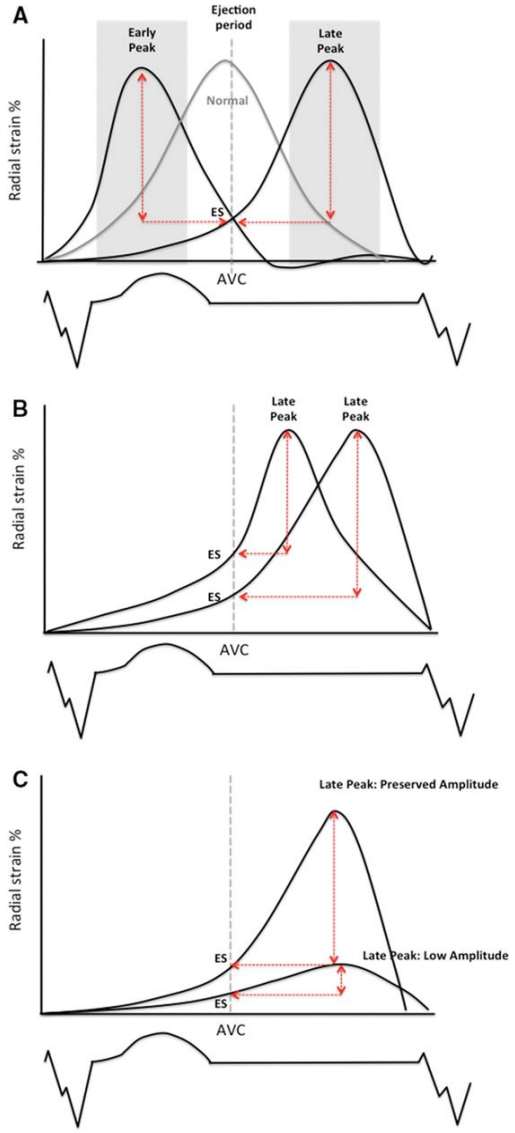

Figure 1-5. Concept of the strain delay

Schematic representation of wasted energy according to timing of myocardial deformation (dyssynchrony) and amplitude (contractility) by radial strain. A, In a normal segment (grey), peak deformation occurs close to aortic valve closure, contributing fully to end-systolic (ES) function. Peak ejection is assumed to occur at end systole, at the point of aortic valve closure (AVC) defined by pulsed wave Doppler. Early and late deformation in segments with preserved contractility will not fully contribute to end-systolic function. The wasted energy is represented by the difference in strain amplitude at peak and end systole for these segments (red). B, The degree of wasted energy increases as segments with preserved contractility become more delayed. C, In delayed segments with preserved amplitude (contractility), the degree of wasted energy is greater than in low-amplitude segments (minimal residual contractility or scar).

(Kydd et al., 2013)

axis stack (Chalil et al., 2007b). Displacement-time curves were constructed for each segment of each slice, and were subject to sine wave fitting. CMR-TSI reflects the standard deviation (SD) of all the segmental phase shifts. In contrast to previous dyssynchrony studies, patients with the greatest baseline dyssynchrony had poorer survival and more frequent hospital admission. This parameter detects dyssynchrony in all patients with heart failure, thus challenging the concept of it being an arbiter of benefit from CRT (Foley et al., 2009a).

Ratios of the spatial uniformity of strain have the same underlying concept as the CMR-TSI, but describe variance in strain rather than motion. A circumferential uniformity ratio estimate (CURE) <0.75 (where 1= total uniformity and 0= complete dyssynchrony), derived from myocardial tagging, had a 90% accuracy for predicting improvement in functional class post CRT (Bilchick et al., 2008).

1.7 Myocardial scar

1.7.1 Myocardial scar assessment

The myocardium consists of myocytes, a variety of non-myocytic cells such as fibroblasts, endothelial cells, mast cells and an extracellular matrix, which are maintained in equilibrium by a variety of hormones, cytokines and growth factors. When this balance is disturbed by an insult, myocardial scar results from expansion of the interstitium, and a net increase in collagen synthesis over its degradation (Baudino et al., 2006). This is physiologically detrimental due to impaired contractility, increased wall stiffness and distorted electrical conductivity that is conducive to cardiac arrhythmogenesis.

Historically the gold-standard for detecting myocardial fibrosis was endomyocardial biopsy (EMB). However, this investigation is limited by sampling error. Fibrosis is often patchy, and in many disease states the composition of the readily sampled RV is not representative of the LV. Along with the small but real risk of serious complications, EMB has been superseded by non-invasive imaging techniques.

1.7.2 CMR and myocardial scar assessment

Coupled with late Gadolinium enhancement (LGE) imaging, CMR is the gold standard for myocardial scar characterisation. It has an unrivalled ability to quantify the size, location and transmural extent of scar. Post injection, Gadolinium is distributed between the intravascular space and the interstitium, but is excluded from the intracellular space by intact cell membranes. It accumulates in areas of scar which have an expanded intracellular space. Gadolinium is paramagnetic, and shortens the T1 relaxation time, thus delayed imaging post administration demonstrates areas of scarred myocardium as having high signal intensity (white) compared to nulled myocardium (black) (Simonetti et al., 2001).

LGE-CMR is not apt for the detection of diffuse fibrotic processes when no reference region exists, but this has been facilitated by advances in the parametric mapping of the T1 magnetic relaxation properties of the myocardium (Flett et al., 2010; Iles et al., 2008). Pulse sequences such as Modified Look-Locker (MOLLI) allow this to be performed in a single breath-hold, greatly reducing acquisition times compared to earlier methodologies and preventing misregistration artefact (Messroghli et al., 2007).

1.7.3 Echocardiography and myocardial scar assessment

Unlike LGE-CMR, echocardiography does not facilitate the delineation of discrete scar, although a variety of surrogates have been evaluated against it. A wall thickness < 0.5cm accompanied by an abnormal increase in echo reflectance has been used (Cwajg et al., 2000; Mele et al., 2009), and further accuracy is gained by combining this approach with examination of regional wall motion abnormalities. Regional myocardial strain measures lend themselves to acting as surrogates for scar, and both longitudinal (Gjesdal et al., 2007) and radial (Becker et al., 2006a) measures have been validated.

The increased collagen content of myocardial scar affects its acoustic reflectivity, and this can be assessed using echocardiographic integrated backscatter (IBS) as a measure of diffuse fibrosis (Picano et al., 1990). IBS correlates with scar content at EMB in aortic stenosis (Di Bello et al., 2004) and IDCM (Mizuno et al., 2007). Even though the accuracy of this is improved by using pericardial backscatter as a control, its technical complexity and poor reproducibility have prevented widespread use (Di Bello et al., 2010).

1.7.4 SPECT and myocardial scar assessment

SPECT (Single Photon Emission Computed Tomography) was the first widely available modality to detect myocardial viability, and thus indirectly define myocardial scar and fibrosis. After the administration of Thallium-201 or Techetium-99 labelled ligands, a series of planar images are taken using a gamma camera at multiple angles. These are reconstructed to form tomographic images through the heart which can be aligned with the hearts axis. Segments with reduced uptake compared to the area of maximal uptake have

the greatest extent of scarring. With Techetium-99 imaging can be performed after administration of the tracer, but with Thallium-201 scar mapping needs to be delayed 2-24 hours post administration of the radionuclide to allow redistribution.

The value of SPECT for identifying scar is limited by its spatial resolution, which is a factor of 60x less than LGE-CMR. A comparison of both against histopathological findings in iatrogenic infarcts in canines found, whilst both modalities were able to detect all transmural scars, SPECT only detected 28% of sub-endocardial scars (c.f. 92% by LGE-CMR) (Wagner et al., 2003). Repeat imaging with SPECT is undesirable due to accumulative ionising radiation exposure.

1.8 Myocardial scar and outcomes from CRT in ischaemic heart failure

Undoubtedly, the quantity of myocardial scar and its location have an influence on the disease course post CRT.

1.8.1 Scar burden

A study of 23 patients who underwent LGE-CMR prior to device implantation showed scar burden was significantly higher in non-responders than responders (Interquartile range [IQR]: 18.1-48.7% vs. 0.0-8.7%, p= 0.002) as assessed using a clinical composite scoring system (White et al., 2006). Scar had an AUC of 0.94 for predicting response. Similarly, a study of 62 patients with pre-implant LGE-CMR found clinical response to be 2.3x greater in those with a scar burden <33%, compared to those whose scar burden was greater than this cut-off (Chalil et al., 2007a). Comparable findings were made when scar burden was

assessed using SPECT. The scar burden of each myocardial segment was graded from 0 (no scar) – 3 (extensive scar). Clinical responders had a mean scar score of 10, and non-responders 25 ($p< 0.001$) (Ypenburg et al., 2007).

Total scar burden predicts survival in patients with heart failure (Kwon et al., 2009) and this trend is not reversed by a CRT device. Over a mean follow up of 2 years post implant, patients with a low scar burden identified by Thallium perfusion imaging were less likely to progress to mechanical circulatory support, transplantation or death than those with a high scar burden ($p<0.001$) (Adelstein et al., 2011).

Significant heterogeneity between studies, in terms of cohort demographics and outcome criteria employed, precludes the identification of a critical level of myocardial scar above which a favourable response to CRT is unlikely. However, there is a linear correlation between scar burden and response, and the prognosis of those with the lowest scar burden is similar to those with NICM (Adelstein et al., 2011). It is probable that there is a scar burden above which CRT will be unsuccessful due to the decreasing quantity of myocardium that can contribute to re-synchronised mechanics.

1.8.2 Scar transmurality

Myocardial segments with a greater transmural extent of scar are more likely to be non-viable and are less likely to recover contractility post revascularisation (Kim et al., 2000; Selvanayagam et al., 2004). A LGE-CMR study of 45 patients showed that, in patients with postero-lateral scar, <51% transmurality was associated with a significant higher likelihood

of response, compared to a greater transmural extent (88% vs. 23%; p<0.001). This remained significant after adjusting for scar burden and location (p=0.004) (Chalil et al., 2007a).

1.9 Idiopathic dilated cardiomyopathy and midwall fibrosis

1.9.1 Diagnosis, prevalence and pathophysiology of midwall fibrosis

The detrimental effects of myocardial fibrosis in IDCM were first described in autopsy studies (Maehashi et al., 1991). Histopathological diagnosis in vivo requires EMB, an imperfect tool due to the variable location and depth from the endocardial surface of fibrotic tissue (Marra et al., 2013), but the evolution of LGE-CMR has facilitated in vivo assessment of myocardial fibrosis and the study of its implication.

LGE-CMR and histopathological techniques have perfect concordance for identifying and delineating the distribution of myocardial fibrosis in IDCM (Gulati et al., 2013) (**Figure 1-6**). The distribution of fibrosis can be patchy, sub-epicardial, or midwall (McCrohon et al., 2003). Problematically, some investigators fail to differentiate between these patterns or clearly specify the definition of myocardial fibrosis, whilst others confine their investigation to true midwall fibrosis (MWF). These differences in the classification of myocardial fibrosis account for the inter-study variance of its prevalence in IDCM, which ranges from 1/3 up to 2/3 if minor insertional fibrosis is included.

The pathophysiology of MWF is unclear. One theory is that MWF is a time dependant processes representing a late pathway of myocardial damage. However, circumstantial

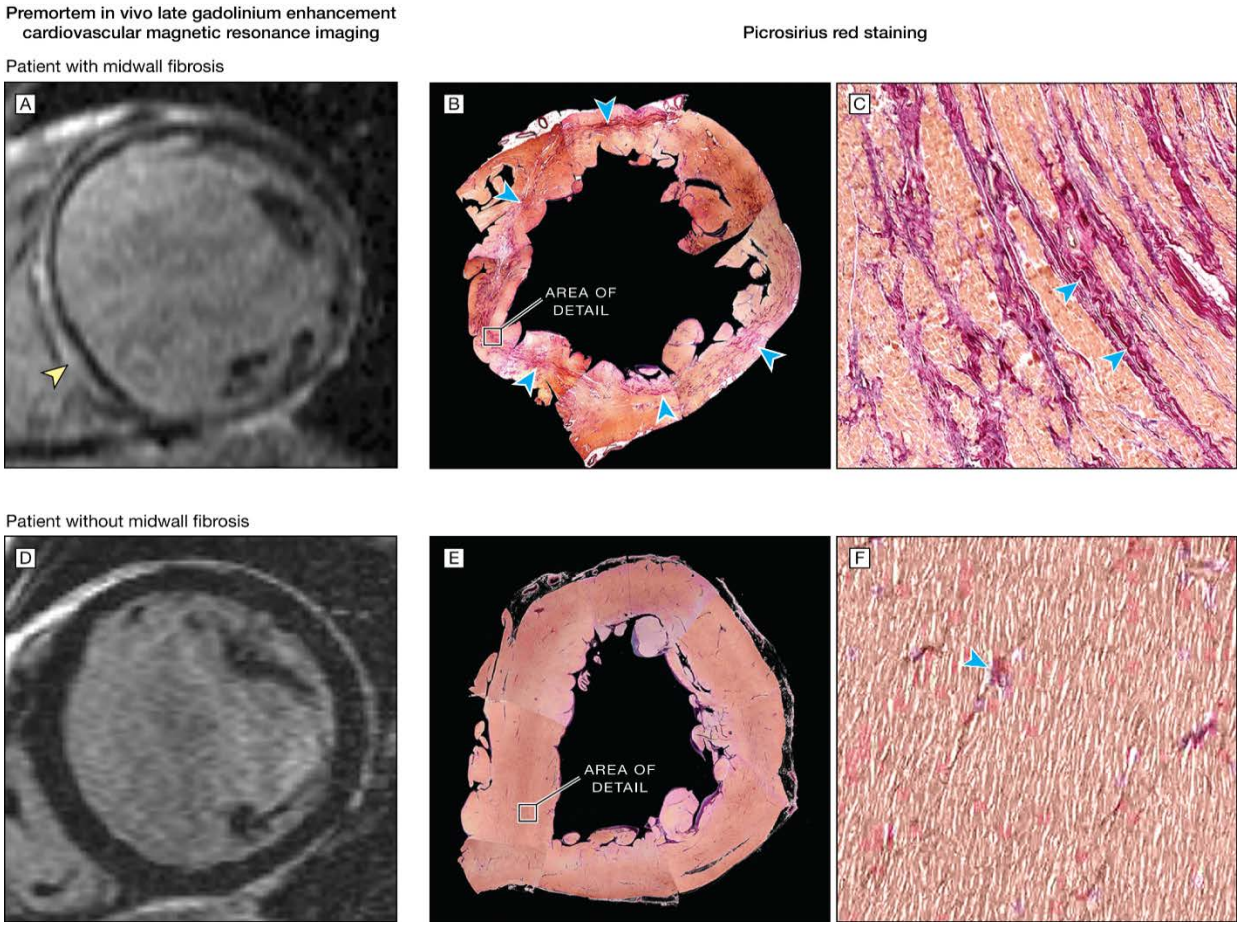

Figure 1-6. Correlation between LGE-CMR, and macroscopic and microscopic histopathological specimens patients with idiopathic dilated cardiomyopathy.

A-C are from a patient with MWF who experienced sudden cardiac death. D-F are from a patient without MWF who underwent cardiac transplantation. A Premortem LGE-CMR demonstrated a near-circumferential pattern of midwall LGE (yellow arrow) in the anterior, septal, inferior, and inferolateral segments at midventricular level. B Picrosirius red staining in the corresponding postmortem macroscopic short-axis section revealed a prominent linear band of collagen (blue arrows), which mirrored the distribution of LGE on CMR. C Microscopic examination confirmed the presence of extensive replacement fibrosis (blue arrows) in an area of staining seen on the macroscopic section (area of detail in part B); magnification × 300. D On LGE-CMR performed prior to cardiac transplantation, there were no areas of LGE. E Following explantation, macroscopic assessment revealed no detectable regions of collagen with Picrosirius red stain. F Microscopic section from the septal midwall (area of detail in part E) showed small amounts of perivascular fibrosis (blue arrow) but no replacement fibrosis; magnification × 300.

(Gulati et al., 2013)

evidence is accruing suggesting an alternative notion that MWF represents a distinct phenotype of IDCM. Patients with MWF are significantly younger and more likely to report a familial link, suggesting a genotypically different disease subset (Assomull et al., 2006). Strengthening this theory, many of the mutations associated with IDCM encode for cytoskeletal proteins (McNally et al., 2013). Further suggestion of separate disease entities comes from a longitudinal study comparing scans performed at baseline with those at a two year time interval. No patient without MWF at baseline developed it during follow-up, in contrast to patients with MWF at baseline, in whom fibrosis never receded but commonly progressed (Masci et al., 2013).

1.9.2 Midwall fibrosis and myocardial pump function

There are conflicting reports with respect to the relationship between LVEF and MWF. The largest studies show that LVEF is reduced in the presence of MWF (Assomull et al., 2006; Gulati et al., 2013), however, two studies restricted to newly diagnosed patients both find equivalent LV function regardless of fibrosis status (Leong et al., 2012; Masci et al., 2013). Nonetheless, these studies observed that following optimal medical therapy, reverse remodelling and improved systolic function were seen in patients without fibrosis, whilst no recovery was seen in ventricles with MWF. Furthermore, over time fibrosis progressed and was associated with a further decline in systolic function.

To date there has been no robust study of the effect that MWF has on contractility. Knappen et al. report that fibrosis does hinder contractile function on the basis of a correlation between regional perfusable tissue index (PTI) calculated with positron emission

tomography and circumferential strain (E_{cc}) (Knaapen et al., 2006). However, segmental reductions in PTI have never been validated as a surrogate for fibrosis (Knaapen et al., 2004), and the authors recognised that 'there is no evidence that the reduction of the PTI in patients with IDCM actually represents myocardial fibrosis.' Furthermore all patients in this study had segmental reductions in PTI, and none had any late Gadolinium enhancement.

Diastolic function is also influenced by MWF. The replacement of normal myocardial tissue with fibrotic tissue increases myocardial stiffness and impedes diastolic function across a broad spectrum of pathologies (Moreo et al., 2009), and findings in IDCM are similar (Karaahmet et al., 2010; Moreo et al., 2013; Nanjo et al., 2009). The most comprehensive study in this field demonstrated a relationship between the number of segments with MWF and LV filling pressures estimated from echocardiography (Moreo et al., 2013). In multivariate analyses the burden of MWF positively correlated with estimated filling pressures, whereas LVEF and LVEDV did not. The only discordant study found that patients without fibrosis had higher LV filling pressures, as estimated from the septal E/E' ratio (Malaty et al., 2011). These results were likely confounded by the inclusion of patterns of fibrosis other than true MWF.

Table 1-1 shows that the impairment in systolic and diastolic function that accompanies MWF translates into worse long term outcomes. In multivariate analyses the presence of MWF was the sole significant predictor of adverse events, even when right and left ventricular function and LV dimensions were considered. Prognosis declined with increasing

Table 1-1. Outcome studies in IDCM stratifying patients according to MWF

Study	Patients n	No MWF n (%)	MWF n (%)	Follow-up (Years)	1^0 Endpoint	Hazard Ratio	2^0 endpoints reaching significance
Assomull 2006	101	66 (65)	35(35)	1.8	All cause mortality/ CV hospitalisation	3.4 (1.4-8.7) p= 0.01	1. SCD/VT
Wu* 2008	65	38 (58)	27 (42)	1.4	CV mortality/ HF hospitalisation/ ICD shock	7.1 (2.0-25.3) P= 0.002	1.CV mortality/ICD shock
Gulati 2013	472	330 (70)	142 (30)	5.3	All cause mortality	2.96 (1.9-4.7) p <0.001	1. CV mortality 2. SCD/VT 3. HF death, hospitalisation or transplant

CV= cardiovascular, HF= heart failure, ICD= Implantable cardioverter-defibrillator, IDCM= idiopathic dilated cardiomyopathy, MWF= midwall fibrosis, SCD= sudden cardiac death, VT= ventricular tachycardia.

***subjects from a population referred for primary prevention ICD**

fibrosis, with particularly poor outcomes for those with more than 5% of the myocardium replaced with fibrotic tissue (Assomull et al., 2006). In the largest study both the presence (HR: 1.62, 95% CI 1.00-2.61, p= .049) and the extent (HR: 1.08, 95% CI 1.04-1.13, P< 0.001) of MWF predicted heart failure events (Gulati et al., 2013).

1.9.3 Midwall fibrosis, ventricular arrhythmias and sudden cardiac death

MWF also increases the risk of both ventricular arrhythmias and sudden cardiac death (Assomull et al., 2006; Gulati et al., 2013). This is unsurprising given that histological specimens from macroscopic sections of MWF show collagen and fibroblasts dispersed with surviving myocytes (de Leeuw et al., 2001). Such areas are prone to slow conduction and functional electrical block; the ideal substrate to facilitate re-entrant arrhythmias (de Bakker et al., 1993). Accordingly, an observational study of patients with IDCM and primary preventative ICDs found that over a 2 year follow up, 9/31 patients with MWF required device therapy, yet no treatments were required in the 30 patients without MWF (Iles et al., 2011). The role for primary prevention ICDs in IDCM remains unclear, and the powerful predictive value of MWF warrants further study.

The location of scar in IDCM makes VT ablation more problematic. In ICM, scar extends to the subendocardium and is usually amenable to endocardial ablation. In contrast, substrate modification of a midwall re-entrant circuit may not be reliably achieved with an endocardial ablation catheter, and in many cases multiple procedures incorporating both endocardial and epicardial ablation are likely to be required (Arya et al., 2010; Soejima et al., 2004).

1.9.4 Midwall fibrosis and dyssynchrony

The solitary study on the influence of MWF on dyssynchrony uses speckle tracking derived SD of time to peak longitudinal strain and interventricular mechanical delay (Leong et al., 2012). At diagnosis, intra- and inter- ventricular dyssynchrony were similar regardless of MWF status. Following 5 months of optimal medical therapy, intra-ventricular dyssynchrony improved in those without MWF. In contrast, patients with MWF had deterioration in both intra- and inter-ventricular synchrony. The observed changes in dyssynchrony paralleled changes in LVEF, and their independence is not scrutinised. The benefit of CRT in patients with MWF requires examination.

1.10 Aetiology and response to CRT

An ischaemic aetiology is inextricably linked to myocardial scarring, and it is generally accepted that response is worse in this cohort (Brignole et al., 2013), although the evidence base is conflicting depending on the outcome metric viewed. Sub-analyses of REVERSE (Linde et al., 2010), MIRACLE (Sutton et al., 2006) and MADIT-CRT (Barsheshet et al., 2011) agree that remodelling is much less pronounced in ischaemic heart failure. This phenomenon is likely due to the lower myocardial viability and reduced substrate for remodelling.

Although these sub-analyses and similar analyses from CARE-HF (Wikstrom et al., 2009) all showed trends towards an improved magnitude of protection from adverse outcomes in NICM, this trend was not statistically significant in any study. Whilst it should be considered that these trials were not powered to detect such differences, these trials did all confirm worse outcomes in those with an ischaemic aetiology, regardless of treatment arm; this may

off-set any differences in outcome modification due to baseline aetiology, as the higher event rate in ischaemic heart failure will be in favour of a greater absolute benefit.

1.11 LV torsional mechanics

The expansion in diversity and availability of techniques to assess cardiac motion has made the assessment of LV rotation and twist accessible. Furthered understanding of normal cardiac mechanics, the deficiencies in various cardiac pathologies, and how CRT modulates these aids our understanding of the benefits and limitations of resynchronisation, and potentially offers the opportunity for a more tailored management strategy.

1.11.1 Normal cardiac architecture and torsion

Using 2D approaches such as 2DE and LV ventriculography, the LV appears to thicken uniformly leading to the common misapprehension amongst cardiologists that the LV functions homogenously with all fibres contracting and then relaxing simultaneously.

The earliest in vivo studies of cardiac torsional mechanics used cine angiography (Hansen et al., 1988) and sonomirometry (Gorman et al., 1996). The left ventricle comprises a counter-directional helical arrangement of myofibrils which smoothly transform from having a right handed orientation at the sub-endocardium, to a circumferential orientation within the mid-myocardium, through to a left handed orientation at the subepicardium. Contraction of these helices not only causes the heart to shorten in a longitudinal direction, but also to twist along its long axis. Contraction of the subepicardial myocardial fibres causes the base to rotate clockwise and the apex to rotate in a counter clockwise direction. The oppositely

aligned subendocardial fibres cause the exact reverse. To appreciate how these oppositely aligned structures exact their mechanical effects, they need to be considered within the context of the coincident electro-activation sequences:

Isovolumic contraction. Electrical activation of the LV myocardium commences at the endocardium, due to the impulse for LV depolarisation being well insulated from surrounding myocardium as it propagates from the base to the apex via the His-Purkinje system. Initial breakout is infero-septal and anterior (Cassidy et al., 1984) (**Figure 1-7**), before the electrical wavefront spreads from the apex in a basal direction. The myocardium is anisotropic, with the wavefront initially being largely confined to the endocardial layer, which is entirely depolarised within 40ms (Durrer et al., 1970), due to the relatively higher concentration of gap junctions longitudinally along the endocardial helix compared to the transmural direction (Saffitz et al., 1995).

Accordingly, there is shortening of the right handed sub-endocardial helix during this phase of the cardiac cycle. The epicardial helix, which is yet to be depolarised, is stretched (Sengupta et al., 2005). These opposing deformations, which have shown by tissue Doppler to be of equal magnitude (Sengupta et al., 2005), counter-balance one another with no net change in cavity dimension. Contraction of the sub-endocardium without a change in volume leads to a rapid rise in LV pressure. Furthermore, the shortening subendocardial helix rotates the apex in a clockwise fashion and the base anti-clockwise. Descriptions of the direction of this twist vary depending on the technique used. Measurements using cine-angiographic markers (Ingels et al., 1989), sonomicrometry (Helle-Valle et al., 2005) or speckle tracking

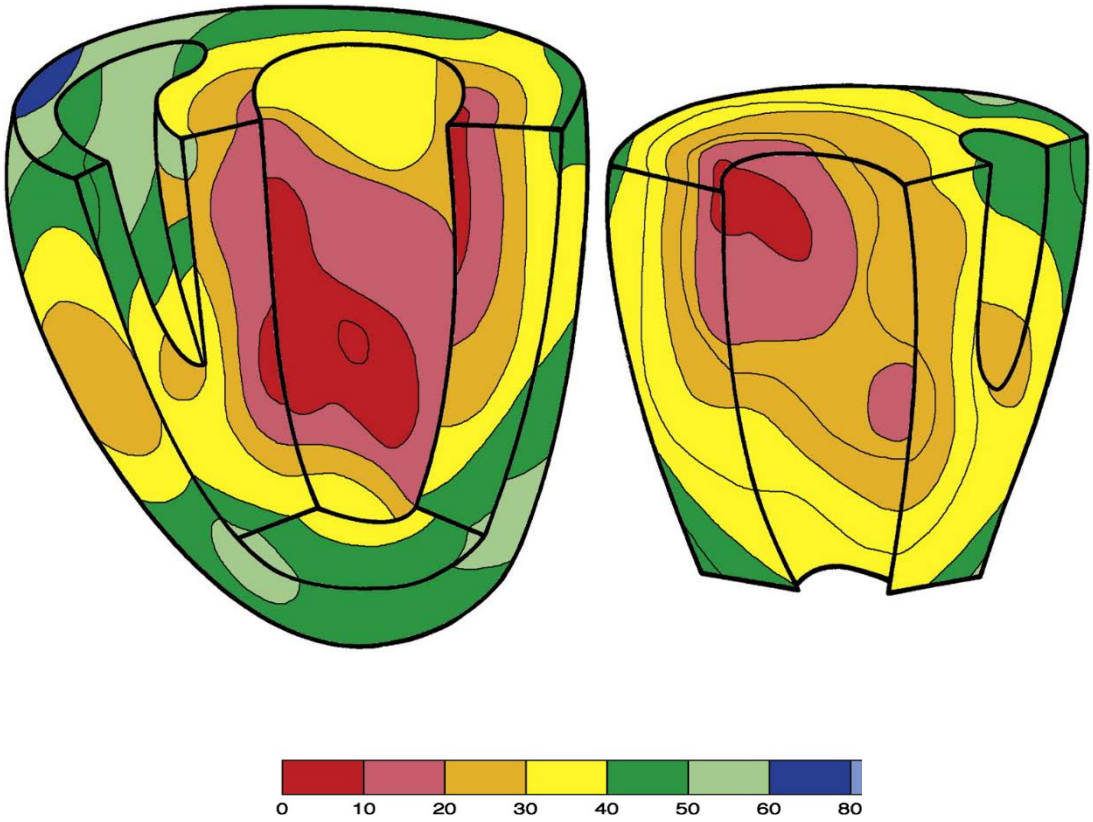

Figure 1-7. Wavefront the electrical activation sequence of the normal heart.

The activation sequence of a normal left ventricle is demonstrated with time colour coding. The anterior wall of the LV has been cut away on the right, but is viewed en face on the left. Activation can be seen to spread in an endocardial to epicardial direction.

(Sengupta et al., 2013)

(Helle-Valle et al., 2005) all concur with the description above, but MRI studies using tagging (Lorenz et al., 2000) and tissue phase mapping (Jung et al., 2006) report a counter-clockwise rotation of both the apex and the base; this incongruity is likely to relate to the lower temporal resolution of MRI.

Ejection phase. Initiation of ventricular ejection correlates with the electrical wavefront reaching the sub-epicardium. Epicardial breakthrough is heterogenous between individuals, but typically occurs either antero-septally, posteriorly or simultaneously at these sites (Ramanathan et al., 2006). Subsequent epicardial activation occurs in a predominantly apico-basal direction, due to a combination of transmural spread of the wavefront and spread of the wavefront directly through the epicardial layer. With contraction of the sub-epicardial helix, the left ventricular cavity shortens along its long axis. As both helices shorten from apex to base, blood is emptied out of the ventricle via the outflow tract. The greater torque of the sub-epicardial helix causes the twisting motion seen during isovolumic contraction to be reversed, with clockwise rotation of the base and anticlockwise rotation at the apex. These counter-directional rotations lead to the LV twisting around its long axis and further enhance the mechanical efficiency of the heart. The motion is analogous to the wringing of a wet towel. As the magnitude of apical rotation is greater than that of basal rotation, it is the former that has the greater influence on total myocardial twist (Gibbons Kroeker et al., 1993).

Diastole. Isovolumic relaxation is a misnomer for the early stage of diastole, as active regional post-systolic shortening continues after aortic valve closure in the subepicardial

layers apically and in the subendocardial layers basally (Sengupta et al., 2006; Voigt et al., 2003). This creates gradients in both a transmural and apico-basal direction, which is thought to provide an active mechanism for restoring LV structure and facilitates rapid expansion of the LV cavity at the apex. The twisted, sheared and thickened myocardium stores potential energy. Rapid recoil during isovolumic relaxation leads to a rapid fall in intra-ventricular pressure. By the time the mitral valve opens, untwisting of the LV has predominantly finished and the above processes have created a pressure gradient from the atrium to the ventricle that drives diastolic suction and rapid filling.

1.11.2 Torsional mechanics and myocardial dysfunction

Whilst one might predict that LV systolic dysfunction results in reduced torsion, this is not singularly true as it is the disturbance of the equipoise between the oppositely aligned myofibrils that modulates the net effect on torsional dynamics. In the initial stages of a myocardial infarction, ischaemia is limited to the sub-endocardium, and increased dominance of the sub-epicardial helix results in hyper-rotation (Kroeker et al., 1995). Similarly, microvascular insufficiency of the subendocardial fibres is seen in hypertension (Yoneyama et al., 2012), hypertrophic cardiomyopathy (HCM) (van Dalen et al., 2009; Young et al., 1994), and as part of physiological ageing (Lumens et al., 2006). In these circumstances augmented twist provides a compensatory mechanism.

Cardiac remodelling leads to changes in fibre orientation and biomechanical models have shown that increasing the angulation between the epicardial and endocardial fibres from the normal +60◦/-60◦ orientation to +90◦/-90◦ leads to a 50% reduction in peak twist (Taber

et al., 1996). This has been confirmed in vivo and **Figure 1-8** shows that in patients with IDCM, a decreasing sphericity index (a more spherical LV) is associated with a linear reduction in LV twist (van Dalen et al., 2010).

In a proportion of patients with heart failure the direction of LV rotation is reversed. Commonly only one extremity of the ventricle is affected, a particularly detrimental scenario as the direction of turn becomes the same at both the base and apex with an absence of net LV twist (Kanzaki et al., 2006; Setser et al., 2003). This torsional pattern is commonly termed 'rigid body rotation' and predictably it is associated with more advanced disease (Popescu et al., 2009).

1.11.3 Torsional mechanics and CRT

The hypothesis that the correction of torsional dysfunction is one mechanism by which CRT mediates its benefits warrants investigation. There are conflicting results as to whether reduced net twist at baseline identifies a population who may derive a greater benefit from CRT. In 33 patients Sade et al., report that responders had lower baseline twist than non-responders (1.5 ^{o} vs. 5.3 ^{o}, $p< 0.01$) and that net twist improved on average by 4.8^{o} in responders ($P< 0.0001$) yet remained unchanged in non-responders (Sade et al., 2008). In contrast, a study of 40 patients showed no net difference in net twist at baseline between responders and non-responders. However, the finding that responders demonstrated a 4.2^{o} improvement in twist at 6 months ($p <0.001$), whilst a reduction was seen in non-responders at 6 months, was in accord with the aforementioned study (-2.1^{o}; $P< 0.001$) (Bertini et al., 2009).

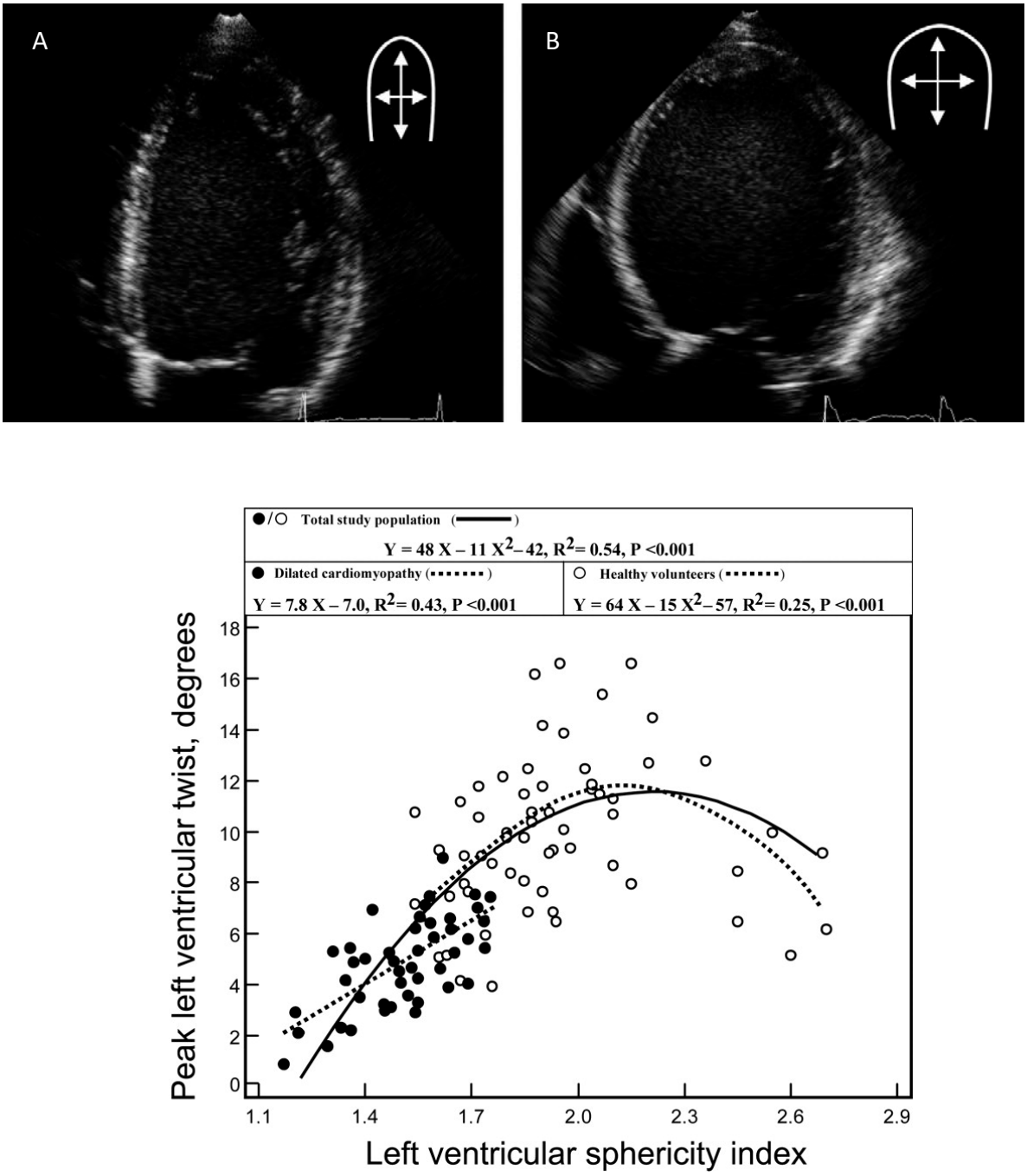

Figure 1-8. Influence of cardiac shape on left ventricular twist

Left ventricular sphericity index (maximal left ventricular long-axis internal dimension divided by the maximal short-axis internal dimension at end-diastole) in (A) a healthy volunteer (sphericity index 1.9) and (B) an IDCM patient (sphericity index 1.4). (C) Healthy controls (open symbols) demonstrate a parabolic relationship beween LV sphericity and peak twist, but a linear reduction in peak twist is seen as LV sphericity index decreases in IDCM patients (closed symbols).

Adapted from (van Dalen et al., 2010)

Potentially, differing lead positions can be used to manipulate torsional mechanics by utilising different electro-mechanical activation sequences. The above small studies found that apical and posterolateral LV pacing was associated with the maximal improvements in twist. Physiological activation stems from the apex, and pacing here should create a depolarisation wavefront that most closely mirrors physiological activation. The thinner apical myocardium also offers closer access to the Purkinje network. Orthodoxly, implanters avoid positioning the LV lead over apical segments, as in all-comers this results in detrimental outcomes (Singh et al., 2011). An apical lead position usually signifies less separation from the RV pacing electrodes and involves pacing a region that has less delayed electro-mechanical activation in typical LBBB (Auricchio et al., 2004). However, patients with ICM are likely to have had a left anterior descending territory infarct and resultant apical scarring. The benefits of avoiding apical placement are less clear in IDCM as the reported enhancement of torsional mechanics may promote response.

1.12 LV pacing site and CRT

Baseline dyssynchrony and low scar burden increase the probability of a response to CRT, but conventionally LV lead positioning is performed 'blind' of these parameters. Via this approach to implantation one might hypothesise that these parameters only improve the probability of an ideal LV lead position being achieved by chance, and specifically targeting a preferential site for lead position might further improve this likelihood.

Elegant support for the impact of individually tailored LV lead position comes from 11 patients who underwent surgical epicardial LV lead placement so that the pacing site was

not restricted by venous anatomy (Dekker et al., 2004). Intra-patient invasive pressure volume loops demonstrated that pacing from different sites engendered very different haemodynamic effects, with some pacing sites even having deleterious effects. Furthermore, there was marked inter-patient heterogeneity with respect to the optimal pacing site, and in 4 patients (in difference to common strategy) apical pacing proved most acutely beneficial.

1.12.1 Site of latest electro-mechanical activation

The basis of CRT is to correct the non-physiological spread of electrical excitation that results in uncoordinated contraction and inefficient cardiac performance (Baller et al., 1988). Early haemodynamic studies found the maximal benefit of LV pacing was derived from pacing at either a lateral or postero-lateral site (Cazeau et al., 1994; Leclercq et al., 1998a). However, in patients with LBBB this is usually the site of latest activation and thus provides maximal correction of dyssynchrony.

The earliest study to demonstate that LV pacing at the site of latest mechanical activation (LMA) could enhance response observed 31 conventional CRT recipients, who had pre-implant assessment of LMA using TDI (Ansalone et al., 2002). CRT improved cardiac performance in the entire cohort, but there were greater improvements in LV volumes (p= 0.04), LVEF (p= 0.04) and ergonometer stress test performance (p= 0.03) in the 13 patients with LV pacing at the site of LMA. All patients had IDCM so there were no confounding effects due to myocardial scarring. These results are re-producible using alternative echocardiographic modalities, including STE (Becker et al., 2007b), 3DE (Becker et al., 2007a) and tissue synchronisation imaging (Murphy et al., 2006) to characterise LMA.

When a larger observational study of 244 patients studied outcomes from CRT in the context of concordance between the site of STE derived LMA and LV lead position, concordance was an independent predictor of hospitalisation free survival over a 32 month follow-up (HR: 0.22, p= 0.004) (Ypenburg et al., 2008). In line with common practice, implanters had preferentially targeted a posterolateral site and in 64% of cases this blind approach led to a concordant lead position. Thus, worse outcomes were seen in patients with alternative sites of LMA.

1.12.2 Relationship between scar and paced segment

Early haemodynamic studies found the maximal benefit of LV pacing was derived from pacing at either a lateral or postero-lateral site (Cazeau et al., 1994; Leclercq et al., 1998a). In patients with LBBB this is usually the site of latest activation and thus provides maximal correction of dyssynchrony. Accordingly, the conventional approach to implantation is to attempt to position the LV lead in a tributary of the coronary sinus that overlies this territory. However, this is disadvantageous if this is scarred. Pacing over scar leads to delayed propagation of the electrical impulse and increased QRS fragmentation (Schwartzman et al., 1999). The greater the transmural depth and area of scar, the longer it will take for the electrical impulse to propagate around the electrical barrier, attenuating any correction of dyssynchrony. Furthermore, scar acts as a substrate for re-entrant rhythms, and pacing over scar can induce monomorphic ventricular tachycardia (VT) (Roque et al., 2014).

In a LGE-CMR study, where response was defined as 1 year survival free from heart failure hospitalisation coupled with a symptomatic improvement, a 33% response rate was observed in 15 patients paced over posterolateral scar vs. 86% in the 14 patients with a similar scar burden but paced at an adjacent site (p= 0.004) (Chalil et al., 2007a). Similarly, a SPECT imaging study found only 20% (3/15) of patients with scar in the region of the LV pacing lead met the response criteria (Ypenburg et al., 2007). Pacing over scar also negatively impacts cardiovascular mortality rate (62% Vs 24%, P= 0.049), and the composite of cardiovascular death or hospitalisation (81% Vs 24%, p=0.0009) (Chalil et al., 2007c).

Approaches to negate the unfavourable effects of pacing over scar have been explored. A study of 57 patients (of whom 16 had posterolateral scar) determined if this could be achieved by ensuring optimal atrioventricular and intraventricular pacing intervals using invasive dp/dt measurement. In multivariate analysis only pre-implant LV dyssynchrony, and not the presence of PL scar (odds ratio [OR] 2.07, p=0.48), independently predicted a LVRR response. The authors concluded that by optimising pacing delays, some of the pacing stimulus could still be propagated to recruit myocardium and still reduce dyssynchrony. Nonetheless, LVRR at 3 months was only seen in 25% of patients with posterolateral scar vs. 89% without (p= 0.001) (Jansen et al., 2008).

1.12.3 Targeted LV lead position

In the context of this support for an individually tailored approach to CRT implantation two randomised control trials have tested whether response can be improved by implanting the LV lead at the site of LMA and over viable myocardium. The STARTER (Speckle Tracking

Assisted Resynchronization Therapy for Electrode Region) sastudies both compared an echocardiography guided LV lead placement against conventional implantation. Both studies used STE radial strain to identify the segments with LMA. In TARGET a prospective evaluation of a surrogate of scar, defined < 10% radial strain, was undertaken. STARTER was implicit in its avoidance of scar within the echocardiography guided arm. Whilst myocardial scar was not formally assessed, segments with low amplitude radial strain were handled as missing data, and therefore not offered to the implanter as a target for LV lead deployment. It follows that, by virtue of study design, segments which may have contained scar were most likely avoided by implanters.

In TARGET both a LVRR response (70 vs. 55%, p= 0.031) and a clinical response (83% vs. 65%, p = 0.003) were seen more frequently in echocardiography guided implantation. Both studies reported longer event free survival with echocardiography guided implants (STARTER: HR 0.48, p=0.006; TARGET: log-rank test, p = 0.031).

1.12.4 Multisite pacing

It must be considered that any added benefit of image guided implantation was restricted to the 17-18% of the participants in STARTER and TARGET in whom an echocardiography guided approach resulted in a more desirable lead position. LV lead placement can be challenging and is constrained by the target branches available, stability, local myocardial excitability and phrenic nerve stimulation. In the imaging guided arm of STARTER only 30% of patients had the LV lead positioned overlying the ‘sweet spot’.

Advances in LV lead technology, and in particular quadripolar leads, are refining our ability to pace over a specific location. Early generation LV leads comprised 1 or 2 electrodes located at the distal tip which had to be wedged into a branch vessel. Having multiple electrodes at more proximal sites means quadripolar leads offer a range of pacing options. This also enhances the capability of an electro-anatomical approach to delivering CRT, as QLV can be measured from multiple electrodes and therapy delivered from a confirmed late activated site.

An early case report demonstrated a quadripolar lead's ability to circumnavigate scar, when the distal portion of a sole tributary of the coronary sinus was overlying scarred myocardium. A bipolar LV lead demonstrated unacceptable pacing thresholds, and stimulation produced a fragmented electrogram (Abozguia et al., 2011). A quadripolar lead was used so that the distal lead aided stability, whilst the proximal poles, straddling non-scarred myocardium, provided an advantageous pacing site (**Figure 1-9**).

Multi-polar leads also offer the possibility of stimulating the LV from several poles simultaneously. Delivering two pacing pulses concurrently may increase the amount of myocardium recruited and early studies suggest this evokes a superior acute haemodynamic (Pappone et al., 2014b) and LVRR response (Pappone et al., 2015). Beneficially the greater possibilities for electro-manipulation of the pacing vector may render the actual position of the lead less important than with the conventional delivery of CRT, and there is as yet unpublished preliminary data to support this (Pappone et al., 2014a).

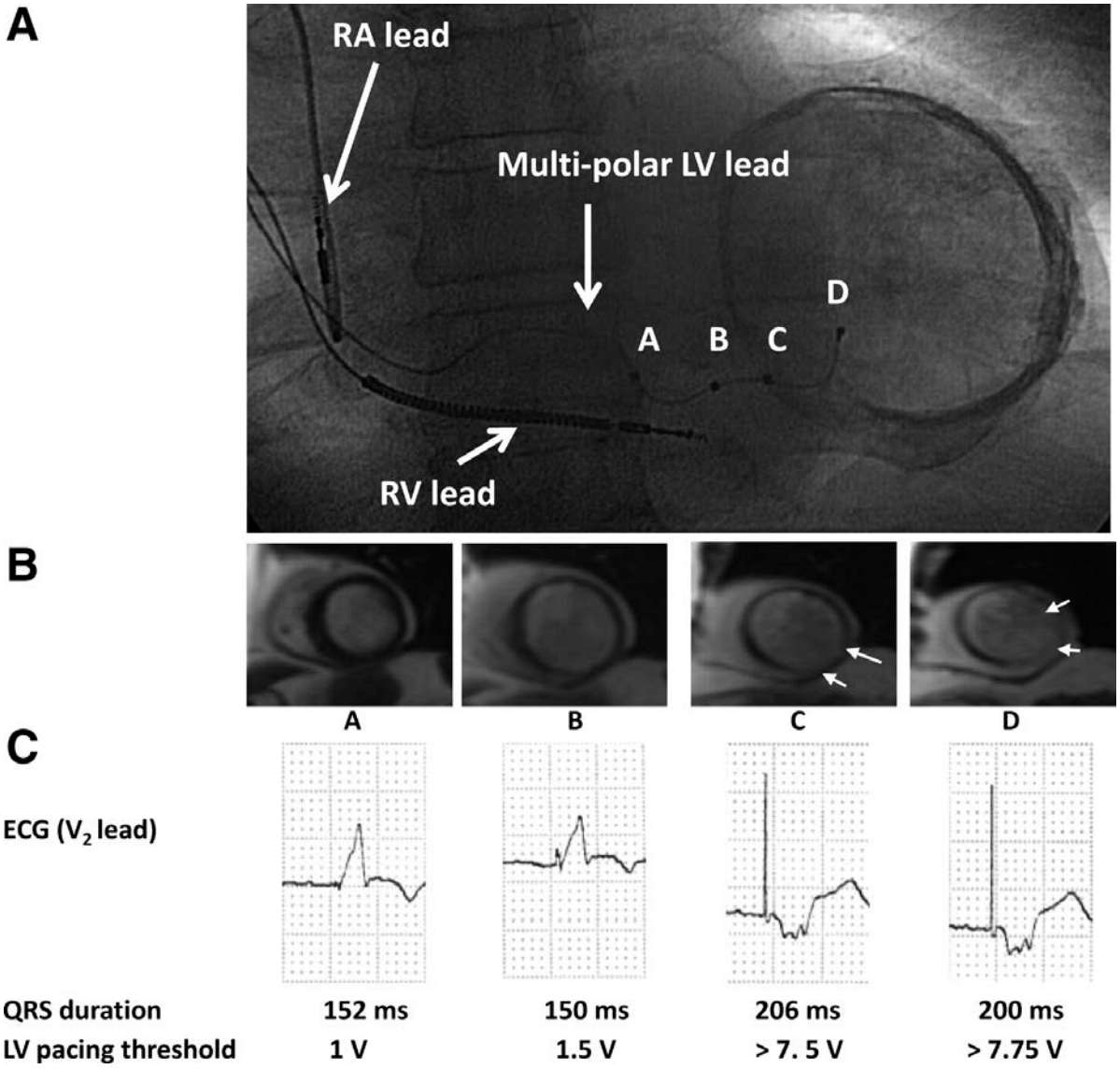

Figure 1-9. Targeting viable myocardium in cardiac resynchronisation therapy using a multipolar left ventricular lead.

A, A 30° right anterior oblique fluoroscopic view of the multipolar LV lead straddling the calcified LV aneurysm. B, The distal poles of the lead subtend scarred myocardium (white, arrows). C, Pacing over poles C and D was associated with a longer QRS duration, a higher pacing threshold, and a markedly different QRS morphology, compared with pacing from poles A and B. The exact positions of the poles were derived by superimposing the fluoroscopic views on the CMR views. CMR indicates cardiovascular magnetic resonance; RA, right atrial; RV, right ventricular; LV, left ventricular.

(Abozguia et al., 2011)

Logically, a targeted approach to CRT delivery would be more feasible if the constraints of individual coronary venous anatomy were overcome. Direct surgical placement of the LV lead via limited thoracotomy provides a greater selection of pacing sites, but in a direct comparison to transvenous CRT, reduced functional improvement and higher mortality rates were reported at one year (Koos et al., 2004). However, this study did not employ a targeted approach to lead positioning and it was probable that surgeons favoured technically easier anterior lead positions which have a lower probability of overlying late activated sites. At present there is no direct comparison as to the potential benefit of surgical LV lead placement guided by electro or mechanical anatomical guidance, but the invasive nature of this technique, coupled with longer hospital stays and recovery time make it an unappealing channel for extensive investigation.

Another method for LV lead placement unrestricted by venous anatomy is endocardially via a transeptal transmitral route. Direct stimulation of the more rapidly depolarised endocardium offers a more physiological solution. The ALSYNC (Alternate Site Cardiac Resynchronization) study showed that outcomes were similar to conventional CRT (Morgan et al., 2016), and one would expect further improvement if this was combined with targeted LV lead placement. However, safety remains a concern and over 10% of the ALSYNC cohort had a cerebrovascular event despite mandated anti-coagulation. A novel alternative for providing endocardial LV pacing is using leadless ultrasound based technology, which should overcome these safety issues, but is currently at a developmental stage (Auricchio et al., 2014).

1.13 Feature-tracking CMR and study hypotheses

1.13.1 Feature tracking CMR

Feature-tracking CMR (FT-CMR) is a novel technique that allows quantification of motion and strain using a standard steady state in free precession (SSFP) sequence, which forms part of a routine LV study protocol.

FT-CMR involves the operator manually defining a border which is then automatically propagated (tracked) through the cardiac cycle by matching individual patterns (features) that represent anatomical structures. These features consist of a group of pixels or a voxel, and are found by the method of maximum likelihood between the regions of interest of consecutive frames by looking for the closest grayscale match (Hor et al., 2011). Accordingly, as with speckle tracking echocardiography, it works on the principle of optical flow. The distance moved by individual points within the two-dimensional matrix between frames facilitates the computation of displacement and strain. Their first order derivatives, velocity and strain rate are calculated from the time interval between frames (Bohs et al., 2000).

The high signal to noise ratio and sharp contrast between the blood pool and myocardium with SSFP cines lend themselves favourably to measuring deformation at the endocardial border. The degree of definition is typically less at the epicardial border and is variable depending on the signal from neigbouring structures. The comparatively homogenous myocardium is poorly tracked. Thus, unlike myocardial tagging which provides a pan-myocardial assessment of deformation, FT-CMR is relatively crude, as it is limited to the assessment of myocardial edges.

Despite its rudimentary nature it offers attractive potential. Theoretically it is substantially less time consuming with no special acquisition sequences, and this aspect also enables retrospective cohorts to undergo assessment of cardiac mechanics.

1.13.2 Study aims

The underlying goals of the studies detailed herein are to:

(1) Confirm the feasibility, reproducibility and accuracy of FT-CMR to assess cardiac strain in multiple dimensions.

(2) Define normal values for myocardial strain with this novel software.

(3) Advance our appreciation of the mechanical effects of myocardial scarring.

(4) Validate FT-CMR as a methodology to calculate novel dyssynchrony parameters and test whether these could enhance patient selection for CRT.

(5) Test whether FT-CMR derived myocardial strain can provide incremental benefit over current functional measures at predicting long term outcomes following CRT.

(6) Validate the concept that using this software to guide LV lead placement could improve response to CRT.

2 VALIDATION OF CARDIOVASCULAR MAGNETIC RESONANCE FEATURE TRACKING MEASURES OF MYOCARDIAL STRAIN AGAINST MYOCARDIAL TAGGING

Principal hypothesis: FT-CMR has acceptable agreement with SPAMM myocardial tagging for the calculation of short and long axis systolic and diastolic strain parameters over a broad spectrum of LV function.

2.1 Introduction

Cardiac strain is a sensitive measure of myofibre deformation and provides a measure of the contractile and relaxation properties of the myocardium. Abnormalities of strain precede declines in more conventional markers of LV function, facilitating the recognition of cardiomyopathies at a pre-clinical stage (Hankiewicz et al., 2008). Strain measurement can enhance the diagnostic utility of ischaemia (Edvardsen et al., 2000) and viability testing (Lyseggen et al., 2005) and it aids risk stratification guiding the timing of therapies or intervention (Yingchoncharoen et al., 2012). The utility of deformation imaging extends beyond the detection of incipient disease and, due to its temporal component, it is of particular interest in the field of cardiac resynchronisation. The dispersion of regional strains underpins dyssynchrony analyses, and regions with late peak strains have been shown to be preferential targets for LV pacing enhancing the delivery of CRT (Khan et al., 2012a).

Myocardial tagging was the first non-invasive measure of myocardial strain, and due to the high signal to noise ratio and spatial resolution of CMR, it is the accepted reference standard by which other techniques are evaluated (Amundsen et al., 2006). Specifically designed

acquisition sequences manipulate the properties of the imaged region so that a grid of magnetically saturated tissue segregates the remaining myocardium into tags (Axel et al., 1989). Theses render myocardial motion more visible and dedicated processing software allows in depth quantitative analysis of myocardial deformation. The evolution of this methodology has seen over 20 different pulse sequences devised for the creation of tagged cines such as spatial modulation of magnetization (SPAMM) or harmonic phase (HARP). Successive techniques have refined shortcomings of forerunners with incremental improvements in tag definition, density, persistence (Ibrahim, 2011). To date, however, myocardial tagging acquisition and its requisite post-processing analysis are largely confined to the research environment, not least because they are laborious and time-consuming.

Feature-tracking CMR (FT-CMR) is a novel technique that allows quantification of motion and strain using SSFP sequences, which forms part of a routine LV study protocol. This technique has shown promising agreement with HARP tagging for the calculation of circumferential strain within the mid LV cavity in a paediatric population (Hor et al., 2010). However, one study reports FT-CMR as inadequate for measuring long axis strain (Augustine et al., 2013) and there has been no attempt to validate its use, against a reference standard, for the measurement of diastolic parameters (Harrild et al., 2012). This study compares the accuracy of FT-CMR for assessing both short and long axis systolic and diastolic strain, using SPAMM myocardial tagging as a reference, in a mixed cohort of healthy volunteers and patients with IDCM.

2.2 Methods

This study was approved by the West Midlands Research Ethics Committee and carried out in accordance with the principles of the Declaration of Helsinki. All patients provided informed written consent.

2.2.1 Study population

Healthy controls. Healthy control subjects were identified from a prospective controlled observational research study examining the effects of living kidney donation on cardiovascular structure and function (NCT01769924)(Moody et al., 2014). Accordingly, all participants met the United Kingdom criteria for living kidney donation and were screened to exclude a previous history of cardiovascular disease, pulmonary disease, hypertension and AF. Both controls and prospective kidney donors from NCT01769924 were used as controls in this study, and baseline CMR studies were used.

IDCM subjects. Patients with IDCM were those enrolled from a prospective investigation into the mechanical effects of midwall fibrosis on cardiac mechanics (REC: 12/WM/0157); IDCM was diagnosed on the basis of clinical features plus echocardiographic evidence of LV systolic impairment in the absence of: severe structural valvular heart disease; hypertrophic or restrictive cardiomyopathy; coronary artery disease on invasive coronary angiography thought to be sufficient to account for the reduced left ventricular systolic function; transmural or subendocardial LGE pattern consistent with a coronary territory.

2.2.2 CMR acquisition

This was performed with a 1.5 Tesla scanner (Magnetom Avanto, Siemens, Erlangen, Germany), using a phased-array cardiac coil.

SSFP. A horizontal long-axis cine imaging plane was mapped from the VLA cine and the short axis scouts, ensuring maximum lateral dimensions of both ventricles were encompassed and avoidance of the LV outflow tract. The short axis stack was piloted from the end-diastolic frames of the HLA and VLA cines; contiguous cines were acquired from the atrioventricular ring to the LV apex (retrospective electrocardiographic gating, repetition time of 3.2 ms; echo time of 1.7 ms; flip angle of 60^{o}; sequential 7 mm slices with a 3 mm interslice gap). There were 25 phases per cardiac cycle resulting in a mean temporal resolution of 40 ms.

Myocardial tagging. Short axis cines at the LV basal, mid cavity and apical level and a HLA cine were acquired with slice positioning from the SSFP data set. SPAMM radiofrequency pulses gated to the R wave produced a grid of magnetisation saturation with tag separation of 8mm using a segmented k-space fast field echo multishot sequence (repetition time 3.9 ms, echo time 1.7 ms, voxel size 1.99/2.04/8.00 mm^3, flip angle 5°, tag grid angle 45° with slice thickness 6 mm, minimum 15 phases per cardiac cycle) (Edwards et al., 2010). For IDCM patients, tagging was performed prior to administration of Gadolinium to maximise T1 relaxation time so as to improved tag persistence.

2.2.3 Myocardial strain and strain rate analysis

A timed off-line analysis was performed on SPAMM and SSFP cines at identical slice positions by two independent blinded observers (R.J.T. and W.M.: 3 and 4 years experience

respectively). Two independent CMR experts (12 and 15 years experience) verified the quality of all cine acquisitions and any deemed of sub-standard quality were excluded from deformation analysis.

CIMTag dynamic tissue-tagging. Tagged acquisitions were analysed with the CIMTag dynamic tissue-tagging (CIMTag2D) analysis package (Cardiac Image Modelling, University of Auckland, Auckland, NZ).

Figure 2-1 provides an overview of the CIMTag analysis platform. LV geometry is rendered in the end-diastolic frame from placing manual guidepoints along the endocardial and epicardial contours, following which a mesh grid is automatically aligned to the stripes of desaturated tissue using linear least squares optimisation with subsequent user fine-tuning. This grid is converted into a visual tissue displacement map which is then automatically distorted through sequential frames to model deformation. The end-systolic displacement map is manually adjusted by the user to provide the optimum overlay of the inherent grid pattern.

FT-CMR. FT-CMR was undertaken using the Diogenes FT-CMR software (TomTec Imaging Systems, Munich, Germany). The four tracked SSFP cines had a matched slice position to the tagged sequences. Endocardial borders were manually drawn in the end-diastolic frame. The papillary muscle was excluded from the endocardial contour. These were then automatically propagated (tracked) through the cardiac cycle by matching individual patterns that represent anatomical structures. These structures are found by the method of

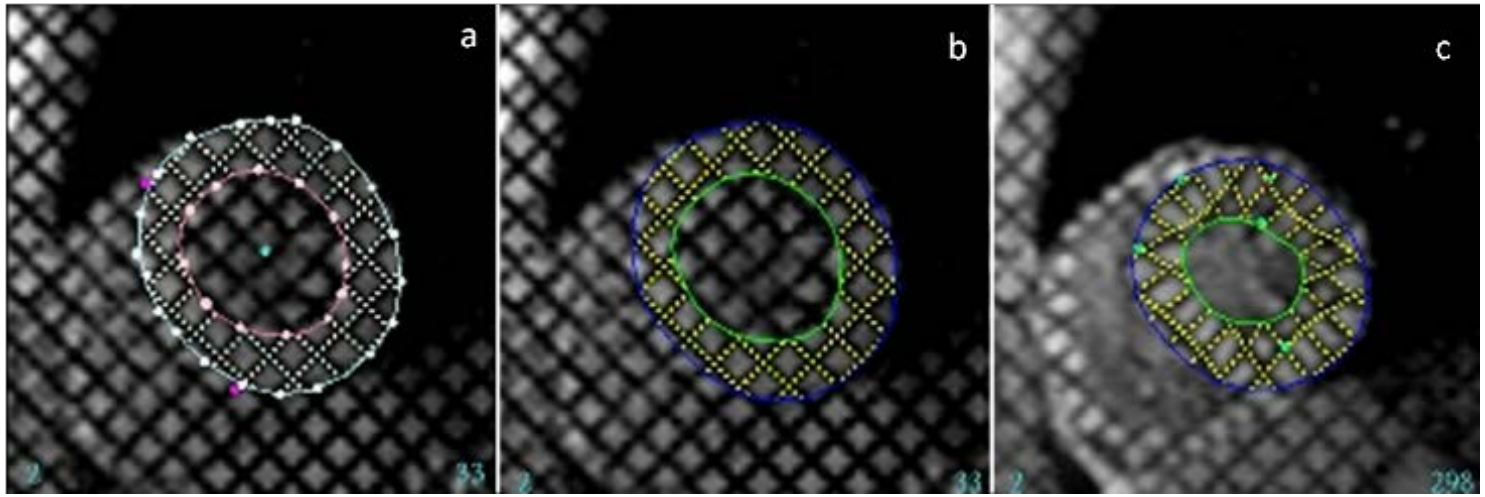

Figure 2-1. Overview of the CIMTag2D analysis platform.

a) Guide points placed by the user on the endocardial and epicardial border of the LV in the first frame (end-diastole) were fitted by the model using linear least squares optimization, resulting in an initial segmentation of the LV with minimal user interaction and subsequent initialization of the finite element model in the first frame of the SPAMM sequence.

b) Visual depiction of the tissue displacement map provided by non-rigid registration image tracking process at end-diastole.

c) User corrected texture map overlay as seen after placing guide points in end-systole, thereby interactively warping the model to provide a best fit between image tags and model stripes.

(Moody et al., 2015)

maximum likelihood between the regions of interest of consecutive frames (Hor et al., 2011). The distance moved by individual points within the two-dimensional matrix between frames facilitates the computation of displacement and strain. Their first order derivatives, velocity and strain rate, are calculated by the process of optical flow, i.e. the ratio between distance and the time interval between frames (Bohs et al., 2000). For each tracked cine, six segmental time-strain plot were constructed, from which a global mean time-strain plot was produced. To minimise variability, user adjustments after the first attempt at tracking were kept to a minimum. However, as with any deformation technique, inaccuracies can arise because the boundary between the trabecular and compact portions of the wall may shift as the blood spaces between the trabeculae close during systole, resulting in an artefactual apparent inward motion of the endocardial contour. If this was deemed to be a significant problem the cine was re-tracked with manual contouring using an end-systolic frame.

For both **CIMTag2D** and **FT-CMR** all strain data was exported into Microsoft Excel and global peak systolic longitudinal strain (ε_{ll}), systolic (SSR_{ll}) and diastolic (DSR_{ll}) longitudinal strain rates were derived from the HLA sequence. Global peak systolic circumferential strain (ε_{cc}) and systolic (SSR_{cc}) and diastolic (DSR_{cc}) circumferential strain rates were derived from each of the short axis acquisitions. Peak DSR was derived during the early rapid filling stage of diastole (**Figure 2-2**). Using CIMTag2D strains were calculated both transmurally, and after subdivision of the myocardium into three equal components (subendocardial, midwall and subepicardial). In contrast, only endocardial equivalents were derived with FT-CMR.

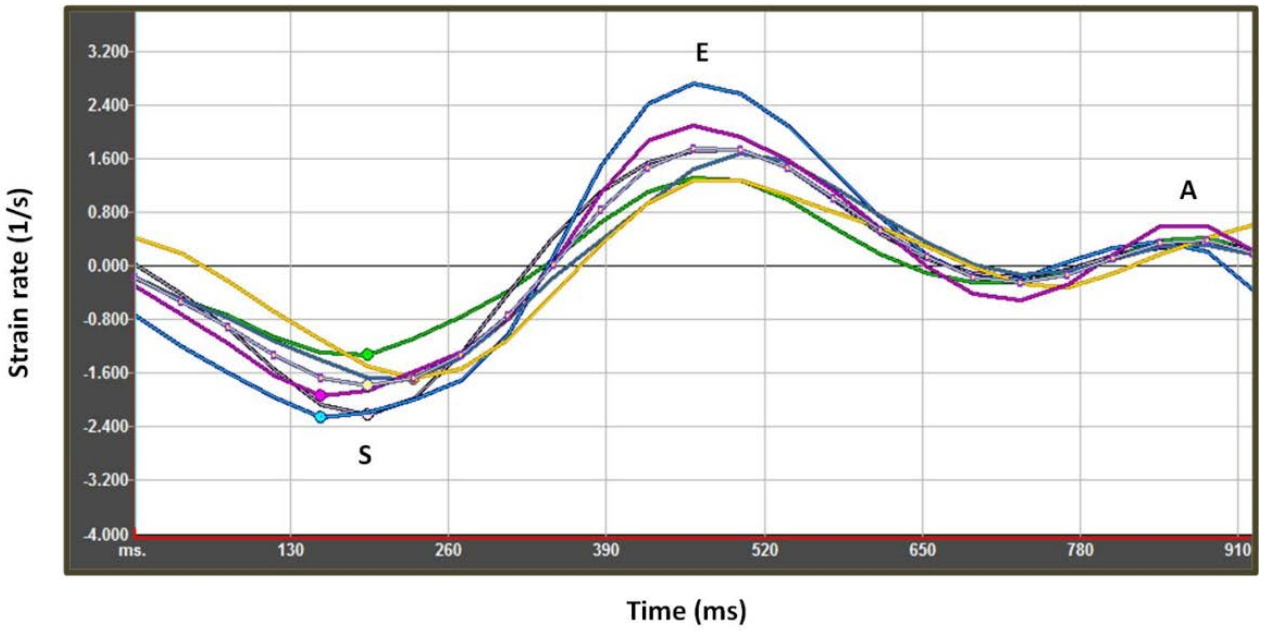

Figure 2-2. Representative circumferential strain rate profile from cardiac magnetic resonance-feature tracking at the mid left ventricular level of a healthy control.

This example demonstrates a typical strain rate pattern with S (systolic), E (early diastolic) and A (late diastolic) waves. The dotted white line represents the global subendocardial circumferential strain rate.

(Moody et al., 2015)

2.2.4 Left ventricular function, volumes and mass

LV mass, LV end-diastolic (LVEDV) and end-systolic (LVESV) ventricular volumes were quantified using manual planimetry of the endocardial and epicardial borders from the short axis stack in accordance with validated methodologies (Maceira et al., 2006) using Argus software (Siemens, Erlangen, Germany). These were indexed to body surface area using the Mosteller formula (Mosteller, 1987).

2.2.5 Statistical analysis

Categorical variables are expressed as a frequency and percentage and continuous variables are presented as either mean $\pm$ SD or median and interquartile range depending on distribution. Normality was assessed using the Kolmogorov-Smirnov test and normality probability plots. Non-parametric data were log-transformed prior to analysis to achieve normality. For continuous variables independent sample t-tests were used for comparisons between healthy controls and IDCM patients. Agreement between techniques was tested using Pearson's correlation coefficient and by calculating mean bias and 95% limits of agreement (confidence intervals) from Bland-Altman analyses. Spearman's rank correlation of the differences with the means for strain parameters calculated by both methods was performed. Paired t-tests were used to compare the mean strain parameters as calculated by the different methods. Comparisons of myocardial tagging derived strain parameters within the different component layers of the myocardial wall were made with repeated measures analysis of variance (ANOVA) with a Greenhouse-Geisser correction. Based on the prior validation of FT-CMR against HARP tagging (Hor et al., 2010), there was no expected mean bias between methodologies, and an expected SD of differences of 2. Accordingly, 15

patients would be required to demonstrate a maximum difference between methods of less than 7.5% (β= 0.2) (Lu et al., 2016). At the time of study design, there was no published data to guide sample size requirements for validating strains in other directions. A p value of < 0.05 was considered statistically significant**.** Statistical analysis was performed using SPSS v21.0. (SPSS Inc. Chicago, Illinois).

2.3 Results

2.3.1 Baseline characteristics

As shown in **Table 2-1** the study included 45 subjects (35 healthy controls, 10 IDCM). Compared to IDCM patients, controls were younger (41 ± 12 yrs [mean ± SD] vs. 58 ± 14 yrs, p< 0.01) and had lower weight (77 ± 11 kg vs. 87 ± 17 kg, p< 0.01). Otherwise, demographics were similar between the two groups. There was a preponderance of male and caucasian participants which was similar across controls and IDCM patients (total cohort: 63% and 88% respectively).

As anticipated, patients with IDCM had larger LV dimensions (LVEDV: 205 ± 51ml vs. 124 ± 25ml; LVESV: 140 ± 60ml vs. 37 ± 15ml, p< 0.01 for both) and lower LVEF (71 ± 6% vs. 33 ± 15%, p< 0.01) and stroke volume (64 ± 21ml vs. 87 ± 14ml, p< 0.01) than healthy controls. LVEF ranged from 19-79% across the entire study cohort.

All SSFP cines were of satisfactory quality for analysis using FT-CMR. In 2 subjects, both healthy controls, SPAMM acquisitions were unsuitable for tagging analysis (due to breathing

Table 2-1. Baseline characteristics of the study population.

Baseline characteristics	Controls (n= 35)	IDCM (n= 10)	Overall (n=45)
Age (years)	41 ± 12	58 ± 14*	44 ± 14
Male gender (%)	26 (62)	6 (60)	32 (63)
Ethnicity			
Caucasian (%)	36 (90)	8 (80)	45 (88)
Asian (%)	3 (8)	1 (10)	4 (8)
Afro-Caribbean (%)	1 (2)	1 (10)	2 (4)
Weight (kg)	77 ± 11	87 ± 17*	79 ± 13
Heart rate (bpm)	66 ± 10	70 ± 10	67 ± 10
Systolic blood pressure (mmHg)	120 ± 11	112 ± 14**	119 ± 12
Diastolic blood pressure (mmHg)	72 ± 6	72 ± 11	72 ± 7
Left ventricular ejection fraction (%)	71 ± 6	33 ± 15†	69 (64 – 74)
End-diastolic volume (mL)	124 ± 25	205 ± 51†	137 ± 43
End-systolic volume (mL)	37 ± 13	140 ± 60†	39 (30 – 59)
Stroke volume (mL)	87 ± 14	64 ± 21†	84 ± 17
Left ventricular mass (g)	122 ± 27	161 ± 21	123 (106 – 141)
Left ventricular mass index (g/m2)	64 ± 11	82 ± 20	64 (59 – 73)
Late gadolinium enhancement result	-	All negative	-

Data are mean ± standard deviation, frequency (percentage) or median (interquartile range).

IDCM, Idiopathic dilated cardiomyopathy

***p<0.01; **p<0.05; †p<0.001 (compared with controls using an independent two-tailed Student's t test).**

[n=1] and ECG gating [n=1] artefact) and they are excluded from comparisons of strain measures.

2.3.2 Comparison of myocardial tagging vs. FT-CMR for global systolic strains

Table 2-2 provides an extensive comparison of all FT-CMR and myocardial tagging derived deformation parameters. For tagging analyses, all deformation parameters were significantly different between the sub-layers of the myocardial wall ($p< 0.001$ for ε_{ll} and ε_{cc}). All deformation parameters were lowest at the sub-epicardium, increasing progressively across the mid-myocardial wall and were greatest at the sub-endocardium. As shown in **Figure 2-3**, FT-CMR derived parameters provide a closer estimate for tagging sub-endocardial strains, rather than other myocardial layers or whole wall strains.

Longitudinal strains. Within the total cohort there was a marginal overestimate of ε_{ll} (-18.1 ± 5.0% vs. -16.7 ± 4.8%, p= 0.03) and SR_{ll} (-1.04 ± 0.29s-1 vs. -0.95 ± 0.32s-1, p= 0.04) by FT-CMR when compared to sub-endocardial myocardial tagging measures. Despite this small systematic difference there was correlation and agreement between the techniques (ε_{ll}: r= 0.70, p< 0.001; bias 1.3 ± 3.8%; SR_{ll}: r= 0.64, p<0.001; bias 0.09 ± 0.26s^{-1}) (**Figure 2-4 & Figure 2-5**). In patients with IDCM there was no overestimation of peak systolic ε_{ll} (-9.7 ± 4.7 vs. -8.8 ±3.9, p= 0.44) and correlation (r= 0.80) and limits of agreement (LoA) (± 2.7%) were tighter than within the total study cohort (**Figure 2-6**). Bland Altman analysis of DSR_{ll} measures show this to be the FT-CMR long axis measure with the greatest overestimation (1.10 ± 0.40 vs. 0.67 ± 0.32; p< 0.001) and weakest LoA (± 0.4) compared to sub-endocardial myocardial tagging, although both techniques remain correlated (r= 0.42, p= 0.007) (**Figure 2-7**).

Table 2-2. Comparison of FT-CMR versus myocardial tagging derived global strain and strain rate parameters for the overall cohort, in healthy controls and in patients with IDCM.

HEALTHY CONTROLS (n=33)	Feature tracking	Tagging whole wall	Tagging sub-epicardium	Tagging mid wall	Tagging sub-endocardium
Long axis function (HLA)					
Peak systolic ε_{ll}					
Mean value ± SD (%)	-19.5 ± 3.5	-18.0 ± 3.5	-15.9 ± 3.0	-17.7 ± 3.2	-18.0 ± 3.5
p-value*	-	0.01	<0.001	0.002	0.04
Pearson's correlation coefficient	-	0.29	0.25	0.27	0.35
p-value**	-	0.09	0.15	0.11	0.04
Bias ± SD (%)	-	2.51 ± 4.0	3.6 ± 4.0	3.6 ± 4.0	1.42 ± 4.0
Peak SSR_{ll}					
Mean value ± SD (1/s)	-1.12 ± 0.22	-0.95 ± 0.24	-0.90 ± 0.23	-0.97 ± 0.24	-1.03 ± 0.26
p-value*	-	0.001	<0.001	0.002	0.07
Pearson's correlation coefficient	-	0.27	0.27	0.27	0.31
p-value**	-	0.12	0.12	0.11	0.06
Bias ± SD (1/s)	-	0.17 ± 0.28	0.22 ± 0.27	0.16 ± 0.28	0.09 ± 0.28
Early DSR_{ll}					
Mean value ± SD (1/s)	1.19 ± 3.5	0.69 ± 0.30	0.67 ± 0.30	0.70 ± 0.30	0.72 ± 0.30
p-value*	-	<0.001	<0.001	<0.001	<0.001
Pearson's correlation coefficient	-	0.20	0.22	0.19	0.19
p-value**	-	0.25	0.20	0.27	0.27
Bias ± SD (1/s)	-	-0.50 ± 0.40	-0.51 ± 0.40	-0.49 ± 0.40	-0.47 ± 0.40
Short axis function (mid LV)					
Peak systolic ε_{cc}					
Mean value ± SD (%)	-24.8 ± 2.9	-18.6 ± 2.5	-12.9 ± 2.0	-18.3 ± 2.6	-24.9 ± 3.0
p-value*	-	<0.001	<0.001	<0.001	0.90
Pearson's correlation coefficient	-	0.15	0.02	0.10	0.26
p-value**	-	0.39	0.92	0.55	0.13
Bias ± SD (%)	-	6.2 ± 3.5	11.9 ± 3.5	6.6 ± 3.7	-0.08 ± 4.0
Peak SSR_{cc}					
Mean value ± SD (1/s)	-1.48 ± 0.27	-1.01 ± 0.18	-0.72 ± 0.13	-0.98 ± 0.18	-1.34 ± 0.31
p-value*	-	<0.001	<0.001	<0.001	0.02
Pearson's correlation coefficient	-	0.22	0.01	0.18	0.28
p-value**	-	0.21	0.99	0.31	0.09
Bias ± SD (1/s)	-	0.48 ± 0.29	0.76 ± 0.30	0.50 ± 0.30	0.14 ± 0.06
Early DSR_{cc}					
Mean value ± SD (1/s)	1.34 ± 0.32	0.79 ± 0.16	0.48 ± 0.11	0.76 ± 0.16	1.15 ± 0.24
p-value*	-	<0.001	<0.001	<0.001	0.001
Pearson's correlation coefficient	-	0.53	0.44	0.52	0.45
p-value**	-	0.001	<0.01	0.001	<0.01
Bias ± SD (1/s)	-	-0.55 ± 0.27	-0.85 ± 0.29	-0.58 ± 0.28	-0.19 ± 0.30

Idiopathic DILATED CARDIOMYOPATHY (n=10)	Feature tracking	Tagging whole wall	Tagging sub-epicardium	Tagging mid wall	Tagging sub-endocardium
Long axis function (HLA)					
Peak systolic ε_{ll}					
Mean value ± SD (%)	-9.7 ± 4.7	-8.2 ± 3.5	-7.6 ± 3.0	-8.3 ± 3.6	-8.8 ± 3.9
p-value*	-	0.26	0.16	0.30	0.44
Pearson's correlation coefficient	-	0.77	0.73	0.75	0.80
p-value**	-	0.08	0.10	0.09	0.05
Bias ± SD (%)	-	1.5 ± 2.9	2.1 ± 3.1	1.4 ± 3.0	0.9 ± 2.7
Peak SSR_{ll}					
Mean value ± SD (1/s)	-0.56 ± 0.19	-0.45 ± 0.19	-0.46 ± 0.15	-0.46 ± 0.19	-0.47 ± 0.23
p-value*	-	0.04	0.16	0.05	0.08
Pearson's correlation coefficient	-	0.88	0.65	0.87	0.91
p-value**	-	0.02	0.16	0.03	0.01
Bias ± SD (1/s)	-	0.11 ± 0.10	0.10 ± 0.15	0.10 ± 0.10	0.09 ± 0.10
Early DSR_{ll}					
Mean value ± SD (1/s)	0.49 ± 0.20	0.31 ± 0.22	0.28 ± 0.18	0.31 ± 0.23	0.35 ± 0.26
p-value*	-	0.07	0.05	0.07	0.17
Pearson's correlation coefficient	-	0.57	0.45	0.59	0.60
p-value**	-	0.24	0.38	0.22	0.21
Bias ± SD (1/s)	-	-0.19 ± 0.20	-0.22 ± 0.20	-0.19 ± 0.19	-0.14 ± 0.22
Short axis function (mid LV)					
Peak systolic ε_{cc}					
Mean value ± SD (%)	-9.6 ± 4.8	-7.2 ± 2.4	-6.3 ± 1.8	-7.2 ± 2.2	-8.1 ± 1.9
p-value*	-	0.15	0.07	0.15	0.36
Pearson's correlation coefficient	-	0.70	0.76	0.73	0.61
p-value**	-	0.12	0.08	0.10	0.20
Bias ± SD (%)	-	2.5 ± 3.5	3.3 ± 3.6	2.4 ± 3.5	1.6 ± 3.8
Peak SSR_{cc}					
Mean value ± SD (1/s)	-0.57 ± 0.23	-0.41 ± 0.10	-0.36 ± 0.09	-0.40 ± 0.10	-0.50 ± 0.23
p-value*	-	0.06	0.04	0.05	0.37
Pearson's correlation coefficient	-	0.80	0.67	0.82	0.73
p-value**	-	0.06	0.14	<0.05	0.10
Bias ± SD (1/s)	-	0.16 ± 0.17	0.20 ± 0.19	0.17 ± 0.16	0.07 ± 0.17
Early DSR_{cc}					
Mean value ± SD (1/s)	0.48 ± 0.26	0.46 ± 0.20	0.30 ± 0.13	0.44 ± 0.20	0.63 ± 0.26
p-value*	-	0.89	0.23	0.79	0.41
Pearson's correlation coefficient	-	0.18	0.20	0.20	0.20
p-value**	-	0.73	0.71	0.71	0.71
Bias ± SD (1/s)	-	-0.03 ± 0.36	-0.18 ± 0.32	-0.04 ± 0.36	0.15 ± 0.41

DSR, diastolic strain rate; Ɛ, Lagrangian strain; HLA, horizontal long axis; LV,left ventricle; SD, standard deviation; SSR, systolic strain rate. *FT-CMR derived means compared with tagging measurements using a paired Student's *t* test. **Using Pearson's *r*, correlation coefficient.

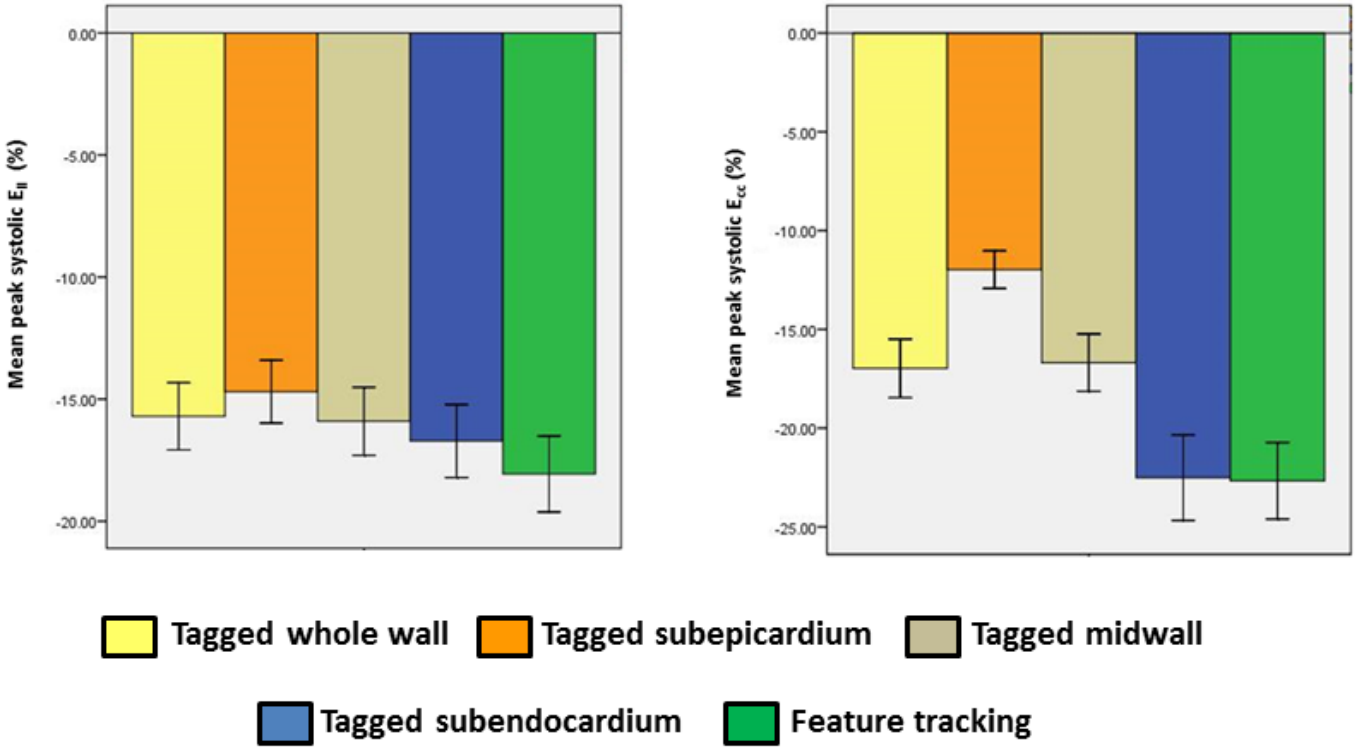

Figure 2-3. Global strain measures calculated from FT-CMR and myocardial tagging analysis across the three layers of the myocardium.

Using an ANOVA with repeated measures with a Greenhouse-Geisser correction, the mean scores for peak systolic strain across the 3 layers of the myocardium were statistically different for both longitudinal and circumferential strain (P<0.001 for both).

(Moody et al., 2015)

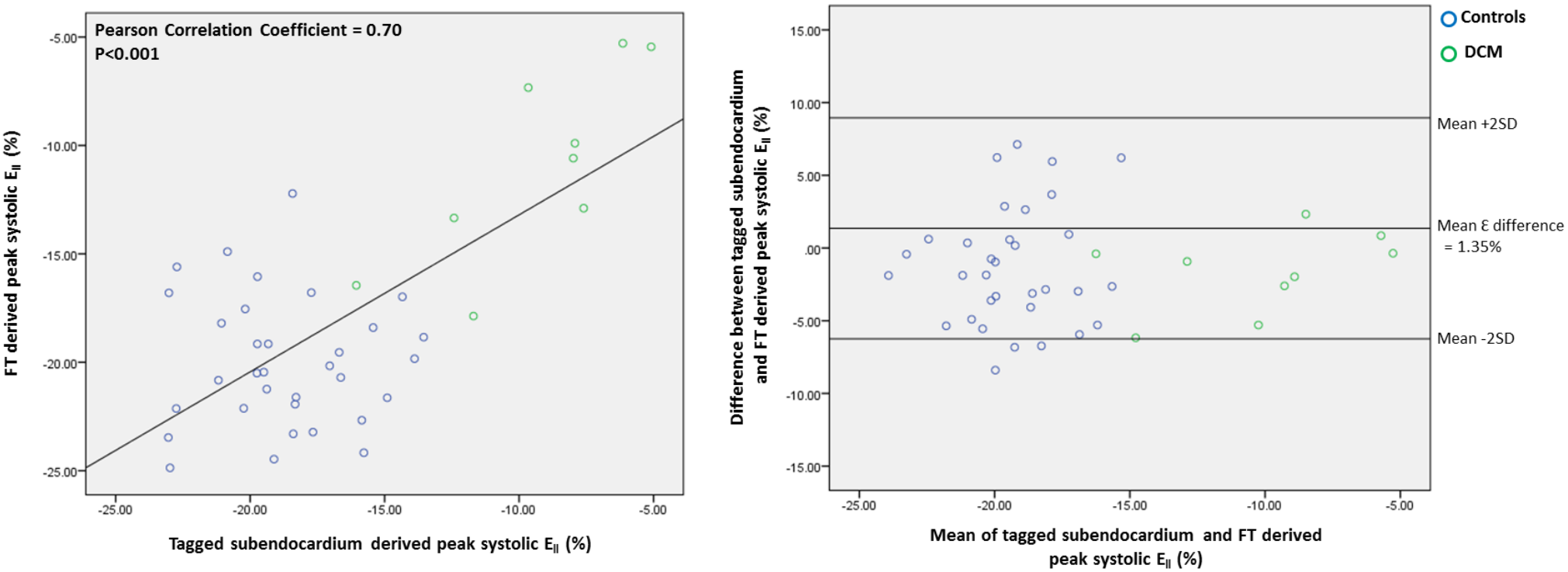

Figure 2-4. (a) Pearson correlation and (b) Bland Altman plots demonstrating agreement for global E_{II} calculation using FT-CMR versus tagging

Spearman's rank correlation of the differences and the means was non-significant (ρ=0.078, P=0.625).

(Moody et al., 2015)

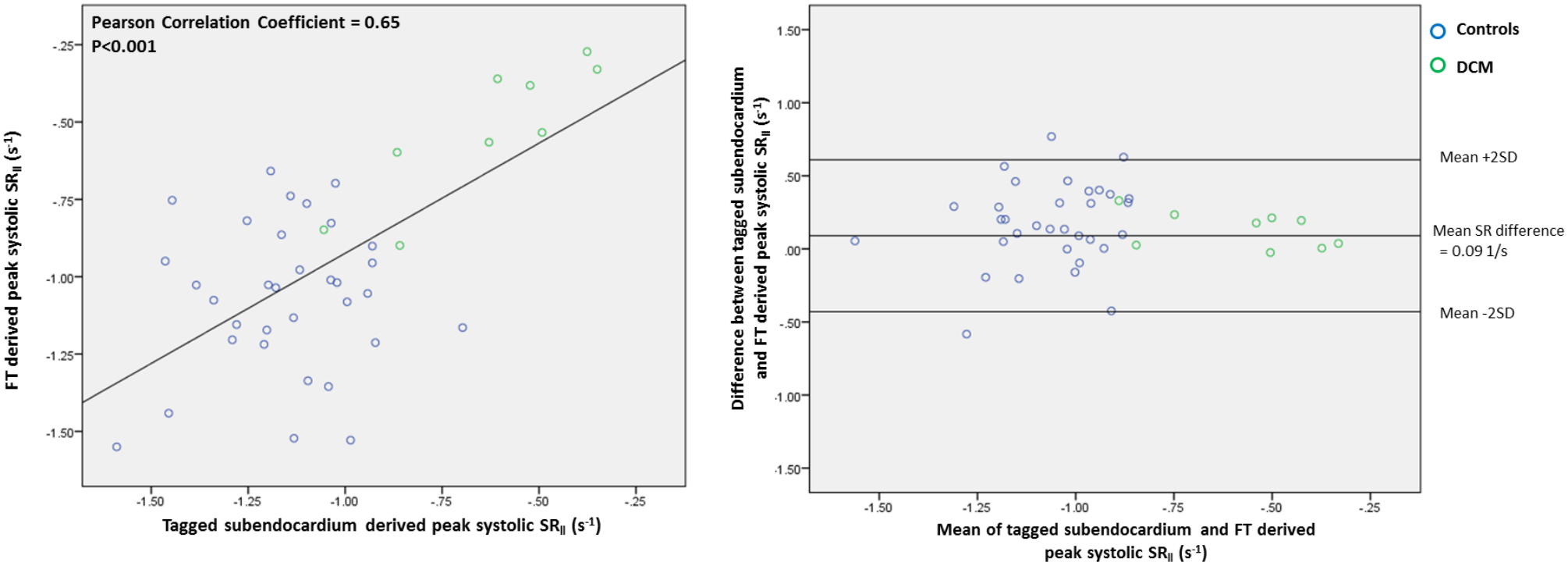

Figure 2-5. (a) Pearson correlation and (b) Bland Altman plots demonstrating agreement for peak systolic global longitudinal strain rate calculation using FT-CMR versus myocardial tagging.

Spearman's rank correlation of the differences and the means was non-significant (ρ=0.196, P=0.213).

(Moody et al., 2015)

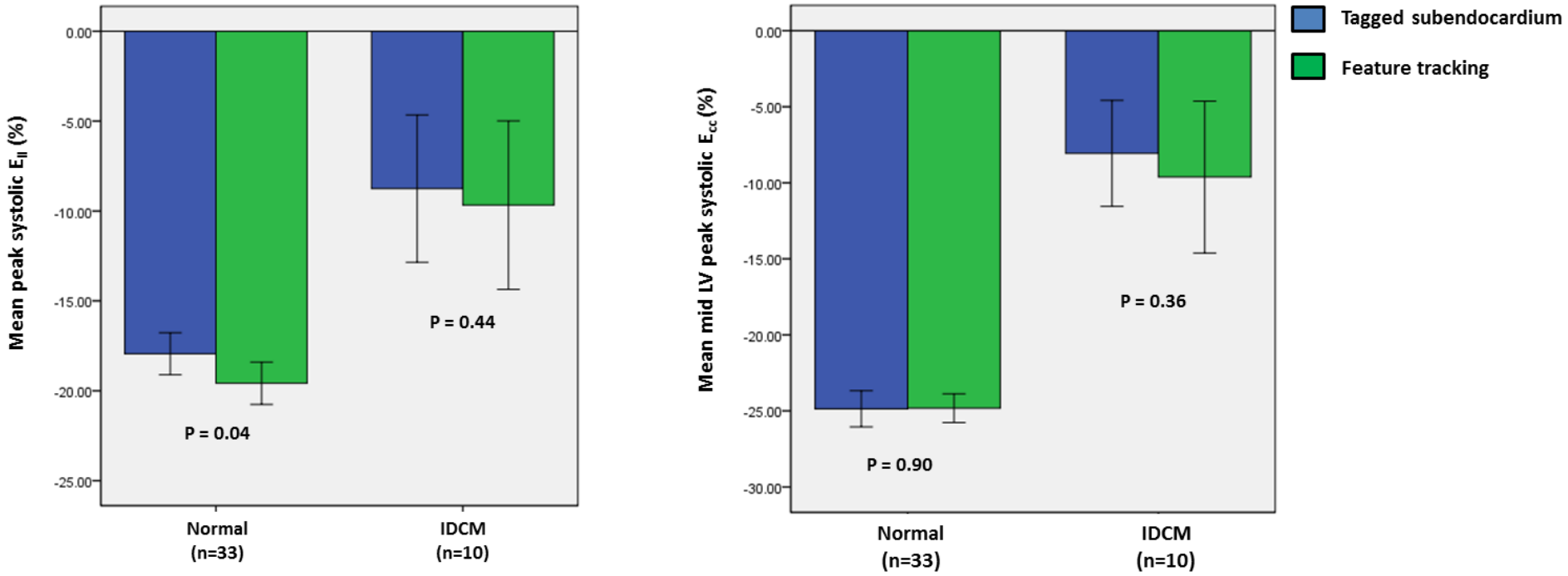

Figure 2-6. Comparison of myocardial tagging versus FT-CMR derived (a) longitudinal and (b) circumferential strain between control and IDCM subjects.

(Moody et al., 2015)

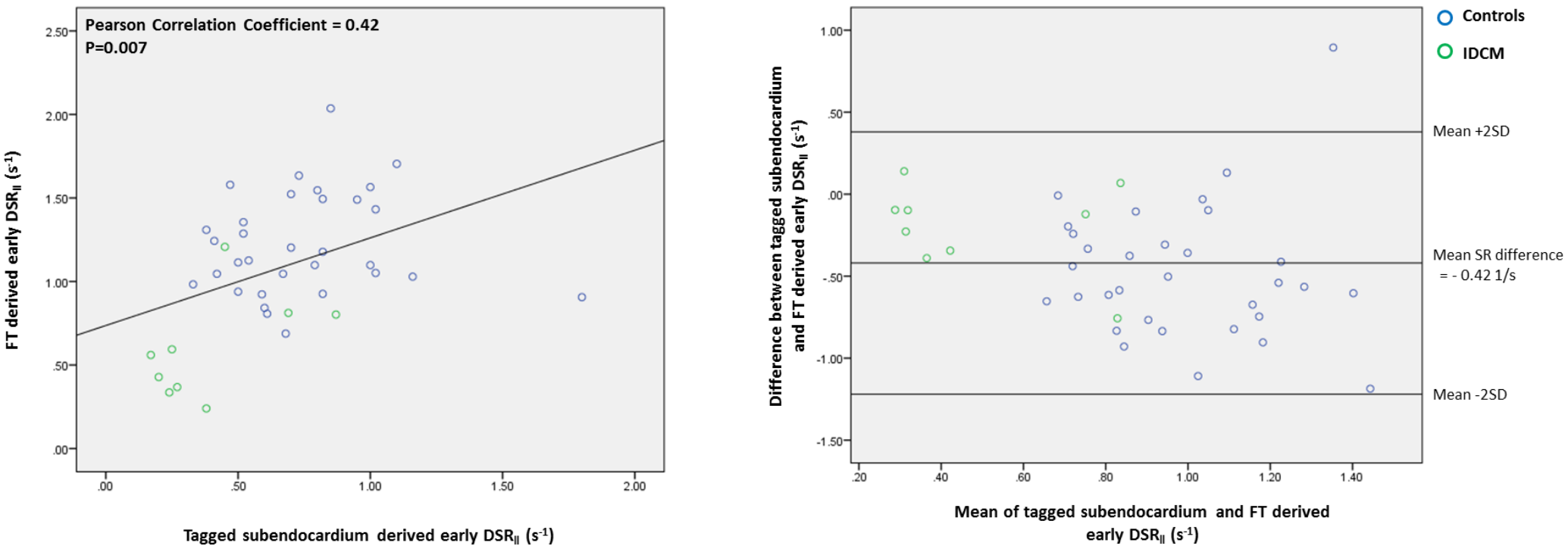

Figure 2-7. (a) Pearson correlation and (b) Bland Altman plots demonstrating agreement for early diastolic global longitudinal strain rate calculation using FT-CMR versus myocardial tagging.

Spearman's rank correlation of the differences and the means was significant (ρ=-0.329, P=0.036) suggesting a proportional error with a downward trend.

(Moody et al., 2015)

Circumferential strains. Within the total cohort FT-CMR closely reproduced sub-endocardial myocardial tagging derived from mid cavity peak systolic E_{cc} with no systematic bias (0.2%, p=0.80), close correlation (r= 0.83, p< 0.001) and LoA of ± 4.0% (**Figure 2-8**).

Figure 2-6b shows that these comparable peak systolic ε_{cc} values between techniques were consistent in both healthy controls and IDCM patients. **Table 2-3** shows that agreement for measures of peak systolic ε_{cc} at the apex and base were inferior to those from the mid cavity. Bland-Altman analysis shows agreement between techniques for peak systolic SR_{cc} (bias 0.13 ± 0.33 s-1; r= 0.69, p< 0.001) and early DSR_{cc} (bias 0.14 ± 0.34 s-1; r= 0.64, p< 0.001) despite a small overestimate by FT-CMR for both measures (**Figure 2-9 and Figure 2-10**).

2.3.3 Rapidity of acquisition and analysis

As shown in **Table 2.4** acquisition of the SSFP cines, a fundamental step of routine CMR imaging, took 12.1 ± 3.4 mins. Acquiring the four SPAMM cines increased scan duration by 8.4 ± 2.3 mins, and their subsequent analysis took 23.2 ± 3.5 mins. In total, MT added 31.6 mins to procedural duration in contrast to the 5.9 ± 0.8 mins to perform FT-CMR (p< 0.001).

2.3.4 Intra- and Interobserver variability

Table 2-5 provides intra- and interobserver variability for myocardial tagging derived strain parameters. Equivalent reproducibility data for FT-CMR is provided in chapter **3**, and it can be seen that it compared favourably to myocardial tagging.

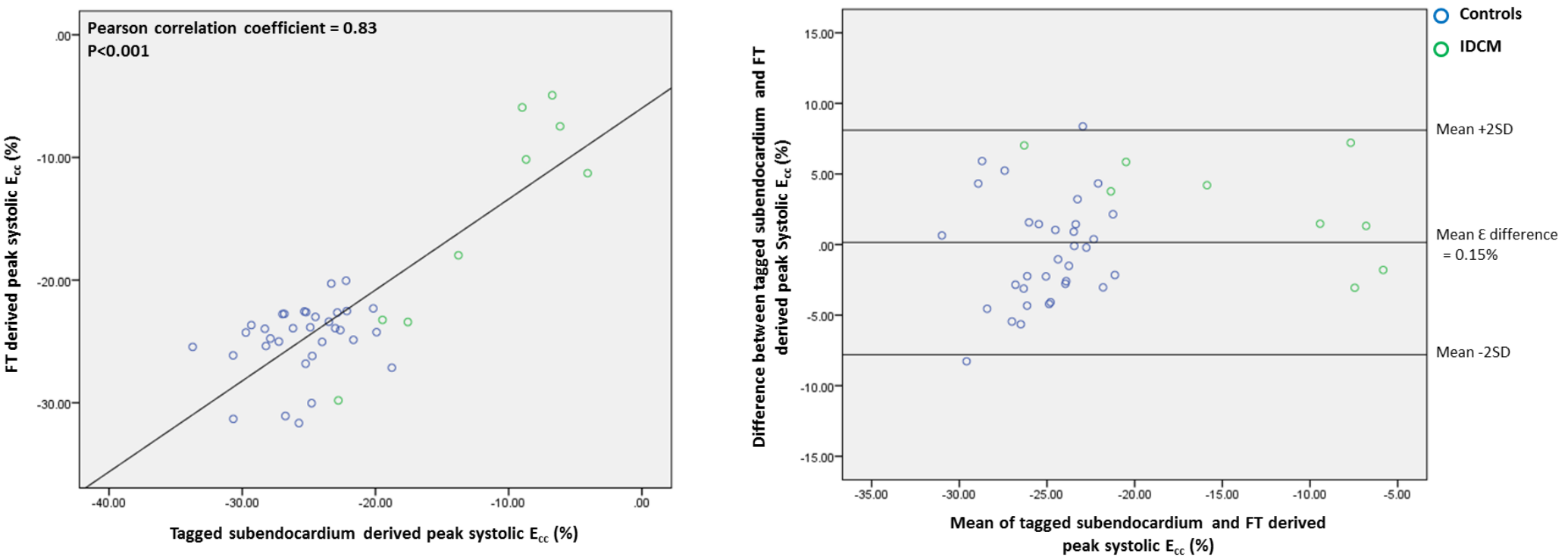

Figure 2-8. (a) Pearson correlation and (b) Bland Altman plots demonstrating agreement for peak systolic global circumferential strain calculation using FT versus tagging.

Spearman's rank correlation of the differences and the means was non-significant (ρ=0.292, P=0.06).

(Moody et al., 2015)

Table 2-3. Comparison of FT versus tagging derived global circumferential strain in the short axis at the apex and base for the overall cohort.

	Feature tracking	Tagging whole wall	Tagging sub-epicardium	Tagging mid wall	Tagging sub-endocardium
Short axis function (base)					
Peak systolic Ɛcc					
Mean value ± SD (%)	-23.9 ± 6.4	-12.8 ± 4.1	-9.6 ± 2.8	-12.6 ± 4.0	-16.7 ± 5.9
p-value*	-	<0.001	<0.001	<0.001	<0.001
Pearson's correlation coefficient	-	0.63	0.52	0.64	0.63
p-value**	-	<0.001	<0.001	<0.001	<0.001
Bias ± SD (%)	-	11.1 ± 5.0	14.4 ± 5.5	11.3 ± 4.9	7.3 ± 5.3
Short axis function (apex)					
Peak systolic Ɛcc					
Mean value ± SD (%)	-26.2 ± 9.2	-18.5 ± 4.7	-12.7 ± 3.3	-18.2 ± 4.6	-24.9 ± 7.0
p-value*	-	<0.001	<0.001	<0.001	0.27
Pearson's correlation coefficient	-	0.56	0.39	0.56	0.59
p-value**	-	<0.001	0.01	<0.001	<0.001
Bias ± SD (%)	-	7.7 ± 7.6	13.5 ± 8.5	7.9 ± 7.6	1.3 ± 7.6

E, Lagrangian strain; SD, standard deviation.

***FT derived means compared with tagging measurements using a paired Student's *t* test.**

****Using Pearson's *r*, correlation coefficient.**

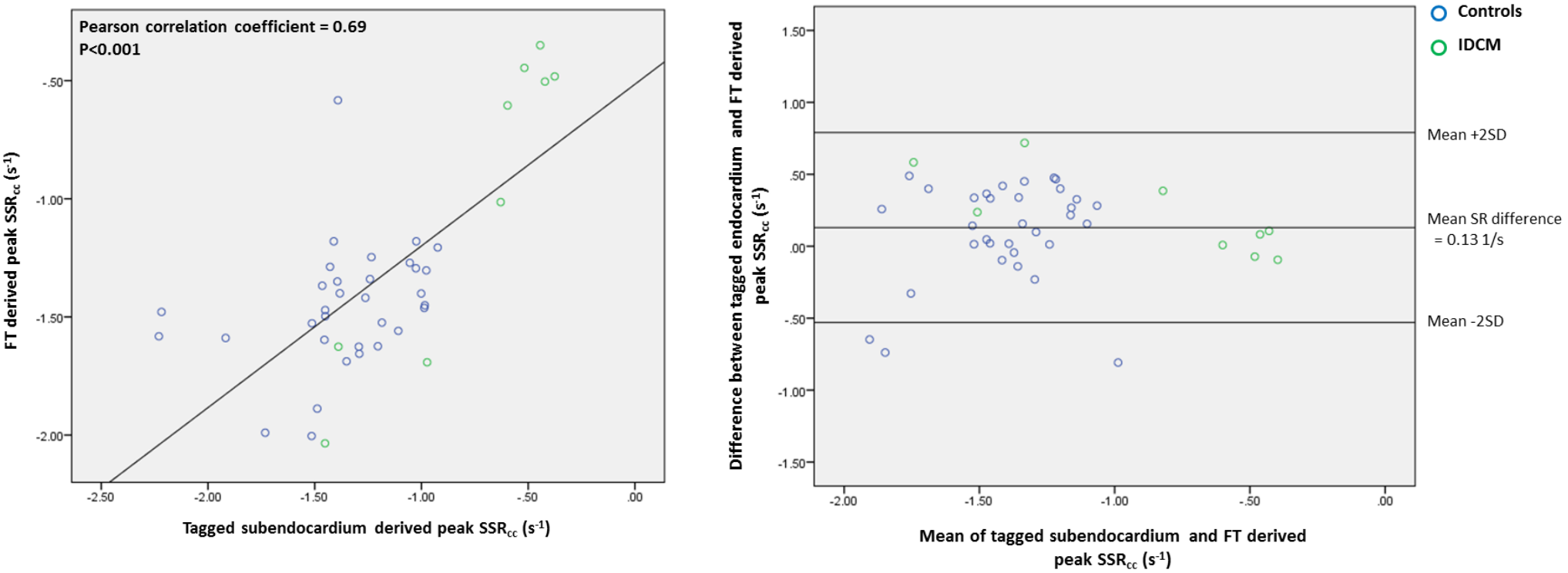

Figure 2-9. (a) Pearson correlation and (b) Bland Altman plots demonstrating agreement for peak systolic global circumferential strain rate calculation using FT versus tagging.

Spearman's rank correlation of the differences and the means was non-significant (ρ=-0.034, P=0.833).

(Moody et al., 2015)

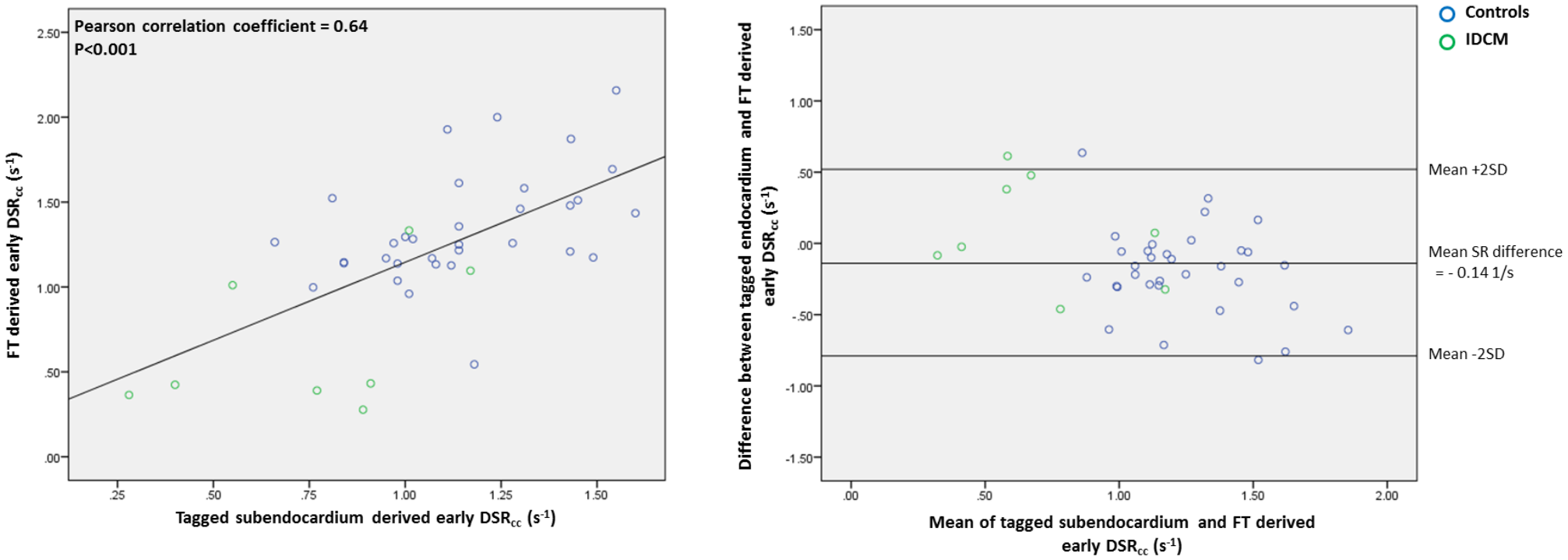

Figure 2-10. (a) Pearson correlation and (b) Bland Altman plots demonstrating agreement for early diastolic global circumferential strain rate calculation using FT-CMR versus tagging.

Spearman's rank correlation of the differences and the means was significant (ρ=-0.315, P=0.045) suggesting a proportional error with a downwards trend (Moody et al., 2015)

Table 2-4. Time taken for image acquisition and post-processing analysis.

	Feature tracking	Tagging
SSFP acquisition time (min)	12.1 ± 3.4	12.1 ± 3.4
SPAMM acquisition time (min)	-	8.4 ± 2.3
Post-processing time (min)	5.9 ± 0.8*	23.2 ± 3.5

Data are mean ± SD. SSFP, steady-state free precession; SPAMM, spatial modulation of magnetization.

***p<0.001 (means compared using a paired Student's *t* test).**

Table 2-5. Intra-observer and inter-observer variability for myocardial tagging derived global strain parameters.

Parameter	Variability	Bias ± SD	p value	Limits of Agreement	Coefficient of Variation (%)	Intra-class Correlation Coefficient (95% CI)
E_{ll} (%)	Intra-observer	-0.47 ± 0.62	0.04	-1.68 to 0.74	3.41	0.97 (0.83 to 0.99)
	Inter-observer	-0.47 ± 2.02	0.49	-4.42 to 3.49	11.44	0.75 (0.29 to 0.93)
SSR_{ll} (1/s)	Intra-observer	0.00 ± 0.06	0.91	-0.11 to 0.11	6.64	1.00 (0.98 to 1.00)
	Inter-observer	-0.01 ± 0.17	0.90	-0.33 to 0.32	17.27	0.60 (-0.04 to 0.89)
DSR_{ll} (1/s)	Intra-observer	0.05 ± 0.10	0.14	-0.14 to 0.24	14.15	0.89 (0.62 to 0.97)
	Inter-observer	0.11 ± 0.20	0.12	-0.28 to 0.49	31.59	0.45 (-0.11 to 0.82)
E_{cc} (%)	Intra-observer	-0.39 ± 1.22	0.39	-2.79 to 2.09	4.79	0.92 (0.74 to 0.98)
	Inter-observer	-0.53 ± 1.53	0.30	-3.54 to 2.48	6.01	0.86 (0.56 to 0.96)
SSR_{cc} (1/s)	Intra-observer	0.00 ± 0.06	0.92	-0.12 to 0.12	4.63	0.95 (0.82 to 0.99)
	Inter-observer	-0.02 ± 0.18	0.71	-0.37 to 0.33	13.86	0.46 (-0.25 to 0.83)
DSR_{cc} (1/s)	Intra-observer	0.03 ± 0.08	0.25	-0.13 to 0.19	7.38	0.95 (0.81 to 0.99)
	Inter-observer	0.09 ± 0.19	0.15	-0.27 to 0.46	16.75	0.78 (0.36 to 0.94)

E_{cc}, Peak systolic global circumferential strain; E_{ll}, Peak systolic global longitudinal strain; SSR_{cc}, Peak systolic global circumferential strain rate; SSR_{ll}, Peak systolic global longitudinal strain rate; DSR_{cc}, Early diastolic circumferential strain rate; DSR_{ll}, Early diastolic longitudinal strain rate.

2.4 Discussion

2.4.1 Major findings

The foremost outcome of this study is the validation of an uncomplicated SSFP based deformation algorithm against the reference standard myocardial tagging, conducted using SPAMM acquisitions and the CIMTag analysis platform. This study supports the recent endorsement of this methodology for the computation of circumferential deformation parameters during systole (Augustine et al., 2013; Harrild et al., 2012; Hor et al., 2010), and further develops its potential by demonstrating its fidelity for longitudinal and diastolic measures. Precision for the longitudinal strain assessment is prerequisite for potential clinical utility. The subendocardium is most exposed to myocardial ischaemia and with its preponderance of longitudinal fibres, reduced deformation in this direction is a key parameter for ischaemia testing. Half of patients presenting with heart failure have preserved systolic parameters, and markers of diastolic dysfunction predict this syndrome at a pre-clinical stage (Kane GC et al., 2011). Myocardial tagging is a sensitive CMR measure of diastolic function in patients with LV hypertrophy (Edvardsen et al., 2006), and on the basis of this study FT-CMR might be a suitable alternative for diastolic assessment. A further key aspect of this study is that by providing the first timed comparison of these techniques, it has been shown that FT-CMR overcomes the major obstacle that has limited the mainstream use of myocardial tagging, as it can be conducted in a fifth of the time.

2.4.2 Differences from previous validations

The demonstration of acceptable agreement for longitudinal measures is in contrast to the work of Augustine et al., who report that in half of their study recruits FT-CMR overestimated peak systolic E_{ll} by a magnitude of 25% and by as much as 50% in extreme cases. This can be explained by flaws in their methodology. The tagging analyses in this study confirm the previously reported strain gradient that exists across the myocardial wall, with greatest deformation recorded at the subendocardium, and least deformation at the subepicardium (Moore et al., 2000a). The systematic overestimation of longitudinal strain by FT-CMR that Augustine et al, report reflects their comparison of myocardial tagging parameters derived from transmural analyses with FT-CMR parameters obtained at the subendocardial border, the location richest in longitudinally orientated fibres (Geyer et al., 2010). It is essential to compare strain from corresponding regions of the myocardial wall, and this justifies the *a priori* decision to compare FT-CMR strain parameters with tagging parameters derived only from the sub-endocardium.

This study also addressed other technical limitations of previous validations. All of the acquisitions were performed on 1.5T MR scanners; other studies employed a combination of 1.5T and 3.T MR scanners (Hor et al., 2010). Validations on retrospective cohorts have selected SSFP images that provided the closest match for tagged acquisitions (Hor et al., 2010), whereas this study used tagging acquisitions matched to the slice location of the SSFP cines used for FT-CMR.

2.4.3 Differences between methodologies

Agreement between the techniques was very close for systolic circumferential deformation parameters and this is in accord with previous validations (Hor et al., 2010)(Augustine et al., 2013). However, Bland-Altman analyses indicate some inter-procedural difference between longitudinal and diastolic parameters. This is small for longitudinal strains and likely relates to inadequacies of the FT-CMR platform to measure these at the very basal region of the LV cavity. The FT-CMR algorithm matches features in consecutive frames based on the maximum probabilities assessed using a hierarchical processing system; whilst this is largely suited to identifying motion at the blood-tissue interface where there is a high signal to noise ratio, it is less apt for discriminating between very basal myocardium and the mitral valve apparatus.

Differences in agreement for diastolic parameters may pertain more to inherent shortcomings of myocardial tagging rather than to FT-CMR. The grid of magnetic saturation that divides the imaged plane into tags is engineered by specific radiofrequency pulses which are gated to the R wave. Longitudinal relaxation occurs exponentially and the sharp contrast outline to the tags fades with increasing time interval from the R wave (Edvardsen et al., 2006), thus myocardial tagging is prone to underestimate diastolic deformation. This likely accounts for the considerably higher values for DSR observed with FT-CMR; and the mean DSR_{cc} of 1.34 s^{-1} observed in these healthy controls matches the defined reference range for STE (Marwick et al., 2009).

In the FT-CMR analysis platform there is little scope for user adjustment to compensate if tracking errors occur, although visual assessment allows for this to be recognised. Nonetheless, this minimal user interaction likely accounts for closer inter-operator agreement with FT-CMR than with myocardial tagging (Moody et al., 2015). In contrast, the myocardial tagging analysis framework allows the user to assign an unlimited number of new guide markers in the end-systolic frame, amending the strain map but enabling far greater inter-operator variability. User proficiency is thus considerably more important for conducting tagging.

2.4.4 FT-CMR beyond the mid-cavity

Circumferential motion parameters at the base and apex have specific clinical relevance as they enable evaluation of cardiac torsion. The significance of reduced cardiac torsion is being increasingly recognised in a spectrum of pathologies including IDCM (Popescu et al., 2009), and manipulation of this offers a potential for individualising CRT delivery (Bertini et al., 2009). The addition of basal and apical tracking will also be essential in the assessment of dyssynchrony and late mechanical activation patterns. FT-CMR derived parameters showed reasonable agreement with tagging for tracking in these regions, although in agreement with Augustine et al. these were not as robust as measures from the mid-LV slice.

Both methodologies have shortcomings for the measurement of deformation at the apex. More prominent trabeculation can make accurate feature tracking difficult apically, a problem compounded if there is end-systolic complete cavity obliteration. Myocardial tagging is immune to this, but the thinner apical myocardium has less substrate available for

tagging, and the smaller strain map leads to magnification of any error. The LV base is particularly exposed to errors in feature tracking due to its greater longitudinal displacement. The software intends to track true in-plane deformations, but as through plane motion is greatest basally, some apparent in plane deformations are doubtlessly due to through plane movement, whilst some voxels tracked in initial frames will be lost out of plane. Myocardial tagging is more resistant to this phenomenon.

2.4.5 Clinical considerations

Considering that FT-CMR measures strain at the endocardial blood interface, it is paradoxical that circumferential deformation is the most accurate and reproducible, as it is longitudinal deformation that is predominantly governed by the sub-endocardial fibres (Greenbaum et al., 1981). However, in common with all deformation imaging techniques, FT-CMR does not directly assess myocardial fibre mechanics which would require precise knowledge of fibre direction, but deformation relative to the central axis of the ventricle. The comparatively reduced fidelity for longitudinal strain may have clinical consequence as longitudinally oriented fibres and strain are the earliest affected in most cardiac pathologies. Peak systolic ε_{ll} (global longitudinal strain) has been used in the surveillance of patients undergoing chemotherapy (Thavendiranathan et al., 2014), and for the early detection of dilated (Hankiewicz et al., 2008), hypertrophic (Nagueh et al., 2001; Sutherland et al., 1994) and restrictive (Quarta et al., 2014) cardiomyopathies. Circumferential strain deteriorates later as this can be compensated by sub-epicardial fibres (Zhang, 2002), and whether global circumferential strain can play a similar role in detecting incipient disease requires investigation.

2.4.6 Limitations

All scans were performed on a 1.5T MR scanner to maintain uniformity, however a 3.0T MR scanning would have improved myocardial tag persistence and diastolic assessment. There were relatively fewer patients with myocardial pathology included in this validation, nonetheless, the study benefits from comparing individuals with a diverse range of LV function.

The number of patients recruited reflects those available from on-going investigations rather than an a priori evaluation. The study design period pre-dated other validations, with the exception of (Hor et al., 2010), to facilitate more accurate power calculations. The true maximum difference between modalities for measuring strain parameters may be greater than that predicted by the LoA. Retrospective power calculations, using a recently described methodology (Lu et al., 2016), show this to be the case for longitudinal parameters; the difference between techniques could be as high as 11.5% for peak systolic ε_{ll} and 1.49 s^{-1} for DSR_{ll} and this magnitude of difference would be deemed unacceptable. The variance in difference between circumferential parameters was as anticipated and the calculated limits of agreement between techniques is more precise.

Intentionally, this study does not validate radial parameters. Myocardial tagging is inaccurate for the determination of these due to the small number of tags covering this dimension (Moore et al., 2000b) (Swoboda et al., 2011). Our experience upholds this, and it would be unconstructive to use this as a comparator. Clearly, the small width over which radial deformation is measured adversely influences measurement regardless of the

algorithm employed, and a recent investigation of inter-study reproducibility suggests that this holds true with FT-CMR, as ε_{rr} was the least reproducible global measure (Morton et al., 2012).

2.5 Conclusions

Tested against the reference standard myocardial tagging, FT-CMR shows reasonable agreement for the derivation of global measures of circumferential and longitudinal systolic and diastolic strains in this study population with a broad spectrum of LV function. In difference to myocardial tagging, FT-CMR does not require additional imaging acquisitions, and its automated processing makes it considerably less time intensive whilst conferring superior inter-operator reproducibility.

3 MYOCARDIAL STRAIN MEASUREMENT WITH FEATURE-TRACKING CARDIOVASCULAR MAGNETIC RESONANCE: NORMAL VALUES

Principal hypothesis: To facilitate the clinical application of FT-CMR, healthy population values for left ventricular systolic and diastolic strains are required.

3.1 Background

The assessment of LV function is, arguably, the most important component of a cardiac imaging study. In routine clinical practice the assessment of systolic function consists of either the quantitative LV volumetric assessment or qualitative regional wall analysis. However, such methods may not be sensitive enough to detect subtle decline in LV function. Assessing diastolic function is even more problematic, and is perceived by many to be too complex due to the vast number of parameters that exist and lack of guidance as to how to integrate these into a unifying grade. Cardiac strain is a sensitive marker of myocardial contractility and abnormalities of strain precede declines in more conventional markers of LV function, facilitating the earlier diagnosis of IDCM (Hankiewicz et al., 2008) , hypertrophic cardiomyopathy (Nagueh et al., 2001) and chemotherapy induced cardiotoxicity (Poterucha et al., 2012).

Cardiac strain is defined as the relative change in fibre length from end-diastole. Whilst measuring this in vivo would require a precise knowledge of the local fibre direction, clinical imaging modalities circumnavigate this by measuring strain in three principle directions (radial, circumferential and longitudinal), relative to the central axis of the ventricle.

Measurements of strain are becoming increasingly popular in both clinical and research environments. However, echocardiographic measurements obtained using tissue Doppler imaging (Edvardsen et al., 2002; Miyatake et al., 1995) are limited by noise interference and angle dependency (Castro et al., 2000). Whilst speckle tracking has largely overcome these issues, it is often limited by image quality (Amundsen et al., 2006). Cardiovascular magnetic resonance imaging combined with myocardial tagging is the reference-standard technique for the assessment of myocardial motion. To date, however, myocardial tagging acquisition and its requisite post-processing analysis are largely confined to the research environment, not least because they are laborious and time-consuming.

Feature-tracking CMR (FT-CMR) is a novel technique that allows quantification of motion and strain using a standard steady state in free precession (SSFP) sequence, which forms part of a routine LV study protocol. Whereas myocardial tagging provides a pan-myocardial assessment of deformation, FT-CMR is relatively crude, as it is limited to the assessment of myocardial edges. Nevertheless, its accuracy has been validated against myocardial tagging using HARP (Hor et al., 2010) and SPAMM (**chapter 2**) (Moody et al., 2015).

In order to facilitate the clinical application of this technique to detect early myocardial dysfunction this study defines normal LV systolic and diastolic strain and strain rates in a large cohort of healthy adults. This study also explores the demographic, haemodynamic and cardiac relationships that influence normal myocardial strain.

3.2 Methods

3.2.1 Study population

One hundred subjects were recruited in a pre-determined stratified fashion to provide 10 participants of each gender representing each age decade from vicenarians to sexagenarians. Healthy control subjects were identified from an ongoing controlled prospective observational research study examining the effects of living kidney donation on cardiovascular structure and function (NCT01769924) (Moody et al., 2014). Rigorous screening criteria were applied: a 10-year risk of a cardiovascular event of less than 20% as evaluated using the QRISK-2 index (Hippisley-Cox et al., 2008; QRISK®2, 2012); normal exercise stress echocardiography and normal haematology and biochemistry profiling. Exclusion criteria included: any history of cardiovascular disease; any history of diabetes or glucose intolerance; renal impairment; anaemia or atrial fibrillation; first degree relative with a proven or potentially inheritable cardiac condition or a history of premature coronary artery disease. Recruits with an office blood pressure greater than 140mmHg systolic, or 90mmHg diastolic had to have a 24 hour ambulatory average of less than 135/85 mmHg to meet our inclusion criteria. However, in such individuals their office blood pressure was used in analyses as not all recruits underwent ambulatory monitoring. Previous prescription of an anti-hypertensive medication was an exclusion criteria.

3.2.2 CMR acquisition

This was performed with a 1.5 Tesla scanner (Magnetom Avanto, Siemens, Erlangen, Germany) as described in section **2.2.2**. A HLA and a short-axis LV stack from the atrioventricular ring to the LV apex were acquired using a SSFP sequence (repetition time of

3.2 ms; echo time of 1.7 ms; flip angle of 60^{o}; sequential 7 mm slices with a 3 mm interslice gap). There were 25 phases per cardiac cycle resulting in a mean temporal resolution of 40 ms

3.2.3 Evaluation of LV dimensions, function and mass.

LV mass, LVEDV and LVESV were quantified using manual planimetry of the endocardial and epicardial borders from the short axis stack in accordance with validated methodologies (Maceira et al., 2006) using Argus software (Siemens, Erlangen, Germany). These were indexed to body surface area using the Mosteller formula (Mosteller, 1987).

3.2.4 Feature tracking

FT-CMR was undertaken using the Diogenes FT-CMR software (TomTec Imaging Systems, Munich, Germany). The base was selected as the slice closest to the annulus without through plane distortion from the LV outflow tract. The horizontal long axis SSFP was used to identify the true mid-cavity at end diastole (equidistant between apex and ring), and the apical slice used was that closest to being equidistant between the apical tip and the mid cavity at end diastole (**Figure 3-1**).

Endocardial and epicardial borders were manually drawn in the end-diastolic frame (**Figure 3-2**). This was in difference to the previously described validation study where tracking was limited to the endocardial border. This advancement of the technique was required to facilitate the derivation of deformation, at the epicardial border, and in a radial direction. Otherwise tracking was performed as described in **2.2.3**.

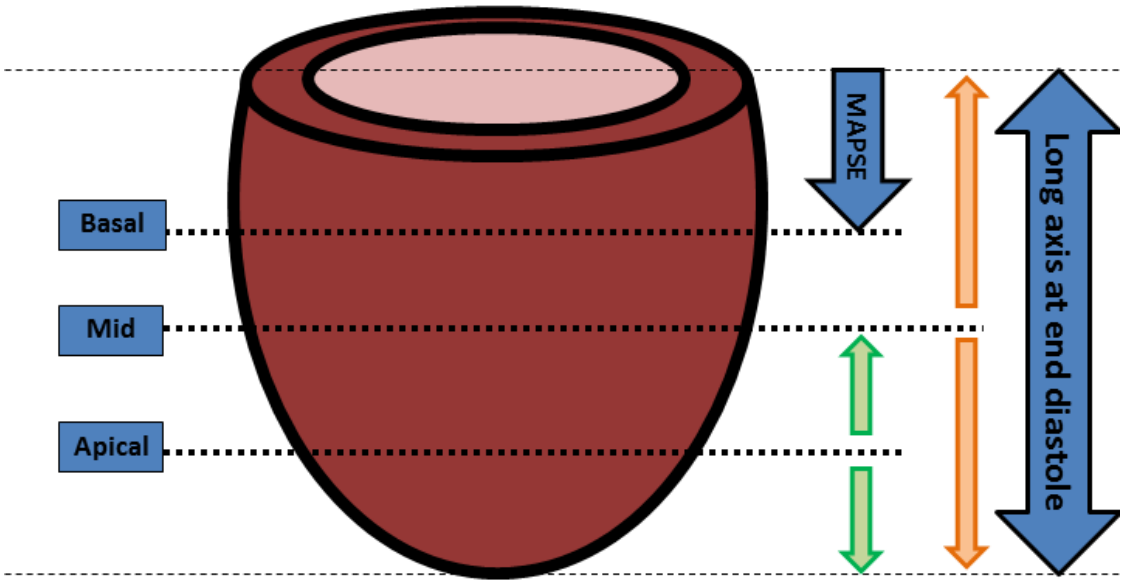

Figure 3-1: Methodology for slice selection for FT-CMR.

A consistent methodology for slice selection is imperative as FT-CMR offers a greater choice of cines for post processing compared to echocardiography or myocardial tagging, particularly as apical images can be tracked. The schematic demonstrates the optimal slices to select for FT-CMR. All slices are selected in end diastole. The mid slice should represent the mid cavity at end diastole (orange arrows). The apical slice is chosen as the mid-point between the mid slice and the apical tip of the LV (green arrows). The basal slice should be the distance of the mitral annular plane systolic excursion away from atrioventricular ring in end-diastole (purple arrow) to prevent extra-ventricular structures distorting the analyses. These are the optimal positions for slices, but an advantage of FT-CMR is that it can be performed on the SSFP sequences which are part of a routine protocol. The slices that correspond closest to these positions should be selected for post processing with FT-CMR.

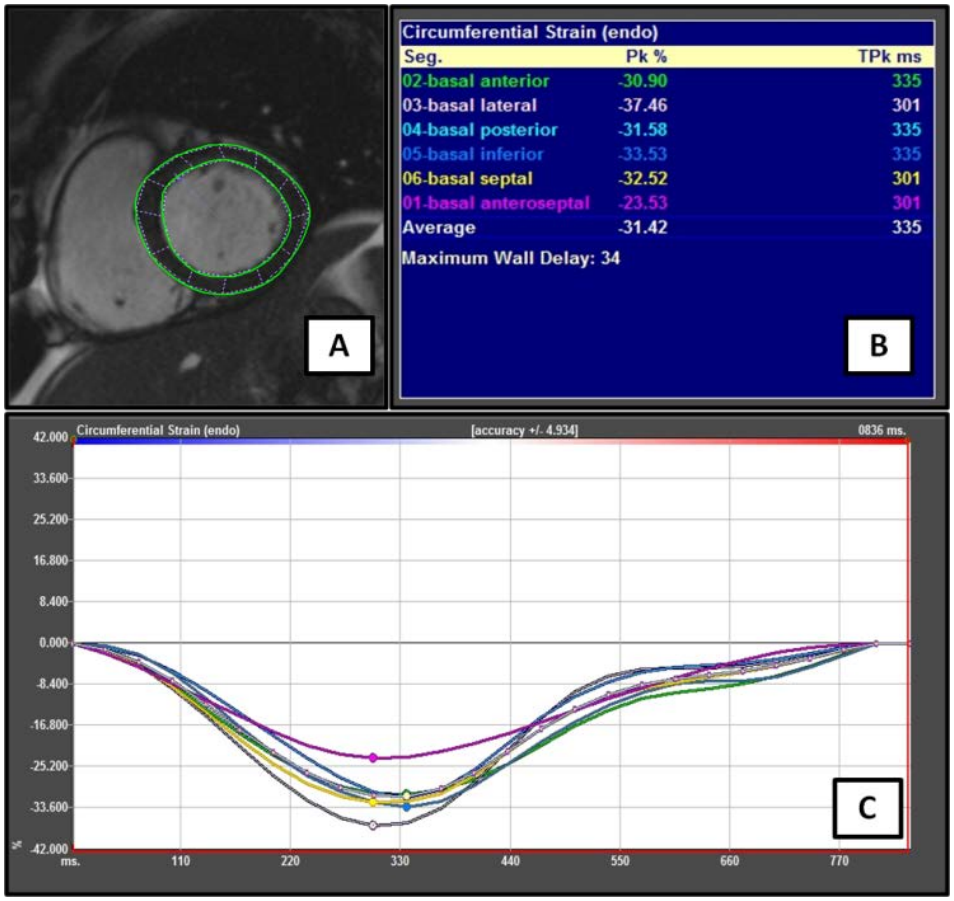

Figure 3-2: Feature-tracking CMR.

a) Endocardial and epicardial contours are traced in the end-diastole frame. b) Peak systolic strain is given for each equiangular segment. The anterior segment is manually delineated starting at the anterior septum. The (global) peak systolic strain is not an average of the peak systolic strain for each segment, but a true instantaneous peak strain (derived from the average global strain at each time point). c) A color coded plot of strain vs. time is shown for each segment. For segmental plots only the peak systolic strain is marked. The average plot is the masked middle white line but this can be easily recognised as strain is plotted at each time point.

The HLA cines were tracked to derive longitudinal displacement and strain, whilst the short axis cines were used to derive circumferential and radial displacements and strains. Separate endocardial and epicardial values were calculated for longitudinal and circumferential strain. Only one measure of strain was calculated in the radial direction, as this direction (myocardial thickening and thinning) is perpendicular to the endocardial and epicardial borders, so both contours are required to derive transmural radial strain.

Global peak systolic longitudinal (ε_{ll}), radial (ε_{rr}) and circumferential (ε_{cc}) strains, global peak longitudinal (SSR_{ll}), radial (SSR_{rr}) and circumferential (SSR_{cc}) systolic strain rates, and global peak early longitudinal (DSR_{ll}), radial (DSR_{rr}) and circumferential (DSR_{cc}) diastolic strain rates were all derived. Segmental peak systolic circumferential strains (in accordance with the American Heart Association's 16 segment model) were also derived.

3.2.5 Reproducibility

For the assessment of inter-observer variability, a randomly generated set of 20 scans were tracked by two investigators (R.J.T. and W.E.M.). The same cine was assessed by each operator, who saved the results independently of the other so a blinded assessment was conducted. Investigator 1 (R.J.T.) repeated this process one month later to assess intra-observer agreement.

3.2.6 Statistical analyses

Continuous variables are expressed as mean $\pm$ SD. Normality was tested using the Shapiro-Wilk test. Comparisons between segments were made using repeated measures ANOVA.

Independent sample t-tests were used to compare inter-gender differences. Curve fitting was performed to assess the relationship between strain and age. Linear regression analysis was used to explore the relationship between strain and baseline variables. Variables reaching a p value <0.10 were included in multivariable models. Reproducibility was tested by calculating mean bias and 95% limits of agreement (confidence intervals) from Bland-Altman analyses, coefficient of variation, and inter-class correlation coefficient (ICC). A p value of < 0.05 was considered statistically significant**.** Statistical analysis was performed using SPSS v21.0. (SPSS Inc. Chicago, Illinois).

3.3 Results

3.3.1 Baseline demographics

The baseline demographics of the entire cohort of 100 healthy individuals are shown in **Table 3-1.** They were normotensive (mean daytime ambulatory systolic blood pressure 123 ± 12 mmHg; mean daytime ambulatory diastolic blood pressure 73 ± 7 mmHg). Fasting total cholesterol was 5.0 ± 1.1 mmol/L, fasting total cholesterol/HDL ratio was 3.4 ± 1.0, and fasting glucose was 4.7 ± 0.4 mmol/L. Estimated glomerular filtration rate, using the modification by diet of renal disease (MDRD) equation, was > 60 ml/min/1.73m^2 in all participants. All participants had a 10 year QRISK-2 score of ≤ 20%. Cardiac volumes, mass and ejection fraction were within normal limits for all participants. (Maceira et al., 2006) There was an age-dependent effect on LVEF, LVESV and LVEDV (p< 0.001 for all) (**Figure 3-3**).

Table 3-1. Baseline characteristics.

	Mean ± SD or n (%)
Demographics	
Age	44.5 ± 14.0
Sex (Male)	50
Height (cm)	170.0 ± 9.6
Weight (kg)	74.3 ± 12.4
Body surface area (m2)	1.85 ± 0.2
Co-morbidities	
Smoker – Current	8
Smoker – Ex	19
Fasting total cholesterol (mmol/L)	5.01 ± 1.1
Fasting total cholesterol/HDL ratio	3.4 ± 1.0
Hypercholesterolaemia (%) *	10
Fasting glucose (mmol/L)	4.7 ± 0.4
eGFR > 60 ml/min/1.73m^2	100
10-year cardiovascular risk (%)	3.6 (0.4-5.8)
Haemoglobin (g/dL)	13.8 ± 1.3
Haemodynamic variables	
Sinus rhythm	100
Heart rate (bpm)	67.3 ± 11.2
Systolic blood pressure† (mmHg)	122.6 ± 12.3
Diastolic blood pressure† (mmHg)	73.1 ± 7.1
Mean blood pressure (mmHg)	89.5.5 ± 8.1
Left ventricular volumes	
LVEDV index (ml/m^2)	63.1 ± 10.4
LVESV index (ml/m^2)	18.1 ± 5.9
LVEF (%)	71.9 ± 6.0
LV mass index (g/m^2)	58.8 ± 11.5

Normally distributed continuous variables are presented as mean ± SD,
Non-normally distributed continuous variables are presented as mean (interquartile limits)
Categorical variables are presented as n (which is also equivalent to the percentage).
***hypercholesterolaemia is defined as a total plasma cholesterol > 6.0 mmol/L or having ever been prescribed a cholesterol lowering therapy.**
†mean of three office blood pressure measures on day of assessment.
eGFR = estimated glomerular filtration rate, HDL = high density lipoprotein, LVEF = left ventricular ejection fraction.

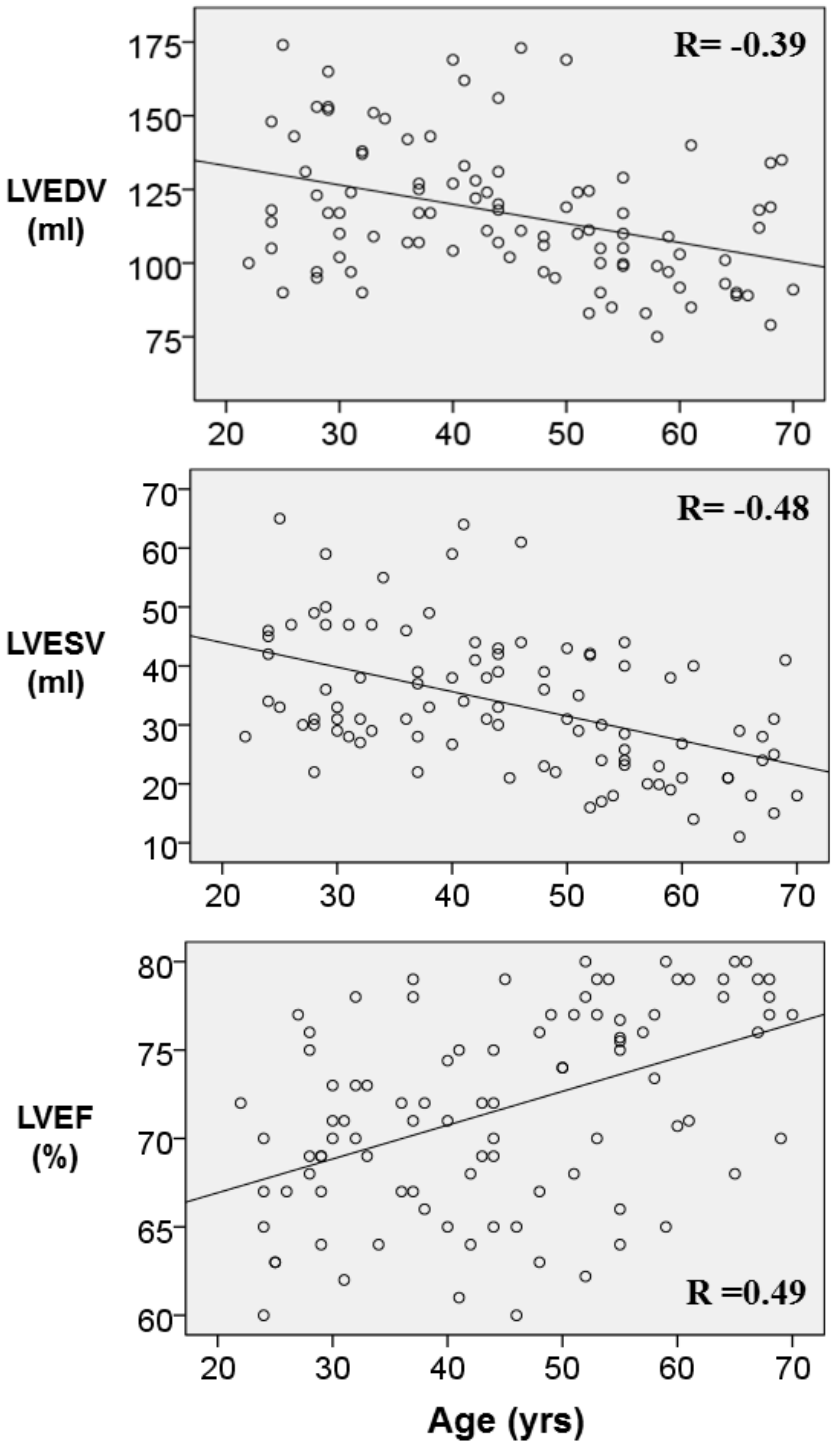

Figure 3-3. The relationship between age and myocardial volumes

Our cohort demonstrated age-related changes which are previously well documented. Age was negatively correlated with LV volumes and positively correlated with LV ejection fraction. The correlation coefficient R is shown for each relationship ($p < 0.001$ for all).

3.3.2 Feasibility

Out of 1600 short-axis and 600 long-axis segments (total 2200) potentially available for the study population, 1600 segments (100%) were adequately tracked. Based on one investigator, semi-automatic border delineation took 5.6 ± 1.2 minutes.

3.3.3 Strain

Peak systolic strains and strain rates are shown in **Table 3-2**. Peak systolic E_{ll} was -21.0 ± 4.1% at the endocardium and -17.3 ± 4.1% at the epicardium. Peak systolic E_{cc} was -26.5 ± 3.8%, and -10.8 ± 2.5% at the endocardium and epicardium, respectively. Peak systolic E_{rr} was the highest, with a transmural value of 39.8 ± 8.3%. All peak systolic strains were higher at the endocardium than at the epicardium; this transmural strain gradient was greatest in the circumferential direction.

The peak systolic E_{cc} was lower in the mid cavity than at the base or apex ($p< 0.001$ for both). Peak systolic E_{cc} measured in the mid cavity correlated strongly with that measured at the base ($r = 0.71$) and apex ($r = 0.60$) ($p< 0.001$ for both). As shown in **Table 3-3**, segmental peak systolic E_{cc} was heterogeneous.

At the endocardium, the margin of error for the calculation of the population peak systolic strains was ± 0.75%, ± 0.94%, and ± 1.63% for E_{cc}, E_{ll} and E_{rr} respectively (these values are presented in absolute terms and represent 2.8%, 4.5% and 4.1% relative to the stated population mean). For segmental peak systolic E_{cc} this margin ranged from a low of ± 1.18%

Table 3-2. Peak systolic strain and diastolic strain rates.

	Peak systolic strain (%)	Peak systolic SR (s^{-1})	Early diastolic SR (s^{-1})
Longitudinal			
Endocardial	-21.3 ± 4.8 -11.9 to -30.7	-1.22 ± 0.36 -0.51 to -1.93	1.25 ± 0.39 0.49 to 2.01
Epicardial	-17.3 ± 4.1 -9.3 to -25.3	-0.99 ± 0.30 -0.40 to -1.58	0.97 ± 0.33 0.32 to 1.62
Mean	-19.1 ± 4.1 -11.1 to -27.1	-1.11 ± 0.30 -0.52 to -1.70	1.11 ± 0.33 0.46 to 1.76
Circumferential			
Endocardial	-26.1 ± 3.8 -18.7 to -33.5	-1.56 ± 0.29 -0.99 to -2.13	1.43 ± 0.35 0.74 to 2.12
Epicardial	-10.8 ± 2.5 -5.9 to -15.7	-0.61 ± 0.13 -0.36 to -0.86	0.53 ± 0.18 0.18 to 0.88
Mean	-18.4 ± 2.9 -12.7 to -24.1	-1.09 ± 0.19 -0.72 to -1.46	0.99 ± 0.24 0.52 to 1.46
Radial			
Transmural	39.8 ± 8.3 23.5 to 56.1	1.63 ± 0.36 0.92 to 2.34	-1.54 ± 0.48 -0.60 to 2.48

Results presented as mean ± SD and 95% confidence intervals.

Table 3-3. Regional circumferential strain.

Peak systolic circumferential strain (%)				
	Apical	**Mid**	**Basal**	**p (all levels)**
Global	-29.3 ± 6.2	-26.1 ± 3.8	-28.4 ±4.2	p<0.001
Anterior	-25.6 ± 7.9	-28.6 ± 6.8	-27.6 ±8.0	p=0.002
Anteroseptal	-30.6 ± 8.2	-24.7 ± 6.1	-28.8 ±8.6	p<0.001
Septal		-24.6 ± 6.0	-32.3 ±8.1	p<0.001
Inferior	-32.1 ± 7.9	-29.0 ± 6.3	-31.7 ±8.5	p=0.001
Inferolateral		-26.0 ± 6.6	-28.5 ±9.3	p=0.006
Lateral	-28.8 ± 7.0	-25.8 ± 7.1	-26.2 ±9.1	p=0.003
p (all segments)	p<0.001	p<0.001	p<0.001	

values presented as mean ±SD.

p values refer to comparison of segments and slices by repeated-measures ANOVA.

at the mid septum, to a high of ± 1.82% at the basal infero-lateral wall (relative error: 4.8-6.4%). A population of 333 would have been required to reduce this absolute margin to less than 1%.

3.3.4 Associations of strain and strain rate

Peak systolic ε_{cc} (-25.6% vs. -26.5%, p = 0.23) and peak systolic ε_{rr} (-38.8% vs. -40.9%, p = 0.20) were similar among males and females. There were significant gender differences (p < 0.001) in peak systolic ε_{ll}, with greater deformation in females (-22.7%) than in males (-19.3%).

There was a linear increase in the magnitude of peak systolic ε_{cc} with advancing age (p = 0.01, β = 0.07), however, the increase in ε_{cc} was greatest for those subjects over the age of 50 years. Accordingly, polynomial regression (with a quadratic curve) had superior modellingpower (R^2= 0.11 [vs 0.06 for linear], p= 0.003) (**Figure 3-4**). **Table 3-4** shows age adjusted values for peak systolic ε_{cc} at the endocardium derived using the best fit regression model. There was no similar relationship when peak systolic ε_{cc} was measured epicardially. There was no association between age and peak systolic ε_{ll} or ε_{rr}. Similarly, there was no association between age and peak systolic SR_{cc} or peak early diastolic SR_{cc} (**Table 3-5**)

As shown in **Table 3-5**, Systolic BP (p= 0.04), LVEDV (p= 0.02) and LVEF (p< 0.001) also emerged as predictors of peak systolic ε_{cc} on linear regression analyses. The relationship between systolic BP and peak systolic ε_{cc} is also shown in **Figure 3-5**. In multivariable analysis SBP (p= 0.02) and LVEDV (p= 0.01) remained significant predictors. With respect to peak

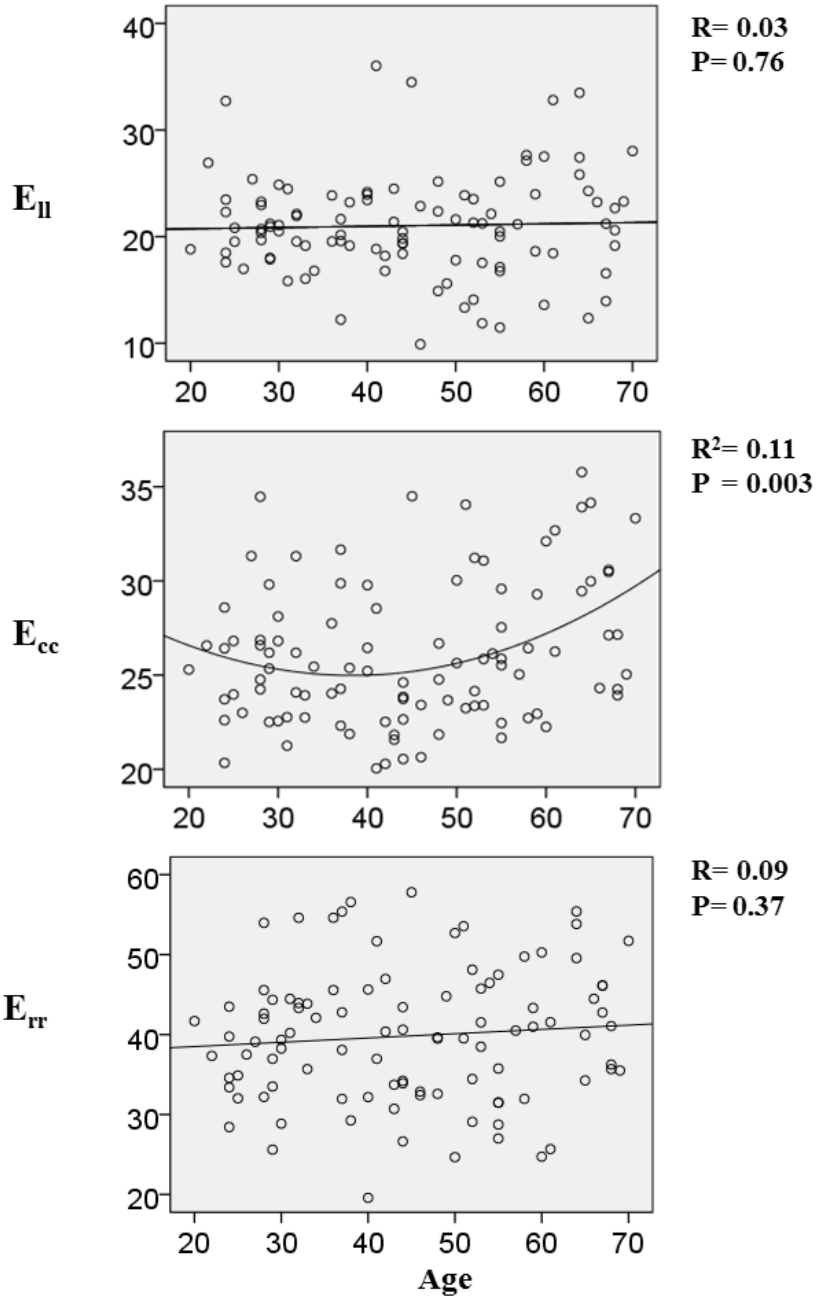

Figure 3-4. The relationship between age and myocardial strain.

These scatter diagrams show the relationship between age and peak systolic longitudinal strain (E_{ll}), peak systolic circumferential strain (E_{cc}) and peak systolic radial strain (E_{rr}). The best fit linear regression line and correlation coefficient R are shown for the relationship between age and E_{ll} and E_{rr}. The relationship between age and E_{cc} is shown as a quadratic curve as this had significantly superior modeling power.

Table 3-4. Age-adjusted mean endocardial peak systolic ε_{cc}.

Age	ε_{cc}
20	26.7
30	25.6
40	25.4
50	26.3
60	28.1
70	31.0

Age adjusted peak systolic E_{cc} calculated using the regression formula, $E_{cc} = 0.005x^2 - 0.363x + 31.94$, where x = age

Table 3-5. Regression analyses of circumferential strain and strain rate measures.

Independent variables	Peak systolic E_{cc}			Peak systolic SR_{cc}			Peak early diastolic SR_{cc}		
	R	Beta coefficient (95% C.I.)	P	R	Beta coefficient (95% C.I.)	P	R	Beta coefficient (95% C.I.)	P
UNIVARIABLE ANALYSES									
Age (yrs)	0.25	0.07 (0.2 to 0.12)	0.01	0.10	0.00 (-0.01 to 0.01)	0.89	0.10	0.00 (-0.01 to 0.00)	0.32
Sex (M=1, F=2)	0.12	0.90 (-0.60 to 2.40)	0.24	0.07	0.04 (-0.08 to 0.16)	0.49	0.13	0.09 (-0.05 to 0.23)	0.21
Height (m)	-0.14	-0.05 (-0.13 to 0.03)	0.19	0.04	0.00 (-0.01 to 0.01)	0.73	-0.12	0.00 (-0.01 to 0.00)	0.26
Weight (kg)	-0.16	-0.05 (-0.11 to 0.01)	0.13	0.00	0.00 (-0.01 to 0.01)	0.99	-0.21	-0.01 (-0.01 to 0)	0.26
BSA (kg/m^2)	-0.16	-3.2 (-7.3 to 0.90)	0.13	0.00	0.03 (-0.31 to 0.31)	0.98	-0.20	-0.38 (-0.76 to -0.01)	0.05
Heart rate (bpm)	0.06	0.02 (-0.11 to 0.03)	0.21	0.27	-0.01 (-0.01 to 0.00)	0.01	0.23	0.01 (0.00 to 0.02)	0.02
SBP (mmHg)	0.21	0.07 (0.00 to 0.13)	0.04	0.11	0.00 (0.00 to 0.01)	0.29	0.06	0.00 (0.00 to 0.01)	0.61
DBP (mmHg)	-0.06	0.03 (-0.14 to 0.08)	0.57	-0.17	-0.01 (-0.02 to 0.00)	0.10	-0.15	-0.01 (-0.02 to 0.00)	0.15
LVEDV (ml)	-0.23	-0.04 (-0.07 to -0.01)	0.02	-0.19	-0.01 (-0.01 to 0.00)	0.07	0.23	0.01 (0.00 to 0.01)	0.02
LVEDV (ml/m^2)	-0.18	-0.07 (-0.14 to 0.01)	0.08	-0.23	-0.01 (-0.01 to 0.00)	0.10	-0.09	0.00 (-0.01 to 0.01)	0.41
LVEF(%)	0.63	0.39 (0.29 to 0.49)	<0.001	0.47	0.02 (0.01 to 0.03)	<0.001	0.38	0.02 (0.01 to 0.03)	<0.001
MULTIVARIABLE ANALYSES									
Age (yrs)	0.02	0.00 (-0.07 to 0.08)	0.90	-	-	-	-	-	-
BSA (kg/m2)	-	-	-	-	-	-	-0.12	-0.19 (-0.55 to 0.18)	0.32
Heart rate (bpm)	-	-	-	0.19	-0.01(-0.01 to 0.00)	0.07	-0.15	0.00 (-0.01to 0.00)	0.15
SBP (mmHg)	0.26	0.08 (0.01 to 0.15)	0.02	-	-	-	-	-	-
DBP (mmHg)	-	-	-	0.14	0.01 (0.00 to 0.01)	0.18	-	-	-
LVEDV (ml)	-0.30	-0.50 (-0.87 to -0.01)	0.01	0.17	0.00 (0.00 to 0.01)	0.11	0.22	0.00(0.00 to 0.01)	0.07

Variables that reached a p value of <0.10 were included in multivariable models (with exception of LVEF given its correlation with strain measures.

Ecc and SRcc have been analysed as positive numbers to aid interpretation of relationships.

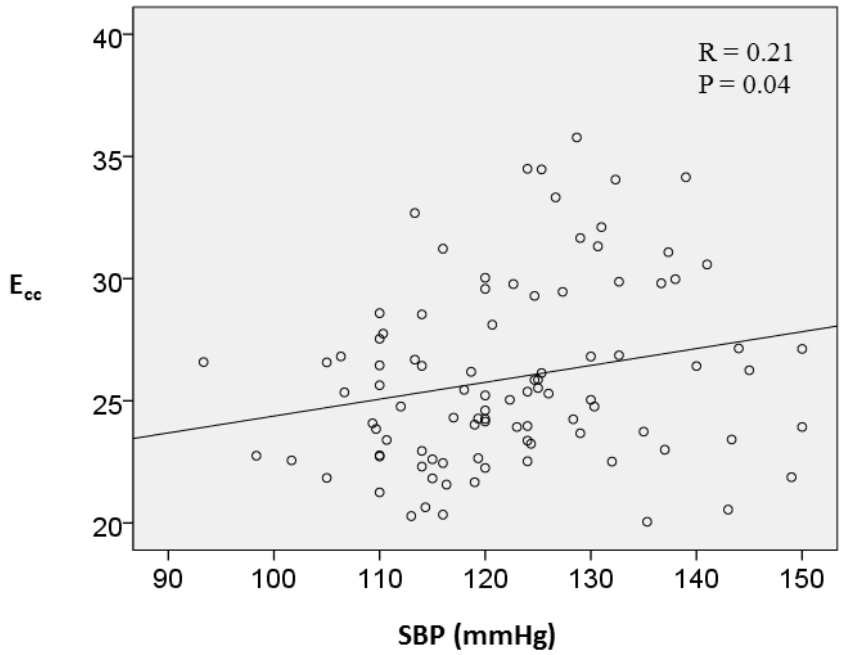

Figure 3-5. The relationship between systolic blood pressure and circumferential strain

This scatter diagram shows the relationship between systolic blood pressure (SBP) and circumferential strain (E_{cc}). The best fit linear regression line and correlation coefficient R are also shown.

systolic SR_{cc}, heart rate (p= 0.01) and LVEF (p< 0.001) emerged as predictors. For peak early diastolic SR_{cc}, body surface area (p= 0.03), heart rate (p= 0.006), LVEDV (p= 0.02) and LVEF (p< 0.001) emerged as predictors.

In **Table 3-6** we have shown that gender (p< 0.001), height (p= 0.001), weight (p= 0.009), body surface area (p< 0.001), SBP (p= 0.09), and LVEDV (p= 0.03) were all predictors of peak systolic ε_{ll} on linear regression analyses. BSA (p =0.08), then gender (p= 0.12) had the greatest influence on E_{ll} in mulitivariate modelling.

3.3.5 Reproducibility

Table 3-7 shows both intra- and inter-observer variability. On Bland-Altman analyses, peak systolic ε_{cc} had the best intra- (bias -0.34 ± 0.87, 95% C.I. -2.05 to 1.36), and inter- (bias 0.63 ± 1.29, 95% C.I. -1.90 to 3.16) observer agreement. Of the three axial strains, peak systolic ε_{rr} had the largest intra- (-0.03 ± 3.65, 95% C.I. -7.2 to 7.1) and inter- (0.13 ± 6.4, 95% C.I. -12.44 to 12.71) observer biases. All parameters had an intra-observer ICC of ≥ 0.85. All circumferential and longitudinal parameters had an inter-observer ICC of ≥ 0.85, but this coefficient was lower for radial parameters.

3.4 Discussion

In this study, we have provided normal reference values for LV myocardial strain using FT-CMR, derived from a well-characterised group of healthy individuals with tailored age and sex stratification. All circumferential and longitudinal based variables had excellent intra- and inter-observer variability, and, although agreement was less for radial parameters, these still had

Table 3-6. Regression analyses of longitudinal strain and strain rate measures.

Independent variables	Peak systolic E_{ll}			Peak systolic SR_{ll}			Peak early diastolic SR_{ll}		
	R	Beta coefficient (95% C.I.)	P	R	Beta coefficient (95% C.I.)	P	R	Beta coefficient (95% C.I.)	p
UNIVARIABLE ANALYSES									
Age (yrs)	0.03	0.01 (-0.6 to 0.08)	0.738	-0.04	0.00 (-0.01 to 0.00)	0.697	-0.34	-0.01 (-0.02 to 0.00)	<0.001
Sex (M=1, F=2)	0.35	3.39 (1.58 to 5.20)	<0.001	0.27	0.19 (0.05 to 0.33)	0.008	0.29	0.22 (0.08 to 0.37)	0.004
Height (m)	-0.35	-0.18 (-0.28 to -0.08)	0.001	-0.29	-0.01 (-0.02 to 0.00)	0.005	-0.21	-0.01 (-0.02 to 0.00)	0.048
Weight (kg)	-0.27	-0.10 (-0.18 to -0.03)	0.009	-0.17	-0.01 (-0.01 to 0.00)	0.098	-0.11	0.00 (-0.01 to 0.00)	0.298
BSA (kg/m^2)	-0.36	-9.27 (-14.20 to -4.35)	<0.001	0.26	-0.47 (-0.84 to -0.10)	0.013	-0.21	-0.40 (-0.79 to -0.01)	0.044
Heart rate (bpm)	0.16	0.07 (-0.02 to 0.16)	0.113	0.24	0.01 (0.00 to 0.01)	0.019	0.34	0.01 (0.01 to 0.02)	0.001
SBP (mmHg)	-0.18	-0.07 (-0.15 to 0.01)	0.088	-0.18	-0.01 (-0.01 to 0.00)	0.093	-0.28	-0.01 (-0.01 to 0.00)	0.007
DBP (mmHg)	-0.13	-0.09 (-0.23 to 0.05)	0.209	-0.10	-0.01 (-0.02 to 0.01)	0.350	-0.18	-0.01 (-0.02 to 0.00)	0.096
LVEDV (ml)	-0.22	-0.05 (-0.09 to 0.00)	0.030	-0.25	0.00 (-0.01 to 0.00)	0.013	-0.14	0.00 (-0.01 to 0.00)	0.170
LVEDV (ml/m^2)	-0.06	-0.03 (-0.12 to 0.07)	0.581	-0.15	-0.01 (-0.01 to 0.00)	0.151	-0.05	0.00 (-0.01 to 0.01)	0.617
LVEF(%)	0.30	0.24 (0.09 to 0.39)	0.003	0.32	0.02 (0.01 to 0.03)	0.002	0.11	0.01 (-0.01 to 0.02)	0.296
MULTIVARIABLE ANALYSES									
Age (yrs)	-	-	-	-	-	-	-0.30	-0.01 (-0.01 to 0.00)	0.006
Sex (M=1, F=2)	0.20	1.92 (-0.51 to 4.35)	0.120	0.19	0.13 (-0.05 to 0.31)	0.152	0.18	0.13 (-0.04 to 0.29)	0.135
BSA (kg/m^2)	-0.25	-6.38 (-13.41 to 0.65)	0.075	-0.11	-0.20 (-0.72 to 0.33)	0.457	-0.13	-0.25 (-0.71 to 0.22)	0.290
Heart rate (bpm)	-	-	-	0.17	0.01 (0.00 to 0.01)	0.116	0.30	0.01 (0.00 to 0.02)	0.002
SBP (mmHg)	-0.03	-0.01 (-0.10 to 0.07)	0.750	-0.05	0.00 (-0.01 to 0.01)	0.620	-0.06	0.00 (-0.01 to 0.01)	0.59
LVEDV (ml)	-0.01	0.00 (-0.05 to 0.05)	0.970	-0.08	0.00 (-0.01 to 0.00)	0.553	-	-	-

Variables that reached a p value of <0.10 were included in multivariable models (with exception of LVEF given its correlation with strain measures.

Ell and SRll have been analysed as positive numbers to aid interpretation of relationships.

DBP was excluded from the diastolic SRll multivariate model due to collinearity with SBP.

Table 3-7. Intra-observer and inter-observer variability.

Variable	Variability	Mean bias ± SD	Limits of agreement	p	Coefficient of variation (%)	Interclass correlation coefficient (95% CI)
Peak systolic E_{rr}	Intra-observer	-0.03 ± 3.65	-7.19 to 7.14	0.97	8.90	0.85 (0.66 to 0.94)
	Inter-observer	0.13 ± 6.41	-12.44 to 12.71	0.93	14.67	0.55 (0.11 to 0.81)
Peak systolic E_{cc}	Intra-observer	-0.34 ± 0.87	-2.05 to 1.36	0.09	3.55	0.96 (0.90 to 0.99)
	Inter-observer	0.63 ± 1.29	-1.90 to 3.16	0.06	4.95	0.93 (0.81 to 0.97)
Peak systolic E_{ll}	Intra-observer	-0.49 ± 1.83	-4.08 to 3.11	0.29	7.68	0.88 (0.72 to 0.96)
	Inter-observer	0.22 ± 1.13	-1.99 to 2.42	0.42	5.48	0.98 (0.94 to 0.99)
Peak systolic SR_{rr}	Intra-observer	-0.01 ± 0.14	-0.29 to 0.27	0.74	8.68	0.89 (0.74 to 0.95)
	Inter-observer	-0.03 ± 0.27	-0.56 to 0.49	0.61	15.01	0.71 (0.38 to 0.88)
Peak systolic SR_{cc}	Intra-observer	-0.02 ± 0.08	-0.18 to 0.13	0.21	5.36	0.96 (0.90 to 0.98)
	Inter-observer	0.02 ± 0.11	-0.20 to 0.23	0.56	6.68	0.94 (0.84 to 0.98)
Peak systolic SR_{ll}	Intra-observer	0.02 ± 0.18	-0.34 to 0.38	0.70	17.89	0.89 (0.72 to 0.96)
	Inter-observer	0.02 ± 0.16	-0.30 to 0.33	0.61	12.95	0.86 (0.67 to 0.95)
Peak early diastolic SR_{rr}	Intra-observer	0.03 ± 0.18	-0.33 to 0.38	0.52	11.67	0.88 (0.72 to 0.95)
	Inter-observer	-0.04 ± 0.48	-0.98 to 0.90	0.72	26.77	0.50 (0.05 to 0.78)
Peak early diastolic SR_{cc}	Intra-observer	0.00 ± 0.07	-0.13 to 0.13	0.92	5.29	0.97 (0.93 to 0.99)
	Inter-observer	-0.01 ± 0.11	-0.24 to 0.21	0.63	7.82	0.96 (0.89 to 0.98)
Peak early diastolic SR_{ll}	Intra-observer	0.05 ± 0.18	-0.30 to 0.40	0.27	14.84	0.85 (0.64 to 0.94)
	Inter-observer	0.01 ± 0.28	-0.53 to 0.55	0.90	20.99	0.85 (0.63 to 0.94)

acceptable reproducibility. Our definition of a normal range for strain and strain rate measures using FT-CMR has emerged in the context of a promising role for this technique to detect preclinical disease, as shown by stress CMR studies (Schuster et al., 2011). Further studies are undoubtedly needed to determine the role of FT-CMR in both clinical and research environments. At this stage, however, an accepted definition of normal values is paramount.

3.4.1 Normal values

There are key differences between the FT-CMR motion analysis techniques presented herein and those reported using other methodologies. In this respect, FT-CMR measures myocardial strain at both the endocardial and epicardial border, whilst speckle tracking measures strain from a region of interest within the myocardium. The presence of a transmural myocardial strain gradient is likely to confound comparisons of strain measures derived from speckle-tracking echocardiography and FT-CMR. Furthermore, there are differences between vendors of speckle-tracking echocardiography in regard to the regions at which strain is calculated. Some manufacturers derive strain from the mid-myocardium, whilst others permit endocardial and epicardial strain computation. The recently published consensus statement aims to standardise strain calculation as at present comparisons of values between software is problematic (Mor-Avi et al., 2011). To allow for such gradients, FT-CMR global peak strain was expressed as the mean strain of values derived from the endocardial and epicardial borders. Accordingly, global strain values are comparable to those reported from the largest single normal reference population (250 patients) studied with speckle tracking echocardiography which determined mid-myocardial strains. Marwick *et al* found a

mean peak systolic ε_{ll} of -18.6% compared with -19.1% in our study (Marwick et al., 2009). Mean peak systolic E_{cc} was also similar (-18.7% vs. -18.4%) and peak systolic SR_{ll} was also comparable (-1.10s^{-1} vs. -1.11s^{-1}).

Since there is no agreed normal reference range for diastolic strain parameters current consensus currently suggests restricting their use to research applications (Mor-Avi et al., 2011). Nevertheless, early diastolic strain rate is a sensitive early marker of diastolic dysfunction and provides important information about LV relaxation as well as being associated with interstitial fibrosis (Park et al., 2006). Moreover, measures of diastolic function predict incident heart failure and, therefore, carry prognostic significance (Kane GC et al., 2011). Thus far, CMR based assessment of diastolic function using myocardial tagging has been restricted by loss of tags. In contrast, FT-CMR offers a more robust method because it is not adversely affected by T1 relaxation. Our derivation of a normal reference range for early diastolic strain rate is therefore a key aspect of this study as it may have future clinical relevance. However the lower temporal resolution of CMR (25Hz in this study) compared to echocardiography raises concerns over whether any CMR based deformation algorithm is apt for the assessment of early diastolic filling which is the fastest part of the cardiac cycle. However, due to the nature of FT-CMR (like speckle tracking) the algorithms are more accurate at detecting rapid movements (there is a lower limit of pixel velocity that can be tracked from one frame to the next). Whilst increasing the frame rate beyond normal acquisition protocols would enhance the quantification of early diastolic strain rate in this population, this may actually reduce the accuracy of strain calculation because of the trade

off in spatial resolution. Further studies to elucidate the optimal spatial and temporal resolution for global and segmental strain assessment in health and disease are required.

The large standard deviation of peak strains within the normal population is similar to that reported with other methodologies (Yingchoncharoen et al., 2013). In view of the small measurement bias for repeated measures (both inter- and intra-observer) in our cohort, and the reported good intra-subject reproducibility in global measures with repeated imaging (Morton et al., 2012), this large spread within this population is likely due to normal biological variation.

3.4.2 Effects of age and sex on strain

Our findings of greater longitudinal deformation in women (but similar circumferential deformation) corroborate with those of Augustine *et al.* who have recently reported on strain values in 116 healthy subjects (Augustine et al., 2013). Their study comprised young healthy volunteers with a narrow age distribution (age 29 ± 7 yrs). Our study also shows that these gender variations persist across a broad age spectrum. Moreover, we also report an age related change in circumferential strain, which is in keeping with a recent 3D speckle tracking echocardiography study (Kleijn et al., 2014). In accordance with this, an age-related increase in LV torsion has been recognised, although the biomechanical reasons for this are still debated (Yoneyama et al., 2012). Our multivariable regression analyses suggest that age related changes in LVEDV and SBP (even within a normotensive population) are important factors in this respect. On the other hand, we have not shown any age-dependent variations in longitudinal strain. This is in contrast with Kuznetsova *et al.*(Kuznetsova et al., 2008) who

reported a decrease in the magnitude of longitudinal strain, associated with ageing, measured using tissue Doppler imaging in a mixed population of healthy individuals and hypertensive patients. Dalen *et al.* (Dalen et al., 2010) also reported an inverse relationship between age and longitudinal strain measured using tissue Doppler imaging in a large population of healthy individuals. Importantly, however, myocardial strain measured using tissue Doppler imaging is not necessarily comparable to speckle-tracking imaging. Notwithstanding, our findings of an absence of age-dependent variations in longitudinal myocardial strain is in keeping with the aforementioned speckle tracking imaging study (Marwick et al., 2009).

3.4.3 Reproducibility and feasibility

In the present study, the best reproducibility was obtained for peak systolic ε_{cc}, followed by peak systolic ε_{ll} and then peak systolic $\varepsilon_{rr.}$ Acceptable intra- and inter-observer agreement was also found for strain rate, in particular for peak systolic and peak early diastolic SR_{cc}. This is consistent with the findings of Morton *et al*., who found that circumferential strain had the best inter-study variability on three serial CMR acquisitions over one day (Morton et al., 2012). Conversely, radial strain had the lowest reproducibility. This may relate to the fact that, as opposed to circumferential strain, radial strain is derived from both endocardial and epicardial motion and, therefore, its quantification relies on the simultaneous tracking of two regions of interest. In this respect, the contrast in signal intensity at the epicardial border is less prominent than that at the endocardial border. This is a likely cause for the comparatively low reproducibility of radial strain.

Reproducibility does not necessarily equate to accuracy. Theoretically any myocardial deformation algorithm could repeatedly quantify strain with a similar but inaccurate result. The robust reproducibility of this myocardial deformation algorithm may be a result of its highly automated process and background smoothing utilised. The agreement with myocardial tagging demonstrated in chapter 2 is reassuring. Peak systolic ε_{cc} can be measured with good agreement and peak systolic ε_{ll} with satisfactory agreement compared to the 'gold standard' myocardial tagging techniques (Hor et al., 2010; Moody et al., 2015). Validation of any radial parameters is more challenging as this is generally less accurately quantified by all deformation algorithms. The 'acid test' for this modality will be whether it can be used to assess pre-clinical disease and these normal values will be beneficial in this respect.

As we have learnt from myocardial tagging, proving feasibility is a necessary step in the development of a clinically applicable imaging modality. In this study, we were able to track 100% of available segments. This is a potential advantage of FT-CMR over echocardiography, insofar as the latter is limited by foreshortening at the apex and 'drop-out' of the apical and anterolateral segments on the apical views. In addition, the sector widths required to image dilated hearts during echocardiography often result in frame rates that are suboptimal for speckle-tracking.

3.4.4 Clinical and research applications

FT-CMR tracks the movement of anatomical structures over time. Tissue inhomogeneities and their variance in signal are important in this regards. Whilst the prominent differences

in signal intensity between the myocardial and blood interface means this methodology is well suited to measuring global strains, motion components parallel to tissue boundaries are more disposed to noise than perpendicular motions and agreement for regional measures is more modest (Harrild et al., 2012; Wu et al., 2014). Thus with its rapidity to execute and the lack of requirement of specialised acquisitions, FT-CMR lends itself to clinical use more favourably than myocardial tagging. An ideal example is the serial assessment of patients undergoing cytotoxic chemotherapy (Thavendiranathan et al., 2014). New guidelines for cardio-oncology mandate the reporting of global longitudinal strain (Plana et al., 2014), and FT-CMR may be appropriate for patients in whom poor acoustic windows prevent repeated speckle tracking echocardiography. However, when the assessment of regional function is required, such as for the assessment of regional ischaemia, the differentiation of adjacent regions of myocardium provided by myocardial tags gives this clear advantages over FT-CMR.

Likewise, speckle tracking echocardiography tracks acoustic interference patterns that are within the myocardium so is better suited to the regional assessment of function than FT-CMR. Neither CMR based methodology can rival the much wider availability or speed of acquisition of echocardiographic based measures. The disadvantages of speckle tracking have already been highlighted.

One attraction of FT-CMR is that cine images do not need any prior manipulation at acquisition equivalent to the myocardial tagging required to facilitate HARP or SPAMM analysis. In addition to saving time this permits the retrospective study of cohorts. However,

such historical data may have suboptimal frame rates for use with the FT-CMR algorithm. Caution is required if such cohorts are compared to the normal values presented within.

3.4.5 Limitations

Our 100% yield relates to the high quality of our SSFP cines, and we acknowledge that the same image quality will not always be obtainable in a clinical environment, not least because arrhythmias may interfere with ECG gating. However, the diagnostic yield reported here compares favourably to that achieved by Marwick et al. who only obtained diagnostic quality images in 79% of healthy enrollees whilst compiling normal values for speckle tracking (Marwick et al., 2009). We present mean segmental values for circumferential but not longitudinal strain as sagittal left ventricular outflow tract cines were not part of our acquisition protocol. Regardless, the margin of error for population mean peak systolic segmental circumferential strains was more than double that for global values, and this will limit their practicality.

Our finding that ε_{cc} was lower in the mid-cavity than at the base is in contrast to tagging studies (Moore et al., 2000a). Although we cannot be assured of the reason for this discrepancy, it is plausible that, despite our slice selection protocol which was designed to negate the influence of through plane distortion from the LV outflow tract, this was an issue; limitations of the software that would account for this are considered in more detail in **2.4.4**.

3.5 Conclusions

We have defined normal values for strain for healthy individuals using FT-CMR. Undoubtedly, this technique will undergo refinements in the future, as data from different disease groups and applications emerge. As with any imaging modality, normal values may vary according to software manufacturer and particular algorithms. It is imperative, therefore, that values quoted herein are expressed in the context of the technology used in the present study.

4 FEATURE-TRACKING CARDIOVASCULAR MAGNETIC RESONANCE AS A NOVEL TECHNIQUE FOR THE ASSESSMENT OF MECHANICAL DYSSYNCHRONY

Principal hypothesis: FT-CMR derived dyssynchrony parameters can act as a biomarker to discriminate between healthy controls and patients with NICM.

4.1 Introduction

The myocardium is a complex, three-dimensional structure in which motion occurs in radial, circumferential and longitudinal directions. These motions are dependent on the intimate interplay between electrical activation and myocardial function. Disturbances of the conducting system or myocardial function can lead to an increase in the temporal dispersion of contraction and relaxation, or dyssynchrony. It is well established that dyssynchrony can leads to myocardial inefficiencies (Prinzen et al., 1990), reduced cardiac output (Park et al., 1985) and cardiac remodeling (Burkhoff et al., 1986).

The assessment of cardiac dyssynchrony has been the focus of increasing attention in the past decade, particularly with the advent of CRT. The concept that pre-implant dyssynchrony is pre-requisite for a benefit from CRT has driven an extensive array of imaging studies. However, the expectation that dyssynchrony measures might predict the response to, or the outcome from CRT (Bax et al., 2004; Pitzalis et al., 2002; Yu et al., 2003b), was not supported by multicenter studies (Chung et al., 2008; Conca et al., 2009; Hawkins et al., 2009; Marwick, 2008). The inability of operators to obtain the various dyssynchrony measures, the inordinately high inter-operator variability, as well as the large overlap in

values between patients with cardiac disease and healthy controls (Chung et al., 2008) are prominent obstacles to the application of dyssynchrony measures in clinical practice.

FT-CMR is the recently developed CMR-equivalent of speckle-tracking echocardiography (Hor et al., 2011). Chapter 2 establishes that it is accurate when compared against myocardial tagging using SPAMM. Furthermore, its superior time efficiency and reproducibility are attractive attributes for clinical practice. In theory, FT-CMR can be used to derive dyssynchrony measures, such as the circumferential uniformity ratio estimate (CURE) and the radial uniformity ratio estimate (RURE), both of which reflect the regional heterogeneity of strain throughout the cardiac cycle. An important aspect of any biomarker is the ability to discriminate between a disease entity and healthy control subjects. The chapter explores whether CURE and RURE derived from FT-CMR can discriminate between healthy controls and patients with NICM.

4.2 Methods

4.2.1 Study population

Healthy controls. Healthy control subjects were identified from a prospective controlled observational research study examining the effects of living kidney donation on cardiovascular structure and function (NCT01769924) (Moody et al., 2014) and are described in detail in **3.2.1**.

NICM subjects. Patients with NICM were enrolled through the heart failure clinic at the regional tertiary centre as part of a prospective investigation into the mechanical effects of

midwall fibrosis on cardiac mechanics. Inclusion criteria were as follows: adults aged of 18 or over with a diagnosis of NICM made on the basis of clinical features plus echocardiographic evidence of LV systolic impairment; Exclusion criteria: hypertrophic or restrictive cardiomyopathy; Coronary artery disease on invasive coronary angiography thought to be sufficient to account for the reduced left ventricular systolic function; transmural or subendocardial LGE pattern consistent with a coronary territory. Coronary angiography was not mandated in all patients, but LGE-CMR was prerequisite for inclusion. All participants gave written informed consent, and the study protocol conforms to the ethical guidelines of the 1975 Declaration of Helsinki as reflected in a priori approval by the National Research Ethics Service.

4.2.2 CMR acquisition

This was performed with a 1.5 Tesla scanner (Magnetom Avanto, Siemens, Erlangen, Germany) as described in section **2.2.2**, although only the cines comprising the short axis stack were utilised for this study.

4.2.3 CURE and RURE

Feature tracking of each SSFP cine of the short axis stack (as described in **3.2.4**.) was used to obtain circumferential and radial strain data along the evenly spaced circumferential segments of a short-axis slice. The user-interface of the FT-CMR platform provides regional strains derived from six equal myocardial segments. Each regional strain is derived from the mean strain from a number of points and this more comprehensive dataset can be

downloaded as a text file. Strain was determined at 48 evenly distributed segments around each slice over the full cardiac cycle.

As shown in **Figure 4-1,** the CURE and RURE are ratios of the spatial uniformity of strain, averaged over time and over all available slices (Helm et al., 2005; Leclercq et al., 2002). These measures assume that, in a perfectly synchronous heart, strain is the same across all segments. In a dyssynchronous heart, strain changes along the circumference, with opposing walls having opposing strain. In a Fourier space, the zero Fourier coefficient A_0 equals the mean strain over all segments, and the modulus of the first Fourier coefficient A_1 equals the sinusoidal amplitude of the strain along all segments, which reflects the discordance of opposing myocardial walls. The CURE and RURE ratios normalise the A_0 amplitude to the total (A_1 and A_0) signal, so that the measures range between 0 (complete dyssynchrony) and 1 (perfect synchrony). Intuitively, a dyssynchrony score that reflects dyssynchrony in both radial and circumferential directions may be more sensitive than one based solely on one direction. On this basis, we also derived the average of CURE and RURE (CURE:$RURE_{AVG}$) to provide an index that reflects both radial and circumferential synchrony.

4.2.4 Statistical methods

Continuous variables are expressed as mean $\pm$ SD. Normality was tested using the Shapiro-Wilk test. Comparisons between continuous variables were made using independent samples t-tests. Pearson's correlation coefficient was used to explore the relationship between CURE and RURE and baseline variables. Receiver-operator characteristics (ROC) curves were constructed to assess the ability of the dyssynchrony measures to discriminate

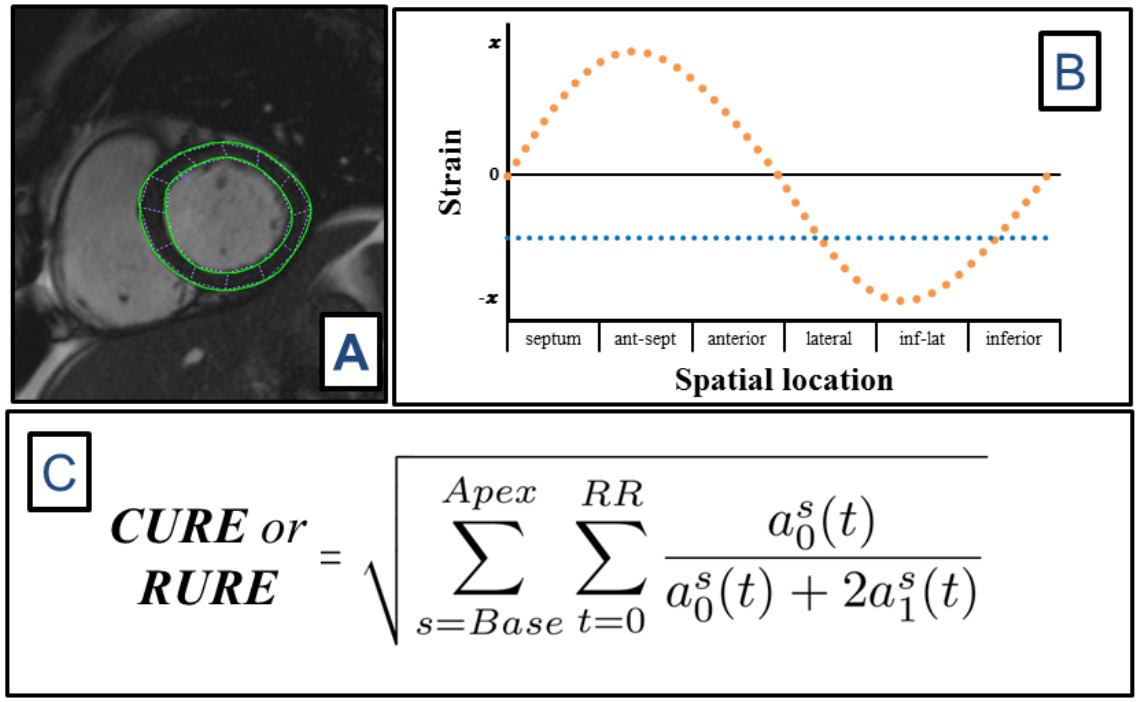

Figure 4-1. Derivation of CURE and RURE.

Tile A shows a basal short axis slice in FT-CMR, with endocardial and epicardial borders traced at end-diastole. This facilitates the calculation of both circumferential and radial strain at 48 evenly spaced regions at each time point. In tile B, these strain measures (at one time point) have been plotted against spatial location. The two hypothetical plots demonstrate perfect synchrony (blue) with all points having identical strains, and perfect dysynchrony (orange) where opposite points have opposite strains. Tile C shows the formula for derivation of CURE or RURE, where a0 and a1 are the zero and first order terms from Fourier analysis of the time-strain graphs, respectively. The final value is an average over time (t) and space (s).

between the groups. Differences between the ROCs were compared using the technique of DeLong (DeLong et al., 1988). Optimal cut-offs for each measure were calculated affording equal value to sensitivity and specificity. Logistic regression analyses were used to explore whether the relationship between the dyssynchrony measures was independent of QRS duration. For the assessment of intra- and inter-observer variability, agreement was tested by calculating mean bias and 95% limits of agreement (confidence intervals) from Bland-Altman analyses. A p value of < 0.05 was considered statistically significant. Statistical analyses were performed using SPSS v21.0. (SPSS Inc. Chicago, Illinois) and MedCalc v12. (MedCalc, Broekstraat, Belgium).

4.3 Results

4.3.1 Baseline variables

There were significant differences between healthy controls (n=55, aged 42.9 ± 13 years) and patients with NICM (n=108, aged 64.7 ± 12 years) for all baseline variables (**Table 4-1**). Healthy subjects had a QRS<120 ms, whereas 66% of patients with NICM had a QRS duration ≥120ms. CURE (0.79 ± 0.14 vs. 0.97 ± 0.02), RURE (0.71 ± 0.14 vs. 0.91 ± 0.04) and CURE:$RURE_{AVG}$ (0.75 ± 0.12 vs. 0.94 ± 0.02) were lower in NICM than in healthy controls ($p<0.0001$ for all) (**Figure 4-2**).

4.3.2 Correlates of CURE and RURE

As shown in **Table 4-2**, neither CURE nor RURE correlated with age in either control subjects or in patients with NICM. Whilst no significant correlations emerged between the three dyssynchrony measures and LVEF or LVEDV in healthy controls, significant correlations were

Table 4-1. Baseline characteristics.

	Healthy controls	Patients with NICM	P
N	55	108	
Age (yrs)	42.9±13	64.7±12	<0.001
Gender (male)	29 (55)	73 (68)	0.06
NHYA functional class			
I	-	14 (13)	
II	-	28 (26)	
III	-	53 (49)	
IV	-	13 (12)	
Medication			
Loop diuretics	-	92 (85)	
ACE-I or ARB	-	102 (94)	
Beta-blockers	-	76 (70)	
Aldosterone antagonists	-	55 (51)	
QRS (ms)	88 ± 9	147 ± 29	<0.001
CMR variables			
LV mass (g)	119 ± 30	139 ± 30	0.046
LVEDV(ml)	122 ± 26	237 ± 87	<0.001
LVESV (ml)	36 ± 14	176 ± 89	<0.001
LVEF (%)	70 ± 5	29 ± 13	<0.001
Dyssychrony measures			
CURE	0.97 ± 0.02	0.79 ± 0.14	<0.001
RURE	0.91 ± 0.04	0.71 ± 0.14	<0.001
CURE:$RURE_{AVG}$	0.94 ± 0.02	0.75 ± 0.12	<0.001

Continuous variables are expressed as mean ± SD. Categorical variables are expressed as n (%)

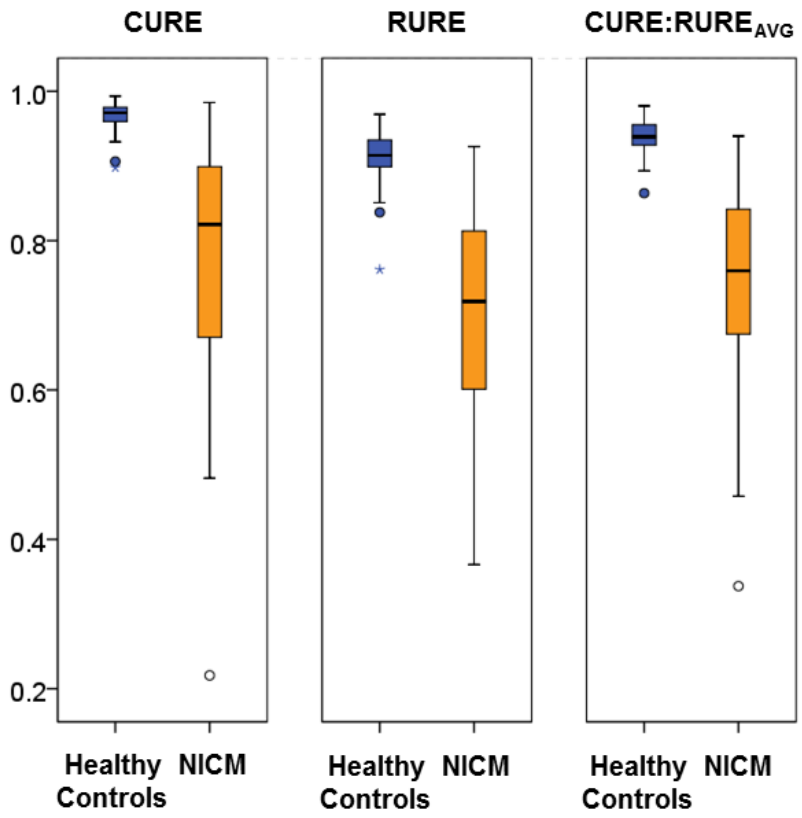

Figure 4-2. Boxplots of dyssynchrony measures.

Comparison of (a) CURE, (b) RURE, (c) CURE:RURE$_{AVG}$ in patients with NICM and healthy controls. The middle horizontals of the boxes represent the median values, the upper and lower horizontals represent the upper and lower interquartile points, respectively. The horizontal lines on the whiskers represent the extreme values not deemed to be outliers. Outliers are defined as values greater than 1.5 times the interquartile range from the interquartile value, and are shown as individual points.

Table 4-2. Correlates of dyssynchrony measures.

	Healthy controls			Patients with NICM			All		
	CURE	RURE	CURE:$RURE_{AVG}$	CURE	RURE	CURE:$RURE_{AVG}$	CURE	RURE	CURE:$RURE_{AVG}$
Age (yrs)	0.21	0.10	-0.09	-0.06	-0.13	0.12	-0.36	0.44	0.45
	(0.13)	(0.46)	(0.50)	(0.52)	(0.18)	(0.24)	(<0.001)	(<0.001)	(<0.001)
QRS (ms)	0.32	0.20	0.23	-0.21	-0.42	-0.38	-0.53	-0.67	-0.66
	(0.83)	(0.19)	(0.12)	(0.04)	(<0.001)	(<0.001)	(<0.001)	(<0.001)	(<0.001)
LVEF (%)	0.26	0.00	-0.04	0.35	0.59	0.55	0.66	0.78	0.80
	(0.06)	(0.99)	(0.79)	(<0.001)	(<0.001)	(<0.001)	(<0.001)	(<0.001)	(<0.001)
LVEDV (ml)	0.14	0.06	0.06	-0.34	-0.47	-0.48	-0.58	-0.67	-0.69
	(0.30)	(0.65)	(0.67)	(0.001)	(<0.001)	(<0.001)	(<0.001)	(<0.001)	(<0.001)

Pearson's correlation coefficient for the correlation between dyssynchrony variables and other baseline variables.

The P value for each analysis is presented in parentheses.

found in both the entire cohort (**Figure 4-3**) and patients with cardiomyopathy. In the latter, CURE, RURE and CURE:$RURE_{AVG}$ correlated positively with LVEF and negatively with LVEDV (all $p< 0.05$).

4.3.3 Relationship between CURE, RURE and QRS duration

Neither CURE, RURE or CURE:$RURE_{AVG}$ correlated with QRS duration within the healthy population, in whom there was minimal variance in the range of QRS duration. All dyssynchrony parameters correlated with QRS duration within the cardiomyopathy population; RURE ($r= -0.42$, $p= <0.001$) was a stronger negative correlate of QRS duration than CURE ($r= -0.21$, $p=0.04$). The relationship between dyssynchrony parameters and QRS duration was not strengthened when only considering individuals in sinus rhythm (CURE: $r= -0.18$, $p=0.12$; RURE: $r= 0.34$, $p=0.003$).

4.3.4 Discriminatory ability of CURE and RURE

Figure 4-4 shows receiver operating characteristic (ROC) curves for the ability of each of the dyssynchrony measures to discriminate between NICM and healthy controls. In line with the traditional academic point system (Metz, 1978), both CURE (area under ROC [AUC]: 0.96, 95% confidence interval [C.I.] 0.93 to 0.99) and RURE (AUC : 0.96, 95% C.I. 0.93 to 0.99) had an excellent ability to discriminate between patients with NICM and healthy control subjects. No differences emerged between the AUC for CURE and RURE ($p = 0.88$). The AUC for CURE:$RURE_{AVG}$ (0.98, 95% C.I. 0.96 to 1.00), however, was greater than that of RURE ($p = 0.03$), but not that of CURE ($p = 0.13$). Cut-off values with the best discrimination between patients with NICM and healthy controls are shown in **Table 4-3.**

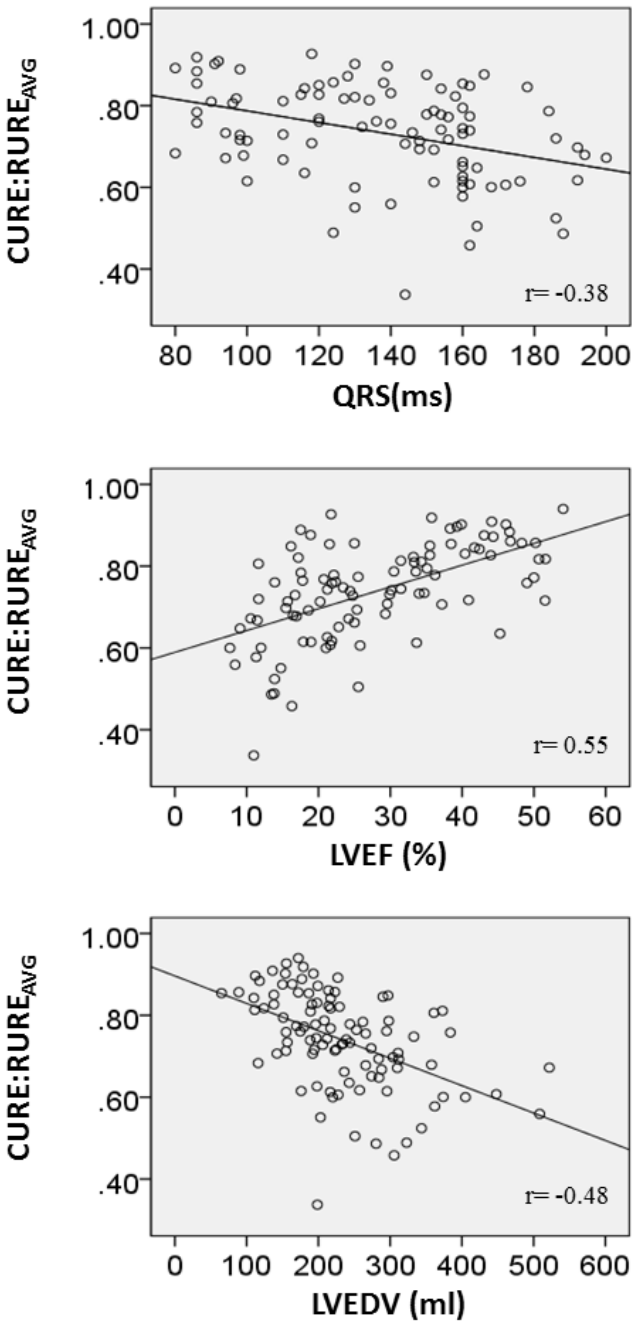

Figure 4-3. Correlates of dyssynchrony.

Scatter diagrams showing the relationship of CURE:RUREAVG in relation to a) QRS, b) LVEF, and c) LVEDV in patients with non-ischaemic cardiomyopathy

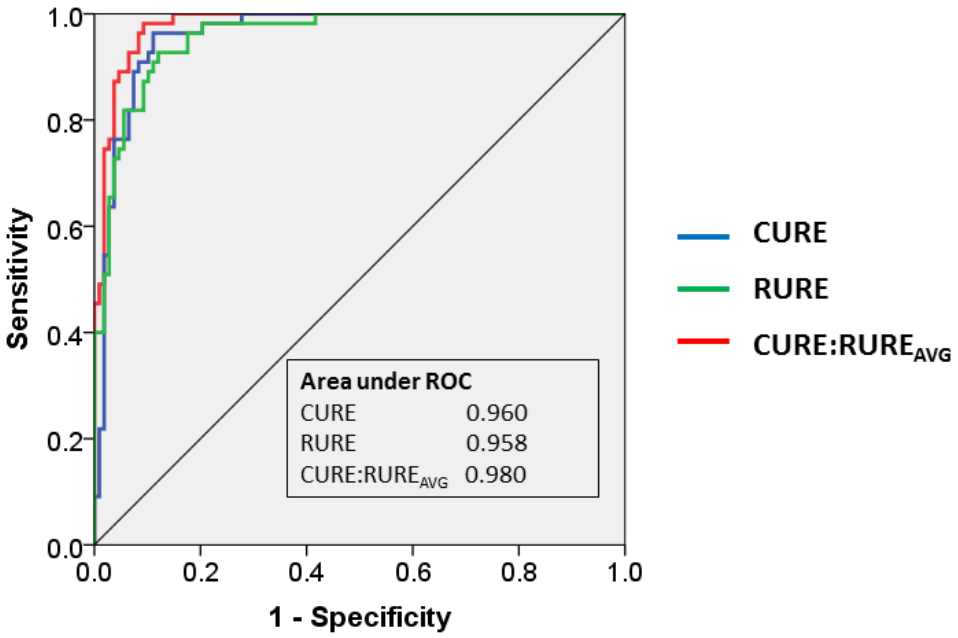

Figure 4-4. Receiver operator characteristics for each dysynchrony measure to discriminate between NICM and healthy controls.

ROC curves for CURE, RURE and CURE:RURE$_{AVG}$ are shown.

Table 4-3. Optimal cut-offs for dyssynchrony measures.

Test	Optimal cut-off	Sensitivity (%)	Specificity (%)	Positive predictive value (%)	Negative predictive value (%)
CURE	0.93	88	96	98	80
RURE	0.87	89	91	95	81
CURE:$RURE_{AVG}$	0.89	90	98	99	83

These relate to the ability of each measure to discriminate between patients and healthy control subjects.

As shown in **Table 4-4**, CURE, RURE and CURE:$RURE_{AVG}$ emerged as strong predictors of cardiomyopathy. In multivariable analyses, CURE (p = 0.001), RURE (p = 0.001) and CURE:$RURE_{AVG}$ (p = 0.006) were able to discriminate between patients with NICM and healthy controls, independent of age and QRS duration.

4.3.5 Dyssynchrony and normal QRS

Amongst patients with NICM, RURE (p < 0.001) and CURE:$RURE_{AVG}$ (p = 0.001), but not CURE (p = 0.14) were lower in patients with electrical dyssynchrony (QRS≥120ms) (**Table 4-5**). As shown in **Figure 4-5**, most patients with NICM and a QRS ≥120ms had both circumferential (95%) and radial (92%) mechanical dyssynchrony, defined as a CURE ≤0.93, or a RURE ≤0.87. Similarly, most patients with NICM and a QRS<120 ms also had circumferential (84%) and radial (91%) dyssynchrony.

4.3.6 Yield and reproducibility

FT-CMR was possible in all patients with NICM and controls recruited into this study. Twenty randomly selected scans of patients with NICM were tracked by two investigators with 4 months (R.J.T.) and 1-month (C.M.) experience in FT-CMR. Bland-Altman analyses were used to compare inter-observer variability for both CURE and RURE. For CURE, the mean bias was 0.003 ± 0.43 (95% CI: -0.08 to 0.09). Almost identical agreement was demonstrated for RURE (mean bias of -0.001 ± 0.44 [95% CI: -0.09 to 0.08]).

Table 4-4. Logistic regression of variables in relation to their ability to differentiate between healthy controls and patients with cardiomyopathy.

	Odds ratio (95% CI)	P
Univariable analyses		
Age	1.10 (1.07-1.13)	<0.001
QRS	1.12 (1.07-1.17)	<0.001
CURE	0.53 (0.42-0.66)	<0.001
RURE	0.67 (0.58-0.78)	<0.001
CURE:$RURE_{AVG}$	0.50 (0.38-0.67)	<0.001
Multivariable analyses		
Model 1		
Age	1.02 (0.96-1.08)	0.53
QRS	1.09 (1.01-1.17)	0.03
CURE	0.58 (0.42-0.80)	0.001
Model 2		
Age	1.05 (0.99-1.11)	0.14
QRS	1.14 (1.03-1.27)	0.009
RURE	0.63 (0.48-0.83)	0.001
Model 3		
Age	1.00 (0.93-1.07)	0.99
QRS	1.16 (1.02-1.32)	0.03
CURE:$RURE_{AVG}$	0.38 (0.19-0.76)	0.006

Uniformity ratio estimates have been entered into logistic regression equations as percentages (0%: perfect dyssynchrony; 100%: perfect synchrony).

Encoding for the dependent variable (disease state) was : healthy control = 0, NICM =1.

Table 4-5. Dyssynchrony measures in patients with cardiomyopathy, according to QRS duration.

Measure	QRS < 120 ms	QRS ≥ 120 ms	P value
CURE	0.81 ± 0.15	0.76 ± 0.14	0.14
RURE	0.77 ± 0.09	0.66 ± 0.14	<0.001
CURE:$RURE_{AVG}$	0.79 ± 0.09	0.71 ± 0.12	0.001

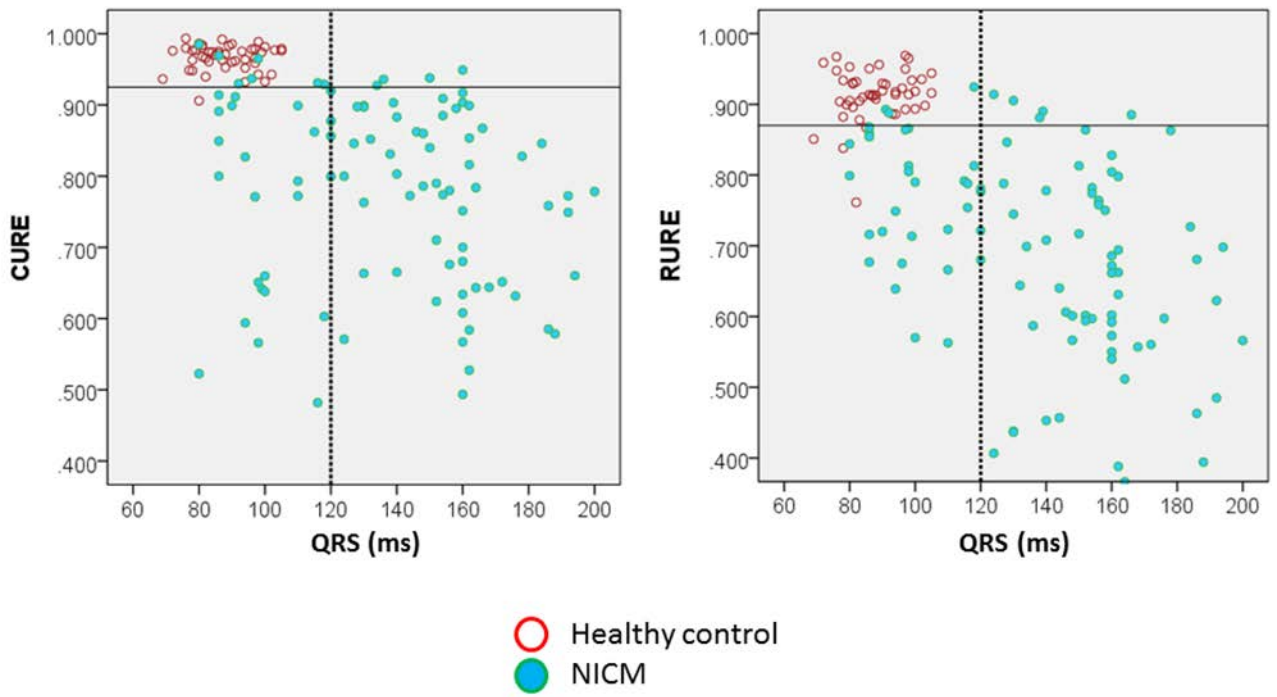

Figure 4-5. Relationship between mechanical and electrical dyssynchrony.

Scatterplot for CURE and RURE against QRS in both healthy controls and patients with NICM. The vertical references mark the conventional discriminator for electrical dyssynchrony (QRS ≥120 ms). The horizontal reference lines mark the optimal cut-offs derived from ROC analyses for each measure.

4.3.7 Rapid assessment of CURE and RURE

The dyssynchrony measures described herein are based on semi-automatically tracking an average of 6.4 ± 1.1 slices per LV stack. The time taken for tracking all short axis slices was 5.9 ± 1.4 mins. We re-calculated CURE and RURE in a sub-group of 50 patients with NICM, based solely on tracking 3 slices (apical, mid and basal). In Bland-Altmann analyses, there was close agreement between the full model and the rapid method for both CURE (bias 0.005 ± 0.05 and 95% C.I. -0.092 to 0.102) and RURE (bias 0.010 ± 0.05 and 95% C.I. -0.091 to 0.112). Using this rapid method time taken was reduced to 3.1 ± 0.8 mins.

4.4 Discussion

4.4.1 Major findings

We have shown that Fourier-based dyssynchrony measures derived from FT-CMR, namely CURE and RURE, provide almost absolute discrimination between patients with NICM and healthy control subjects, independent of age and QRS duration. Important aspects of these measures are the rapidity of post-processing and the fact that they are based on SSFP imaging, which is part of a routine CMR scan.

4.4.2 FT-CMR vs myocardial tagging

CURE and RURE can be calculated from any imaging technique that analyzes wall motion. Our results are of importance in the context of a study of 20 CRT candidates, in which CURE, derived from myocardial tagging, predicted improvements in functional capacity after CRT (Bilchick et al., 2008). Although myocardial tagging is the gold-standard for the assessment

of myocardial motion, it has not gained popularity in clinical practice. This has been due to the need for specialised tagging sequences and lengthy breath-holds, and to the laborious and time-consuming post-processing involved. In contrast, FT-CMR requires no acquisitions other than a SSFP sequence, the 'workhorse' sequence in CMR. As a further advantage over SPAMM, with which myocardial tags fade toward the end of diastole, FT-CMR permits measurement of motion and strain throughout the cardiac cycle.

If QRS duration and dyssynchrony parameters demonstrated perfect negative association, this would imply that the assessment of mechanical dyssynchrony was futile as it comprises no additional information. Undoubtedly, an association between these parameters is anticipated, and provides one potential inspection of this novel technique. The association between CURE and QRS duration in this study (r= -0.21) is weaker than that reported within an analogous population using myocardial tagging (r= -0.58) (Bilchick et al., 2008). This may indicate that some of the sophistication of this Fourier transformation based index has been lost due to the comparative crudeness of FT-CMR. Radial based Fourier measures are not previously described in humans, but it is encouraging that the association of RURE with QRS duration was stronger than that seen with CURE and closer to that predicted.

4.4.3 Yield and reproducibility

The PROSPECT investigators found that the ability to obtain dyssynchrony measures was poor, even in elite centers that had served as echocardiographic core laboratories in other studies (Chung et al., 2008). In this study, CURE and RURE were obtained in 100% of patients with NICM and healthy controls. In agreement with other studies (Morton et al., 2012), we

have found that CURE and RURE derived using FT-CMR have an excellent inter-observer reproducibility. This may relate to the fact that the method is semi-automated, requiring the operator to manually delineate contours on only one phase (end-diastole) per slice, leaving the software to automatically delineate contours in other phases. This, combined with the high spatial resolution of SSFP CMR, may contribute to the low interobserver variability.

4.4.4 Rapidity of acquisition and post-processing

We have found that operators were able to quantify CURE and RURE after only 1 to 4 months training in FT-CMR. Moreover, post-processing was as short as 6 min for a whole short-axis stack and 3 min for 3 short-axis slices. Although we have not compared FT-CMR with other CMR techniques, it is well recognised that myocardial tagging with HARP as well as Displacement Encoding with Simulated Echoes (DENSE) involve laborious post-processing. This also applies to some echocardiographic techniques. For example, the standard deviation of the time-to-peak systolic motion derived from tissue Doppler imaging involves manually identifying and computing myocardial wall motion peaks in 12 myocardial segments (Yu et al., 2002). In contrast, the FT-CMR described herein, together with the Fourier transformation-based indices such as CURE and RURE, do not involve time-consuming manual selection of motion or strain peaks.

4.4.5 Dyssynchrony and narrow QRS duration

In the field of CRT, there is a debate as to how measures of mechanical dyssynchrony, rather than electrical dyssynchrony, can help predict clinical outcome. Major outcome trials of CRT, such as CARE-HF (Cleland et al., 2005), adopted a QRS > 120 ms as an arbitrary surrogate

marker of electrical dyssynchrony. Echocardiographic (Haghjoo et al., 2007; Takemoto et al., 2007; Yu et al., 2003a) and radionuclide phase analysis (Marcassa et al., 2007) studies, however, have shown that that mechanical dyssynchrony is also present in patients with a QRS ≤120 ms. Cardiovascular magnetic resonance has shown that intraventricular dyssynchrony is almost universal in patients with heart failure, regardless of QRS duration (Chalil et al., 2007b; Foley et al., 2009a). This is consistent with the present study, in which most patients with NICM and a QRS<120 ms had circumferential (84%) and radial (91%) dyssynchrony. Despite this, in the RethinQ study, in which 172 patients with heart failure and a QRS duration < 130 ms were randomly assigned to CRT-defibrillation or implantable cardioverter defibrillator therapy (Beshai et al., 2007), CRT did not lead to an improvement in the peak VO_2 during cardiopulmonary exercise testing. In the light of observational studies (Achilli et al., 2003; Bleeker et al., 2006a; Foley et al., 2011b; Yu et al., 2006), some have proposed that mechanical dyssynchrony may help to identify patients with a QRS<120 ms who may respond to CRT. The role of FT-CMR in this context remains to be explored.

4.4.6 Study limitations

Our two cohorts are heterogeneous in terms of age. This led to a spurious correlation between age and dyssynchrony measures. However, this correlation was not present when healthy controls or patients were analysed as individual cohorts. Similarly, multivariate models showed that age had no discriminative ability between health and disease.

4.5 Conclusions

Dyssynchrony measures derived from FT-CMR, such as CURE and RURE, provide almost absolute discrimination between patients with NICM and healthy control subjects. This, together with rapidity of post-processing, the fact that these measures do not require specialized CMR sequences and excellent inter-operator reproducibilty offers potential for FT-CMR as a clinically applicable imaging modality for the assessment of mechanical dyssynchrony. An important focus will be its ability to contribute to patient selection for CRT.

5 LEFT VENTRICULAR MIDWALL FIBROSIS AS A PREDICTOR OF MORTALITY AND MORBIDITY AFTER CARDIAC RESYNCHRONISATION THERAPY IN PATIENTS WITH IDIOPATHIC DILATED CARDIOMYOPATHY

Principal hypothesis: In a IDCM population of guideline driven CRT recipients, the presence of pre-implant left ventricular midwall fibrosis is associated with an increased risk of mortality post-implant.

5.1 Introduction

CRT has revolutionised the treatment of selected patients with HF (Bristow et al., 2004; Cleland et al., 2005; Gervais et al., 2009; Moss et al., 2009). The clinical outcome of CRT, however, is influenced by the underlying aetiology of HF, with an ischaemic aetiology being associated with a worse outcome (Barsheshet et al., 2011; Gasparini et al., 2003; Wikstrom et al., 2009). This outcome has been linked to the extent (burden) and location of myocardial scarring (Adelstein et al., 2007; Bleeker et al., 2006b; Chalil et al., 2007a; Chalil et al., 2007c; Leyva et al., 2011).

In ICM, fibrosis usually follows a subendocardial or transmural distribution, in line with the perfusion territories of epicardial coronary arteries. In IDCM, fibrosis tends to be patchy, subepicardial, or midmyocardial in distribution (Gottlieb et al., 2006; Mahrholdt et al., 2004; McCrohon et al., 2003). It has been shown that non-CRT patients with IDCM and midwall fibrosis have a higher risk of mortality and unplanned hospitalisations, as well as a higher risk of sudden cardiac death (Assomull et al., 2006). We hypothesised that in patients with IDCM,

the presence of LV midwall fibrosis, assessed using LGE-CMR imaging, predicts the clinical outcome of CRT.

5.2 Methods

5.2.1 Study population

This retrospective analysis was conducted on a historical prospectively followed cohort of consecutive heart failure patients (n= 258) who had undergone successful CRT implantation with pre-implant CMR imaging (mean: 1.1 month pre-implant; range: 1 day – 3.2 months). All patients were recruited from a dedicated heart failure service at a single centre (Good Hope Hospital, Birmingham) between October 2000 and September 2009.

Inclusion criteria were as follows: clinical HF with NYHA class II-IV symptoms diagnosed on the basis of the clinical features plus echocardiographic evidence of LV systolic dysfunction; maximum tolerated pharmacological therapy with ACE-I or ARBs, beta-blockers and MRAs; a QRS duration ≥120ms and any QRS morphology; Exclusion criteria were: a history of myocardial infarction or acute coronary syndrome within the previous month; severe structural valvular heart disease; hypertrophic or restrictive cardiomyopathy; pre-existing cardiac implantable electronic devices; any non-cardiac comorbidities that significantly reduced the likelihood of survival beyond 12 months.

Patients were classified as ICM if LV systolic dysfunction was associated with a history of prior myocardial infarction (Alpert et al., 2000) or angiographically documented coronary heart disease. LGE-CMR was also used in the assessment of aetiology, and in the absence of

the above features a diagnosis of an ischaemic aetiology was still made in the presence of a transmural or subendocardial LGE pattern consistent with a coronary territory. Patients with presumed IDCM, but with fibrosis in distributions other than midwall (subepicardial, epicardial, or patchy) suggestive of an alternative NICM were excluded. The study conforms with the Declaration of Helsinki and was approved by the local Ethics Committee.

5.2.2 Device therapy

Device prescription was based on contemporary indications. Accordingly CRT-P was the predominant therapy as NICE guidance and funding for CRT-D in the United Kingdom did not exist until 2007. In contrast to other international guidelines, NICE recommended CRT-P rather than CRT defibrillation (CRT-D) in patients with IDCM (Barnett et al., 2007). With the exception of 2 patients who received CRT-D for secondary prevention, all others with IDCM received CRT-P.

All devices were implanted via a trans-venous approach using either the subclavian, cephalic or femoral vein. Right ventricular leads were preferentially deployed at the apex, and right atrial leads in the appendage. Subsequent to coronary sinus (CS) balloon venography, the LV lead was positioned in a CS tributary, preferentially overlying the LV free wall.

Patients in sinus rhythm had their device programmed to a DDD pacing mode, with a back-up atrial rate of 60 beats per minute and no intra-ventricular delay. Patients with atrial fibrillation had the atrial port plugged and the device set to a ventricular triggered mode.

Patients in sinus rhythm underwent atrioventricular optimising using a transmitral Doppler based iterative technique at 6 weeks and at each 6 month check.

5.2.3 Cardiovascular magnetic resonance imaging

This was performed using a 1.5 Tesla Signa (GE Healthcare Worldwide, Slough, England) scanner and a phased-array cardiac coil.

A short-axis LV cine stack (from the atrioventricular ring to the LV apex) was acquired using a steady state-in-free precession sequence (repetition time of 3.0 to 3.8 ms; echo time of 1.7 ms; flip angle of 45^{o}; sequential 8 mm slices with a 2 mm interslice gap). There were 20 phases per cardiac cycle resulting in a temporal resolution of 40-50ms.

LV volumetric analyses, comprising LVEDV and LVESV and LVEF, were quantified using manual planimetry of the endocardial and epicardial borders from the short axis stack in accordance with validated methodologies (Maceira et al., 2006) using MASS analysis software (Medis, Leiden, the Netherlands).

5.2.4 Scar imaging

For scar imaging, horizontal and vertical long-axis as well as short-axis slices identical to the LV stack were acquired using a segmented inversion-recovery technique 10 minutes after the intravenous administration of gadolinium-diethylenetriamine pentaacetic acid (0.1 mmol/kg). Inversion times were adjusted to null normal myocardium (260 to 400 ms). To exclude artefact, the scar pattern was required to be visible in the short-axis and long-axis acquisitions, in two different phase encoded directions.

Scars were classified into subendocardial, midwall, epicardial, transmural, or patchy, according to McCrohon et al. (McCrohon et al., 2003). Scars in a subendocardial or transmural distribution following coronary artery territories were regarded as ischaemic in aetiology, whereas midwall scars and absence of scar were regarded as indicative of IDCM. Patients with IDCM were dichotomized according to the presence or absence of MWF, assessed visually. Examples of scars typical of ICM, and IDCM with MWF are shown in **Figure 5-1**. Scar volume was calculated by multiplying the manually planimetered area of LGE in each slice by the slice thickness. Scar burden was expressed as a percentage of LV myocardial volume in the diastolic phase.

5.2.5 Dyssynchrony

Intraventricular dyssynchrony was assessed using the CMR–tissue synchronisation index (TSI), as previously described (Chalil et al., 2007b). Briefly, segmental radial wall motion data were quantified for up to 20 phases (time points) in each RR interval and fitted to an empirical sine wave function $y = a + b \times \sin(2\pi t/RR + c)$. The mean segmental radial wall motion (a), the segmental radial wall motion amplitude (b), and the segmental phase shift of the maximum radial wall motion (c) were extracted from the fit. The CMR-TSI, a global measure of radial dyssynchrony, was expressed as the standard deviation of all segmental phase shifts of the radial wall motion extracted from the fit. This measure was previously shown to predict mortality and morbidity after CRT (Chalil et al., 2007b; Leyva et al., 2009). In a previous study (Chalil et al., 2007b), intraobserver and interobserver variabilities for CMR-TSI were 3.01% and 8.84%, respectively.

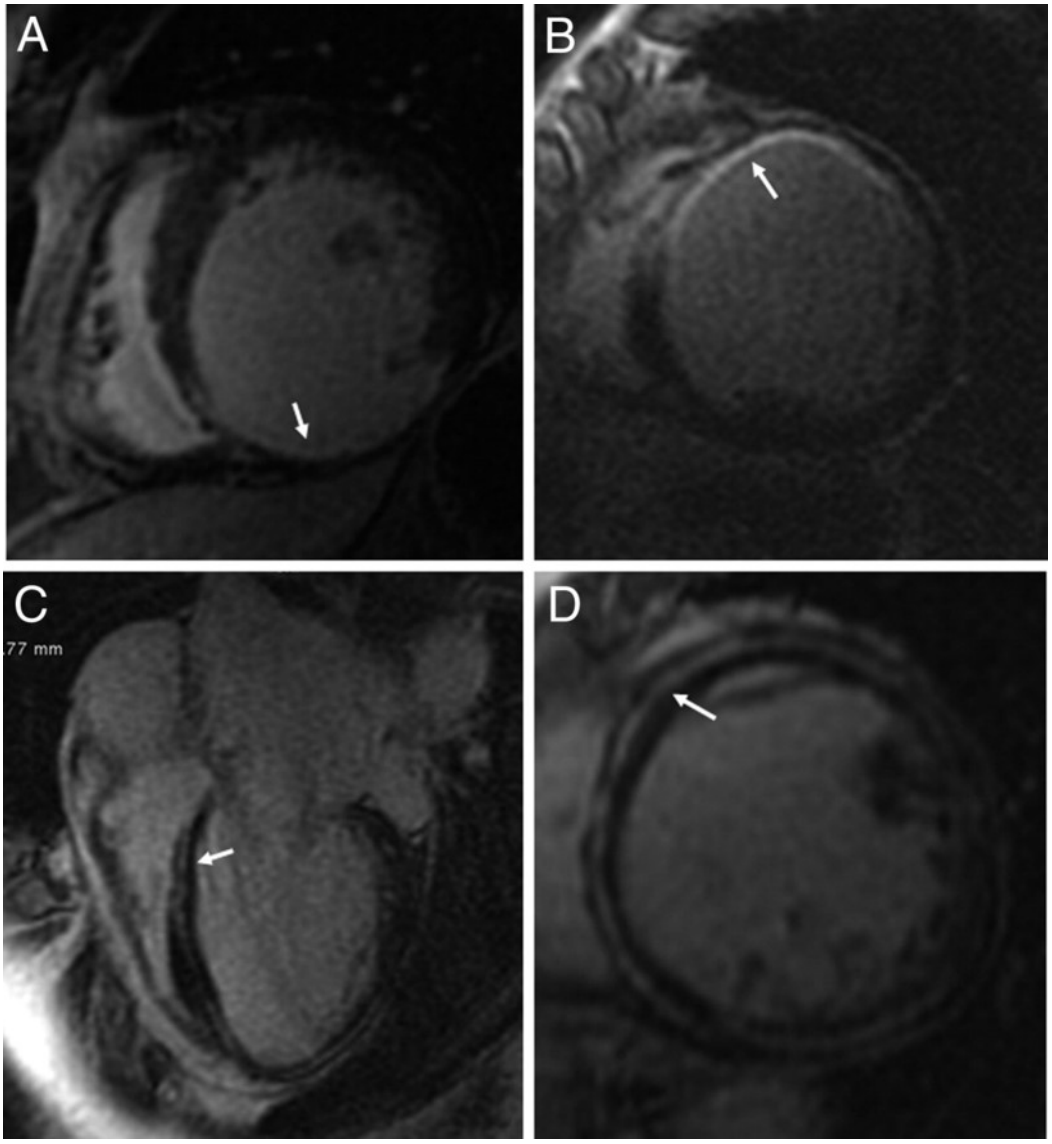

Figure 5-1. Patterns of myocardial scarring in ischaemic and idiopathic dilated cardiomyopathy

(A) Short-axis inversion-recovery late gadolinium enhancement cardiovascular magnetic resonance (LGE-CMR) image showing a transmural, inferior myocardial infarction in a patient with ischaemic cardiomyopathy. (B) Short-axis inversion-recovery LGE-CMR image showing a transmural, anterior myocardial infarction in a patient with ischaemic cardiomyopathy. (C) Four-chamber and (D) short-axis inversion-recovery LGE-CMR images showing midwall LGE, denoting fibrosis, in a patient with idiopathic dilated cardiomyopathy.

5.2.6 Baseline and follow-up assessment

Patients underwent a clinical assessment one day pre-implant, then at 1, 3 and 6 months and every 6 months thereafter. This comprised assessment of the NYHA functional classification, a 6MWT and echocardiography. 2DE was performed using either Vivid 5 or 7 cardiovascular ultrasound systems (General Electric Healthcare Worldwide, Slough, United Kingdom). LVEDV, LVESV and LVEF were calculated using Simpson's biplane method in accordance with the American Society of Echocardiography guidelines (Schiller et al., 1989). Analysis was contemporaneous with the study, and performed by an accredited physiologist who was not aware of the CMR findings.

5.2.7 Study endpoints.

Clinical response was quantified according to the composite clinical score (survival to one year, without HF hospitalisation, and improvement by either (a) ≥ 1 NHYA class or (b) ≥ 25% in 6MWT distance). A LVRR response at echocardiography was defined as a ≥15% reduction in LVESV at the 6 month visit (Konstam et al., 1992) (mean timing of study: 6.4 months; range: 5.0 months – 7.9 months). The studies primary endpoint was cardiac mortality, defined as death from myocardial infarction, arrhythmia or heart failure (or transplantation). Secondary endpoints included death from any cause, and the composite of cardiac mortality/unplanned hospitalisation for worsening HF, death from any cause/unplanned hospitalisation for major adverse cardiovascular events (MACE), and sudden cardiac death/hospitalisation for major arrhythmic events (hospitalisations for worsening HF, myocardial infarction, unstable angina, arrhythmia, stroke, or pulmonary embolism were included in this endpoint. The first event was included in the analysis. Sudden cardiac death

was defined as a “natural, unexpected death due to cardiac causes, heralded by an abrupt loss of consciousness within 1 hour of the onset of acute symptoms” (Braunwald et al., 2011). Death from pump failure was defined as “death after a period of clinical deterioration in signs and symptoms of heart failure despite medical treatment”(Rockman et al., 1989). Outcome data was collected prospectively through medical records and, when appropriate, from interviews with patients' caregivers. Clinical outcome data were collected every 3 months by an investigator who was blinded to clinical and imaging data. Events were adjudicated by the investigators every 3 months.

5.2.8 Statistical analysis

Continuous variables are expressed as mean ± SD. Normality was tested using the Shapiro-Wilk test. Comparisons between normally distributed continuous variables were made using analysis of variance with the Scheffe F procedure for multiple comparisons. Variables that did not follow a normal distribution, such as NT pro–brain natriuretic peptide, were log-transformed for statistical analyses. Categorical variables were analyzed using chi-square tests and the Scheffe post hoc test. Changes in variables from baseline to follow-up were analyzed using paired t tests and Wilcoxon matched-pairs analyses. The ability of MWF to predict the various endpoints was assessed using Kaplan-Meier survival curves and the log-rank (Mantel-Cox) test, as well as Cox proportional hazards analyses. The first event was included in the analyses. For large estimates of the coefficient, as in our case of sudden cardiac deaths in the IDCM +MWF group, the standard error is typically inflated, resulting in a lower Wald statistic, falsely considering the variable not relevant in the model. To overcome this, we used the likelihood ratio test, which is considered superior for testing the

Cox regression model. The profile likelihood was used to estimate the lower 95% confidence interval (CI) bound. Variables reaching $p < 0.10$ on univariate analyses were considered for entry in multivariable models. Given the sample size of patients with IDCM (n=97), the proportion of these with MWF, and a total mortality rate of 15% within the IDCM population, this study was powered ($\beta=0.2$) to detect a 6.0x greater risk of death in either sub-cohort during the follow-up period (HyLown Consulting, 2013). Statistical analyses were performed using Statview (Cary, North Carolina) and SPSS version 15.0 (Chicago, Illinois). A 2-tailed $p < 0.05$ was considered statistically significant.

5.3 Results

5.3.1 Baseline characteristics

The baseline characteristics of patients with ICM and IDCM are shown in **Table 5-1**. Of the 97 patients with IDCM, 20 (26%) had MWF (7.8% of the entire cohort), and the rest of the IDCM group had no myocardial scarring at all. The IDCM +MWF and IDCM −MWF groups were well matched for age, device type, comorbidities, presence of permanent atrial fibrillation, and QRS duration. The +MWF group had a worse NYHA class ($p = 0.0271$) and LVEF ($p= 0.0007$), a higher LVEDV and LVESV (both $p < 0.0001$), lower systolic ($p= 0.0048$) and diastolic ($p= 0.008$) blood pressures, higher NT pro–brain natriuretic peptide levels ($p= 0.0064$), higher plasma creatinine levels ($p= 0.0070$), but similar estimated glomerular filtration rates than the IDCM −MWF group. These groups were also matched for treatment with ACE-Is/ARBs, beta-blockers, and MRAs, but the +MWF group was more likely to require loop diuretics ($p = 0.0257$). In comparison with the IDCM groups, the ICM group had a higher proportion of men and was more likely to receive CRT-D (as required by contemporaneous guidelines) but

Table 5-1. Characteristics of the study groups.

	Group A IDCM +MWF (n = 20)	Group B IDCM -MWF (n = 77)	Group C ICM (n = 161)	P value * A vs B	P value * A vs C	P value * B vs C
Demographics						
Age, yrs	63.6 ± 9.58	66.7 ± 13.0	69.3 ± 9.4	0.25	0.09	0.10
Male, n (%)	12 (60)	48 (62)	142 (88.2)	0.85	0.0008	<0.0001
NYHA class, n (%)	3.50 ± 0.51	3.21 ± 0.41	3.25 ± 0.44	0.03	0.0428	0.84
III	10 (50)	61 (79)	122 (76)			
IV	10 (50)	16 (21)	39 (24)			
SBP, mmHg	103.7 (14.6)	120.8 (18.4)	119.5 (20.4)	0.0048	0.0061	0.69
DBP, mmHg	63.7 (11.3)	73.5 (12.8)	70.3 (11.6)	0.008	0.06	0.09
NT pro-BNP, ng/L	5045.9 (1027.9)	1838.3 (2012.7)	3117.2 (4108.9)	0.0064	0.07	0.07
Creatinine, µmol/L	130.8 (56.1)	103.2 (33.4)	122.0 (37.1)	0.0070	0.36	0.0013
eGFR	56.6 (26.6)	67.3 (20.8)	58.8 (20.5)	0.06	0.68	0.0082
CRT-D, n. (%)	0	2 (2.6)	33 (20.4)	0.4664	0.0657	0.0006
Co-morbidity, n. (%)						
Diabetes mellitus	1 (5)	12 (16)	33 (20.4)	0.22	0.09	0.32
Hypertension	4 (20)	22 (29)	46 (28.6)	0.44	0.38	0.90
CABG	0	0	54	-	0.0017	<0.0001
Medication, n. (%)						
Loop diuretics	20 (100)	61 (79)	140 (87.0)	0.0257	0.09	0.10
ACE-I or ARB	17 (85)	73 (95)	148 (92)	0.13	0.25	0.51
Beta-blockers	11 (55)	39 (51)	102 (63.4)	0.73	0.45	0.05
MRAs	8 (40)	32 (42)	60 (37.2)	0.88	0.92	0.78
ECG variables						
Permanent AF, n. (%)	3 (15)	16 (21)	27 (16.7)	0.74	0.84	0.22
QRS duration, ms	154.1 ± 35.5	144.2 ± 29.1	136.9 ± 32.6	0.4	0.08	0.24
CMR variables						
LVEDV, mL	314.0 ± 107.6	205.6 ± 79.7	230.6 ± 97.5	<0.0001	0.0018	0.18
LVESV, mL	269.4 ± 103.2	166.5 ± 74.2	194.5 ± 89.4	<0.0001	0.0022	0.08
LVEF, %	16.0 ± 6.06	23.9 ± 9.7	23.9 ± 10.9	0.0007	0.0053	0.99
CMR-TSI (ms)	91.8 ± 31.9	75.8 ± 33.8	108.6± 44.7	0.44	0.36	<0.0001

Variables are expressed as mean ± SD, unless indicated otherwise.*, refers to differences between the groups from ANOVA with Scheffe's post hoc test for continuous variables and from chi-squared tests for categorical variables.

was well matched to the IDCM +MWF for age, medication, and LV volumes and LVEF. The CMR-TSI was higher in the ICM group than in the IDCM +MWF group ($p < 0.0001$).

5.3.2 Endpoints

After a maximum follow-up period of 3,166 days (8.7 years; median follow-up time 1,038 days [2.84 years]), total mortality was 10 of 20 (50%) in IDCM +MWF and 5 of 77 (6.5%) in

IDCM −MWF. Cardiovascular mortality was 9 of 20 (45%) and 2 of 77 (2.6%) in the IDCM +MWF and IDCM −MWHF groups, respectively. In the ICM group, total mortality was 53 of 161 (31.8%) and cardiovascular mortality was 49 of 161 (30.4%).

Among patients with IDCM, +MWF predicted cardiovascular mortality (HR: 18.1; $p< 0.0001$), the composite of total mortality or hospitalisation for MACE (HR: 7.57; $p< 0.0001$), and the composite endpoint of cardiovascular mortality or HF hospitalisations (HR: 9.90; $p= 0.0004$), independent of NYHA class, QRS duration, presence of atrial fibrillation, LV volumes, LVEF, and CMR-TSI (**Table 5-2**).

Kaplan-Meier survival curves for the IDCM and ICM groups are shown in **Figure 5-2** In multivariable analyses comprising the IDCM and ICM subgroups, both IDCM +MWF (HR: 18.5 in model 1; HR: 18.6 in model 2; both $p = 0.0002$) and ICM (HR: 21.0; $p < 0.0001$) emerged as strong predictors of cardiovascular mortality, independent of NYHA class, treatment with beta-blockers, QRS duration, presence of atrial fibrillation, LV volumes, LVEF, and CMR-TSI (**Table 5-3)**.

Table 5-2. Cox proportional hazards analyses of baseline variables in relation to clinical outcome in patients with Idiopathic dilated cardiomyopathy.

	Cardiovascular mortality		Total mortality or hospitalisations for MACE		Cardiovascular mortality or heart failure hospitalisations	
	HR (95% CI) *	**p**	**HR (95% CI) ***	**p**	**HR (95% CI) ***	**p**
Univariate analyses						
+ MWF	22.0 (4.73 to 102.0)	<0.0001	7.24 (3.09 to 16.9)	<0.0001	11.9 (4.09 to 34.7)	<0.0001
NYHA class (III)	0.41 (0.12 to 1.33)	0.13	0.56 (0.24 to 1.43)	0.19	0.29 (0.11 to 0.78)	0.014
QRS duration (ms)	1.02 (1.00 to 1.05)	0.0339	1.01 (1.00 to 1.03)	0.11	1.02 (1.00 to 1.04)	0.07
Permanent atrial fibrillation	0.77 (0.17 to 3.57)	0.73	0.99 (0.36 to 2.68)	0.97	0.74 (0.21 to 2.59)	0.63
LVESV, mL	1.01 (1.00 to 1.01)	0.0232	1.00 (0.99 to 1.01)	0.12	1.01 (1.00 to 1.01)	0.0316
LVEDV, mL	1.01 (1.00 to 1.01)	0.0181	1.00 (0.99 to 1.01)	0.13	1.00 (1.00 to 1.01)	0.0297
LVEF, %	0.93 (0.86 to 1.01)	0.08	0.97 (0.92 to 1.01)	0.16	0.95 (0.89 to 1.01)	0.08
CMR-TSI (ms)	1.04 (0.99 to 1.08)	0.09	1.02 (0.99 to 1.04)	0.17	1.03 (0.99 to 1.06)	0.08
Multivariable analyses **						
Model 1						
+ MWF	18.6 (3.51 to 98.5)	0.0008	7.57 (2.71 to 21.2)	<0.0001	9.56 (2.72 to 33.6)	0.0004
NYHA class (III)	-		-		0.58 (0.21 to 1.66)	0.31
QRS duration (ms)	1.01 (0.99 to 1.03)	0.16	-		1.01 (0.99 to 1.02)	0.44
LVEF, %	0.99 (0.91 to 1.09)	0.92	-		1.00 (0.94 to 1.07)	0.95

Model 2						
+ MWF	18.7 (3.53 to 98.7)	0.0008	7.57 (2.71 to 21.2)	<0.0001	9.62 (2.74 to 33.8)	0.0004
NYHA class (III)	-		-		0.59 (0.21 to 1.65)	0.31
QRS duration (ms)	1.01 (0.99 to 1.03)	0.16	-		1.01 (0.99 to 1.02)	0.45
CMR-TSI (ms)	1.00 (0.96 to 1.05)	0.93	-		1.00 (0.97 to 1.03)	0.94

***, Hazard ratios (HR) and 95% confidence intervals (CI). Only variables with p<0.10 on univariate analyses were included in multivariable models. Variables that interact with each other, such as LV volumes, were excluded from the multivariable analyses. **, In addition to +MWF, includes NYHA class, QRS duration, presence of atrial fibrillation, LVEF and the CMR-TSI as independent variables. None of the latter reached statistical significance.**

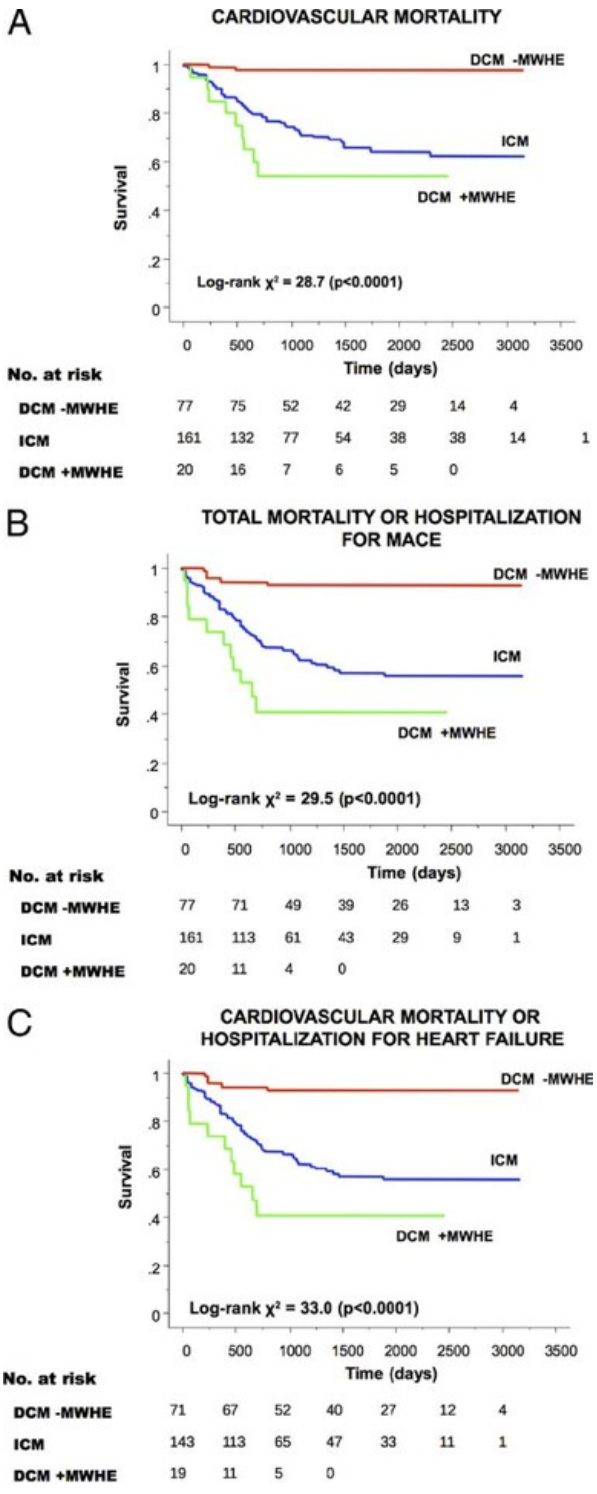

Figure 5-2. Survival curves after cardiac resynchronisation therapy

Patients with idiopathic dilated cardiomyopathy (IDCM) were categorised according to presence of midwall hyperenhancement (+MWHE) or the absence of midwall hyperenhancement (−MWHE) on late Gadolinium enhancment CMR. ICM = ischaemic cardiomyopathy; MACE = major adverse cardiovascular events.

Table 5-3. Cox proportional hazards analyses of baseline variables in relation to cardiovascular mortality in patients with idiopathic dilated cardiomyopathy or ischaemic cardiomyopathy.

	Cardiovascular mortality	
	HR (95% CI) *	**p**
Univariate analyses		
IDCM + MWF	24.1 (5.20 to 111.7)	<0.0001
ICM	14.3 (3.46 to 58.7)	0.0002
NYHA class	2.07 (1,23 to 3.48)	0.0063
Beta-blocker (no)	1.68 (1.01 to 2.79)	0.0451
QRS duration (ms)	1.01 (1.00 to 1.02)	0.06
Permanent AF	1.23 (0.68 to 2.24)	0.49
LVESV, mL	1.00 (1.00 to 1.01)	0.0039
LVEDV, mL	1.00 (1.00 to 1.01)	0.0087
LVEF, %	0.95 (0.92 to 0.98)	0.0018
CMR-TSI (ms)	1.01 (1.01 to 1.02)	<0.0001
Multivariable analyses **		
Model 1		
+ MWF	18.5 (3.93 to 87.3)	0.0002
ICM	21.0 (5.06 to 87.2)	<0.0001
NYHA class	1.55 (0.88 to 2.75)	0.13
Beta-blocker use (no)	2.28 (1.32 to 3.93)	0.0031
QRS duration (ms)	1.01 (1.00 to 1.02)	0.07
LVEF, %	0.96 (0.93 to 0.99)	0.0281
Model 2		
+ MWF	18.6 (3.94 to 87.4)	0.0002
ICM	21.0 (5.07 to 87.3)	<0.0001
NYHA class	1.55 (0.88 to 2.75)	0.13
Beta-blocker use (no)	2.28 (1.32 to 3.93)	0.0031
QRS duration (ms)	1.01 (1.00 t 1.02)	0.07
CMR-TSI (ms)	1.02 (1.00 to 1.03)	0.0282

***, Hazard ratios (HR) and 95% confidence intervals (CI). Only variables with p<0.10 on univariate analyses were included in multivariable models. Variables that interacted with each other, such as LV volumes, were excluded from the multivariable analyses. **, In addition to +MWF, includes NYHA class, QRS duration, presence of atrial fibrillation, LVEF and the CMR-TSI as independent variables. None of the latter reached statistical significance.**

Scar burden in the IDCM group was 2.12% ± 4.96% (range 0 to 26.9%). In Cox proportional hazards analyses, scar burden did not emerge as a predictor of total mortality (HR: 0.99; 95% CI: 0.87 to 1.14; p = 0.94) or cardiovascular mortality (HR: 1.02; 95% CI: 0.89 to 1.16; p = 0.82).

5.3.3 Pump failure

Of the 60 cardiovascular deaths, 46 were due to pump failure (IDCM +MWF 6 of 20 [30%]; IDCM −MWF 2 of 77 [2.6%]; ICM 38 of 161 [23.6%]). In univariate analyses comprising the IDCM and ICM subgroups, both ICM (HR: 10.5; 95% CI: 2.52 to 43.5; p = 0.0012) and IDCM +MWF (HR: 14.1; 95% CI: 2.85 to 70.0; p = 0.0012) emerged as predictors of death from pump failure.

5.3.4 Sudden cardiac death and arrhythmic events

Of the 60 cardiovascular deaths, 14 were sudden cardiac deaths (IDCM +MWF 3 of 20 [15%]; IDCM −MWF 0 of 77 [0%]; ICM 11 of 161 [6.8%]). In univariate and multivariate analyses comparing with IDCM −MWF, both IDCM +MWF and ICM significantly improved the Cox regression model using the likelihood ratio test (p = 0.0029), and both IDCM +MWF (HR lower 95% CI: 2.65) and ICM (HR lower 95% CI: 4.54) emerged as predictors of sudden cardiac death.

Five patients had unplanned hospitalisations for major arrhythmic events (IDCM +MWF 1 of 20 [5.0%] for atrial fibrillation; IDCM −MWF 1 of 77 [1.3%]; ICM 1 atrial fibrillation, 1 ventricular tachycardia, and 1 ventricular fibrillation [total 3 of 161 (5.0%)]). In univariate

analyses comprising the IDCM and ICM subgroups, IDCM +MWF emerged as a predictor of sudden cardiac death or major arrhythmic events (HR: 16.7; 95% CI: 1.87 to 149.7; p = 0.0118), whereas ICM reached only borderline significance (HR: 7.03; 95% CI: 0.92 to 53.4; p = 0.06). In univariate analyses comprising the IDCM subgroups, IDCM +MWF emerged as a predictor of sudden cardiac death or major arrhythmic events (HR: 16.1; 95% CI: 1.81 to 144.8; p = 0.0128).

5.3.5 Clinical variables

Whereas no significant changes in NYHA class were observed in the IDCM +MWF group (−1.25; p= 0.17) or the IDCM −MWF group (−1.20; p= 0.07), a significant reduction in NYHA class was observed in the ICM group (−1.10; p= 0.0429). The 6-min walking distance, however, increased in all groups (IDCM +MWF +101.6 ± 75.8 m, p= 0.0007; IDCM-MWF +54.9 ± 74.2 m, p< 0.0001; ICM +63.1 ± 98.17, p< 0.0001). Quality of life scores (a reduction denoting an improvement in quality of life) decreased in all groups (IDCM +MWF −13.7 ± 40.6, p= 0.0202; IDCM −MWF −25.7 ± 29.6, p< 0.0001; ICM −18.5 ± 21.7, p< 0.0001). Responder rates, in terms of the clinical composite score, were similar across the groups (IDCM +MWF 65.0%; IDCM −MWF 80.5%; ICM 68.2%; p= 0.19).

5.3.6 Echocardiographic variables

As shown in **Figure 5-3**, LVRR was observed in the IDCM −MWF (p= 0.0007) and ICM groups (p= 0.0428) but not in the IDCM +MWF group. Similarly, significant reductions in the LVEDV were observed in the IDCM −MWF group (p= 0.0019) and the ICM group (p= 0.0238) but not

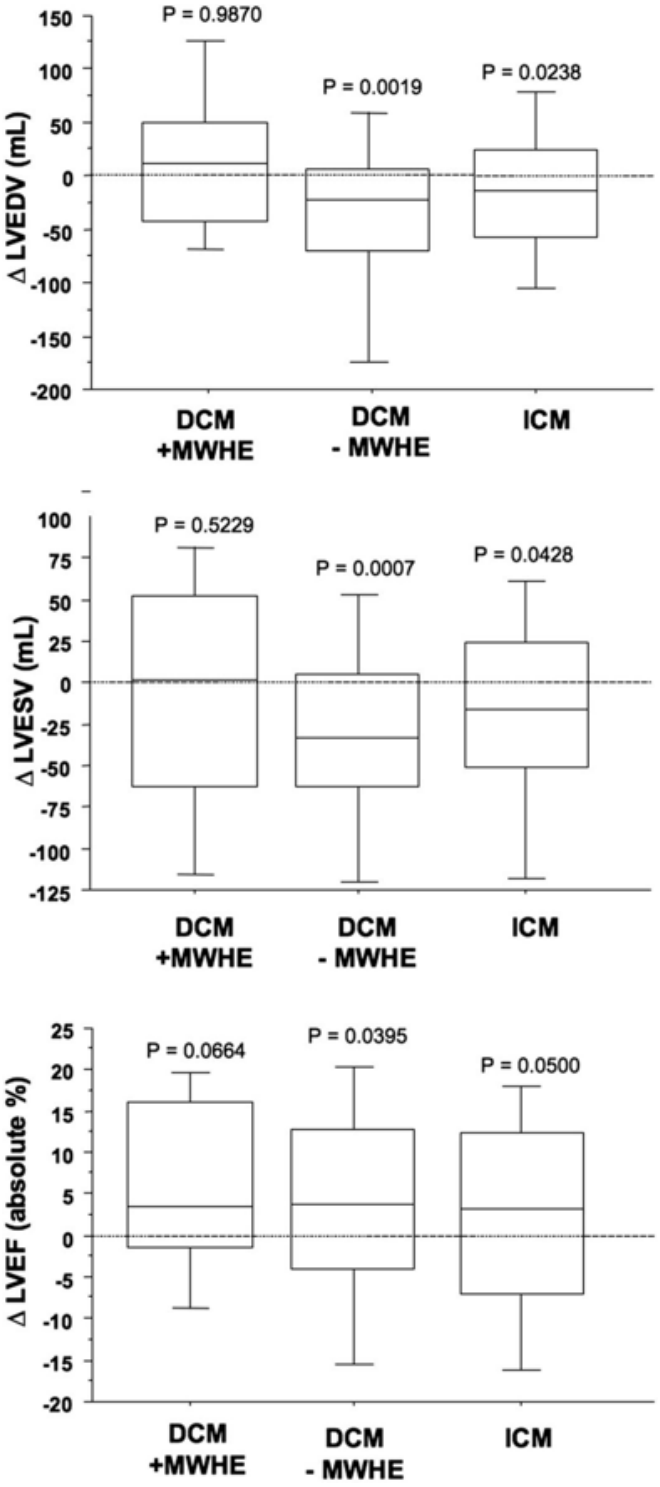

Figure 5-3. Echocardiographic Response to Cardiac Resynchronisation Therapy

Changes from baseline are shown in box and whisker plots, in which the 5 horizontal lines represent the 10th, 25th, 50th, 75th, and 90th percentiles from bottom to top. For left ventricular (LV) volumes, the change is shown in terms of the percent change in relation to baseline volumes. For left ventricular ejection fraction (LVEF), changes are shown in terms of the absolute percentage change.

in the IDCM +MWF group. The LVEF increased in the IDCM −MWF group (p= 0.0395) and the ICM group (p = 0.05) but not in the IDCM +MWF group.

5.4 Discussion

5.4.1 Major findings

This study shows that in patients with IDCM, MWF (detected by midwall hyper-enhancement on LGE-CMR imaging) predicts mortality and morbidity after CRT. Compared with patients without MWF, patients with MWF were 18 times more likely to die from cardiovascular causes after adjustment for NYHA class, beta-blocker use, QRS duration, atrial fibrillation, LVEF, and dyssynchrony. MWF was also predictive of the combined endpoint of total mortality or hospitalisations for MACE and the combined endpoint of cardiovascular mortality or HF hospitalisations. Patients with MWF were less likely to exhibit LVRR, assessed by echocardiography.

5.4.2 Midwall fibrosis as an adverse prognostic marker in IDCM

A novel finding from this study is that the outcome after CRT of patients with MWF was similar to that of patients with ICM. Conversely, the outcome of patients with IDCM and without MWF was dramatically better. These findings have emerged in the context of major CRT trials showing that patients with IDCM have a better clinical outcome (Wikstrom et al., 2009), as well as a better LVRR response (Barsheshet et al., 2011; Gasparini et al., 2003; Linde et al., 2010) to CRT. Importantly, however, no major trial has used CMR in the characterisation of the aaetiology of HF, nor have they used CMR in the differentiation between IDCM with and without MWF. It therefore remains unknown whether the super-

responders to CRT described in such studies are patients with IDCM without MWF. Our findings have major implications for prognostic stratification in clinical practice as well for the design of CRT outcome trials. It would appear that patients with IDCM without MWF have a particularly low clinical event rate.

Since its description in autopsy studies (Maehashi et al., 1991), and in an LGE-CMR study (McCrohon et al., 2003), MWF has been recognised as a prognostic marker for patients with IDCM. A prospective cohort study of 65 patients with IDCM and LVEF ≤35% undergoing implantable cardioverter defibrillator therapy showed that LGE on CMR in any distribution was associated with an 8.2-fold increase in the risk of the composite endpoint of hospitalisation for HF, appropriate implantable cardioverter defibrillator shocks, and cardiac death (Wu et al., 2008). Assomull et al., showed that MWF on LGE-CMR predicted the risk of death or hospitalisations in non-CRT patients with IDCM (Assomull et al., 2006). Our findings are largely consistent with these studies and extend the application of this technique to the risk stratification of patients undergoing CRT.

We found that the degree of dyssynchrony was similar in the +MWF and −MWF groups. Yet, the clinical outcome was worse in the +MWF group. This suggests that the detrimental effects of MWF on clinical outcome is mediated through mechanisms that are independent of dyssynchrony. Several aspects may be relevant in this respect. Fibrosis effectively replaces viable myofibrils, thus reducing the amount of functional myocardium. It interacts mechanically with the complex fiber architecture of the myocardium, which may lead to global mechanical effects remote from the affected area, such as LV stiffness, reduced

compliance, and reduced contractile reserve. The observation that patients with MWF did not exhibit LVRR or an improvement in LVEF is consistent with this notion. Myocardial scars are not readily excitable (Soejima et al., 2001; Tedrow et al., 2004), and therefore reduce the volume of excitable myocardium available to ventricular depolarization.

It has been shown that myocardial fibrosis can form a substrate for ventricular arrhythmias (Hsia et al., 2002; Wu et al., 1998). Accordingly, midwall fibrosis has been linked to a higher risk of sudden cardiac death in patients with IDCM. We too have found that MWF predicts sudden cardiac death, as well as the composite endpoint of sudden cardiac death or major arrhythmic events. In fact, the association between MWF (HR: 16.7; p = 0.0118) and this endpoint was stronger than for ICM (HR: 7.03; p = 0.0597). The occurrence of only 3 sudden cardiac deaths in the whole IDCM group in this study, however, precluded reliable statistical analysis of MWF in relation to sudden cardiac death. On the other hand, the LVEF was very low (16%) in comparison with that of CRT-D trials (20% to 22%) (Bristow et al., 2004), and deaths from pump failure occurred relatively early in the follow-up period. Therefore, the possibility arises that patients succumbed to pump failure before the occurrence of lethal ventricular arrhythmias.

5.4.3 Midwall fibrosis and clinical response to CRT

Despite worse outcomes, the symptomatic response in patients with MWF was similar to that in patients without MWF. This discordance between outcomes and symptomatic response after CRT is well recognised. Yu et al., for example, found no relationship between LVRR and changes in NYHA class, 6-min walking distance, or quality of life scores after CRT

(Yu et al., 2005). Ypenburg et al., also showed similar improvement in NYHA class, quality of life scores, and 6-min walking distance in patients exhibiting ≥15% reduction in LVESV and in those exhibiting a reduction in LVESV of <14% after CRT (Ypenburg et al., 2009). Foley et al., found similar symptomatic response rates in survivors and nonsurvivors 1 year after CRT device implantation (Foley et al., 2011a). There is, in addition, evidence of a discordance between outcomes and symptomatic response according to aetiology. In the REVERSE study, in which patients in NYHA class I or II and LVEF ≤40% were randomized to CRT or no CRT for 12 months, HF aetiology was not predictive of the composite clinical response (Linde et al., 2010). This is in keeping with our finding of similar symptomatic response rates in patients with and without MWF.

5.4.4 Clinical application

CMR has already gained credence as an ideal investigation for patients with HF because it provides unparalleled quality of information on cardiac function and disease aetiology. In addition, LGE-CMR is also unique in its ability to allow quantification and localisation of myocardial scarring in patients with ICM, in whom it has proven to be valuable in prognostic stratification (Chalil et al., 2007a; Chalil et al., 2007c; Leyva et al., 2011). Our findings extend the utility of CMR to the prognostic stratification of patients with IDCM undergoing CRT.

5.4.5 Study limitations

This study was observational and did not include a control group on maximum tolerated pharmacological therapy only. We therefore cannot ascertain whether patients with MWF have a worse outcome than patients not undergoing CRT, and we cannot therefore assume

that patients with MWF do not benefit from CRT. In addition, the number of patients in the +MWF group was small. Therefore, the lack of an effect of CRT on LVRR may be attributable to statistical underpowering. Moreover, we have not quantified the severity of mitral regurgitation, which could also contribute to differences in outcomes between the groups. The lack of systematic collection of arrhythmic events at device interrogation is also a limitation. The relatively small number of events in some multivariable models render these liable to overfitting, and further validation is desirable. The strength of the association between the IDCM +MWF group and the various endpoints is, however, unlikely to be affected by further validation. In contrast to other studies in patients with IDCM (Assomull et al., 2006) or coronary heart disease (Kwong et al., 2006), we have not found a graded relationship between scar burden and mortality in patients with IDCM. This, however, is likely to be due to statistical underpowering.

5.5 Conclusions

We conclude that MWF, detected by midwall hyper-enhancement on LGE-CMR, is a powerful predictor of mortality and morbidity in patients with IDCM undergoing CRT, independent of QRS duration, NYHA class, LVEF, atrial fibrillation, LV volumes, and mechanical dyssynchrony. Pump failure as well as sudden cardiac death and arrhythmic events mediate this association. These findings provide further evidence for CMR in the prognostic stratification of patients undergoing CRT.

6 MECHANICAL EFFECTS OF LEFT VENTRICULAR MIDWALL FIBROSIS IN IDIOPATHIC DILATED CARDIOMYOPATHY

Principal hypothesis: In a population of patients with IDCM, individuals with MWF observed with LGE-CMR have reduced deformation in a circumferential direction and reduced net left ventricular twist as compared to individuals without midwall fibrosis.

6.1 Introduction

IDCM is a common cause of heart failure (Codd et al., 1989). The IDCM phenotype ranges from patients who remain largely asymptomatic to those who succumb to multiple hospitalisations and premature death. In a study of 603 patients with IDCM followed up over 9 years, Castelli et al found that 45% died or underwent cardiac transplantation (Castelli et al., 2013).

Left ventricular MWF was first described as an autopsy finding in 1991 (Maehashi et al., 1991). Clinical studies using LGE-CMR have subsequently shown that in patients with IDCM, MWF is associated with an increased risk of heart failure hospitalisations, ventricular arrhythmias and cardiac death (Assomull et al., 2006; Dweck et al., 2011; Gulati et al., 2013; McCrohon et al., 2003; Wu et al., 2008). Patients with IDCM and MWF are also less responsive to pharmacologic therapy (Leong et al., 2012) and cardiac resynchronisation therapy (**chapter 5**) (Leyva et al., 2012). Whilst the evidence linking MWF and poor patient outcomes is compelling, the mechanism remains unexplored.

The LV twists in systole and untwists, or recoils, in diastole. In systole, the LV base rotates clockwise and the apex rotates counter-clockwise. This wringing motion is effected by the helical arrangement of myocardial fibres, which run in a left-handed direction in the subepicardium and in a right-handed direction in the subendocardium. Contraction of subepicardial myocardial fibres cause the base to rotate clockwise and the apex to rotate in counterclockwise (Nakatani, 2011). Because the radius of rotation of the subepicardium is greater than that of the subendocardium, the former provides a greater torque. Consequently, the LV gets smaller in systole and LV ejection occurs (Nakatani, 2011). Circumferential fibres, which run in the mid-myocardium, are crucial to this process. During ejection, they shorten simultaneously with oblique fibres in the right- and left-handed helices. In effect, circumferential fibres provide a horizontal counterforce throughout ejection (Buckberg et al., 2008).

This study tests the hypothesis that injury to mid-myocardial, circumferential myocardial fibres, (Wu et al., 2007) as might be expected from MWF, leads to impairment of LV circumferential contraction and relaxation and therefore, to disturbances in LV twist and torsion. In this study, FT-CMR is used to explore the mechanical effects of MWF in patients with IDCM.

6.2 Methods

6.2.1 Study population

Patients with IDCM were recruited through dedicated heart failure units from two centres. To ensure adequate numbers of patients with +MWF, prospective recruitment (Queen

Elizabeth Hospital, Birmingham, United Kingdom) was supplemented with retrospective inclusion (Good Hope Hospital, United Kingdom). Both groups conformed to the identical eligibility criteria: Adults aged 18 or over with a diagnosis of IDCM made on the basis of clinical history, echocardiographic evidence of LV chamber dilatation (≥112% predicted value corrected for age and BSA)(Henry et al., 1980), LV systolic impairment and absence of coronary artery disease at invasive coronary angiography (performed in all patients) thought to be sufficient to account for LV systolic dysfunction. Exclusion criteria: history of chronic alcohol excess; valvular heart disease; congenital heart disease; hypertension (BP >160/100 mmHg), transmural or sub-endocardial LGE pattern consistent with a coronary territory (McCrohon et al., 2003); fibrosis in distributions other than midwall (subepicardial, epicardial, or patchy) suggestive of an alternative NICM. The study conforms to the Declaration of Helsinki and was approved by the local Ethics Committee.

6.2.2 CMR

It is routine clinical practice at the two recruiting dedicated heart failure units to perform CMR as part of the diagnostic work-up. Accordingly, all patients underwent CMR at the time of the diagnosis. This was undertaken using 1.5 Tesla Magnetom Avanto (Siemens, Erlangen, Germany) or Signa (GE Healthcare Worldwide, Slough, England) scanners and a phased-array cardiac coil. The acquisition protocols were broadly equivalent between the two units and are as described in **2.2.2** (Queen Elizabeth Hospital cohort) and **5.2.3** (Good Hope Hospital Cohort). Mean temporal resolution was 38ms, range 24-49ms.

Scar imaging was conducted as described in **5.2.4**. Patients were dichotomised according to the presence or absence of MWF, assessed visually using CVI[42] software (Circle Cardiovascular Imaging Inc., Calgary, Canada) and only deemed to be present if a crescentic or circumferential area of mid-wall signal enhancement (2 SD above the mean intensity of remote myocardium in the same slice (Mahrholdt et al., 2004)), surrounded by non-enhanced epicardial and endocardial myocardium was evident. To exclude artefact, the typical scar pattern was required to be visible in the short-axis and long-axis acquisitions, in two different phase encoded directions. Assessment was conducted by an experienced observer (F.L.), blinded to FT-CMR data, and on anonymised scans uploaded to the viewing platform in a random order determined using online software (Random.org, Dublin, Ireland).

6.2.3 Cardiac mechanics

Assessment of cardiac mechanics was undertaken using FT-CMR (Tomtec Imaging Systems, Munich, Germany) as previously described in **3.2.4.**

Global peak systolic $Ɛ_{cc}$ and $Ɛ_{rr}$, SSR_{cc} and SSR_{rr} and DSR_{cc} and DSR_{rr} were assessed using FT-CMR of the mid-cavity LV short-axis cine. $Ɛ_{ll}$, SSR_{ll} and DSR_{ll} were assessed using the HLA cine. Only the SSFP sequences were uploaded onto the FT-CMR software, ensuring that the operator (R.T.) was blinded to MWF status. In addition, MWF status was decided by an investigator (F.L.) who was blinded to the findings of FT-CMR.

Peak systolic rotation was measured using the basal and apical short axis cines. In health, peak systolic rotation, as viewed from the apex, is typically clockwise (+) at the base, and

anti-clockwise (-) at the apex. Peak systolic rotation was calculated in degrees and expressed as both the maximum extent of rotation in the anticipated direction (i.e. if systolic rotation at the apex was solely in a clockwise direction this would equate to 0^o) and the total magnitude of rotation (regardless of direction). Torsional parameters are derived from the peak instantaneous net difference in apical and basal rotation. LV twist was defined as ($\Phi_{apex} - \Phi_{base}$), twist per unit length ($\Phi_{apex} - \Phi_{base}/D$), and LV torsion (circumferential-longitudinal shear angle) as ($\Phi_{apex} - \Phi_{base}$)($\rho_{apex} - \rho_{base}$) / 2D (where Φ = the rotation angle; ρ = epicardial radius, and; D = base-to-apex distance) in accordance with agreed methodologies (Russel et al., 2009).

Systolic torsion was classified as either: a) normal torsion, in which there is predominantly anticlockwise rotation of the apex and clockwise rotation of the base; b) rigid body rotation: both the apex and base rotating in the same direction; and c) reverse torsion: predominantly clockwise rotation of the apex and anti-clockwise rotation of the base (**Figure 6-1**).

6.2.4 Statistical analysis

Categorical variables were expressed as a percentage and continuous variables as mean $\pm$ standard deviation (SD). Normality was tested using the Shapiro-Wilk test. Comparisons between variables were made with Fisher's exact test for categorical variables and independent samples t-tests for continuous variables, after adjustment by the Welch-Satterthwaite method where Levene's test showed unequal variance between groups. Post-hoc power calculations accepted a risk of type II error of 0.20. A p value of < 0.05 was

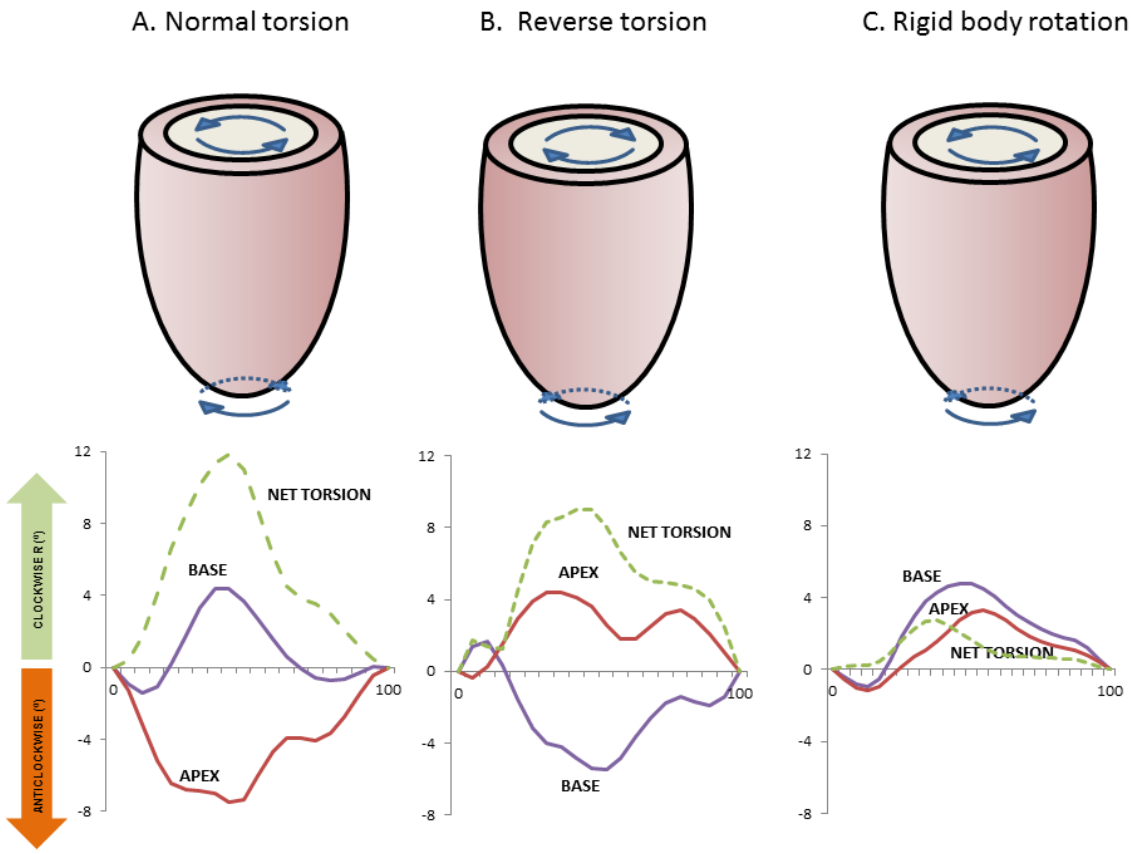

Figure 6-1. Rotational mechanics in IDCM.

Diagrammatic representation of torsional and rotational patterns identified using feature-tracking cardiovascular magnetic resonance. In the bottom tiles, the time in the cardiac cycle, expressed as a percentage of the R-R interval on the ECG, is shown in the x axes. Rotation at the base and apex of the LV as well as net torsion (the instantaneous difference between apical and basal rotation) is shown on the y axis (in degrees) (A) shows a preserved torsional pattern from a patient with IDCM without MWF with predominantly anticlockwise rotation at the apex and clockwise rotation at the base. (B) shows reverse torsion, where the direction of both apical and basal rotation is reversed. (C) shows rigid body rotation in a patient with IDCM and MWF. The apex and base both twist in the same direction so that the heart rotates as one solid body with minimal net torsion.

considered statistically significant for all tests. Statistical analyses were performed using SPSS v21.0. (SPSS Inc. Chicago, Illinois).

6.3 Results

The characteristics of the study group are shown in **Table 6-1**. Amongst the entire cohort, 32/116 patients (28%) had MWF. Patients were of similar age (63.8 vs. 62.3 yrs, p= 0.29), but more patients with MWF were men (84% vs. 61%, p= 0.02). There were no differences in NHYA class, atrial rhythm, QRS duration, LVEF, co-morbidities, pharmacological therapy for heart failure.

6.3.1 Systolic deformation

As shown in **Table 6-2**, patients with MWF had a lower, global circumferential strain (ε_{cc}: -6.6% vs -9.4%, P=0.004), but similar longitudinal (ε_{ll}: -7.6% vs.-9.4%, p-0.053) and radial (ε_{rr}: 14.6% vs. 17.8% p= 0.18) strain. Systolic strain rate was reduced in the circumferential direction (SSR_{cc}: -0.38 s^{-1} vs. -0.56 s-1, p= 0.005), but not in radial or longitudinal directions.

Figure 6-2 shows typical examples. As shown in **Figure 6-3**, ε_{cc} (r = 0.70), ε_{rr} (0.57, p <0.001 and ε_{ll} (r = 0.62, p<0.001) correlated positively with LVEF. In the case of ε_{cc}, the slope of the regression line was 0.17 in the +MWF group and 0.31 in the -MWF group, indicating that ε_{cc} is lower in the +MWF group than in the -MWF at a given LVEF.

Table 6-1. Baseline characteristics

	No MWF (n = 84)	**MWF (n = 32)**	**P**
Age, yrs	62.3 ± 13.7	63.8 ± 11.9	0.29
Male, n (%)	51 (61)	27 (84)	0.02
Height, m	1.68 ± 0.09	1.74±0.09	0.02
Weight, Kg	83.4 ± 18.6	83.3 ± 12.6	0.97
NYHA class			0.20
I	4 (5)	3 (9)	
II	15 (18)	8 (25)	
III	47 (56)	11 (34)	
IV	9 (11)	5 (16)	
Unknown	9 (11)	5 (16)	
Diabetes mellitus, n (%)	13 (16)	7 (24)	0.42
Hypertension, n (%)	18 (22)	5 (17)	0.61
Atrial fibrillation, n (%)	15 (18)	8 (24)	0.44
Medication, n (%)			
Loop diuretics	62 (81)	26 (89)	0.47
ACE-I or ARB	77 (97)	27 (90)	0.31
Beta-blockers	51 (65)	20 (66)	1.00
Aldosterone antagonists	36 (46)	10 (35)	0.29
Systolic blood pressure, mmHg	124.3 ± 20.5	119.6 ± 23.1	0.38
Diastolic blood pressure, mmHg	71.5 ± 11.9	71.7 ± 13.8	0.96
QRS duration (ms)	144 (28)	149 (32)	0.48

ACE-I: angiotensin-converting enzyme inhibitors; ARB: angiotensin receptor blockers.

Table 6-2. Mechanical variables in patients with or without MWF.

	No MWF (n = 84)	MWF (n = 32)	P
LV dimensions			
LVEDV, mL	222 ± 80	277 ± 79	0.002
LVESV, mL	166 ± 79	214 ± 83	0.007
LV mass, g	137.6 ± 46.6	155.5 ± 71.1	0.052
Systolic deformation			
LVEF, %	27.5 ±10.8	24.3 ± 12.9	0.20
Ɛcc (%)	-9.4 ± 4.76	-6.6 (2.57	0.004
SSR_{cc} (s^{-1})	-0.56 ± 0.25	-0.38 (0.12	0.005
$Ɛ_{rr}$ (%)	17.8 ± 11.0	14.6 ± 10.1	0.18
SSR_{rr} (s^{-1})	0.84 ± 0.37	0.74 ± 0.40	0.31
$Ɛ_{ll}$ (%)	-9.4 ± 4.35	-7.6 ± 3.34	0.053
SSR_{ll} (s^{-1})	0.56 ± 0.20	-0.49 ± 0.18	0.13
Diastolic deformation			
DSR_{cc} (s^{-1})	0.46 ± 0.19	0.34 ± 0.11	0.010
DSR_{rr} (s^{-1})	-0.75 ± 0.35	-0.55 ± 0.44	0.038
DSR_{ll} (s^{-1})	0.50 ± 0.20	0.38 ± 0.14	0.006
Systolic torsion			
Basal systolic rotation (°)			
Net Clockwise	3.40 ± 3.00	3.00 ± 2.23	0.513
Magnitude	4.63 ± 2.64	3.67 ± 1.97	0.082
Basal rotation rate (° s^{-1})	31.3 ± 14.5	22.1 ± 8.2	0.002
Apical systolic rotation (°)			
Net anti-clockwise	-3.50 ± 3.28	-1.99 ± 1.97	0.024
Magnitude	5.18 ± 3.15	3.52 ± 2.45	0.013
Apical rotation rate (° s^{-1})	-38.9 ± 21.8	-26.1 ± 15.8	0.005
Average basal/apical rotation(°)	9.81 ± 4.48	7.20 ± 3.44	0.002
LV twist (°)	6.31 ± 3.30	4.65 ± 2.18	0.004
LV twist per unit length (°/cm)	1.34 ± 0.76	0.94 ± 0.55	0.005
Torsional shear angle	0.83 ± 0.06	0.52 ± 0.07	0.008
LV twist rate (° s^{-1})	48.4 ± 23.1	36.1 ± 17.1	0.01

Torsional pattern			<0.001
Normal torsion, n (%)	39 ± 46	10 ± 32	
Rigid body rotation, n (%)	23 ± 28	21 ± 64	
Reverse torsion, n (%)	22 ± 26	1 ± 4	
Diastolic torsion			
Basal rotation rate (^{o} s^{-1})	-34.1 ± 14.8	-28.0 ± 11.8	0.053
Apical rotation rate (^{o} s^{-1})	38.3 ± 20.1	24.9 ± 13.1	0.001
LV untwist rate (^{o} s^{-1})	44.5 ± 21.0	30.5 ± 14.9	<0.001

Variables are expressed as mean ± SD. MWF: mid-wall fibrosis; SSR = systolic strain rate; DSR = diastolic strain rate; Ɛ = strain

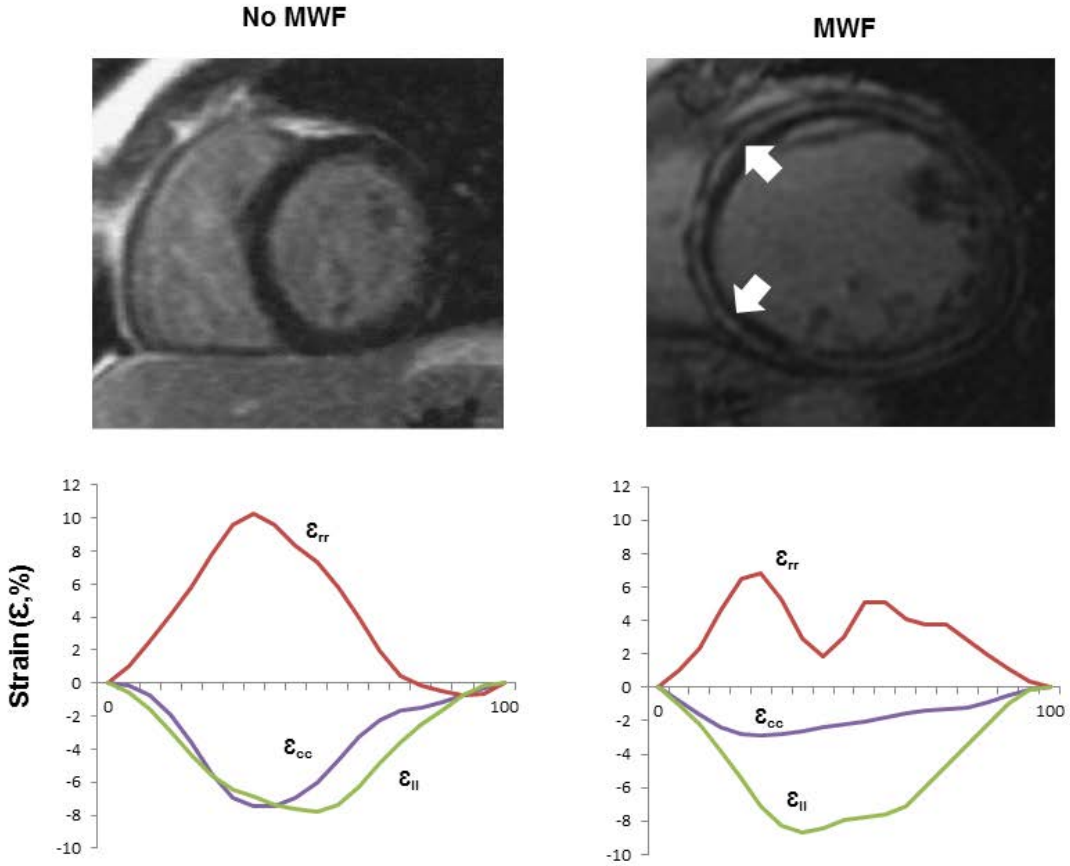

Figure 6-2. Typical examples of strain parameters from patients with and without midwall fibrosis.

Short-axis, late gadolinium enhancement views of patients with idiopathic dilated cardiomyopathy, without (a) and with (b) mid-wall fibrosis (MWF, white arrows). The bottom tiles show plots of global circumferential strain (Ɛcc, purple), global radial strain (Ɛrr, red) and global longitudinal strain (Ɛll, green) over a cardiac cycle. Note the marked reduction in Ɛcc in the patient with MWF.

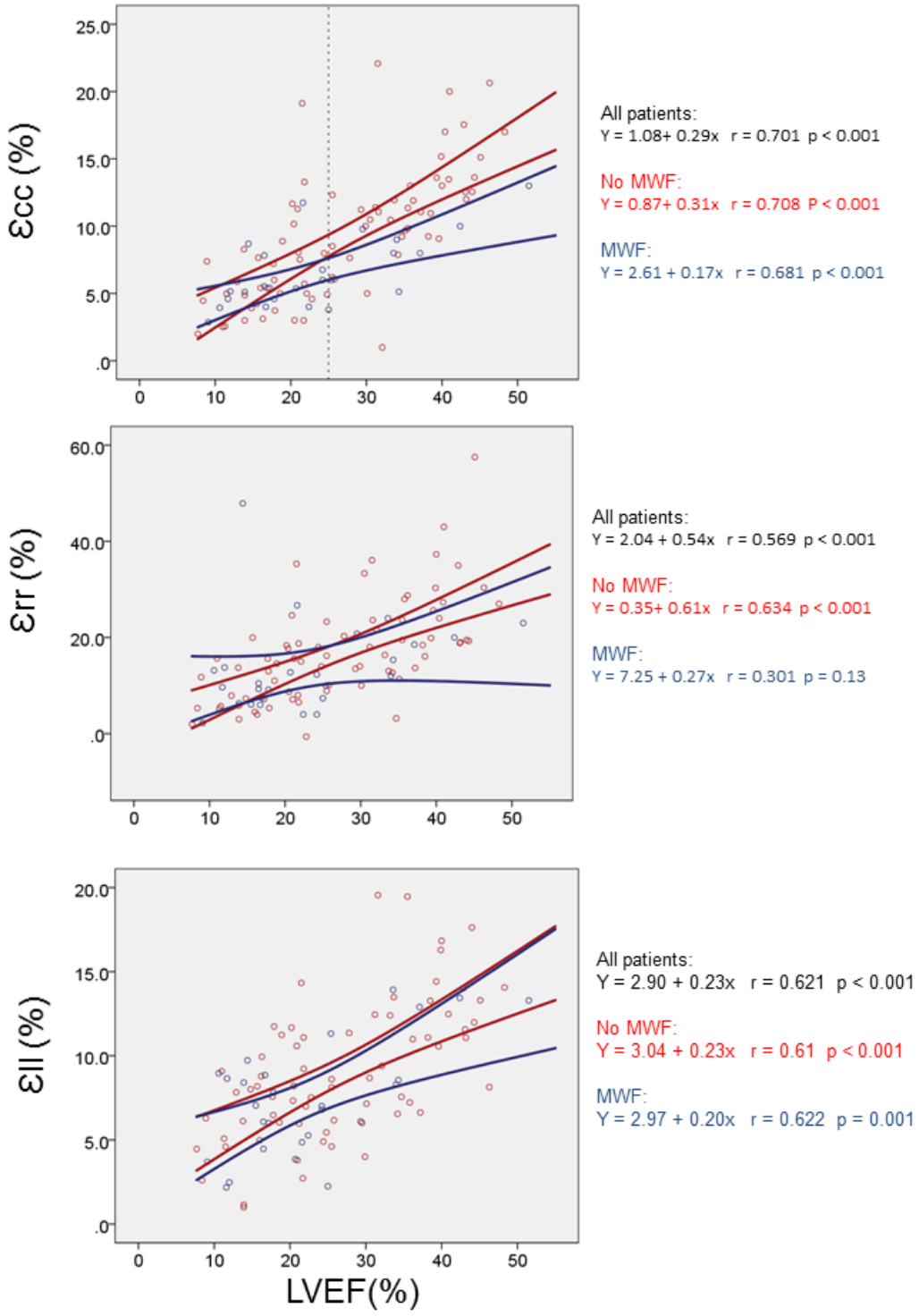

Figure 6-3. Relationship between LVEF and myocardial strain

Scattergrams for each of the Lagrangian strains plotted against LVEF. Cases are classified according to presence (blue circles) or absence (red circles) of mid-wall fibrosis (MWF). The lines correspond to the 95% confidence intervals for strain. The top scattergram demonstrates that above an LVEF of 25% (dashed reference line) MWF alters the relationship between E_{cc} and LVEF: patients with MWF have lower E_{cc} than those with similar LVEF but without MWF.

6.3.2 Diastolic deformation

In patients with MWF, diastolic strains rates were lower in all three directions in patients with MWF (DSR_{cc}: 0.34 vs 0.46 s^{-1}, p= 0.01; DSR_{rr}: -0.55 vs -0.75 s^{-1}, p= 0.04; DSR_{ll}: 0.38 vs 0.50 s^{-1}, p= 0.006).

6.3.3 Torsional mechanics

Whilst basal rotation was unaffected by MWF (net clockwise: 3.00^o vs. 3.30, p = 0.51; total magnitude: 3.67^o vs. 4.63^o,p = 0.08), the rate of basal rotation was reduced (22.1 $^o s^{-1}$ vs 31.3 $^o s^{-1}$, p= 0.002). In patients with MWF, apical rotation was also reduced in terms of both the total magnitude (3.52^o vs 5.18^o, p=0.013) and the net anti-clockwise rotation (-1.99^o vs. -3.50^o, p= 0.024). The rate of apical rotation was lower in patients with MWF (-26.1 $^o s^{-1}$ vs -38.9 $^o s^{-1}$, p= 0.005). This reduction in the magnitude of apical rotation was associated with a reduction in LV twist (peak LV twist : 4.65 ^{o} vs. 6.31 ^{o}, p=0.004; LV twist per unit length: 0.94 ^{o}/cm vs.1.34 ^{o}/cm, p= 0.005; torsional shear angle: 0.52 vs. 0.83, p= 0.008). The rate of LV twist (36.1 $^o s^{-1}$ vs. 48.4 $^o s^{-1}$, P= 0.001) and untwist (30.5 $^o s^{-1}$ vs. 44.5 $^o s^{-1}$, P< 0.001) was also reduced in patients with MWF. A normal torsion pattern, in which there is predominantly anti-clockwise rotation of the apex and clockwise rotation of the base, was observed more frequently in patients without MWF (32 vs 46%). Rigid LV body rotation was more frequently observed in patients with MWF (64 vs 28%, p< 0.001).

6.3.4 Sample size

Retrospective calculation shows that this study was able to resolve similar reductions in E_{cc} (20%) or E_{ll} (22%) within the +MWF group compared to the –MWF. This study was only powered to detect a 34% reduction in E_{rr}. The study would have required 336 patients to have the capability of identifying a 20% reduction in E_{rr}.

6.4 Discussion

6.4.1 Major findings

In this study, we have shown that in patients with IDCM, MWF is associated with a selective impairment of circumferential LV myocardial strain. In addition, MWF is associated with impaired apical rotation and a reduction in rotation rate, from base to apex. MWF is also associated with impaired diastolic function, reflected in reductions in untwist in all directions, from base to apex. Together, these findings are consistent with the notion that, by affecting predominantly circumferential myocardial fibres, MWF leads to disturbances in myocardial contraction and diastolic function. The result is a 'stiff' LV, which is less able to twist to an applied torque (rotation) and more likely to move as a solid body. These disturbances may be related to the known associations of MWF with reduced pump function, heart failure hospitalisations and a poor response to medical and device therapy. (Assomull et al., 2006; Dweck et al., 2011; Gulati et al., 2013; Lehrke et al., 2011; Leong et al., 2012; Leyva et al., 2012; McCrohon et al., 2003; Wu et al., 2008)

6.4.2 Systole

During ejection, circumferential fibres shorten simultaneously with the oblique fibres in the right- and left-handed helices to thicken the myocardium and empty the heart. We have found that MWF was associated with a selective reduction in circumferential strain, suggesting that MWF preferentially affects mid-myocardial, circumferential fibres. As noted by Buckberg (Buckberg et al., 2008), circumferential fibres provide a horizontal counterforce, or 'buttress' to the simultaneously contracting oblique fibres. Impaired circumferential contraction would be expected to lead to impaired rotation, as we have found in patients with MWF. Our finding of more frequent rigid LV body rotation supports the notion that MWF renders the LV less capable of twisting and more liable to move as a rigid body.

Chapter 5 shows that patients with IDCM and MWF treated with CRT are more likely to suffer pump failure than patients without MWF (Leyva et al., 2012). On the other hand, Lamia et al found that CRT improved torsion, stroke volume and stroke work in an animal model (Lamia et al., 2011). Using 3-dimensional speckle-tracking echocardiography, others found that in patients with IDCM, CRT led to an improvement in LV torsion (Matsumoto et al., 2012). If torsion is indeed influenced by CRT, we might expect that the higher risk of pump failure observed in patients with MWF undergoing CRT may be due to a permanent inability of the LV to twist and untwist. This hypothesis requires further exploration.

6.4.3 Diastole

In diastole, release of energy stored in systole (recoil) causes rapid untwisting and a mitral-to-apical negative gradient (Steine et al., 1999) that 'sucks' blood from the left atrium to the

LV (Wu et al., 2006). Untwisting occurs mainly during the isovolumic relaxation period and is followed by diastolic filling. Several studies (Beyar et al., 1989) (Moon et al., 1994; Rademakers et al., 1992) have shown that whilst cavity volume is fixed during isovolumic relaxation, there is a rapid recoil of about 40% of the torsion effected during systole. We have found that MWF leads to both a multi-directional impairment in diastolic strain rate, as well as to impairment of apical untwist rate. This is likely to account for the higher LV filling pressures observed using echocardiography in patients with NICM and MWF (Moreo et al., 2009). Conceivably, impaired apical untwisting leads to impaired LV suction and to increased LV filling pressures.

6.4.4 Limitations

The LGE-CMR technique described herein only detects replacement fibrosis. The more recent technique of T1 mapping, which detects interstitial fibrosis, was not undertaken. We cannot therefore comment as to whether our findings are also influenced by the latter. In addition, we have not routinely undertaken myocardial biopsy, nor have we quantified myocardial oedema. Therefore, we cannot exclude the possibility that our findings were influenced by active myocarditis, despite the absence of evidence from clinical and laboratory screening.

This study was inadequately powered to determine if ε_{rr} was reduced in –MWF. However, the study was powered to detect reductions in deformation in other directions. Problematically, this study investigates a diverse range of different mechanical effects of MWF, accordingly multiple simultaneous comparisons are made. No correction is made for

this, and the study is insufficiently powered to manage this. It is probable that some reported differences are due to type I errors and further testing is required to substantiate the hypotheses generated.

In this study each parameter is calculated only once, in difference to a recent recommendation that reproducibility can be maximised with 3 repeated measures, analogous to the methodology commonly employed with STE (Schuster et al., 2015). However, in a population of 16 healthy volunteers, the same group reports reassuring inter-study reproducibility and minimal diurnal fluctuation when FT-CMR is utilised for the assessment of peak torsional parameters, with torsional shear angle having the greatest reproducibility (Kowallick et al., 2016). They calculated that a sample size of only 15 is required to demonstrate a 20% difference in peak torsion between groups. Standardisation of slice selection with FT-CMR is likely to be an important contributor facilitating smaller sample sizes compared to echo based studies. Cautionary, FT-CMR was much less robust for the assessment of diastolic torsion rate due to the loss of tracked features owing to through plane motion during the rapid isovolaemic relaxation phase. Furthermore, reproducibility does not necessarily equate to precision, and the accuracy of FT-CMR to measure torsional mechanics still lacks validation against either phantom models, currently utilised echo-based modalitities or myocardial tagging.

6.5 Conclusions

In patients with IDCM, MWF is associated with profound disturbances in LV global circumferential strain, strain rate, LV twist and torsion, in both systole and diastole. In

addition, MWF is associated with rigid LV body rotation. These findings provide a mechanistic link between MWF and a poor clinical outcome in patients with IDCM, despite pharmacologic and device therapy.

7 MECHANICAL DYSSYNCHRONY AND BASELINE LEFT VENTRICULAR SYSTOLIC FUNCTION AS PREDICTORS OF RESPONSE AND OUTCOME AFTER CRT: A FEATURE-TRACKING CARDIOVASCULAR MAGNETIC RESONANCE STUDY

Principal hypothesis: The assessment of baseline dyssynchrony using FT-CMR on pre-implant acquisitions predicts response following CRT.

7.1 Introduction

Improving the proportion of patients who respond, and outcomes following CRT remain the focuses of investigational efforts within this field of cardiovascular medicine. One strategy for improving outcomes is to refine patient selection; this forms an important aspect of the provision of any therapy, and is of particular relevance in publically funded healthcare systems, such as the UK, where financial resources are finite. Under current national (NICE, 2014) and international (Brignole et al., 2013) guidelines patient selection is based on assessment of an individual's symptoms, the electrocardiogram and left ventricular systolic function.

With the exception of patients who have a concomitant pacing indication (Curtis et al., 2007), the functional cut-off for allocating CRT remains a LVEF <35% based on the selection criteria used in landmark studies (Bristow et al., 2004; Cleland et al., 2005). Investigating the benefit of CRT in recipients with more moderate LV impairment has proved challenging and MIRACLE EF was abandoned due to poor recruitment, with the long follow-up required to prove benefit proving unacceptable to potential recruits (Linde et al., 2016). Investigations in

this field, are further complicated by our reliance on 2DE for LVEF assessment, with its inherent high interobserver variability (Wood et al., 2014), and even within the clinical trial forum this has proved an inprecise measure (Chung et al., 2010; Kutyifa et al., 2013). Global systolic strain is a more sensitive marker of LV function measuring myocardial contractility. STE global strain measures are independent predictors of prognosis in heart failure and superior to LVEF (Sengelov et al., 2015). However, STE measures are more susceptible to image quality than 2DE measures.

The underlying paradigm of CRT that it rectifies disordered cardiac synchrony has driven extensive search for an imaging based measure of mechanical dyssynchrony that can enhance patient selection. Nonetheless, no single dyssynchrony parameter has proven clinical utility (Chung et al., 2008; Miyazaki et al., 2010), and this is reflected in major guidelines that continue to recommend electrocardiographic QRS duration and morphology as the sole arbitrators of the presence of dyssynchrony (Brignole et al., 2013; Tracy et al., 2012). One component of the failure of non-invasive dyssynchrony markers has been their reliance on regional delays in time to peak contractions. This is a particular problem in the setting of infarcted myocardium, where the identification of low peak amplitudes is inaccurate, contributing to poor inter-operator reproducibility, and disregards the negligible contribution of late activated non-viable segments to overall performance. In this respect, measures of the potential contractile reserve that could be recruited (Kydd et al., 2013; Lim et al., 2008; Tatsumi et al., 2011), or Fourier transformations of regional strains that encompass a more universal assessment of the entire myocardium throughout the cardiac

cycle have both shown promise (Bilchick et al., 2008; Chalil et al., 2007b). The superior type of measure remains unknown.

Most dyssynchrony and strain assessment has utilised echocardiography, but CMR based dyssynchrony assessment using myocardial tagging has shown promise in single centre studies (Bilchick et al., 2008). FT-CMR overcomes the time inefficiencies limiting other CMR methodologies and its highly automated processing coupled with the high spatial resolution of CMR could resolve the poor reproducibility that hamper echocardiographic based measures. This study tests the hypothesis that baseline strain and dyssynchrony assessment using FT-CMR predicts response to and outcomes from CRT, and examines which type of these measures is superior for this purpose.

7.2 Methods

7.2.1 Study population

This retrospective study was conducted on an historical prospectively followed cohort of 118 consecutive heart failure patients who had undergone successful CRT-P implantation based on contemporaneous indications. All patients were recruited from a dedicated heart failure service at a single centre (Good Hope Hospital, Birmingham) between June 2002 and December 2007. Inclusion criteria were: Clinical HF with NYHA class II-IV symptoms diagnosed on the basis of the clinical features plus echocardiographic evidence of LV systolic dysfunction; maximum tolerated contemporary pharmacological therapy; a QRS duration ≥120ms and any QRS morphology; availability of original CMR acquisitions including the entire LV short axis stack. Exclusion criteria were: a history of myocardial infarction or acute

coronary syndrome within the previous month; severe structural valvular heart disease; hypertrophic or restrictive cardiomyopathy; CRT-D as device therapy, pre-existing cardiac implantable electronic devices; any non-cardiac comorbidities that significantly reduced the likelihood of survival beyond 12 months.

Baseline and follow-up assessments (**5.2.6**), and study end-points (**5.2.7**) are as previously described.

7.2.2 Device therapy and follow-up

Device prescription was based on contemporary indications. This study examines a population exclusively of patients with CRT-P. Device implantation, programming and optimisation is as described in **5.2.2**.

7.2.3 LV volumetric and myocardial strain analysis

CMR acquisition is as described in **5.2.3**. LV volumetric analyses, comprising LVEDV and LVESV and LVEF, were quantified using manual planimetry of the endocardial and epicardial borders from the short axis stack in accordance with validated methodologies (Maceira et al., 2006) using CVI[42] software (Circle Cardiovascular Imaging Inc.,Calgary, Canada). FT-CMR was undertaken as detailed in **3.2.4.** Global peak systolic ε_{ll}, ε_{rr} and ε_{cc} were derived. ε_{3D} was calculated as summation of the 3 peak systolic axial strains and provides a three-dimensional measure of myocardial contractility.

7.2.4 Dyssynchrony analyses

Feature tracking of each SSFP cine of the short axis stack (as described in **3.2.4**) was used to obtain circumferential and radial strain data along the evenly spaced circumferential segments of a short-axis slice. The strain data was processed in different ways to derive 3 distinct classes of dyssynchrony parameter.

i) Time to peak contraction. Circumferential deformation data was obtained from feature tracking of the LV basal, mid and apical slices (slice selection was as described in **Figure 3-1**). Time-ε_{cc} curves were derived for each of the 16 myocardial segments (in accordance with the American Heart Association's 16 segment model) from which the SD of time to peak ε_{cc} ($SDT2P_{16}$) was calculated. All time data was expressed as a percentage of the cardiac cycle; giving a final parameter which is expressed as a percentage, thus adjusting for differences in heart rates, both between slice acquisitions and between different patients.

ii) Fourier transformation. CURE and RURE ratios were derived as detailed in **4.2.3** and provide an index of the spatial uniformity of strain from all available slices over the entire cardiac cycle.

iii) Contractile reserve. To quantify the myocardial inefficiency that could be recruited by resynchronisation, the strain delay index (SDI_{16}) was calculated from all 16 segmental Time-ε_{cc} curves using the formula $\sum_{16} (\varepsilon_{cc\ peak} - \varepsilon_{cc\ es})$; where $\varepsilon_{cc\ peak}$ represents segmental peak systolic ε_{cc}, and $\varepsilon_{cc\ es}$ represents segmental instantaneous systolic ε_{cc} at end-systole(Lim et al., 2008). Segments with positive strain or biphasic strain patterns with a greater positive

(stretch) peak than the absolute negative (contraction) peak were not included in the summation as predominantly stretched segments have been shown not to contribute to cardiac resynchronisation (Carasso et al., 2009). In accordance with published methodologies, end-systole was taken as the time of global peak ε_{cc} from all 16 segments (Lim et al., 2008). In a sub-set of 20 patients, absolute concordance between this method, the minimum LV volume derived from the co-ordinates of the tracked endocardial borders and visual inspection of the LV short axis cines was demonstrated. The entire process of calculating SDI_{16} was performed using a custom produced excel spreadsheet and **Figure 7-1** illustrates the methodology.

7.2.5 Statistical analysis

Comparisons between LVRR responders and non-responders were made using an independent samples t-test for continuous variables and either Chi-squared test or log-likelihood ratio test for categorical variables (when the expected cell count was less than 5). The percentage increase in baseline dyssynchrony (compared to the non-response cohort) that the study would detect (β= 0.2) was determined in post-hoc analysis using an online calculator (Kane, 2016). ROC curves were constructed to assess the ability of each dyssynchrony measure to predict LVRR, and were rated according to the traditional academic point system (Metz, 1978). The study population was dichotomised into those with more or less dyssynchrony according to each dyssynchrony index and within group changes in LVESV were compared using paired sample t-tests and between group differences using independent sample t-tests. Cox proportional hazards analyses were used to assess the ability of baseline indexes to predict clinical outcomes. Variables reaching $p< 0.10$ on

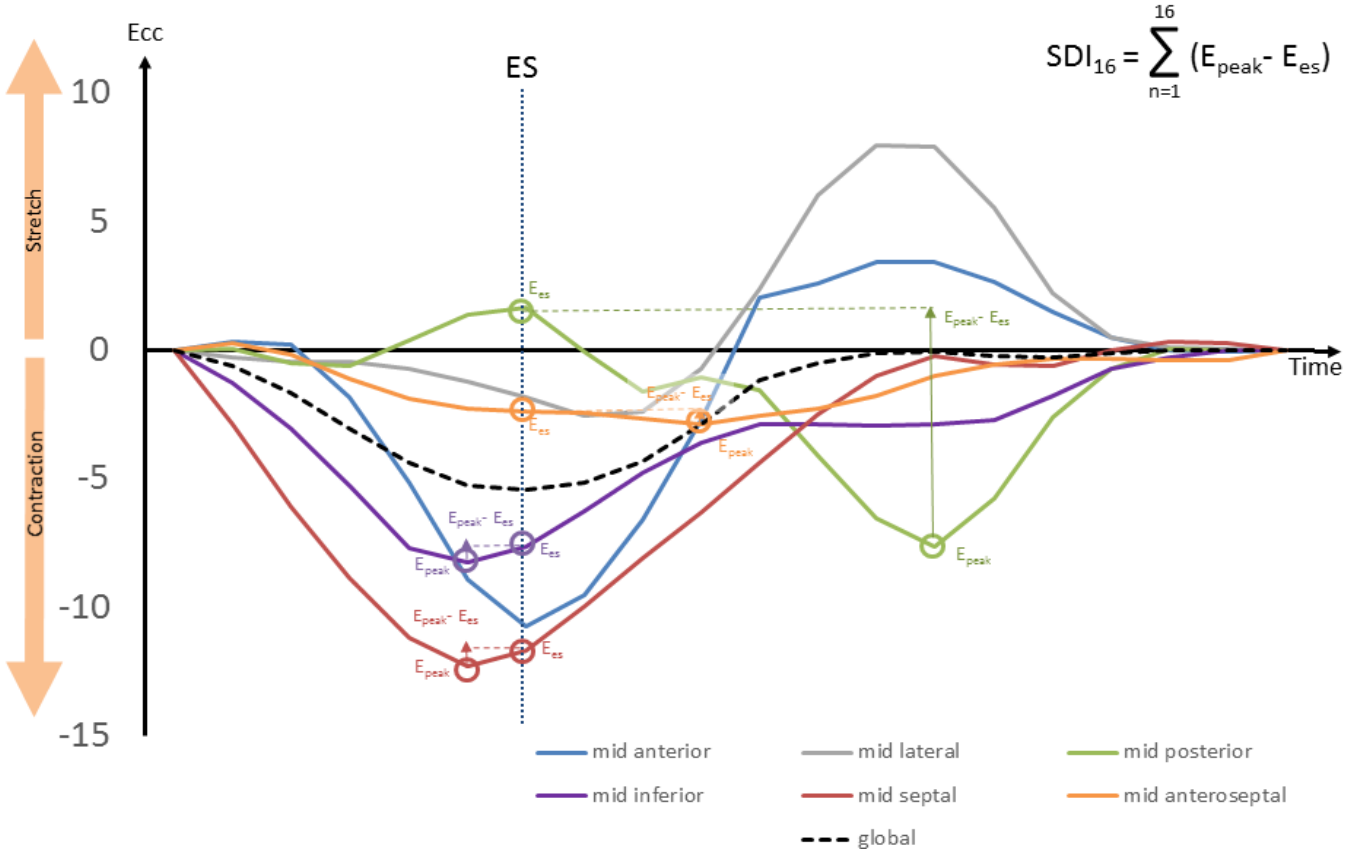

Figure 7-1. Derivation of SDI_{16}

This figure illustrates the derivation of SDI_{16} in a typical subject, a 69 yr old man with a previous LAD territory infarct and LBBB. For clarity only the 6 mid cavity segments are shown (in practice all 16 segments are analysed). Time-Ecc graphs are produced for each segment. The mean of these represents global Ecc (black dash), and the time of peak contraction (negative peak) represents end systole (ES) (dotted reference line). For each segment Ecc is noted at peak contraction (E_{peak}) and at end systole (E_{es}), and the differences (Epeak-Ees), represented by the vector magnitude of the coloured arrows, is the wasted work that can potentially recruited by resynchronisation. The summation of these quantifies total myocardial inefficiency due to dyssynchrony. Late activation of the posterior segment, which maintains good contractility but is which is stretched at ES, provides the greatest inefficiency and will contribute greatest to the summation. The antero-septum (orange) appears late, but the accuracy of identifying a E_{peak} is poor in a scarred segment. Nonetheless, indifference to time to peak contraction methods where the selection of the peak would have a great influence on the final index, the low Epeak-Ees minimises the contribution of this scarred segment to the SDI_{16}. The lateral segment (grey) is predominantly stretched and excluded from summation as it will not contribute to the benefit of resynchronisation.

univariable analyses were entered into multivariable models after inspection for collinearity. The $\chi 2$ of the model was used to assess its power. ROC analyses were conducted to assess the ability of LV functional parameters to predict 5 year survival from cardiac mortality. Optimal cut-offs for each measure were calculated affording equal value to sensitivity and specificity, and the cohort dichotomised around this value and was subjected to Kaplan-Meier survival analyses. Statistical analyses were performed using SPSS v21.0. (SPSS Inc. Chicago, Illinois). A p value of < 0.05 was considered statistically significant.

7.3 Results

7.3.1 Baseline characteristics

The study cohort included 118 CRT recipients, who were 67.8 ± 11 yrs old at implant, 88 (75%) were male, and 66 (56%) had an ischaemic aetiology. 89 patients underwent follow-up echocardiography at 6 months and **Table 7-1** shows the baseline demographics of the entire cohort, and after dichotomisation according to LVRR response.

There were no differences in age, gender, aetiology, NHYA class, co-morbidities, baseline LVEF or QRS duration between the dichotomised cohorts. There were more patients within the non-response cohort who were prescribed beta-blockade compared to responders (71% vs. 45%, p= 0.01), but otherwise the groups were similarly matched for prognostic therapies.

7.3.2 LVRR

Within the entire cohort 42/89 (47%) exhibited LVRR at 6 months. As shown in **Table 7-1** there was no difference in ε_{cc} (-6.5% vs. -6.8%, p= 0.68), ε_{rr} (-10.4% vs. 10.5%, p=0.89), ε_{ll} (-

Table 7-1. Baseline differences between LVRR Responders and Non-responders

	Total Cohort (n = 118)	**LVRR Responder (n = 42)**	**LVRR Non-responder (n = 47)**	**P***
Demographics				
Age (yrs)	67.8 ± 10.9	68.9 ± 10.8	65.0 ± 10.6	0.09
Gender (male)	88 (75)	32 (76)	35 (74)	0.85
Aetiology (ischaemic), n (%)	66 (56)	24(57)	27 (57)	0.98
NHYA class				0.07
II	5 (4)	0 (0)	4 (9)	
III	89 (75)	33 (79)	34 (72)	
IV	24 (20)	9 (21)	9 (19)	
QRS, ms	150.1 ± 23.6	150.9 ± 25.0	148.9 ± 24.9	0.71
Comorbidities, n (%)				
Diabetes mellitus	22 (19)	11 (26)	5 (11)	0.10
Hypertension	27 (23)	9(21)	11 (23)	0.82
Atrial fibrillation	24 (20)	8 (19)	9 (19)	0.99
CABG	21 (18)	6(14)	10 (21)	0.39
Medication, n (%)				
Loop diuretics	100 (85)	33 (79)	40 (85)	0.42
ACEi or ARB	108 (92)	39 (93)	42 (89)	0.57
BB	71 (60)	19 (45)	33 (70)	0.02
MRA	53 (45)	19(45)	21(45)	0.96
Echocardiogram				
LVEF (%)	22.8 ± 9.9	24.8 ± 10.9	21.1 ± 8.2	0.08
CMR LV volumes				
LVEDV (ml)	248.9 ± 95.6	235.2 ± 74.0	274.0 ± 113.1	0.07
LVESV (ml)	198.9 ± 93.5	182.2 ± 74.5	224.1 ± 110.4	0.04

CMR LV functional measures				
LVEF (%)	22.4 ± 9.9	24.6 ± 11.4	20.8 ± 9.3	0.09
$Ɛ_{cc}$ (%)	-7.1 ± 4.0	-6.5 ± 3.0	-6.8 ± 4.1	0.68
$Ɛ_{rr}$ (%)	11.3 ± 4.3	10.4 ± 6.7	10.5 ± 6.9	0.89
$Ɛ_{ll}$ (%)	-8.5 ± 4.3	-9.0 ± 3.5	-8.0 ± 4.6	0.26
E_{3d} (%)	26.9 ± 12.5	25.9 ± 10.5	25.3 ± 12.5	0.81
Dyssynchrony parameters (all patients)				
$SDT2P_{16}$ (%)	17.4 ± 11.6	15.7 ± 8.5	19.3 ± 14.5	0.17
CURE	0.74 ± 0.13	0.75 ± 0.11	0.73 ± 0.12	0.28
RURE	0.63 ± 0.14	0.62 ± 0.13	0.63 ± 0.14	0.71
SDI_{16}	-19.5 ± 10.6	-19.7 ± 10.4	-19.0 ± 10.9	0.78
Dyssynchrony parameters (patients in sinus rhythm)				
$SDT2P_{16}$ (%)	17.9 ± 13.1	15.9 ± 9.1	19.6 ± 15.8	0.24
CURE	0.75 ± 0.12	0.77 ± 0.11	0.74 ± 0.13	0.38
RURE	0.64 ± 0.14	0.63 ± 0.14	0.64 ± 0.14	0.68
SDI_{16}	-19.3 ± 10.8	-20.1 ± 11.4	-18.6 ± 10.3	0.55

Continous variables are presented as mean (± standard deviation), categorical variables are presented as n (%)

P* is given for the difference between responders and non-responders using independent samples t-tests and Pearson's Chi-Square for continuous and categorical variables respectively

ACEi = Angiotensin converting enzyme inhibitor, ARB = Angiotensin receptor blocker, BB = Beta-blocker, MRA = Mineralocorticoid receptor antagonist.

9.0% vs. -8.0%, p= 0.26) or $Ɛ_{3D}$ (25.9% vs. 25.3%, p= 0.81) between LVRR responders and non-responders. Similarly, there was no significant difference in $SDT2P_{16}$ (15.7% vs. 19.3%, p= 0.17), CURE (0.75 vs 0.73, p= 0.28), RURE (0.62 vs. 0.63, p= 0.71) or SDI_{16} (-19.7 vs. -19.0, p=0.78) between responders and non-responders.

Compared to the non-response cohort, this study was able to detect an increase in baseline dyssynchrony of the magnitude of 45% for $SDT2P_{16}$, 10% for CURE, 13% for RURE and 34% for SDI_{16} with a power of 80%.

When analysis was restricted to the sub-group of patients in sinus rhythm, no dyssynchrony parameter emerged as a predictor of LVRR ($SDT2P_{16}$: 15.9% vs. 19.6%, p= 0.24; CURE: 0.77 vs. 0.74, p= 0.38; RURE: 0.63 vs. 0.64, p= 0.68; SDI_{16}: -20.1% vs. -18.6%, p= 0.55).

7.3.3 Symptomatic response

Data on symptomatic response was not collected for 2 patients who survived to 6 months. 92/116 patients met the composite clinical response criteria. When stratifying the cohort according to the composite clinical response criteria there was no difference in LVEF between responders and non-responders (22.3% vs. 22.1%, p=0.92). However, global peak systolic $Ɛ_{rr}$ was significantly lower in those who met the composite clinical response criteria ($Ɛ_{rr}$: 10.5 ± 6.5% vs. 14.9 ± 9.5%, p=0.009), a similar non-significant effect was observed for strain in other directions (Ɛ 1: -6.7 ± 3.4% vs. -8.8 ± 5.6%, p= 0.09; Ɛll: -8.3 ± 4.1% vs. -9.7 ± 4.9%, p= 0.18), and $Ɛ_{3D}$ was significantly lower in clinical responders (-25.5 ± 11.9% vs. -33.4 ± 14.4%, p= 0.006).

There was a non-significant trend towards lower QRS duration in responders (148ms vs. 154ms, p= 0.22). None of the baseline dyssynchrony indexes showed any significant difference according to symptomatic response ($SDT2P_{16}$: 17.7% vs. 14.3%, p= 0.19; CURE: 0.74 vs. 0.74, p= 0.93; RURE: 0.63 vs. 0.64, p= 0.87; SDI_{16}: -17.7% vs. -18.4%, p= 0.82). $SDT2P_{16}$ (17.9% vs. 14.6%, p= 0.32), CURE (0.75 vs 0.75, p= 0.94), RURE (0.64 vs. 0.64, p= 0.97) or SDI_{16} (-17.9 vs. -14.6, p=0.39) remained unable to differentiate between responders and non-responders when only patients in sinus rhythm were considered.

7.3.4 Dyssynchrony as a predictor of response.

The ROC analyses in **Figure 7-2** and **Table 7-2** demonsrate the ability of each dyssynchrony index to predict the likelihood of a LVRR or symptomatic response 6 months post CRT implant. CURE had the highest AUROC of 0.58 (0.45-0.70, p= 0.25), but in accordance with the traditional academic point system (Metz, 1978), all the examined dyssynchrony indexes fail to demonstrate predictive value. **Figure 7-3** shows the study population split into halves with more or less dyssynchrony using the population median value for each index. SDI_{16} was the only index with which patients with more dyssynchrony had a significant reduction in LVESV post CRT (baseline: 208.2 ± 97.6ml, post-CRT 172.1 ± 84.6ml, p= 0.007), but this reduction was not significant when compared to that observed in those with less baseline dyssynchrony (ΔLVESV: 12.6 ± 91.1ml, p= 0.20).

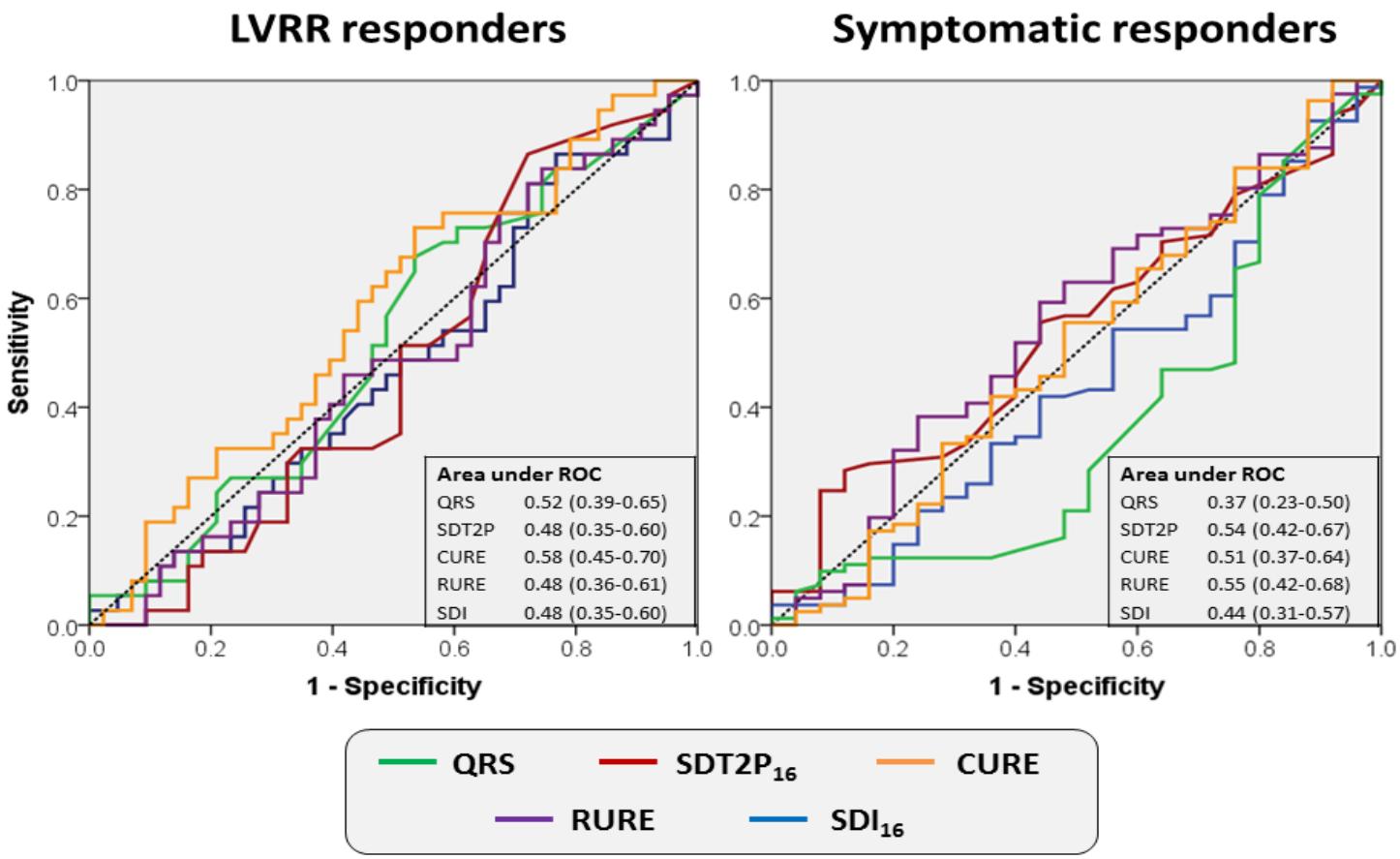

Figure7-2. Receiver operator characteristics for each dysynchrony measures ability to predict response.

ROC curves for each index to predict a) a left ventricular reverse remodelling, and b) a symptomatic response (according to the composite clinical score)

Table 7-2. Receiver operator characteristics for baseline dyssynchrony parameters to act as predictors of symptomatic and echocardiographic response

	AUC	95% C.I.	P
LVRR response			
QRS	0.52	0.39 - 0.65	0.77
$SDT2P_{16}$	0.48	0.35 - 0.60	0.70
CURE	0.58	0.45 – 0.70	0.25
RURE	0.48	0.36 – 0.61	0.80
SDI_{16}	0.48	0.35 – 0.60	0.70
Symptomatic response			
QRS	0.37	0.23-0.50	0.047
$SDT2P_{16}$	0.54	0.54-0.67	0.53
CURE	0.51	0.37-0.64	0.92
RURE	0.55	0.42-0.68	0.47
SDI_{16}	0.44	0.31-0.57	0.38

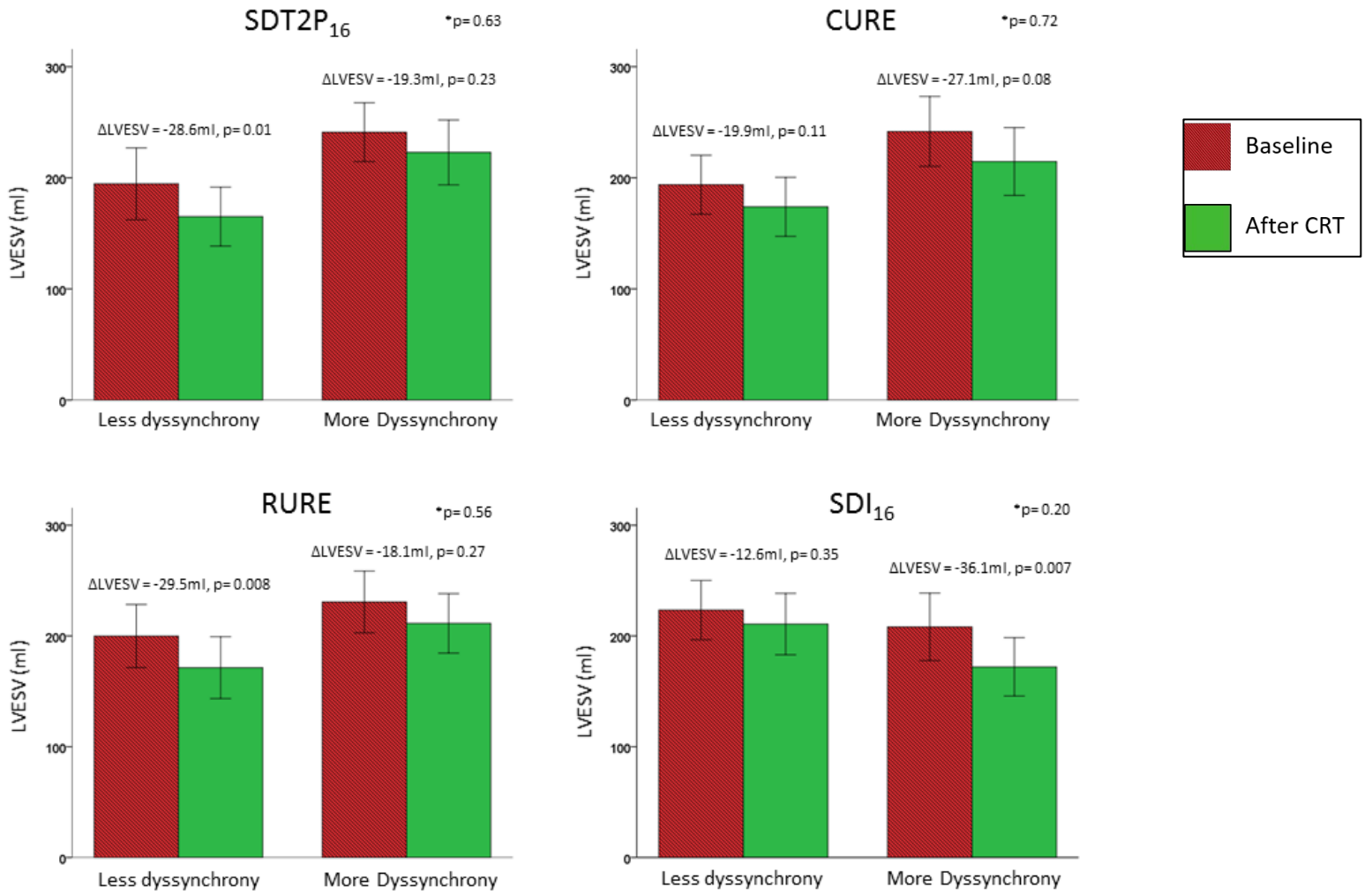

Figure 7-3. Reduction in LVESV according to baseline dyssynchrony

Bar charts of LVESV at baseline and after CRT, with the cohort split into halves above and below the study population median value for each index.

***p= difference in reduction between subgroups.**

7.3.5 Clinical outcomes

Over a 0.1-8.7 yrs (range; median: 3.2 yrs; mean: 3.8 yrs), 34 patients died from cardiac causes, including 1 patient who underwent cardiac transplantation, and there were 27 HF hospitalisations.

The Cox proportional hazard modelling in **Table 7-3** shows that of the baseline variables, increasing age at time of implant and ischaemic aetiology were predictive of cardiac mortality, and ischaemic aetiology was predictive of the composite of cardiac mortality or HF Hospitalisation.

The model shows that baseline LVEF as assessed by CMR (HR 0.93, 95% C.I. 0.89-0.97) but not by 2DE (HR 0.97, 95% C.I. 0.93-1.004) was a univariable predictor of cardiac mortality in Cox proportional hazards analyses. Both predicted the composite of cardiac mortality or hospitalisation for heart failure, although CMR LVEF (HR 0.93, 95% C.I. 0.89-0.97) was more powerful than 2DE LVEF (HR 0.96, 95% C.I. 0.92-0.997). ε_{3D} was a strong univariable predictor of cardiac mortality (HR 0.94, 95% C.I. 0.90-0.97) and cardiac mortality or hospitalisation for heart failure (HR 0.93, 95% C.I. 0.90-0.97). Of the individual strains ε_{ll} (HR 0.88, 95% C.I. 0.80-0.97) and ε_{rr} (HR 0.93, 95% C.I. 0.87-0.99), but not ε_{cc} (HR 1.10, 95% C.I. 0.99-1.21) predicted cardiac mortality, and all individual strains predicted the composite outcome.

No dyssynchrony parameter predicted cardiovascular mortality ($SDT2P_{16}$: HR 0.98-1.04; CURE: HR 0.1 -22.0; RURE: HR 0.01 - 1.78; SDI_{16}: HR 0.99-1.07). Greater baseline

Table 7-3. Cox proportional Hazards Analyses of Baseline Variables in Relation to Clinical Outcome.

	Cardiac Mortality			Cardiac Mortality / HF Hospitalisation		
	HR	**95% C.I.**	**P**	**HR**	**95% C.I.**	**P**
UNIVARIABLE ANALYSES						
Baseline variables						
Age (yrs)	1.04	1.00-1.07	0.03	1.02	0.99-1.06	0.12
Gender (male)	2.20	0.85-5.68	0.104	2.26	0.88-5.81	0.09
Aetiology of HF (ischaemic)	4.24	1.76-10.3	0.001	3.08	1.41-6.74	0.005
NYHA class	1.80	0.91-3.56	0.09	1.85	0.96-3.57	0.067
Atrial Fibrillation	2.01	0.98-4.12	0.06	1.04	0.47-2.30	0.92
QRS duration (ms)	1.00	0.99-1.01	0.59	1.00	0.99-1.02	0.54
LV systolic function						
2DE LVEF (%)	0.97	0.93-1.004	0.08	0.96	0.92-0.997	0.03
CMR LVEF (%)	0.93	0.89-0.97	0.002	0.93	0.89-0.97	0.001
E_{cc} (%)	1.10	0.99 - 1.21	0.08	0.88	0.80-0.98	0.02
E_{rr} (%)	0.93	0.87-0.99	0.01	0.91	0.86-0.97	0.004
E_{ll} (%)	0.88	0.80-0.97	0.01	0.87	0.79-0.96	0.004
E_{3D} (%)	0.94	0.90-0.97	0.001	0.93	0.90-0.97	<0.001
Dyssynchrony parameters (entire cohort)						
CURE	1.48	0.10-22.0	0.77	0.36	0.24-53.6	0.36
RURE	0.14	0.01-1.78	0.13	0.06	0.01-0.68	0.02
$SDT2P_{16}$ (%)	1.01	0.98-1.04	0.48	1.02	1.00-1.04	0.13
SDI_{16} (%)	1.03	0.99-1.07	0.11	1.04	1.01-1.09	0.03
Dyssynchrony parameters (patients in sinus rhythm only)						
CURE	4.4	0.15-132.6	0.39	7.97	0.34-186.3	0.20
RURE	0. 22	0.01-4.26	0.32	0.09	0.01-1.32	0.08
$SDT2P_{16}$ (%)	1.01	0.99-1.04	0.36	1.02	0.995-1.05	0.11
SDI_{16} (%)	1.03	0.98-1.08	0.20	1.04	0.996-1.08	0.08

MULTIVARIABLE ANALYSES						
Model 1						
RURE	-	-	-	0.15	0.01-0.61	0.02
SDI_{16} (%)	-	-	-	1.05	1.01-1.09	0.03
Model 2a						
Age (yrs)	1.02	0.98-1.05	0.31	-	-	-
Gender (male)	-	-	-	0.37	0.13-1.11	0.08
Aetiology of HF (ischaemic)	4.25	1.70-10.6	0.002	3.02	1.31-6.94	0.009
NYHA class	1.83	0.89-3.78	0.10	1.99	0.96-4.13	0.07
RURE	-	-	-	0.35	0.02-7.89	0.51
SDI_{16} (%)	-	-	-	1.03	1.00-1.07	0.09
CMR LVEF (%)	0.94	0.90-0.99	0.01	0.93	0.88-0.98	0.009
Model 2b						
Age (yrs)	1.04	1.00-1.08	0.048	-	-	-
Gender (male)	-	-	-	0.63	0.20-1.95	0.42
Ischaemic aetiology	2.62	0.99-6.97	0.053	2.19	0.86-5.52	0.10
NYHA class	1.93	0.88-4.22	0.10	2.18	1.02-4.65	0.045
RURE	-	-	-	0.41	0.01-12.1	0.61
SDI_{16} (%)	-	-	-	1.06	1.01-1.10	0.01
E_{3D} (%)	0.94	0.90-0.99	0.009	0.94	0.90-0.99	0.01
Model 2						
CMR LVEF (%)	0.94	0.91-1.003	0.06	0.95	0.90-0.998	0.04
E_{3D} (%)	0.96	0.89-0.999	0.047	0.95	0.91-0.99	0.02
Model 3						
2DE LVEF (%)	0.99	0.91-1.003	0.06	0.98	0.93-1.02	0.25
E_{3D} (%)	0.94	0.90-0.98	0.005	0.94	0.90-0.98	0.002

dyssynchrony as measured by RURE (HR 0.01 - 0.68) or SDI_{16} (HR: 1.01-1.09), but not by $SDT2P_{16}$ (HR 1.00-1.04) or CURE (HR 0.24-53.6) predicted the composite of cardiovascular mortality and HF hospitalisation. RURE and SDI_{16} were not collinear and both remain independently predictive when modelled together (model 1); neither remained predictive when only the smaller sub-cohort of patients in sinus rhythm was considered.

A multivariate model was constructed consisting of all non-colinear univariate predictors (**Table 7-3)**. Incorporating CMR LVEF as the functional metric (model 2a), LVEF (cardiac mortality: HR 0.94, 95% C.I. 0.90-0.99; cardiac mortality or hospitalisations for HF: HR 0.93 95% C.I. 0.88-0.98) and an ischaemic aetiology (cardiac mortality: HR 4.25, 95% C.I. 1.70-10.6; cardiac mortality or hospitalisations for HF: HR 3.02 95% C.I. 1.31-6.94) were the main determinants of outcome. When LVEF was substituted for $Ɛ_{3D}$, $Ɛ_{3D}$ (HR: 0.94 95% C.I. 0.90-0.99), but not ischaemic aetiology (HR 2.62, 95% C.I. 0.99-6.97) was predictive of cardiac mortality (model 2b). The same trend was observed when predicting cardiac mortality or hospitalisations for HF ($Ɛ_{3D}$: HR 0.94 95% C.I. 0.90-0.99; Ischaemic aetiology: HR 2.19 95% C.I. 0.86-5.52); NYHA class (HR 2.18, 95% C.I. 1.02-4.65) and SDI_{16} (HR 1.06, 95% C.I. 1.01-1.10) were further independent predictors.

When CMR LVEF and $Ɛ_{3D}$ were considered together, $Ɛ_{3D}$ (HR 0.96, 95% C.I. 0.89-0.999) but not LVEF (HR 0.94, 95% C.I. 0.91-1.003) was an independent predictor of cardiac mortality. Both parameters predicted the composite outcome ($Ɛ_{3D}$: HR 0.94, 95% C.I. 0.91-0.99; LVEF: HR 0.95, 95% C.I. 0.90-0.998).

Table 7-4 shows the optimum cut-off for each functional measure to predict 5 year survival from cardiac mortality from ROC analyses; E_{3D} has the greatest AUROC (0.75 95% C.I. 0.65-0.85) but all parameters were significant predictors. As shown in **Figure 7-4,** above an optimum cut-off of 20.3%, ε_{3D} predicted survival free from cardiac mortality (Log Rank [LR] $\chi 2 = 11.63$, $p= 0.001$) and cardiac mortality and HF hospitalisation (LR $\chi 2 = 15.34$, $p< 0.001$). Above an optimum cut-off of 16.6%, LVEF similarly predicted event free survival (cardiac mortality: LR $\chi 2 = 12.97$, $p< 0.001$; cardiac mortality and HF hospitalisation: LR $\chi 2 = 17.08$, $p< 0.001$).

7.3.6 Moderate LV systolic dysfunction

Based on CMR volumetrics, 15 patients would be reclassified as having an LVEF >35% and thus moderate rather than severe LV systolic dysfunction. This sub-group had a better LVRR (62% vs. 45%, p= 0.19) and clinical response (93% vs. 77%, p= 0.37) than the rest of the cohort although the small numbers meant that these were not significant. Only 1 patient reclassified as moderate LVSD had an event (cardiac death preceeded by a HF hospitalisation) which translated into significantly better outcomes than other patients (cardiac mortality: LR $\chi 2 = 3.85$, $p= 0.05$; cardiac mortality and HF hospitalisation: LR $\chi 2 = 4.95$, $p= 0.03$).

Table 7-4. Optimal cut-offs for functional measures to predict 5 year survival free from cardiac mortality.

	Optimum cut-off	AUC	95% C.I.	P
2DE LVEF (%)	17.0	0.59	0.46-0.73	0.01
CMR LVEF (%)	16.6	0.69	0.58-0.79	0.002
Ecc (%)	5.97	0.70	0.59-0.80	0.002
Err (%)	9.98	0.74	0.64-0.84	<0.001
Ell (%)	5.5	0.67	0.56-0.78	0.009
E3D (%)	20.28	0.75	0.65-0.85	<0.001

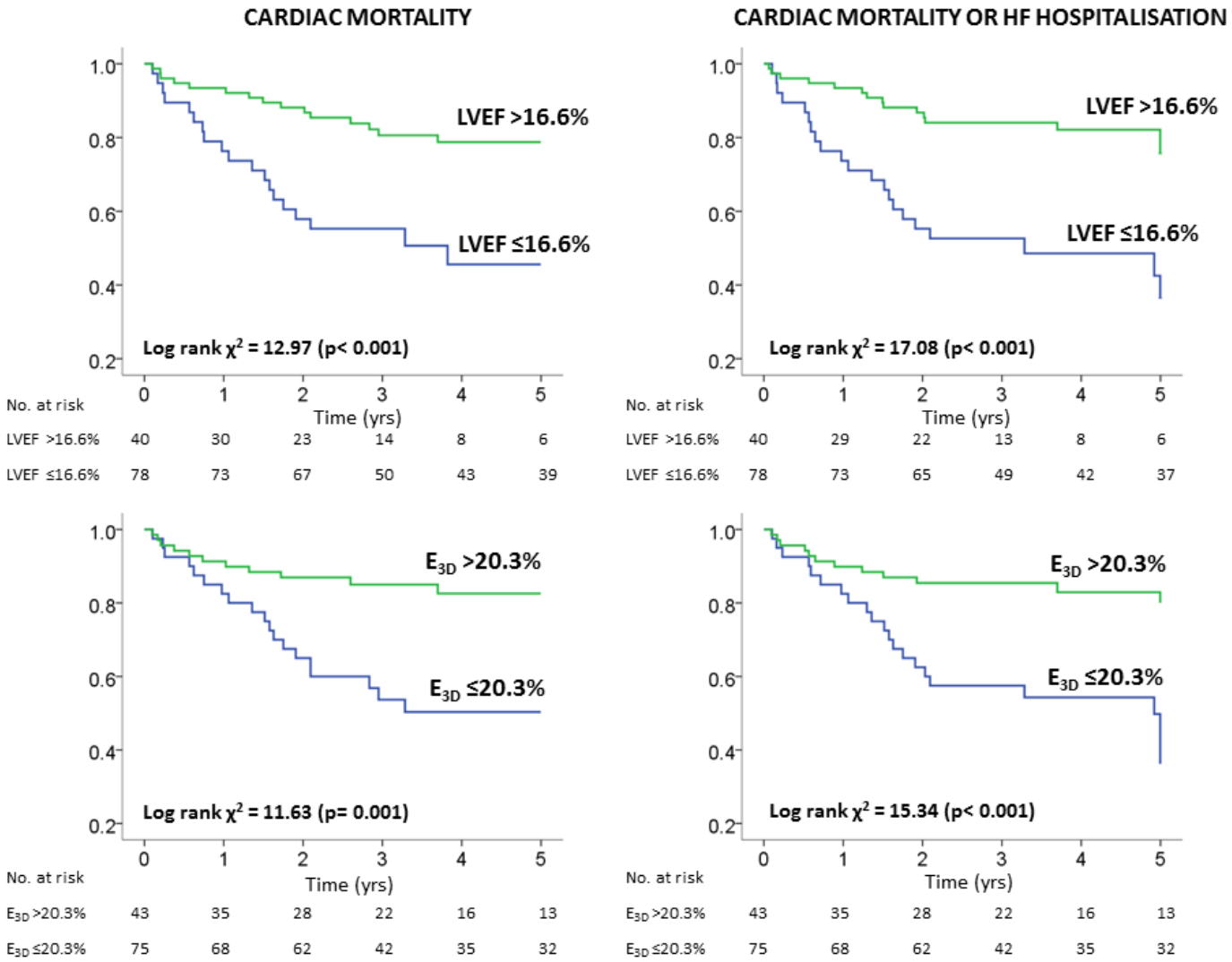

Figure 7-4. Cardiovascular mortality and hospitalisations after CRT according to baseline LV function.

7.4 Discussion

7.4.1 Major findings

In this study we derived 3 distinct classes of CMR based dyssynchrony parameters; none proved apt to refine patient selection for CRT implant. More severe dyssynchrony at baseline when measured by Fourier or contractile reserve techniques was associated with poorer long term outcomes, although this was not independent of LV function and scar.

This study also provides the first comparison of the utility of 2DE and CMR derived functional measures to predict outcomes following CRT. Poorer LV function at baseline regardless of the modality used predicted a worse long-term outcome. LVEF is a more powerful predictor of outcomes post CRT when it is measured by CMR as opposed to with 2DE. This likely relates to 2DEs inferior precision for the quantification of LVEF, and this could explain why this relationship is not universally reported (Kreuz et al., 2012).

In numerous cardiac populations, 2DE studies' measures of myocardial strain have been shown to be more powerful predictors of outcome than LVEF (Ersboll et al., 2013; Mignot et al., 2010; Stanton et al., 2009). This phenomenon is not merely due the inaccuracies of 2DE for the measurement of LVEF as this concept remains valid when both LVEF and strain are measured with CMR.

7.4.2 Baseline dyssynchrony assessment and patient selection

The concept behind cardiac resynchronisation is the correction of the disordered electrical and mechanical activation sequence that is frequently associated with HF, and the notion of a marker that enhances the quantification of this defect, and thus predicts the possible benefit from CRT remains highly desirable yet elusive. This study examined the predictive value of FT-CMR derived dyssynchrony and none of the major classes of dyssynchrony index demonstrated potential for enhancing patient selection; the implication is that there is a deficiency of either this methodology, or of the underlying concept of dyssynchrony analysis.

At this early stage in its evolution the appropriateness of FT-CMR to assess dyssynchrony requires scrutiny. Kuetting et al., have recently studied the ability to use FT-CMR to discriminate between healthy controls and HF patients with velocity encoding (VENC) proven dyssynchrony using differences between the timing of peak longitudinal velocity at the basal septal and lateral basal myocardium (Kuetting et al., 2016). Whilst FT-CMR could correctly differentiate 100% of healthy controls, 18% of patients with dyssynchrony were misclassified as normal. FT-CMR is a crude tool and the technique used in this investigation has a reliance on unfavourable aspects of this methodology. Instantaneous measures such as velocity rely on differences between two frames, and are more prone to error than time integrals such as strain, which rely on measures over a series of frames. This is compounded by using time to peak methodology that is prone to estimation variance. Fourier transformation indexes such as CURE and RURE utilised in this study were designed to smooth out such errors by incorporating strain measures at over 7000 spatial and temporal

points, and **chapter 4** demonstrates their excellent ability for discrimination between healthy controls and NICM patients (Taylor et al., 2014).

Dyssynchrony assessment is intimately related to the temporal resolution of the acquisitions and the mean temporal resolution of cines in this study is < 3-4x the suggested optimum for STE. Whilst it is plausible that increased temporal resolution would improve our markers' clinical value, this alone should not explain the failure of CURE or RURE to act as predictors of response. Our temporal resolution is typical of standard CMR acquisitions, and higher than that used in a study by Bilchick et al., who reported that CURE derived from myocardial tagging could predict symptomatic response. Our findings are also in difference to the MUSIC (Multicentre study using strain delay index for predicting response to cardiac resynchronization therapy) study where a contractile reserve approach to dyssynchrony assessment, using STE derived longitudinal strain, had a positive and negative predictive value of 80% and 84% above a SDI threshold of 25% (Lim et al., 2011).

Further support that FT-CMR derived dyssynchrony is a valid technique comes from demonstration of its clinical utility in a recent Italian study, where it was used to provide incremental value to SSFP imaging for the diagnosis of Arrhythmogenic right ventricular cardiomyopathy (ARVC) (Prati et al., 2015). RV dyssynchrony measures based on the SD of time to peak strains had an AUROC of 0.80 to differentiate between true ARVC and patients with more benign RV outflow tract arrhythmias, even in patients who had an absence of conventional CMR criteria for diagnosing ARVC (Marcus et al., 2010).

Whilst failure of multi-study trials such as PROSPECT (Chung et al., 2008) and EchoCRT (Ruschitzka et al., 2013) to demonstrate a role for dyssynchrony testing to aid patient selection may relate to the inability of operators to obtain the various measures, and high inter-operator variability, there may be a more fundamental floor in the concept of dyssynchrony testing. Response is a difficult entity to measure, and it is dependent on the interplay of multiple factors. The notion of a simple parameter that predicts response overlooks the contribution of lead position, underlying myocardial substrate, device timing optimisation, RV function, valvular incompetence and comorbid states such as anaemia and renal dysfunction. A final possibility is that baseline mechanical dyssynchrony is not a pre-requist to derive benefit from CRT. This theory is supported by MADIT-CRT, where the relationship between baseline dyssynchrony and benefit was not linear. Those with the greatest dyssynchrony pre-implant fared worse than those with mild-moderate dyssynchrony (Kutyifa et al., 2013).

7.4.3 Atrial fibrillation, CRT and dyssynchrony

There is a paucity of data to confirm the benefit of CRT in patients with AF, primarily due to their under representation in clinical studies. The percentage of biventricular pacing is a key determinant of success following CRT (Hayes et al., 2011), this is sub-optimal in the setting of AF as irregular and faster ventricular rates result in intrinsic ventricular activation as well as fusion and pseudofusion. Furthermore, in AF the loss of atrial transport restricts benefits to improved inter-ventricular and intra-ventricular co-ordination, whereas patients in sinus rhythm also benefit from improved atrio-ventricular synchrony. Nonetheless, national (NICE, 2014) and international (Brignole et al., 2013) guidelines have been updated to

allocate CRT to AF patients with the same clinical indications as those in sinus rhythm, reflecting widespread consensus of the benefit in this patient population and corroboration from a meta-analysis of prospective cohorts (Upadhyay et al., 2008). European registries show that a quarter of CRT recipients are in AF, this has remained uniform over the last decade (Dickstein et al., 2009; Dickstein et al., 2018). Accordingly, it is important not to restrict patients with atrial fibrillation from research in this field.

The majority of research in the field of dyssynchrony has excluded patients with AF. It must be considered that AF may interfere with the accuracy of dyssynchrony assessment. FT-CMR has been validated against STE for radial based time to peak methods, but patients in atrial fibrillation were excluded (Onishi et al., 2013). Such patients pose a greater concern in CMR studies as in difference to echocardiography, which makes use of real time imaging, acquisitions are periodic with a cine loop reconstructed from ECG gated data over several cycles. Fourier-based dyssynchrony assessment is likely to be most at risk of diminished quality in AF as these incorporate diastolic frames into the total index score, but these are likely to be preferentially hindered with prospective gating at R-R intervals shorter than the longest seen, as was employed in this cohort. Nonetheless, there was an even spread of atrial fibrillation between responders and non-responders, and analysis within the sinus rhythm sub-cohort failed to reveal any benefit of dyssynchrony assessment.

7.4.4 LV function as a predictor of outcome

The landmark pharmacotherapy trials demonstrate that lower LVEF is associated with reduced survival in HF (Quinones et al., 2000; Solomon et al., 2005; Wong et al., 2004). This study suggests that CRT does not break this relationship.

The predictive value of a parameter will naturally be affected by the precision with which it can be measured, and this is the probable explanation for LVEF having greater univariate predictive power when derived by CMR as opposed to with 2DE. 2DE volumetric analysis relies on the geometric modelling of the LV as a prolate ellipsoid, and this assumption loses validity in the remodelled ventricle.

Higher baseline values of all three axial strains predicted survival after CRT implantation, and their summation produced a powerful predictor. It is not surprising that ε_{3D} and LVEF predict outcome independently, as whilst they correlate in healthy controls, there is discordance between them in the failing heart (Delgado et al., 2008). This stems from the unique yet complimentary detail on cardiac function they convey. LVEF is a marker of cardiac output and is influenced by the compensatory neurohumoral and systemic vascular responses. In difference, myocardial strain is a purer gauge of the myocardium's contractile function. In this respect, global strain measures are affected by the degree of myocardial scarring (Becker et al., 2006b), and this is reflected in the survival modelling. LVEF and ischaemic aetiology are strong independent predictors of outcome, but when ε_{3D} is utilised as an alternative functional measure, it carries a greater weight than LVEF and ischaemic aetiology combined (**Figure 7-5**).

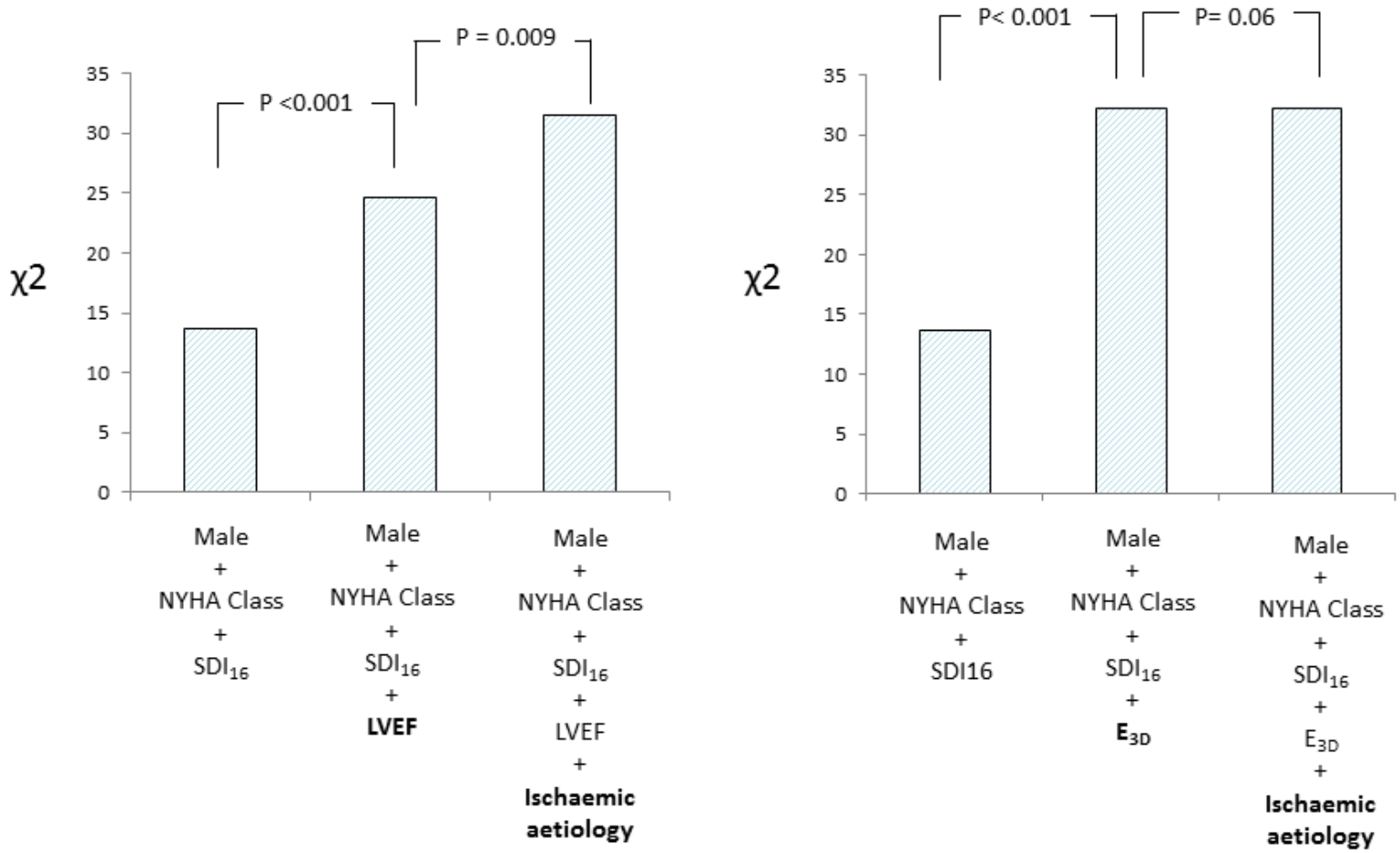

Figure 7-5. Multivariate analysis illustrating the incremental value of LV functional measures and ischaemic aetiology when modelling survival from cardiac mortality and heart failure hospitalisation.

These findngs are in accord with a model to predict survival in a population of 546 all-comers, attending an echocardiography department for LV function assessment. The addition of either LVEF or ε_{II} added substantial predictive power, but the latter provided greater incremental power (Stanton et al., 2009). Comparable findings are reported in the modelling of populations with a less diverse spread of LV function, such as those with HFrEF (Mignot et al., 2010), or preserved LVEF post MI (Ersboll et al., 2013).

7.4.5 Baseline dyssynchrony as a predictor of outcome

Patients with the greatest dyssynchrony as measured by either RURE or SDI_{16} had a greater event rate even despite resynchronisation. This may reflect that greater dyssynchrony is one manifestation of more advanced heart failure. However, that patients with the greatest myocardial inefficiency according to the SDI_{16} had poorer outcomes even despite CRT is in difference to the findings of Kydd et al. who reported that higher pre-implant SDI was associated with improved outcomes over a 2 year follow-up (Kydd et al., 2013). It is intuitive that wasted work is directly associated with poorer long term outcomes, and in MUSIC, although this metric was reduced post-implant in responders, it remained higher than in those who had minimal wasted work pre-implant (Lim et al., 2011). Conceivably, the quantification of wasted work post CRT is a better determinant of outcome, and as yet no study has evaluated this relationship.

7.4.6 CRT and moderate LVSD

Clinical studies to test whether CRT is a viable proposition for those with more moderate LV systolic dysfunction may prove implausible due to the long follow-up period required as

exemplified by the failure of MIRACLE EF. However, in this study, where CMR has been used to re-classify 15 patients as having moderate LVSD, this group showed improved rates of LVRR and symptomatic response compared to those with confirmed severe LV systolic dysfunction, although small numbers prevent meaningful statistical analysis. This sub-group, as anticipated, had an exceptionally low event rate.

These findings corroborate a subgroup analysis of the 696 patients in MADIT-CRT who were adjudged to have more moderate LVSD, where the best remodelling response was seen in the least impaired ventricles (Kutyifa et al., 2013). The availability of a control arm in this study shows that this group also saw the greatest protection from hospitalisation and death (HR: 0.56). Similarly, an observational study of 520 patients, which defined HF remission as improvement to NYHA class I functional status and a normalisation of LVEF (to >50%), found that greater function at baseline was a predictor of remission (Gasparini et al., 2008).

7.4.7 Limitations

The main limitation is that this is a single-centre study which includes only a moderate number of patients. As FT-CMR is applied to standard acquisitions it has the capacity to study retrospective cohorts. A drawback to this is that the cine images were not optimised for this purpose and it is indeterminable as to whether greater temporal resolution would have improved the value of dyssynchrony testing. Unfortunately, we have not systematically collected data on QRS morphology, and this may have had an influence on response.

As no dyssynchrony parameter has a proven clinical utility, selecting an adequate sample size to test novel indices is challenging. However, the presence of pre-implant dyssynchrony has been shown to predict response in single centre studies, and the magnitude of the difference in dyssynchrony between responders and non-responders, seen when analogous parameters to those herein were calculated with STE, suggests that this study cohort was of ample size. 64% and 84% differences in baseline dyssynchrony have been observed between echocardiographic responders and non-responders using SDI_{16} (Lim et al., 2011) and time to peak methodologies (Tanaka et al., 2010) respectively in similar sized cohorts.

7.5 Conclusions

In this study, FT-CMR derived dyssynchrony variables were not useful in predicting LV reverse remodelling or symptomatic improvement in patients undergoing CRT. Greater dyssynchrony at baseline as measured by RURE and SDI_{16} predicted a higher subsequent event rate. Baseline functional assessment with CMR was a better predictor of long term outcomes following CRT as compared to 2DE derived measures. For CMR measures of LV function, myocardial strain was a more powerful predictor of outcomes than LVEF.

8 LEFT VENTRICULAR LEAD POSITION, MECHANICAL ACTIVATION, AND MYOCARDIAL SCAR IN RELATION TO LEFT VENTRICULAR REVERSE REMODELING AND CLINICAL OUTCOMES AFTER CARDIAC RESYNCHRONISATION THERAPY: A FEATURE-TRACKING AND CONTRAST-ENHANCED CARDIOVASCULAR MAGNETIC RESONANCE STUDY

Principal hypothesis: The deployment of the LV lead over non-scarred segments with LMA, assessed using LGE-CMR and FT-CMR, is associated with increased likelihood of a LVRR response from CRT.

8.1 Introduction

CRT is a standard treatment for patients with HF, impaired LV systolic function and a wide QRS complex. In addition to prolonging survival (Bristow et al., 2004; Cleland et al., 2005), CRT reduces HF hospitalisations and improves symptoms, including exercise capacity and quality of life (Abraham et al., 2002; Bristow et al., 2004; Cleland et al., 2005). As with any other therapy (Foley et al., 2009b), CRT leads to a variable treatment response. This has led to the concept of 'non-responders' (Molhoek et al., 2002).

Whilst patient selection is important in reducing 'non-responders', the response to CRT is still variable and unpredictable, even when the LV lead is deployed in fluoroscopically 'optimal' LV pacing positions. This variability is not surprising, as fluoroscopy is opaque to biological properties of the LV myocardium. Echocardiographic studies have suggested that better LV resynchronisation, LV reverse remodeling and clinical outcomes after CRT can be

achieved by pacing the 'latest mechanically activated' (LMA) LV segments (Khan et al., 2012a; Saba et al., 2013). FT-CMR has been validated against the gold-standard of CMR-tagging for the assessment of myocardial deformation (**chapter 2**) (Moody et al., 2015).

Studies using LGE-CMR (Chalil et al., 2007a; Chalil et al., 2007c; Leyva et al., 2011) and nuclear scintigraphy (Adelstein et al., 2007) have shown that myocardial scarring in the segment subtended by the LV lead leads to a suboptimal response to CRT. These findings are consistent with the observation that pacing scar is associated increased duration (Schwartzman et al., 1999) and fragmentation of the QRS complex, as well as suboptimal resynchronisation. (Bleeker et al., 2006b) Moreover, myocardial scars are not readily excitable (Tedrow et al., 2004) and effectively reduce the volume of myocardium available for LV pacing (Breithardt et al., 2002). We hypothesized that deployment of the LV lead over non-scarred segments with LMA, assessed using LGE-CMR and FT-CMR, leads to a better LVRR response and outcome from CRT.

8.2 Methods

8.2.1 Study population and study design

This study utilises the same historical CRT population recruited through the dedicated heart failure service at a single centre who were the subject of previous chapters. Inclusion and exclusion criteria are as described in **7.2.1**. Device therapy (**5.2.2**), CMR acquisition (**5.2.3**), follow-up (**5.2.6**) and study end-points (**5.2.7**) are as described in **chapter 5**.

8.2.2 Scar analysis

The myocardium was divided into 16 segments (Cerqueira et al., 2002) and scar was recorded as present or absent in each segment based on visual assessment by an experienced observer (R.T.) using CVI^{42} software (Circle Cardiovascular Imaging Inc.,Calgary, Canada). Myocardial segments were considered scarred or not in a binary fashion; a segment was delineated as scar if it contained an area of enhancement >10% of the total segment area.

8.2.3 Identification of site of latest mechanical activation

FT-CMR (Tomtec Imaging Systems, Munich, Germany) of the basal, mid and apical short axis slices was undertaken as previously described **3.2.4.** In contrast to speckle-tracking echocardiographic studies (Khan et al., 2012b; Saba et al., 2013), which have employed radial strain to define LMA, this study used circumferential strain on the basis of previous validation against CMR-tagging (**chapter 2**)(Hor et al., 2010; Moody et al., 2015), and a superior reproducibility (**chapter 1**) (Morton et al., 2012; Taylor et al., 2015). On the basis of an initial validation study (**Appendix 2**: FT-CMR derived myocardial strain as a surrogate for scar), a cut-off of -6.3% was selected to favour specificity for scar rather than sensitivity, as the latter was more optimally provided by LGE-CMR. The LMA segments were those with the latest peak systolic circumferential strain within the imaged cardiac cycle (as a percentage of the R-R interval). Only the 11 free wall segments were considered. Segments with a peak systolic circumferential strain above zero or between zero and -6.3% were excluded from the LMA analysis.

8.2.4 Lead positions

The final position of the LV lead was assessed using the 30^{o} right anterior (RAO) and left anterior (LAO) fluoroscopic projections at the time of implantation by an investigator who was blinded to all other study data. According to Albertsen et al. (Albertsen et al., 2005), the 30^{o} RAO projection was used to identify the long-axis position of the LV lead (basal, mid or apical) and the 30^{o} LAO projection was used to identify the circumferential position (anterior, anterolateral, posterior, posterolateral or inferior). In addition, the LV lead tip was mapped to a specific segment based on the AHA 16-segment model. Concordance was defined as a LV lead position that met two criteria: i) subtended a non-scarred segment, ii) subtended LMA or the adjacent segment. Non-concordance was defined as LV lead tip position in scarred and/or earlier-activated segments (**Figure 8-1**).

8.2.5 Statistical analysis

Categorical variables are expressed as a percentage and continuous variables as mean ± SD. Normality was tested using the Shapiro-Wilk test. Comparisons between concordant and non-concordant lead positions were made using independent samples t-tests for continuous variables and either Chi-squared test or Fishers exact test for categorical variables (when the expected cell count was less than 5). Within-group comparisons were made using paired sample t-tests. Predictors of LVRR were analysed using logistic regression. The influence of LV lead position in relation to outcomes was assessed using Kaplan-Meier survival curves, the log-rank (Mantel-Cox) test and Cox proportional hazard analyses. Statistical analyses were performed using SPSS v21.0. (SPSS Inc. Chicago, Illinois). A p value of < 0.05 was

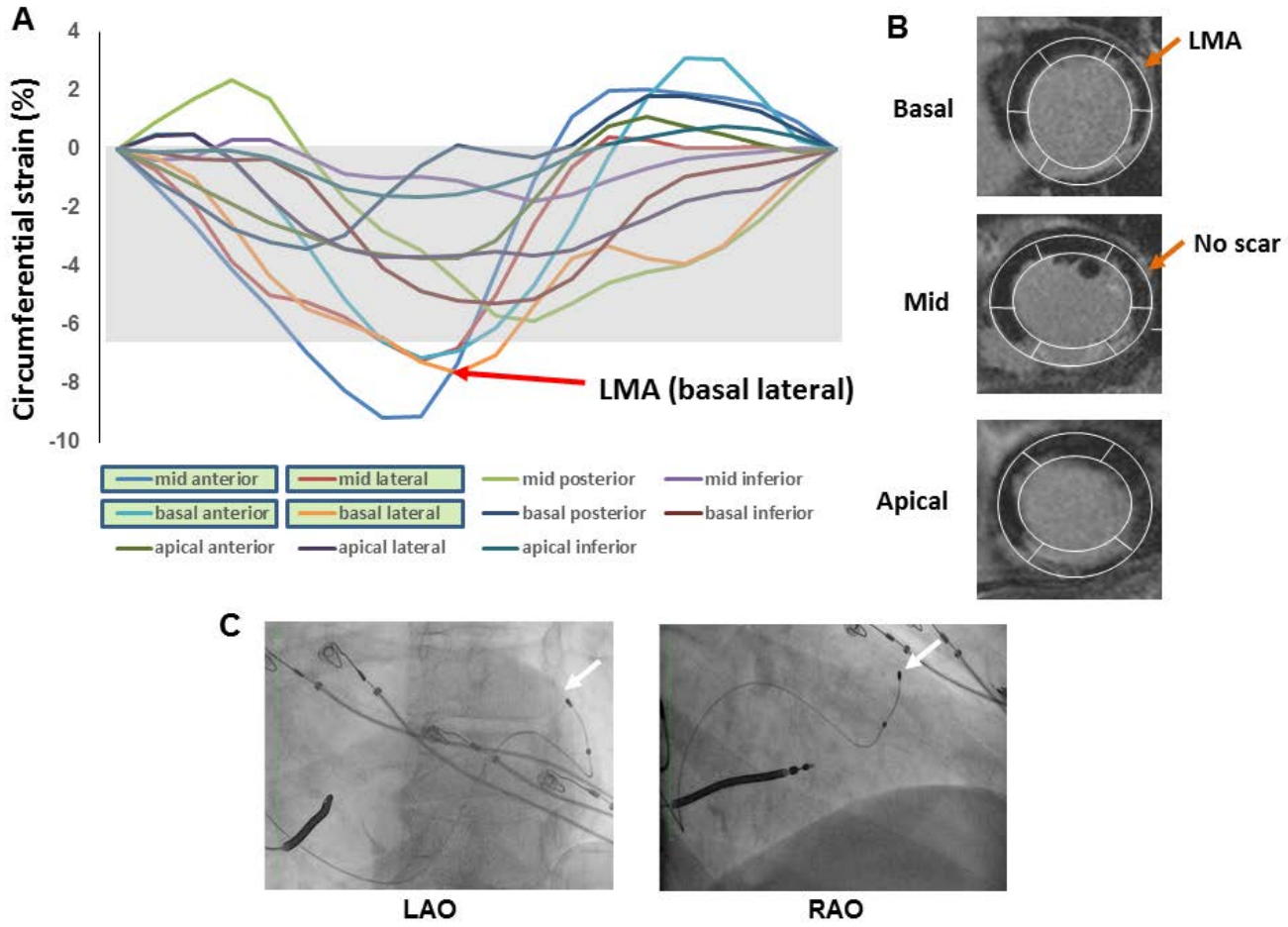

Figure 8-1. Left Ventricular Lead Position, Scar and Mechanical Activation.

Panel A shows circumferential strain (%) curves over one cardiac cycle, derived using FT-CMR. Segments with a peak circumferential strain above zero or between zero and -6.3% were considered scarred and excluded (gray zone) from analysis of LMA. Segments with a peak strain ≤-6.3% included the basal anterior and lateral, and the mid anterior and lateral (green boxes). Out of these, the basal lateral segment is the latest to reach peak systolic strain and was selected as the LMA segment. Panel B shows short-axis LGE-CMR images, from LV base to apex, with myocardial scar showing in white. Panel C shows the final fluoroscopic LV lead position in a mid lateral segment, at a 1 o'clock position on the left anterior oblique [LAO] view and mid position on the right anterior oblique [RAO] views)(white arrows), which is considered concordant (non-scarred segment adjacent to the LMA segment).

considered statistically significant. Variables reaching p<0.10 on univariable analyses were entered into multivariable models.

In TARGET, a guided approach led to a 15% increase in LVRR compared to the control arm (70% vs 55%). Accepting β= 0.2, 160 patients would be required to replicate a similar finding; 89 patients power this study to demonstrate a 20% difference in LVRR (70% vs. 50%). However, substantially greater benefit was anticipated in this study which compared LV concordance against non-concordance; the 15% improvement in LVRR in TARGET was seen despite LV concordance only being achieved in 63% with an echocardiographic guided approach, compared to 47% of controls.

8.3 Results

8.3.1 Baseline characteristics

As shown in **Table 8-1**, patients were 66.8 ± 10.8 yrs old (mean ± SD), 67 (75%) were male and in 50 (56%), HF was ischaemic in aetiology. The QRS duration was 149.0 ± 25.7 ms and the LVEF was 23.1±9.9%. No differences emerged with respect to age, gender, NYHA class, co-morbidities, pharmacologic therapy or baseline LV function between patients with concordant or non-concordant LV lead positions. Patients with concordant LV lead positions had a wider QRS complex (155.3 ± 28.4 vs 143.0 ± 21.4 ms, p=0.02). The LV lead was positioned over 'no scar' in 71 patients (80%) and over a LMA segment or adjacent segments in 57 (64%). Concordant LV lead positions were found in 44 (49%) patients.

Table 8-1. Baseline Characteristics

	All (n = 89)	Concordant (n = 44)	Non-concordant (n= 45)	P
Demographics				
Age, yrs	66.8 ± 10.8	68.4 ± 11.6	65.3 ± 9.9	0.17
Gender (male), n (%)	67(75)	30 (68)	37 (82)	0.13
Aetiology (ischaemic), n (%)	50 (56)	20(45)	30(67)	0.04
NYHA class				0.19
II	4 (5)	1 (2)	3 (7)	
III	67 (75)	31 (70)	36 (80)	
IV	18 (20)	12 (27)	6 (13)	
QRS duration (ms)	149.0 ± 25.7	155.3 ± 28.4	143.0 ± 21.4	0.02
Echocardiographic LVEF *	23.1 ± 9.9	23.5 ± 10.7	22.7 ± 9.2	0.71
Comorbidities, n (%)				
Diabetes mellitus	13 (14)	6 (14)	7 (16)	0.80
Hypertension	17 (22)	11 (25)	6 (13)	0.16
Atrial fibrillation	17 (19)	9 (20)	8 (18)	0.75
CABG	18 (20)	11 (25)	7 (16)	0.30
Medication, n (%)				
Loop diuretics	72 (81)	37 (84)	35 (78)	0.45
ACE-Is or ARBs	81 (91)	39 (89)	42 (93)	0.44
Beta-blockers	53 (60)	27 (61)	26 (58)	0.73
MRAs	39 (43)	20 (45)	19 (42)	0.76
CMR variables				
LVEDV, ml	255.1 ± 100.3	256.4 ± 106.4	253.7 ± 94.6	0.90
LVESV, ml	204.4 ± 98.1	204.7 ± 104.7	204.2 ± 92.4	0.98
LVEF, %	22.4±10.0	22.7 ± 10.7	22.0 ± 9.5	0.76
Fluoroscopic LV lead position				
Longitudinal position				0.26
Basal	61 (69)	27 (61)	34 (76)	
Mid	27 (30)	16 (36)	11 (24)	
Apex	1 (1)	1 (2)	0 (0)	
Circumferential position				0.57
Anterior	8 (9)	3 (7)	5 (11)	
Lateral	48 (54)	21 (48)	17 (38)	
Posterior	43 (48)	20 (45)	23 (51)	
Latest contracting segments				
Basal	50 (56)	25 (57)	25 (56)	0.90
Mid	26 (29)	18 (41)	8 (18)	0.02
Apex	34 (38)	17(39)	17 (38)	0.94

p values refer to differences between the groups: no scar and late contraction (LC) or scar and earlier contraction (EC) at the paced left ventricular segment. CABG = coronary artery bypass graft operation; ACE-Is = angiotensin-converting enzyme inhibibitors; ARBs = angiotensin receptor blockers; MRAs = mineralocorticoid receptor antagonists; LVEDV = left ventricular end-diastolic volume; LVESV = left ventricular end-systolic volume.

8.3.2 LVRR

In the entire cohort, 41/89 (46%) exhibited LVRR at 6 months. As shown in **Table 8-2**, LVRR was observed in patients with a concordant LV lead position (ΔLVESV = -56.3 ml, p<0.001), but not in patients with non-concordant positions (ΔLVESV = -0.1 ml, p=0.62) (p = 0.003 for group difference) (**Figure 8-2**). This corresponds to a LVRR rate of 30/44 (68%) patients with concordant LV lead positions and11/45 (24%) in patients with non-concordant positions. Similarly, LV lead concordance was associated with a reduction in LVEDV (ΔLVEDV = -55.6 ml, p<0.001), but no change was observed in patients with non-concordant positions (ΔLVEDV =+2.1 ml, P= 0.68) (p=0.006 for group difference). In addition, an increase in LVEF was observed with concordant but not non-concordant LV lead positions (7.05 ± 12.5 vs 0.23 ± 11.8%, p=0.006 for group difference).

In univariable regression analyses (**Table 8-3**) LV concordance emerged as a predictor of LVRR (OR: 6.62, 95% C.I. 2.61-16.79). When LMA was considered in isolation, LMA in the paced segment or adjacent segments predicted LVRR (OR: 3.27; 95% C.I. 1.29-8.30). When scar was considered in isolation, 'no scar' failed to emerge as a predictor of LVRR. Age, gender, HF aetiology, QRS duration and LVEF did not emerge as predictors.

In further analyses of the group of patients with concordant LV lead positions, LV lead concordance exactly over a segment with LMA was associated with more marked LVRR (18/20 [90%]; ΔLVSV = -84.0 ml, p< 0.001; OR: 18.9 (95%C.I. 3.84-84.31), p<0.001).

Table 8-2. Clinical and Echocardiographic Measures According to LV lead position.

	Concordant (n = 44)	**Non-concordant (n = 45)**	**P**
NHYA			
Baseline	3.25 ± 0.49	3.07 ± 0.45	
Follow-up	1.98 ± 0.70	2.09 ± 0.85	
Change	1.27 ± 0.73	0.98 ± 0.81	0.08
	p< 0.001*	p< 0.001*	
NYHA responders, n (%)	38(86)	32 (71)	0.08
6MWD, m			
Baseline	246.3 ± 109.3	278.0 ± 105.2	
Follow-up	323.7 ± 125.6	306.7 ± 110.6	
Change	70.0 ± 76.0	27.2. ± 72.5	0.03
	p< 0.001*	p= 0.04*	
LVEDV,ml			
Baseline	296.0 ± 115.1	255.6 ± 90.7	
Follow-up	240.4 ± 116.9	260.7 ± 88.4	
Change	-55.6 ± 104.3	2.07 ± 82.3	0.006
	p< 0.001*	p= 0.68*	
LVESV,ml			
Baseline	232.2 ± 107.2	198.9 ± 78.5	
Follow-up	179.6 ± 104.7	204.2 ± 76.7	
Change	-56.30 ± 93.4	-0.10 ± 79.8	0.003
	p< 0.001*	p= 0.62*	
LVRR **	30 (68)	11 (24)	<0.001
LVEF, %			
Baseline	23.5 ± 10.7	22.7 ± 9.2	
Follow-up	30.5 ± 10.4	23.0 ± 9.4	
Change	7.05 ± 12.5	0.23 ± 11.8	0.006
	p= 0.001*	p= 0.83*	

*** refers to p value for within-group changes at 6 months.**

**** left ventricular reverse remodeling (LVRR) defined as a 15% reduction in LVESV from baseline**

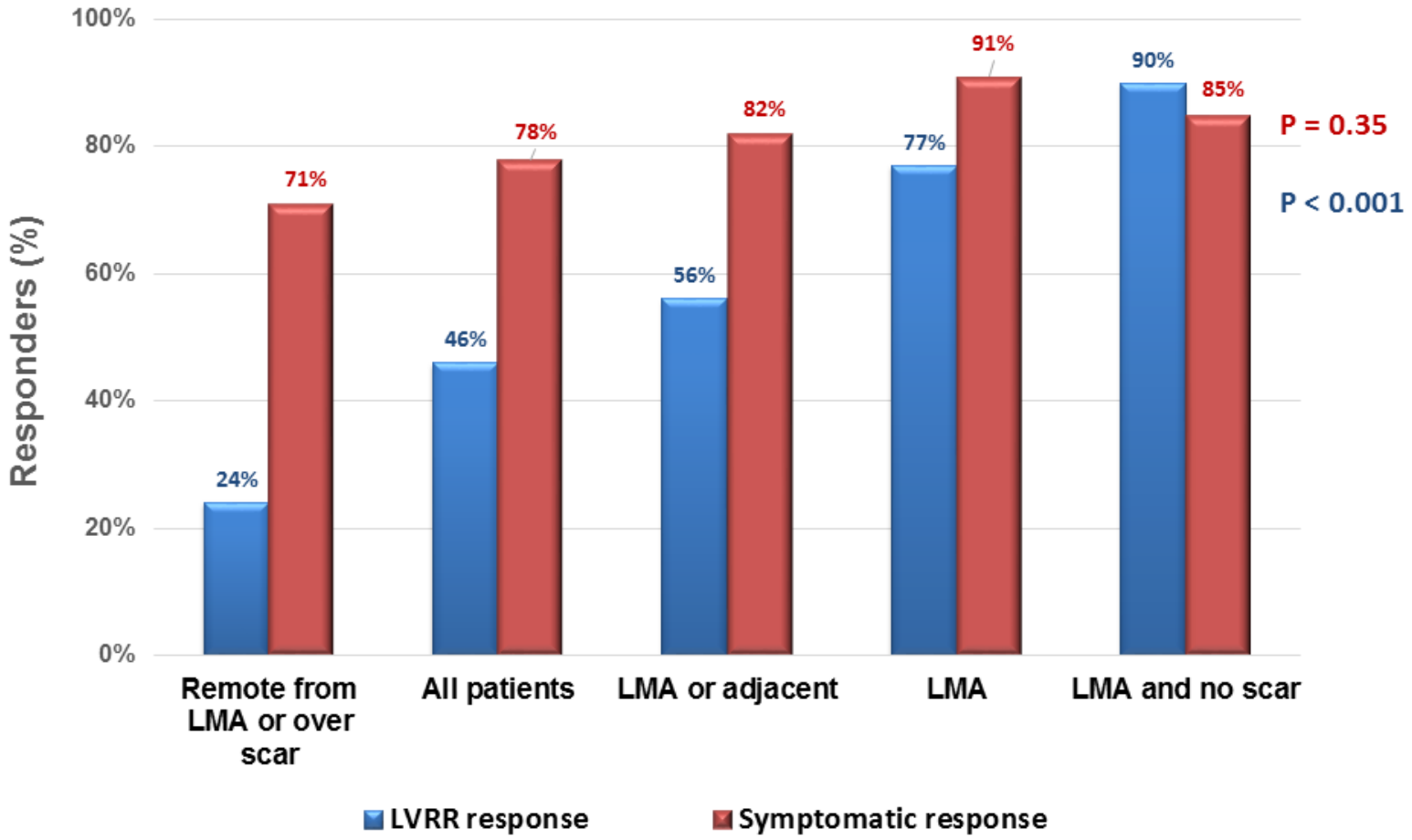

Figure 8-2. Clinical and Left Ventricular Reverse Remodeling Response.

This figure shows the clinical and LVRR response after CRT according to LV lead position.

Table 8-3. Logistic Regression Analyses of Predictors of LV Reverse Remodeling.

	Odds ratio	95% C.I.	P
UNIVARIABLE ANALYSES			
Age (yrs)	1.04	1.00-1.08	0.07
Gender (male)	1.03	0.40-2.72	0.95
Aetiology of HF (non-ischaemic)	0.99	0.43-2.30	0.99
QRS duration (ms)	1.01	0.99-1.02	0.54
LVEF (%)	1.03	0.98-1.07	0.22
Left ventricular pacing position			
No scar in paced segment	2.60	0.86- 8.29	0.09
LMA in paced or adjacent segments	3.27	1.29-8.30	0.01
LMA in paced segment	6.09	2.00-18.58	0.001
Concordant LV lead position	6.62	2.61-16.79	<0.001
MULTIVARIABLE ANALYSES			
Model 1			
Age (yrs)	1.04	0.99-1.08	0.09
No scar in paced segment	4.17	1.23-14.12	0.02
LMA in paced or adjacent segments	3.55	1.32-9.54	0.01
Model 2			
Age (yrs)	1.03	0.98-1.08	0.24
No scar in paced segment	4.85	1.24-18.94	0.02
LMA in paced or adjacent segments	7.01	1.96-25.10	0.003
Model 3			
Age (yrs)	1.03	0.99-1.08	0.17
Concordant LV lead position	6.28	2.45 -16.08	<0.001

8.3.3 Clinical outcomes.

Over a 4.4 yrs (median; range: 0.1-8.7 yrs), 28 patients died from cardiac causes, including 1 patient who underwent cardiac transplantation (8 deaths in concordant arm and 20 in the non-concordant arm). There were 3 HF hospitalisations in the concordant arm and 10 in the non-concordant arm. In Kaplan-Meier survival analyses (**Figure 8-3**) and Cox proportional hazards analyses (**Table 8-4**), patients with a concordant LV lead position had a lower cardiac mortality (Log Rank [LR] χ^2 = 7.32, p= 0.007; adjusted odds ratio [aOR]: 0.27, 95% C.I. 0.12-0.62) and a lower cardiac mortality or hospitalisations for HF (LR χ^2: 8.31., p<0.004; aOR: 0.26, 95% C.I. 0.12-0.58) than patients with a non-concordant LV lead position. When mechanical activation was considered in isolation, no difference emerged in these endpoints emerged between patients with LV lead positions over LMA segments or in remote segments. When scar was considered in isolation, a LV lead position over a segment with scar emerged as a strong predictor of cardiac mortality (LR χ^2 = 21.3, p< 0.001; aOR: 0.24, 95% C.I. 0.11-0.52) and cardiac mortality or hospitalisations for HF (LR χ^2: 22.3, p<0.001; aOR: 0.24, 95% C.I. 0.12- 0.49).

In terms of symptomatic response **Table 8-2** shows that CRT was associated comparable reductions in NYHA class in patients with either concordant or non-concordant LV lead positions (both p<0.001). Similarly, an increase in 6MWT distance was observed in patients with concordant LV positions (p<0.001), and to a lesser extent in patients with non-concordant positions (p=0.04). No differences in the composite clinical score was observed

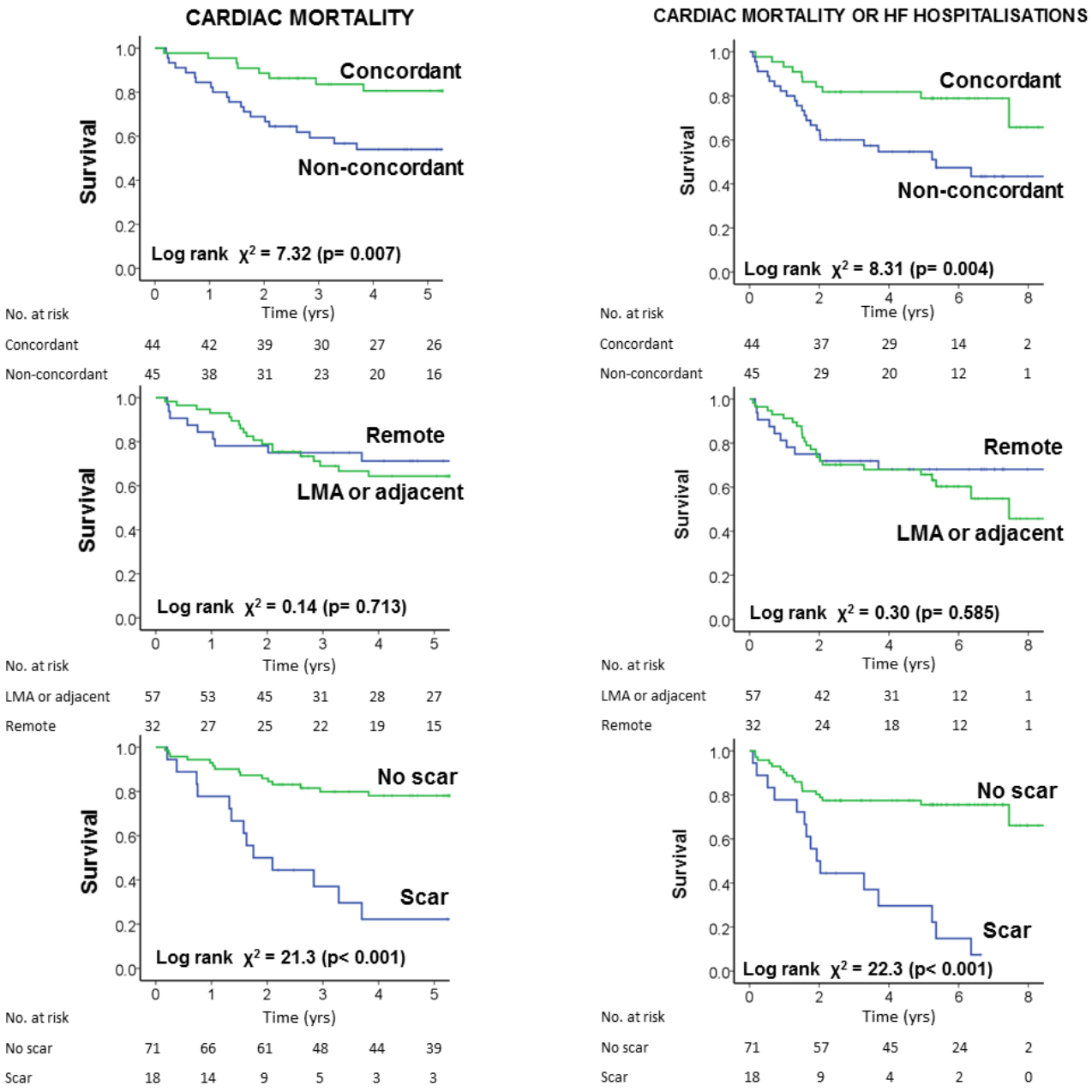

Figure 8-3. Cardiovascular mortality and hospitalisations after CRT according to lead position.

Kaplan-Meyer survival curves for cardiac mortality (a) and the composite endpoint of cardiac mortality or heart failure hospitalizations (b), according to characteristics of paced LV segment.

Table 8-4. Cox Proportional Hazards Survival Analyses

	Cardiac Mortality			Cardiac Mortality / HF Hospitalisation		
	HR	**95% C.I.**	**P**	**HR**	**95% C.I.**	**P**
UNIVARIABLE ANALYSES						
Age (yrs)	1.04	1.00-1.07	0.046	1.03	1.00-1.06	0.08
Gender (male)	2.10	0.72-6.05	0.17	1.90	0.73-4.91	0.19
Aetiology of HF (ischaemic)	4.15	1.57-10.91	0.004	3.10	1.34-7.15	0.008
QRS duration (ms)	1.00	0.98-1.01	0.78	1.00	0.98-1.01	0.57
LVEF (%)	0.92	0.87-0.97	0.002	0.93	0.88-0.97	0.001
Left ventricular pacing site						
No scar	0.20	0.10-0.43	<0.001	0.22	0.11-0.44	<0.001
LMA in paced or adjacent segments	0.82	0.33-2.02	0.662	1.19	0.57-2.51	0.64
LMA in paced segment	1.16	0.52-2.57	0.713	1.37	0.65-2.89	0.42
Concordant LV lead position	0.34	0.15-0.77	0.01	0.35	0.17-0.74	0.006
MULTIVARIABLE ANALYSES						
Model 1						
Age (yrs)	1.04	1.00-1.08	0.03	1.03	1.00-1.07	0.051
LVEF (%)	0.93	0.88-0.98	0.004	0.93	0.89-98	0.003
No scar	0.24	0.11-0.52	<0.001	0.24	0.12-0.49	<0.001
Model 2						
Age (yrs)	1.06	1.02-1.10	0.002	1.05	1.02-1.09	0.003
LVEF (%)	0.92	0.87-0.97	0.001	0.92	0.88-0.97	0.001
Concordant LV lead position	0.27	0.12-0.62	0.002	0.26	0.12-0.58	0.001

(37/43 and 36/45, respectively, p = 0.45). As shown in **Figure 8-2**, a higher symptomatic response rate was observed in paced LV segments with LMA, and in segments with LMA and no scar, but this was not statistically significant.

8.4 Discussion

8.4.1 Major findings

We have shown that in patients undergoing CRT, a concordant LV lead position was associated with marked LVRR and better clinical outcomes than a non-concordant position. In addition, LV lead concordance was associated with a 73% lower cardiac mortality and a 74% lower cardiac mortality or hospitalisations for HF. When scar was considered in isolation, 'no scar' was associated with a 76% lower risk of both endpoints. When LMA was considered in isolation, no difference in either endpoint was observed, but LV lead positions over LMA was associated with marked LVRR.

8.4.2 Myocardial scar

This study has emerged in the context of the STARTER (Saba et al., 2013) and TARGET (Khan et al., 2012b) studies, which employed speckle-tracking echocardiography to identify segments with LMA prior to CRT device implantation. The findings of STARTER have been adopted in support for targeting segments with LMA. Whilst myocardial scar was not formally assessed, segments with low amplitude radial strain were handled as missing data, and therefore not offered to the implanter as a target for LV lead deployment. It follows that, by virtue of study design, segments which may have contained scar were most likely avoided by implanters. Therefore, it is possible that the findings of STARTER were at least partly attributable to scar. In this respect, the TARGET study (Khan et al., 2012b) also

explored LMA as a target for LV lead deployment but in addition, a prospective evaluation of a surrogate of scar, defined < 10% radial strain, was undertaken. Whilst TARGET has also been interpreted as supporting the use of LMA as a target for LV lead deployment, the difference in outcome between the intervention and control groups could largely be explained by scar alone (Khan et al., 2012b). In the present study, we have found that a LV lead position over 'no scar', assessed using LGE-CMR, was associated with a 76% lower risk of cardiac mortality and the combined endpoint of cardiac mortality or hospitalisations for HF. In fact, the ORs for 'no scar' (0.24) and concordance (0.27) were almost identical, indicating that it is scar rather than LMA that primarily relates to clinical outcomes.

8.4.3 Latest mechanical activation

Intuitively, pacing segments with LMA should provide a more effective synchronisation than pacing earlier activated segments (Becker et al., 2007b). We have found that a LV lead position over segments with LMA is associated with marked LVRR, particularly when it is deployed exactly over the segment with LMA. When LMA was considered in isolation, however, it did not predict clinical outcomes. These findings further support our interpretation of the TARGET (Khan et al., 2012b) and STARTER (Saba et al., 2013) studies that it is myocardial viability rather than LMA at the paced LV segment that influences clinical outcomes. In this respect, we should consider that that speckle-tracking strain measures are not a reliable surrogates of myocardial scarring (Popovic et al., 2007). Accordingly, LV leads over LMA segments may actually be over scarred segments.

8.4.4 Clinical implications

This study provides further support for a role of CMR guiding LV lead deployment in patients undergoing CRT. The assessment of myocardial strain does not add value in predicting

cardiac mortality or HF hospitalisations, over and above the assessment of myocardial scar. Nevertheless, a LV lead position over LMA segments is associated with LVRR. Importantly, LGE-CMR is part of a routine CMR scan and FT-CMR does not require additional imaging. Using novel software, FT-CMR analysis can be performed using routine CMR images in under 6 mins (Taylor et al., 2015).

8.4.5 Limitations

The main limitation is that this is a single-centre study which includes only a moderate number of patients. It is also an observational study and does not demonstrate that LV lead deployment guided by LGE-CMR and FT-CMR is superior to a fluoroscopic approach. Importantly, however, the assessment of myocardial strain was undertaken on pre-implantation CMR scans which were analysed years later. Effectively, therefore, investigators were blinded to the findings of FT-CMR. Unfortunately, we have not systematically collected data on QRS morphology, which may have influenced our results.

8.5 Conclusions

In patients undergoing CRT, a LV lead position over non-scarred segments with LMA, assessed using CMR, was associated with marked LVRR and a better clinical outcome than deploying the lead over scarred and/or earlier activated segments. Clinical events were primarily related to scar, whereas LVRR was mainly related to LMA. These findings add support for the use of LGE- and FT-CMR in guiding LV lead deployment.

9 FUTURE STUDIES

9.1 Summary of main findings

This collection of investigations was undertaken in the context of exploring the potential for FT-CMR to be used to optimise the response to CRT. However, at the outset of this project, FT-CMR was an innovative technology with a published evidence base limited to two pilot studies. First and foremost a comprehensive validation was required. In a study comprising of healthy controls and patients with IDCM, as compared to the reference standard myocardial tagging, FT-CMR showed reasonable agreement for the derivation of global measures of circumferential and longitudinal systolic and diastolic strains. Agreement for systolic deformation parameters at the mid cavity was extremely precise, and although less robust, remained acceptable at the LV apex and base. Furthermore, excellent intra- and inter-observer variability was demonstrated for FT-CMR derived circumferential and longitudinal deformation parameters; a product of the largely automated tracking process. Additionally, FT-CMR was conducted in a fifth of the time of myocardial tagging. These steps were essential to justify further clinical or investigational utility.

Left ventricular MWF, detected on LGE-CMR, occurs in a quarter of patients with IDCM, and predicts mortality. This work shows that midwall fibrosis is a powerful and independent predictor of mortality and morbidity after CRT. LVRR was observed in patients without, but not in those with, MWF. The LV midwall is the site of circumferential myocardial fibres, and FT-CMR analysis found MWF to be associated with a reduction in global systolic circumferential strain and strain rate, as well as torsion. In addition, MWF was associated

with rigid LV body rotation. These mechanical disturbances may explain the high risk of pump failure associated MWF.

A retrospective study of patients undergoing CRT implantation has shown that no FT-CMR based dyssynchrony index derived from a pre-implant CMR predicts clinical or LVRR response. Greater dyssynchrony at baseline, as measured by either RURE or SDI_{16}, was a predictor of a higher subsequent event rate, although not independently of other baseline variables. However, baseline LV function was a strong marker of outcomes, and ε_{3D} was more powerful than CMR volumetric analysis in this respect. When considering LV lead position, LVRR and better clinical outcomes occur in patients in whom the LV lead has been deployed in non-scarred late-activated LV myocardial segments.

9.2 Limitations

9.2.1 Validation of FT-CMR techniques

Validation of any new modality against an accepted standard is a required starting point. Shortcomings of the FT-CMR validation study (**chapter 2**) include the exclusion of radial and segmental strains. Radial parameters had poorer intra- and inter-observer variability. However, they are less precisely evaluated by any deformation algorithm, as the small diameter of this dimension leads to a greater propensity for error. Myocardial tagging is not immune to this and would have been an unconstructive comparator. The exclusion of regional parameters was in the context of reports of suboptimal reproducibility, and our acknowledgement that these were being addressed by the manufacturer's scientific

department. Although the pathological cohorts were tracked with the benefit of these enhancements, it is important to appreciate that FT-CMR remains less apt for determining motion components parallel to tissue boundaries.

The torsional, dyssynchrony and LMA parameters used all lack prior validation against an accepted imaging modality. This was not feasible within the time constraints of this project, but remains fundamental to the development of work in this field. As discussed below, a validation between STE and FT-CMR for some dyssynchrony indexes has been conducted.

9.2.2 Study endpoints

Several chapters explore the clinical potential for FT-CMR based analyses to enhance patient selection for CRT and guide implant. The raison d'être behind such investigation is to evaluate if the strengths of CMR as an imaging technique can overcome some of the limitations of echocardiography; thus there is an illogicality in the use of echocardiographic LVRR as a primary endpoint. Section **1.4.1.1** reviews limitations that have been reported in landmark CRT studies using Simpson's biplane volumetric analysis. LVRR was performed by 2 experienced and accredited physiologists, but these studies lack an assessment of intra- or inter-operator variability; it is thus difficult to quantify the risk of a type II error in some analyses such as the failure of dyssynchrony parameters to predict response.

Nonetheless, LVESV is an attractive measure of CRT response as it incorporates not only LV reverse remodelling, but also function by virtue of any improvement in LVEF lowering LVESV. Accordingly, LVESV has been shown to be the strongest echocardiographic surrogate of long

term prognosis in both medical (Konstam et al., 1992) and CRT investigations (Yu et al., 2005). Early CRT studies utilised a 15% reduction in LVESV as a marker of response (Stellbrink et al., 2001), and this has been adopted by hundreds of subsequent studies as the predominant metric of CRT response.

These retrospective studies are constrained by the contemporaneous assessments conducted. A prospectively designed trial could benefit from the reduced variability in LVESV measurement by using ultrasound contrast agents (Thomson et al., 2001) or 3DE (Thavendiranathan et al., 2013). More attractively for studies designed to evaluate the role of CMR in this field, a future prospective study could now benefit from MRI conditional implants and pre- and post- implant CMR could facilitate LV volumetric analysis utilising the gold standard. Additionally, this would address a further deficiency of these studies, permitting post implant analysis of the FT-CMR metrics used.

The other major class of response parameters are functional. Whilst the studies herein employed our validated composite clinical score, this was weighted towards recognising an improvement in NHYA class. This scale predominantly reflects the participants' health status from the assessors' perspective, not that of the patient. The validity of NHYA as a research tool is uncertain with little more than a 50% agreement between physicians in differentiating between NHYA class II and III (Raphael et al., 2007).

A recent FDA guidance has suggests that HF trials move towards using clinically meaningful end-points; improvement in 6MWD and quality of life scores are advised as they

demonstrate clinical benefit and likely act as a surrogate for improved long-term outcomes (U.S. Department of Health and Human Services: Food and Drug Administration, 2015). However, a recent meta-analysis encompassing 83 heart failure trials found that in only half of studies where treatment provided a mortality benefit, there was an improvement in 6MWD or peak VO2 during cardiopulmonary exercise testing. A trans-Atlantic consort of prominent investigators within the field have suggested combining 6MWD or quality of life scores with natriuretic peptides to produce consequential endpoints (Ferreira et al., 2016).

9.2.3 Generic CMR acquisitions

A major advantage of FT-CMR, the potential to access historical CMR acquisitions, is also the source of a major limitation. A number of the chapters make use of this, but these were not necessarily optimised to address the study question contributing to a risk of type II error.

In the study of the predictive role of dyssynchrony assessment it is possible that the use of tailored acquisitions with higher temporal resolution would produce different findings. Recently, a London based research group reported good inter-study reproducibility for the computation of CURE, RURE and time to peak methodologies between the repeated exams in healthy volunteers. Uniformity ratio estimates derived with an analogous technique to that described in **4.2.3**, had the lowest inter-study variability (Coefficient of Variance 6.4%–8.5%). In difference, their prospectively planned acquisitions consisted of 30 phases per cardiac cycle, affording a superior temporal resolution of 25–35 ms (Kowallick et al., 2017). Onishi et al, also used similar temporal resolution when validating FT-CMR dyssynchrony against STE (Onishi et al., 2013). However, in isolation improved temporal resolution would

reduce the ability of FT-CMR to track tissue motion due to smaller displacements between phases, unless matched by improved spatial resolution. The study by Kowallick et al, used a 3T scanner which will have provided the necessary higher resolution.

In the same cohort, Kowallick et al. demonstrated good reproducibility and minimal diurnal fluctuation when FT-CMR is utilised for the assessment of peak torsional parameters (Kowallick et al., 2016). The superior spatial and temporal resolution they employed was inadequate to resolve the problem of through plane motion causing loss of tracked features during the rapid isovolaemic relaxation phase; reproducibility of diastolic torsion was significantly less robust. Again, despite analogous methodology, differences in scanner strength and scan protocol raise doubt about the translation of their reported reproducibility to the torsional mechanics described in **chapter 6**.

A further factor influencing diastolic assessment is differences in ECG gating between studies. The diseased populations had CMR studies as part of their routine clinical assessment and gating was at the discretion of the scan operator. The majority of patients underwent SSFP cine imaging with retrospective gating thus providing coverage of the full cardiac cycle. However, in a number of patients, including those in atrial fibrillation, cine images were acquired with prospective triggering, with loss of data from the end-diastolic portion of the cardiac cycle. Unfortunately, data on gating procedures was not systematically collected and this variable may have had particular influence on diastolic parameters and Fourier-based dyssynchrony assessment.

Future studies to assess the effect of spatial and temporal resolution on the precision of FT-CMR measures are essential. Nonetheless, any consensus on the ideal acquisition technique must balance the risk of counteracting a major benefit that FT-CMR is utilised on routinely acquired SSFPs.

9.2.4 Methodology for parameter assessment

For some parameters, such as those of dyssynchrony, FT-CMR facilitates the derivation of such a vast array of indexes that measuring everything would have been excessively time consuming and testing them all in the CRT population and would have predisposed to a high risk of a number of false positive findings. The FT-CMR parameters calculated in each chapter were largely chosen with the benefit of the wealth of knowledge generated by the STE experience. One difference was the use of circumferential rather than radial parameters to utilise the strengths of FT-CMR. However, STE studies that have demonstrated a predictive utility for dyssynchrony assessment have focused on radial mechanics, which also benefit from being the predominant contributor to systolic function. Similarly, STARTER (Saba et al., 2013) and TARGET (Khan et al., 2012b) used radial strains to both define LMA, and act as a surrogate for scar. Albeit limited to assessment from the short axis mid-cavity, reasonable agreement has been reported between FT-CMR and STE radially based time to peak measures of dyssynchrony (Onishi et al., 2013). The failure of $SDT2P_{16}$ and SDI_{16} to predict response may be partly attributable to the decision to use circumferential segmental strains. Nonetheless the RURE index, which was based on radial strain, was also inept to predict response (**7.3.2**). Future validation studies to identify the optimal way to assess dyssynchrony using FT-CMR are required.

The evolved wisdom from STE has been to perform a number of repeated measures of deformation parameters that are subsequently averaged. All the studies reported herein calculate each parameter only once. This is in difference to a recent recommendation that reproducibility for FT-CMR parameters can be maximised with 3 repeated measures (Schuster et al., 2015).

9.2.5 Observational design

The investigations of CRT recipients are observational in design. Missing data due to 'loss to follow-up' has been described within the relevant chapters. An example of this was not having the follow-up echocardiogram performed on all patients to assess for LVRR, and it is possible that differential losses to follow up have biased some analyses. Blinding methods vary for different analyses and are not of the same rigor that would be feasible with prospective research. Nonetheless, whilst the operators performing the echocardiograms studies may have had some awareness of the patients' clinical status, they are not believed to have been aware of patients' MWF status and could not have been aware of FT-CMR data that was performed years later. Thorough blinding was conducted with FT-CMR analyses which were conducted on anonymised acquisitions.

The historical cohort was taken from a single centre and only moderate in size; this leads to the possibility of some negative findings being attributable to statistical under-powering rather than the lack of a true effect. Finally, without a control arm, deductions of the benefits of CRT in patients with adverse prognostic features such as MWF or low baseline

strain cannot be made. Similarly, one cannot state that LV lead deployment guided by LGE-CMR and FT- CMR is superior to a fluoroscopic approach.

9.3 Future directions

This work provides further evidence of a role for CMR in the prognostic stratification of IDCM patients undergoing CRT. My initial research plan had been to examine the mechanical effects of MWF both pre- and post CRT implant. A major obstacle was the inability to acquire 2DE images of adequate temporal resolution and quality for STE, due to the sector widths required to image dilated hearts and 'drop-out' of the apical and anterolateral segments on the apical views. With the advent of CMR conditional CRT devices, FT-CMR offers potential to address this. This would be an important step in considering the ethics of planning a trial randomising patients with IDCM and MWF to either optimal pharmacotherapy or CRT.

The final study shows that it is the avoidance of scar rather than targeting LMA that primarily relates to clinical outcomes; this is also a possible interpretation of the 2 recent randomised controlled echocardiographic studies examining target LV lead placement. This is important as LGE-CMR is superior to STE for identifying scar. This study provides further support for a role of CMR guiding LV lead deployment in patients undergoing CRT, and this warrants further investigation in a multi-centre randomised study.

The scope for utility of FT-CMR reaches far beyond the field of CRT. The assessment of LV function is key to clinical decision-making both within the field of cardiovascular medicine and beyond. At the outset of this project there was no consensus on the best practice for

using FT-CMR. A combination of the best practice methodologies reported herein, coupled with the normal values from a population with a broad age range will form a platform for its use. Further manufacturers have recently released analogous applications and it is important to appreciate that normal values are likely to differ between platforms. An inter-vendor comparison of the Tomtec Imaging Systems (Munich, Germany) platform used herein with CVI42 software (Circle Cardiovascular Imaging Inc., Calgary, Canada) showed that newer application consistently calculated lower E_{cc} and with poorer reproducibility (Schuster et al., 2015). However, CVI[42] had superior reproducibility for ε_{rr}. There is a need for industry compliance to make algorithms more visible, and to work towards a more standardised methodology; otherwise a lack of inter-vendor agreement will limit the clinical utility of feature tracking.

A more readily accessible alternative to myocardial tagging with preserved accuracy will increase the utility of deformation assessment in the research environment. One in-house example of its use has been in a controlled observational research study examining the effects of living kidney donation on cardiovascular structure and function. These volunteers had formed the normal values population, and in view of the precision of FT-CMR deformation assessment this was used in preference to myocardial tagging to investigate the cardiovascular effects of unilateral nephrectomy in living kidney donors. Compared to controls, FT-CMR demonstrated a small but significant decline in peak systolic ε_{cc} at one year contributing to the evolving picture that living kidney donation is not a benign state (Moody et al., 2016).

The FT-CMR variables evaluated through this collection of studies makes use of only an infinitesimal proportion of the data collected. At each phase, a tracked border has its spatial location registered within the software framework by 48 coordinate pairs. Considering a stack of 6 cines, this would represent 28800 data points just detailing short axis mechanics. Whilst CURE and RURE were designed to harness greater detail from this data, much of the subtlety is lost in Fourier transformation. To maximise the potential within the dataset, we are collaborating with the department of biomedical engineering with the goal of developing a computational model that predicts myocardial mechanics. Using the data sets from healthy controls, coupled with clinical parameters, the model will use finite element analysis to predict myocardial behaviour. The model will then be upscaled to incorporate pathological states with tissue characterisation provided by LGE-CMR to solve how the myocardium reacts to structural insults. The intention is to predict myocardial mechanical behaviour in response to a given stress, and to identify mechanical markers which predict greater time-dependant predisposition to myocardial dysfunction with the goal of informing preventative and therapeutic decisions.

10 APPENDICES

10.1 Appendix 1 - Patient cohorts

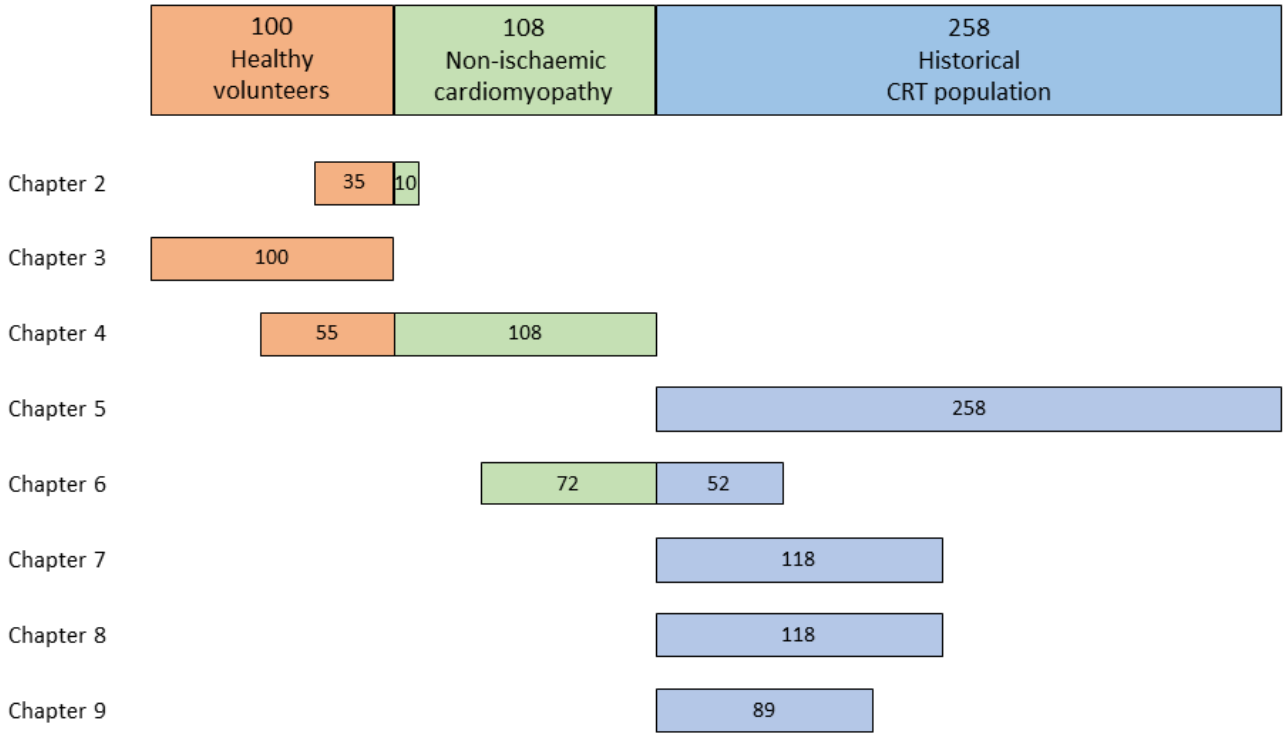

Figure 10-1. Patient cohorts.

This provides a visual representation of the overlap between healthy volunteers and patients between the different investigations.

The participants from all three cohorts gave written informed consent, and the studies protocol conforms to the ethical guidelines of the 1975 Declaration of Helsinki as reflected in a priori approval by the National Research Ethics Service.

10.2 Appendix 2: FT-CMR derived myocardial strain as a surrogate for scar

In TARGET and STARTER, strain assessment was used to guide LV lead placement. A preliminary pilot as part of **chapter 8** involved determining whether FT-CMR derived myocardial strain below a specific threshold can act as a surrogate for scar.

20 consecutive patients with angiographically documented coronary artery disease and conventional indications for CRT were prospectively recruited through a heart failure clinic. CMR acquisition (**2.2.2**) and scar imaging (**5.2.4**) were performed as described. Scar analysis was performed using CVI[42] software. A segment with >10% LGE was considered scarred, and this was sub-classified on the basis of trans-mural extent, as being either sub-endocardial (<50%) or trans-mural (>50%). Non-scarred segments were sub-classified as being either adjacent or distant to scar (depending on the presence of a scar-free border of at least 1/3 of a segment's width from a neighbouring circumferential segment). FT-CMR assessment of segmental peak ε_{cc} was performed as described (**3.2.4**). Both scar assessment and strain quantification were performed by the same operator, but for both analysis platforms the scans were loaded in an anoymised and randomised manner. All analyses were in accordance with the American Heart Association's 16-segment model.

All 20 patients (62 ± 13 yr, 70% male) had multiple scarred segments; in total 126 (39%) of the 320 analysed segments had scar. ε_{cc} did not discriminate between segments with sub-endocardial or transmural scar (-4.9% vs -5.5%; p= 0.42). The mean ε_{cc} of scarred segments was lower than that in non-scarred segments in 17/20 patients studied (**Table 10-1**). Overall ε_{cc} was significantly lower in scarred myocardium compared to non-scarred myocardium (-

5.3% vs. -9.2%, P<0.001). The magnitude of this difference was less when scarred segments were compared against segments adjacent to scar (-5.3 vs -7.6; p= 0.003).

$Ɛ_{cc}$ had an area under the ROC curve of 0.71 for discriminating between scarred and non-scarred segments (**Figure 10-2**). At the Youden index (Youden, 1950), $Ɛ_{cc}$ < -9.2% predicts scar with a sensitivity of 87% and specificity of 45%. This cut-off was felt to provide too great an emphasis on sensitivity over specificity. This cut-off would be prone to misclassify segments adjacent to scar as scar, preventing from them being classified as LMA. $Ɛ_{cc}$ < -6.3 provides a cut-off with only minimal reduction in the vertical distance from the line of equality, but provides the cut-off closest to the (0,1) point (Perkins et al., 2006), predicting scar with a 67% sensitivity and 64% specificity. Favouring specificity rather than sensitivity was preferable as the latter was more optimally provided by LGE-CMR.

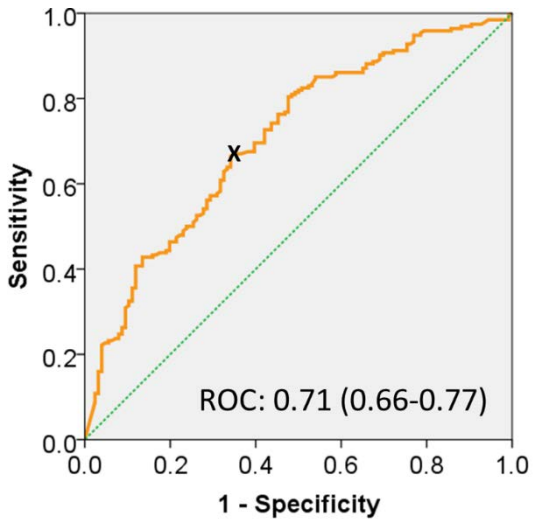

Figure 10-2. Receiver operator characteristics for segmental $Ɛ_{cc}$ to predict scar.

At the cut-off closest to the (0,1) point X, $Ɛ_{cc}$ predicts scar with a 67% sensitivity and 64% specificity

Table 10-1. Mean segmental Ecc in relation to myocardial scar.

	Mean Peak segmental Ecc (%)						P
Patient	**Scar**	**Full thickness**	**Subendocardial**	**No scar**	**Adjacent scar**	**Distant Scar**	**Scar vs. no scar**
1	-2.8 (5)	-2.7 (4)	-3.3 (1)	-11.4 (11)	-6.8 (5)	-15.2 (6)	0.01
2	-2.0 (5)	-2.1 (2)	-2.0 (3)	-7.4 (11)	-4.1 (4)	-9.2 (7)	0.002
3	-6.3 (7)	-6.8 (3)	-6.0 (4)	-12.6 (9)	-11.8 (2)	-12.8 (7)	0.003
4	-4.9 (8)	-5.1 (6)	-4.6 (2)	-4.6 (8)	-4.4 (7)	-5.9 (1)	0.79
5	-4.6 (5)	-4.6 (5)	-	-7.1 (11)	-5.8 (6)	-8.7(5)	0.18
6	-4.5 (7)	-3.8 (6)	-8.9 (1)	-7.6 (9)	-8.4 (8)	-1.2 (1)	0.25
7	-6.9 (5)	-7.7 (4)	-3.5 (1)	-12.3 (11)	-11.9 (5)	-12.7 (6)	0.12
8	-5.5(9)	-5.4 (8)	-6.2 (1)	-7.5 (7)	-7.2 (5)	-8.2 (2)	0.43
9	-1.9 (7)	-2.1 (6)	-0.8 (1)	-9.3 (9)	-6.8 (5)	-12.4 (4)	0.005
10	-7.6 (5)	-7.6 (5)	-	-11.0 (11)	-10.3(6)	-12.0 (5)	0.30
11	-5.7 (7)	-4.4 (2)	-6.2 (5)	-10.0 (9)	-6.4 (1)	-10.4 (8)	0.01
12	-6.1 (7)	7.0 (5)	-3.8 (2)	-10.5 (9)	-9.5 (3)	-11.0 (6)	0.21
13	-5.1 (6)	-	-5.1 (6)	-13.9 (10)	-	-13.9 (10)	0.007
14	-4.6 (8)	-1.3 (2)	-5.6 (6)	-6.4 (8)	-3.0 (1)	-6.9 (7)	0.33
15	-5.3 (7)	-5.3 (6)	-5.7 (1)	-5.5 (9)	-4.8 (5)	-6.3 (4)	0.93
16	-12.1 (4)	-12.9 (3)	-9.9 (1)	-8.4 (12)	-8.2 (5)	-8.6 (7)	0.26
17	-2.5 (5)	-2.5 (5)	-	-7.0 (11)	-6.4 (2)	-7.2 (9)	0.02
18	-7.0 (9)	-6.6 (6)	-7.8 (3)	-14.2 (7)	-10.4 (3)	-17.0 (4)	0.10
19	-10.0 (5)	-11.8 (4)	-2.9 (1)	-10.0 (11)	-10.1 (5)	-10.0 (6)	0.99
20	-2.3 (5)	-	-2.3 (5)	-7.8 (11)	-	-7.8 (11)	0.004
Total	-5.3 (126)	-5.5 (82)	-4.9 (44)	-9.2 (194)	-7.6 (78)	-10.3 (116)	<0.001

The number of segments considered is indicated in parentheses

10.3 Appendix 3: List of publications arising from this work

10.3.1 List of scientific papers arising directly from this work

- **Taylor RJ**, Umar F, Panting JR, Stegemann B, Leyva F. Left ventricular lead position, mechanical activation, and myocardial scar in relation to left ventricular reverse remodeling and clinical outcomes after cardiac resynchronization therapy: A feature-tracking and contrast-enhanced cardiovascular magnetic resonance study. Heart Rhythm 2016; 13: 481-489.

- **Taylor RJ**, Umar F, Lin EL, Ahmed A, Moody WE, Mazur W, Stegemann B, Townend JN, Steeds RP, Leyva F. Mechanical effects of left ventricular midwall fibrosis in non-ischemic cardiomyopathy. J Cardiovasc Magn Reson 2016; 18: 1.

- **Taylor RJ**, Moody WE, Umar F, Edwards NC, Taylor TJ, Stegemann B, Townend JN, Hor KN, Steeds RP, Mazur W, Leyva F. Myocardial strain measurement with feature-tracking cardiovascular magnetic resonance: Normal values. Eur Heart J Cardiovasc Imaging 2015; 16(8): 871-881.

- Moody WE*, **Taylor RJ***, Edwards NC, Chue CD, Umar F, Taylor TJ, Ferro CJ, Young AA, Townend JN, Leyva F, Steeds RP. Comparison of magnetic resonance feature tracking for systolic and diastolic strain and strain rate calculation with spatial modulation of magnetization imaging analysis. J Magn Reson Imaging 2015; 41: 1000-1012.

  * Joint first authors

- **Taylor RJ**, Umar F, Moody WE, Meyyappan C, Stegemann B, Townend JN, Hor KN, Miszalski-Jamka T, Mazur W, Steeds RP, Leyva F. Feature-tracking cardiovascular magnetic resonance as a novel technique for the assessment of mechanical dyssynchrony. Int J Cardiol 2014; 175(1): 120-125.

- Leyva F, **Taylor RJ**, Foley PWX, Umar F, Mulligan LJ, Patel K, Stegemann B, Haddad T, Smith REA, Prasad SK. Left ventricular midwall fibrosis as a predictor of mortality and morbidity after cardiac resynchronization therapy in patients with nonischemic cardiomyopathy. J Am Coll Cardiol 2012; 60: 1659-1667.

10.3.2 List of scientific papers related to this work

- Leyva F, Umar F, **Taylor RJ**, Steeds RP, Frenneaux MP. The clinical outcome of cardiac resynchronization therapy in post-surgical valvular cardiomyopathy. Europace 2016; 18: 732-738.

- Umar F, **Taylor RJ**, Stegemann B, Marshall H, Flannigan S, Lencioni M, De Bono J, Griffith M, Leyva F. Haemodynamic effects of cardiac resynchronization therapy using single-vein, three-pole, multipoint left ventricular pacing in patients with ischaemic cardiomyopathy and a left ventricular free wall scar: The maestro study. Europace 2016; 18: 1227-1234.

- Moody WE, Ferro CJ, Edwards NC, Chue CD, Lin EL, **Taylor RJ**, Cockwell P, Steeds RP, Townend JN. Cardiovascular effects of unilateral nephrectomy in living kidney donors. Hypertension 2016; 67: 368-377.

- Mehmood M, Ambach SA, Taylor MD, Jefferies JL, Raman SV, **Taylor RJ**, Sawani H, Mathew J, Mazur W, Hor KN, Al-Khalidi HR. Relationship of right ventricular size and function with respiratory status in duchenne muscular dystrophy. Pediatr Cardiol 2016; 37: 878-883.

- Moody WE, Edwards NC, Chue CD, **Taylor RJ**, Ferro CJ, Townend JN, Steeds RP. Variability in cardiac MR measurement of left ventricular ejection fraction, volumes and mass in healthy adults: Defining a significant change at 1 year. Br J Radiol 2015; 88: 831.

10.3.3 List of other publications related to this work

Letters

- **Taylor RJ**, Umar F, Leyva F. Letter by Taylor et al regarding article, "myocardial fibrosis as a key determinant of left ventricular remodeling in idiopathic dilated cardiomyopathy: A contrast-enhanced cardiovascular magnetic study". Circ Cardiovasc Imaging 2013; 6: e78.

Chapters

- **Taylor RJ**, Umar F, Leyva F. The use of cardiovascular magnetic resonance to guide left ventricular lead deployment in cardiac resynchronization therapy. In: Yu C-M, Hayes DL, Auricchio A, eds. Cases in cardiac resynchronization therapy. Philadelphia: Elsevier; 2014: 235-244.

Abstracts

- **Taylor RJ**, Umar F, Stegemann B, Leyva F. Left ventricular lead position, mechanical activation and myocardial scar in relation to the clinical outcome of cardiac resynchronisation therapy: The role of feature-tracking and contrast-enhanced cardiovascular magnetic resonance. Europace 2015; 17(suppl S5): V1. **Finalist for British Heart Rhythm Society's Young Investigators Research in Device Therapy Award, Heart Rhythm Congress, Birmingham, October 2015.**

- Umar F, **Taylor RJ**, Stegemann B, Marshall H, Flannigan S, Leyva F. Haemodynamic effects of single-vein, simultaneous, multipoint pacing compared with bipolar pacing in patients undergoing cardiac resynchronisation therapy. Europace 2015; 17(suppl S5): V20.

- **Taylor RJ**, Umar F, Lin ELS, Mankaryous G, Stegemann B, Leyva F. Feature-tracking cardiovascular magnetic resonance to predict response following cardiac resynchronisation therapy. Europace 2015; 17(suppl3): iii122.

- **Taylor RJ**, Umar F, Lin ELS, Moody WE, Mazur W, Stegemann B, Townend JN, Steeds RP, Leyva F. The influence of left ventricular midwall fibrosis on torsional mechanics. The implications for cardiac resynchronisation therapy. Europace 2015; 17(suppl 3): iii219.

- Moody WE, Ferro CJ, Edwards N, Chue CD, Lin ELS, **Taylor RJ**, Cockwell P, Steeds RP, Townend JN. Effects of nephrectomy on cardiovascular structure and function in living kidney donors. J Am Col Cardiol 2015; 65: 2150.

- **Taylor RJ**, Umar F, Lin ELS, Ahmed A, Moody WE, Stegemann B, Townend JN, Steeds RP, Leyva F. Mechanical effects of midwall fibrosis in non-ischemic dilated cardiomyopathy. J Cardiovasc Magn Reson 2014; 16 (Suppl 1): 308.

- Moody WE, Edwards N, Chue CD, **Taylor RJ**, Li AYK, Ferro CJ, Townend JN, Steeds RP. Normative annual changes in left ventricular volumes, mass and function among healthy adults: A prospective cardiac magnetic resonance imaging study. J Cardiovasc Magn Reson 2014; 16(Suppl 1): 99.

- **Taylor RJ**, Moody WE, Umar F, Edwards N, Townend JN, Steeds RP, Leyva F. The effects of age and gender on myocardial strain: A feature tracking cardiac magnetic resonance study. Eur Heart J Cardiovasc Imaging 2013; 14(suppl 2): ii235.

- Moody WE, Lin ELS, Bloxham N, Fraser H, **Taylor RJ**, Holloway B, Edwards N, Ferro CJ, Townend JN, Steeds RP. Real-world relative utility of stress testing and coronary calcium score for the detection of coronary artery disease in prospective renal transplant recipients. Eur Heart J Cardiovasc Imaging 2013; 14(suppl 2): ii43-ii44.

- **Taylor RJ**, Umar F, Lin EL, Ahmed A, Steeds RP, Leyva F. Systolic circumferential strain derived from feature-tracking cardiovascular magnetic resonance predicts survival after cardiac resynchronization therapy. Circulation 2013; 128: a18413.

- **Taylor RJ**, Umar F, Moody WE, Meyyappan C, Stegemann B, Townend JN, Leyva F. Feature-tracking cardiovascular magnetic resonance as a novel technique for the assessment of mechanical dyssynchrony. Europace 2013; 15(suppl 2): ii14.

- **Taylor RJ**, Umar F, Moody WE, Townend JN, Steeds RP, Leyva F. The reproducibility and analysis time of cardiac magnetic resonance feature tracking: Potential for clinical application. Heart 2013; 99(suppl 2): A64.

- Moody WE, **Taylor RJ**, Edwards NC, Umar F, Chue CD, Taylor TJ, Ferro CJ, Townend JN, Leyva F, Steeds RP. Comparison of magnetic resonance feature tracking for longitudinal strain calculation with spatial modulation of magnetization imaging analysis. J Cardiovasc Magn Reson 2013; 14(suppl 1): 123.

- Umar F, **Taylor RJ**, Vakharia A, Marshall H, Leyva F. The cost of upgrading implantable cardioverter defibrillators to cardiac resynchronization therapy with defibrillation in patients with left ventricular dysfunction. Heart Rhythm 2013; 10(suppl 5): S516.

- **Taylor RJ**, Umar F, Foley PWX, Mulligan LJ, Patel K, Stegemann B, Smith R, E, A., Prasad SK, Leyva F. Left ventricular midwall fibrosis as a predictor of mortality and morbidity after cardiac resynchronization therapy in patients with non-ischemic cardiomyopathy. Europace 2012; 14(suppl 4): iv18.

11 REFERENCES

Abozguia, K.,Leyva, F. 2011. Targeting Viable Myocardium in Cardiac Resynchronization Therapy Using a Multipolar Left Ventricular Lead. ***Circulation**, 123* (22): e617-e618.

Abraham, W. T., Fisher, W. G., Smith, A. L., et al. 2002. Cardiac resynchronization in chronic heart failure. ***N Engl J Med**, 346* (24): 1845-1853.

Achilli, A., Peraldo, C., Sassara, M., et al. 2006. Prediction of Response to Cardiac Resynchronization Therapy: The Selection of Candidates for CRT (SCART) Study. ***Pacing Clin Electrophysiol**, 29* S11-S19.

Achilli, A., Sassara, M., Ficili, S., et al. 2003. Long-term effectiveness of cardiac resynchronization therapy in patients with refractory heart failure and "narrow" QRS. ***J Am Coll Cardiol**, 42* 2117-2124.

Adelstein, E. C.,Saba, S. 2007. Scar burden by myocardial perfusion imaging predicts echocardiographic response to cardiac resynchronization therapy in ischemic cardiomyopathy. ***Am Heart J**, 153* (1): 105-112.

Adelstein, E. C.,Saba, S. 2009. Usefulness of baseline electrocardiographic QRS complex pattern to predict response to cardiac resynchronization. ***Am J Cardiol**, 103* (2): 238-242.

Adelstein, E. C., Tanaka, H., Soman, P., et al. 2011. Impact of scar burden by single-photon emission computed tomography myocardial perfusion imaging on patient outcomes following cardiac resynchronization therapy. ***Eur Heart J**, 32* (1): 93-103.

Albertsen, A. E., Nielsen, J. C., Pedersen, A. K., et al. 2005. Left ventricular lead performance in cardiac resynchronization therapy: impact of lead localization and complications. ***Pacing Clin Electrophysiol**, 28* (6): 483-488.

Alpert, J. S., Thygesen, K., Antman, E., et al. 2000. Myocardial infarction redefined--a consensus document of The Joint European Society of Cardiology/American College of Cardiology Committee for the redefinition of myocardial infarction. ***J Am Coll Cardiol**, 36* (3): 959-969.

Amundsen, B. H., Helle-Valle, T., Edvardsen, T., et al. 2006. Noninvasive Myocardial Strain Measurement by Speckle Tracking Echocardiography: Validation Against Sonomicrometry and Tagged Magnetic Resonance Imaging. ***J Am Coll Cardiol**, 47* (4): 789-793.

Ansalone, G., Giannantoni, P., Ricci, R., et al. 2002. Doppler myocardial imaging to evaluate the effectiveness of pacing sites in patients receiving biventricular pacing. ***J Am Coll Cardiol**, 39* (3): 489-499.

Arya, A., Bode, K., Piorkowski, C., et al. 2010. Catheter ablation of electrical storm due to monomorphic ventricular tachycardia in patients with nonischemic cardiomyopathy: acute results and its effect on long-term survival. ***Pacing Clin Electrophysiol**, 33* (12): 1504-1509.

Assomull, R. G., Prasad, S. K., Lyne, J., et al. 2006. Cardiovascular magnetic resonance, fibrosis, and prognosis in dilated cardiomyopathy. ***J Am Coll Cardiol**, 48* (10): 1977-1985.

Augustine, D., Lewandowski, A. J., Lazdam, M., et al. 2013. Global and regional left ventricular myocardial deformation measures by magnetic resonance feature

tracking in healthy volunteers: comparison with tagging and relevance of gender. ***J Cardiovasc Magn Reson**, 15* (1): 8.

Auricchio, A., Delnoy, P. P., Butter, C., et al. 2014. Feasibility, safety, and short-term outcome of leadless ultrasound-based endocardial left ventricular resynchronization in heart failure patients: results of the wireless stimulation endocardially for CRT (WiSE-CRT) study. ***Europace**, 16* (5): 681-688.

Auricchio, A., Fantoni, C., Regoli, F., et al. 2004. Characterization of left ventricular activation in patients with heart failure and left bundle-branch block. ***Circulation**, 109* (9): 1133-1139.

Auricchio, A., Sommariva, L., Salo, R. W., et al. 1993. Improvement of cardiac function in patients with severe congestive heart failure and coronary artery disease by dual chamber pacing with shortened AV delay. ***Pacing Clin Electrophysiol**, 16* (10): 2034-2043.

Axel, L.,Dougherty, L. 1989. MR imaging of motion with spatial modulation of magnetization. ***Radiology**, 171* (3): 841-845.

Baller, D., Wolpers, H. G., Zipfel, J., et al. 1988. Comparison of the effects of right atrial, right ventricular apex and atrioventricular sequential pacing on myocardial oxygen consumption and cardiac efficiency: a laboratory investigation. ***Pacing Clin Electrophysiol**, 11* (4): 394-403.

Barnett, D., Phillips, S.,Longson, C. 2007. Cardiac resynchronisation therapy for the treatment of heart failure: NICE technology appraisal guidance. ***Heart**, 93* (9): 1134-1135.

Barsheshet, A., Goldenberg, I., Moss, A. J., et al. 2011. Response to preventive cardiac resynchronization therapy in patients with ischaemic and nonischaemic cardiomyopathy in MADIT-CRT. ***Eur Heart J**, 32* (13): 1622-1630.

Baudino, T. A., Carver, W., Giles, W., et al. 2006. Cardiac fibroblasts: friend or foe? ***Am J Physiol Heart Circ Physiol**, 291* (3): H1015-H1026.

Bax, J. J., Bleeker, G. B., Marwick, T. H., et al. 2004. Left ventricular dyssynchrony predicts response and prognosis after cardiac resynchronization therapy. ***J Am Col Cardiol**, 44* 1834-1840.

Becker, M., Bilke, E., Kuhl, H., et al. 2006a. Analysis of myocardial deformation based on pixel tracking in two dimensional echocardiographic images enables quantitative assessment of regional left ventricular function. ***Heart**, 92* (8): 1102-1108.

Becker, M., Hoffmann, R., Kühl, H. P., et al. 2006b. Analysis of myocardial deformation based on ultrasonic pixel tracking to determine transmurality in chronic myocardial infarction. ***Eur Heart J**, 27* (21): 2560-2566.

Becker, M., Hoffmann, R., Schmitz, F., et al. 2007a. Relation of optimal lead positioning as defined by three-dimensional echocardiography to long-term benefit of cardiac resynchronization. ***Am J Cardiol**, 100* (11): 1671-1676.

Becker, M., Kramann, R., Franke, A., et al. 2007b. Impact of left ventricular lead position in cardiac resynchronization therapy on left ventricular remodelling. A circumferential strain analysis based on 2D echocardiography. ***Eur Heart J**, 28* (10): 1211-1220.

Belghitia, H., Brette, S., Lafitte, S., et al. 2008. Automated function imaging: a new operator-independent strain method for assessing left ventricular function. ***Arch Cardiovasc Dis**, 101* (3): 163-169.

Bertini, M., Marsan, N. A., Delgado, V., et al. 2009. Effects of cardiac resynchronization therapy on left ventricular twist. ***J Am Coll Cardiol**, 54* (14): 1317-1325.

Beshai, J., Grimm, R., Nagueh, S., et al. 2007. Cardiac-resynchronization therapy in heart failure with narrow QRS complexes. ***N Eng J Med**, 357* 2461-2471.

Beyar, R., Yin, F. C., Hausknecht, M., et al. 1989. Dependence of left ventricular twist-radial shortening relations on cardiac cycle phase. ***Am J Physiol**, 257* (4 Pt 2): H1119-1126.

Bilchick, K. C., Dimaano, V., Wu, K. C., et al. 2008. Cardiac Magnetic Resonance Assessment of Dyssynchrony and Myocardial Scar Predicts Function Class Improvement Following Cardiac Resynchronization Therapy. ***JACC Cardiovasc Imaging**, 1* (5): 561-568.

Blanc, J. J., Etienne, Y., Gilard, M., et al. 1997. Evaluation of different ventricular pacing sites in patients with severe heart failure: results of an acute hemodynamic study. ***Circulation**, 96* (10): 3273-3277.

Bleeker, G. B., Holman, E. R., Steendijk, P., et al. 2006a. Cardiac resynchronization therapy in patients with a narrow QRS complex. ***J Am Coll Cardiol**, 48* (11): 2243-2250.

Bleeker, G. B., Kaandorp, T. A., Lamb, H. J., et al. 2006b. Effect of posterolateral scar tissue on clinical and echocardiographic improvement after cardiac resynchronization therapy. ***Circulation**, 113* (7): 969-976.

Blessberger, H.,Binder, T. 2010. NON-invasive imaging: Two dimensional speckle tracking echocardiography: basic principles. ***Heart**, 96* (9): 716-722.

Bohs, L. N., Geiman, B. J., Anderson, M. E., et al. 2000. Speckle tracking for multi-dimensional flow estimation. ***Ultrasonics**, 38* (1-8): 369-375.

Borlaug, B. A., Olson, T. P., Lam, C. S., et al. 2010. Global cardiovascular reserve dysfunction in heart failure with preserved ejection fraction. ***J Am Coll Cardiol**, 56* (11): 845-854.

Braunwald, E., Myerburg, R. J.,A., C. (2011). Cardiac arrest and sudden cardiac death. *Braunwald's Heart Disease: A Textbook of Cardiovascular Medicine.* (pp. 742-749). New York, NY: WB Saunders Publishing Co.

Brecker, S. J., Xiao, H. B., Sparrow, J., et al. 1992. Effects of dual-chamber pacing with short atrioventricular delay in dilated cardiomyopathy. ***Lancet**, 340* (8831): 1308-1312.

Breithardt, O. A., Stellbrink, C., Kramer, A. P., et al. 2002. Echocardiographic quantification of left ventricular asynchrony predicts an acute hemodynamic benefit of cardiac resynchronization therapy. ***J Am Coll Cardiol**, 40* (3): 536-545.

Brignole, M., Auricchio, A., Baron-Esquivias, G., et al. 2013. 2013 ESC Guidelines on cardiac pacing and cardiac resynchronization therapy: The Task Force on cardiac pacing and resynchronization therapy of the European Society of Cardiology (ESC). Developed in collaboration with the European Heart Rhythm Association (EHRA). ***Eur Heart J**, 34* (29): 2281-2329.

Bristow, M. R., Saxon, L. A., Boehmer, J., et al. 2004. Cardiac-Resynchronization Therapy with or without an Implantable Defibrillator in Advanced Chronic Heart Failure. ***N Engl J Med**, 350* (21): 2140-2150.

Buckberg, G., Hoffman, J. I., Mahajan, A., et al. 2008. Cardiac mechanics revisited: the relationship of cardiac architecture to ventricular function. ***Circulation**, 118* (24): 2571-2587.

Burkhoff, D., Oikawa, R. Y.,Sagawa, K. 1986. Influence of pacing site on canine left ventricular contraction. ***Am J Physiol**, 251* H428-H435.

Byrne, M. J., Helm, R. H., Daya, S., et al. 2007. Diminished left ventricular dyssynchrony and impact of resynchronization in failing hearts with right versus left bundle branch block. ***J Am Coll Cardiol**, 50* (15): 1484-1490.

Camm, A. J., Luscher, T. F.,Serruys, P. W. (2009). *The ESC Textbook of Cardiovascular Medicine* (Vol. 2nd). New York: Oxford.

Carasso, S., Rakowski, H., Witte, K. K., et al. 2009. Left ventricular strain patterns in dilated cardiomyopathy predict response to cardiac resynchronization therapy: timing is not everything. ***J Am Soc Echocardiogr**, 22* (3): 242-250.

Cassidy, D. M., Vassallo, J. A., Marchlinski, F. E., et al. 1984. Endocardial mapping in humans in sinus rhythm with normal left ventricles: activation patterns and characteristics of electrograms. ***Circulation**, 70* (1): 37-42.

Castelli, G., Fornaro, A., Ciaccheri, M., et al. 2013. Improving survival rates of patients with idiopathic dilated cardiomyopathy in Tuscany over 3 decades: impact of evidence-based management. ***Circ Heart Fail**, 6* (5): 913-921.

Castro, P. L., Greenberg, N. L., Drinko, J., et al. 2000. Potential pitfalls of strain rate imaging: angle dependency. ***Biomed Sci Instrum**, 36* 197-202.

Cazeau, S., Leclercq, C., Lavergne, T., et al. 2001. Effects of multisite biventricular pacing in patients with heart failure and intraventricular conduction delay. ***N Engl J Med**, 344* (12): 873-880.

Cazeau, S., Ritter, P., Bakdach, S., et al. 1994. Four chamber pacing in dilated cardiomyopathy. ***Pacing Clin Electrophysiol**, 17* (11 Pt 2): 1974-1979.

Cazeau, S., Ritter, P., Lazarus, A., et al. 1996. Multisite pacing for end-stage heart failure: early experience. ***Pacing Clin Electrophysiol**, 19* (11 Pt 2): 1748-1757.

Cerqueira, M. D., Weissman, N. J., Dilsizian, V., et al. 2002. Standardized myocardial segmentation and nomenclature for tomographic imaging of the heart. A statement for healthcare professionals from the Cardiac Imaging Committee of the Council on Clinical Cardiology of the American Heart Association. ***Circulation**, 105* (4): 539-542.

Chahal, N. S.,Senior, R. 2010. Clinical applications of left ventricular opacification. ***JACC Cardiovasc Imaging**, 3* (2): 188-196.

Chalil, S., Foley, P. W. X., Muyhaldeen, S. A., et al. 2007a. Late gadolinium enhancement-cardiovascular magnetic resonance as a predictor of response to cardiac resynchronization therapy in patients with ischaemic cardiomyopathy. ***Europace**, 9* (11): 1031-1037.

Chalil, S., Stegemann, B., Muhyaldeen, S., et al. 2007b. Intraventricular Dyssynchrony Predicts Mortality and Morbidity Following Cardiac Resynchronization Therapy: A Study Using Cardiovascular Magnetic Resonance Tissue Synchronization Imaging ***J Am Coll Cardiol**, 50* 243-252.

Chalil, S., Stegemann, B., Muhyaldeen, S. A., et al. 2007c. Effect of posterolateral left ventricular scar on mortality and morbidity following cardiac resynchronization therapy. ***Pacing Clin Electrophysiol**, 30* (10): 1201-1209.

Chitwood, W. R., Jr., Hill, R. C., Sink, J. D., et al. 1980. Measurement of global ventricular function in patients during cardiac operations using sonomicrometry. ***J Thorac Cardiovasc Surg**, 80* (5): 724-735.

Chung, E. S., Katra, R. P., Ghio, S., et al. 2010. Cardiac resynchronization therapy may benefit patients with left ventricular ejection fraction >35%: a PROSPECT trial substudy. ***Eur J Heart Fail**, 12* (6): 581-587.

Chung, E. S., Leon, A. R., Tavazzi, L., et al. 2008. Results of the Predictors of Response to CRT (PROSPECT) Trial. ***Circulation**, 117* (20): 2608-2616.

CIBIS-II Investigators and Committees. 1999. The Cardiac Insufficiency Bisoprolol Study II (CIBIS-II): a randomised trial. ***Lancet**, 353* (9146): 9-13.

Cleland, J. G. F., Daubert, J.-C., Erdmann, E., et al. 2005. The Effect of Cardiac Resynchronization on Morbidity and Mortality in Heart Failure. ***N Engl J Med**, 352* (15): 1539-1549.

Codd, M. B., Sugrue, D. D., Gersh, B. J., et al. 1989. Epidemiology of idiopathic dilated and hypertrophic cardiomyopathy. A population-based study in Olmsted County, Minnesota, 1975-1984. ***Circulation**, 80* (3): 564-572.

Cohn, J. N., Ferrari, R.,Sharpe, N. 2000. Cardiac remodeling--concepts and clinical implications: a consensus paper from an international forum on cardiac remodeling. Behalf of an International Forum on Cardiac Remodeling. ***J Am Coll Cardiol**, 35* (3): 569-582.

Cohn, J. N.,Tognoni, G. 2001. A Randomized Trial of the Angiotensin-Receptor Blocker Valsartan in Chronic Heart Failure. ***N Engl J Med**, 345* (23): 1667-1675.

Cojoc, A., Reeves, J. G., Schmarkey, L., et al. 2006. Effects of Single-Site Versus Biventricular Epicardial Pacing on Myocardial Performance in an Immature Animal Model of Atrioventricular Block. ***J Cardiovasc Electrophysiol**, 17* (8): 884-889.

Conca, C., Faletra, F. F., Miyazaki, C., et al. 2009. Echocardiographic Parameters of Mechanical Synchrony in Healthy Individuals. ***Am J Cardiol**, 103* (1): 136-142.

Curtis, A. B., Adamson, P. B., Chung, E., et al. 2007. Biventricular versus right ventricular pacing in patients with AV block (BLOCK HF): clinical study design and rationale. ***J Cardiovasc Electrophysiol**, 18* (9): 965-971.

Cwajg, J. M., Cwajg, E., Nagueh, S. F., et al. 2000. End-diastolic wall thickness as a predictor of recovery of function in myocardial hibernation: Relation to rest-redistribution Tl-201 tomography and dobutamine stress echocardiography. ***J Am Coll Cardiol**, 35* (5): 1152-1161.

Dalen, H., Thorstensen, A., Aase, S. A., et al. 2010. Segmental and global longitudinal strain and strain rate based on echocardiography of 1266 healthy individuals: the HUNT study in Norway. ***Eur J Echocardiogr**, 11* (2): 176-183.

Daubert, J. C., Ritter, P., Le Breton, H., et al. 1998. Permanent left ventricular pacing with transvenous leads inserted into the coronary veins. ***Pacing Clin Electrophysiol**, 21* (1 Pt 2): 239-245.

Daubert, J. C., Saxon, L., Adamson, P. B., et al. 2012. 2012 EHRA/HRS expert consensus statement on cardiac resynchronization therapy in heart failure: implant and follow-up recommendations and management. ***Europace**, 14* (9): 1236-1286.

de Bakker, J. M., van Capelle, F. J., Janse, M. J., et al. 1993. Slow conduction in the infarcted human heart. 'Zigzag' course of activation. ***Circulation**, 88* (3): 915-926.

de Leeuw, N., Ruiter, D. J., Balk, A. H., et al. 2001. Histopathologic findings in explanted heart tissue from patients with end-stage idiopathic dilated cardiomyopathy. ***Transpl Int**, 14* (5): 299-306.

Dekker, A. L., Phelps, B., Dijkman, B., et al. 2004. Epicardial left ventricular lead placement for cardiac resynchronization therapy: optimal pace site selection with pressure-volume loops. ***J Thorac Cardiovasc Surg**, 127* (6): 1641-1647.

Delgado, V., Mollema, S. A., Ypenburg, C., et al. 2008. Relation Between Global Left Ventricular Longitudinal Strain Assessed with Novel Automated Function Imaging and Biplane Left Ventricular Ejection Fraction in Patients with Coronary Artery Disease. ***J Am Soc Echocardiogr**, 21* (11): 1244-1250.

DeLong, E. R., DeLong, D. M.,Clarke-Pearson, D. L. 1988. Comparing the areas under two or more correlated receiver operating characteristic curves: a nonparametric approach. ***Biometrics**, 44* (3): 837-845.

Di Bello, V., Cucco, C., Giannini, C., et al. 2010. Myocardial tissue characterization and aortic stenosis. ***J Am Soc Echocardiogr**, 23* (10): 1067-1070.

Di Bello, V., Giorgi, D., Viacava, P., et al. 2004. Severe aortic stenosis and myocardial function: diagnostic and prognostic usefulness of ultrasonic integrated backscatter analysis. ***Circulation**, 110* (7): 849-855.

Dickstein, K., Bogale, N., Priori, S., et al. 2009. The European cardiac resynchronization therapy survey. ***Eur Heart J**, 30* (20): 2450-2460.

Dickstein, K., Normand, C., Auricchio, A., et al. 2018. CRT Survey II: a European Society of Cardiology survey of cardiac resynchronisation therapy in 11 088 patients-who is doing what to whom and how? ***Eur J Heart Fail***.

Durrer, D., van Dam, R. T., Freud, G. E., et al. 1970. Total excitation of the isolated human heart. ***Circulation**, 41* (6): 899-912.

Dweck, M. R., Joshi, S., Murigu, T., et al. 2011. Midwall fibrosis is an independent predictor of mortality in patients with aortic stenosis. ***J Am Coll Cardiol**, 58* (12): 1271-1279.

Edvardsen, T., Aakhus, S., Endresen, K., et al. 2000. Acute regional myocardial ischemia identified by 2-dimensional multiregion tissue Doppler imaging technique. ***J Am Soc Echocardiogr**, 13* (11): 986-994.

Edvardsen, T., Gerber, B. L., Garot, J., et al. 2002. Quantitative Assessment of Intrinsic Regional Myocardial Deformation by Doppler Strain Rate Echocardiography in Humans. ***Circulation**, 106* (1): 50-56.

Edvardsen, T., Rosen, B. D., Pan, L., et al. 2006. Regional diastolic dysfunction in individuals with left ventricular hypertrophy measured by tagged magnetic resonance imaging--the Multi-Ethnic Study of Atherosclerosis (MESA). ***Am Heart J**, 151* (1): 109-114.

Edwards, N. C., Ferro, C. J., Kirkwood, H., et al. 2010. Effect of spironolactone on left ventricular systolic and diastolic function in patients with early stage chronic kidney disease. ***Am J Cardiol**, 106* (10): 1505-1511.

Egoavil, C. A., Ho, R. T., Greenspon, A. J., et al. 2005. Cardiac resynchronization therapy in patients with right bundle branch block: analysis of pooled data from the MIRACLE and Contak CD trials. ***Heart Rhythm**, 2* (6): 611-615.

Elliott, P. 2000. Cardiomyopathy. Diagnosis and management of dilated cardiomyopathy. ***Heart**, 84* (1): 106-112.

Ersboll, M., Valeur, N., Mogensen, U. M., et al. 2013. Prediction of all-cause mortality and heart failure admissions from global left ventricular longitudinal strain in patients with acute myocardial infarction and preserved left ventricular ejection fraction. ***J Am Coll Cardiol**, 61* (23): 2365-2373.

Fantoni, C., Kawabata, M., Massaro, R., et al. 2005. Right and left ventricular activation sequence in patients with heart failure and right bundle branch block: a detailed analysis using three-dimensional non-fluoroscopic electroanatomic mapping system. ***J Cardiovasc Electrophysiol**, 16* (2): 112-119.

Felker, G. M., Thompson, R. E., Hare, J. M., et al. 2000. Underlying causes and long-term survival in patients with initially unexplained cardiomyopathy. ***N Engl J Med**, 342* (15): 1077-1084.

Ferreira, J. P., Duarte, K., Graves, T. L., et al. 2016. Natriuretic Peptides, 6-Min Walk Test, and Quality-of-Life Questionnaires as Clinically Meaningful Endpoints in HF Trials. ***J Am Coll Cardiol**, 68* (24): 2690-2707.

Flather, M. D., Shibata, M. C., Coats, A. J. S., et al. 2005. Randomized trial to determine the effect of nebivolol on mortality and cardiovascular hospital admission in elderly patients with heart failure (SENIORS). ***Eur Heart J**, 26* (3): 215-225.

Flett, A. S., Hayward, M. P., Ashworth, M. T., et al. 2010. Equilibrium contrast cardiovascular magnetic resonance for the measurement of diffuse myocardial fibrosis: preliminary validation in humans. ***Circulation**, 122* (2): 138-144.

Foley, P. W., Chalil, S., Khadjooi, K., et al. 2011a. Left ventricular reverse remodelling, long-term clinical outcome, and mode of death after cardiac resynchronization therapy. ***Eur J Heart Fail**, 13* (1): 43-51.

Foley, P. W., Khadjooi, K., Ward, J. A., et al. 2009a. Radial dyssynchrony assessed by cardiovascular magnetic resonance in relation to left ventricular function, myocardial scarring and QRS duration in patients with heart failure. ***J Cardiovasc Magn Reson**, 11* (1): 50.

Foley, P. W., Leyva, F.,Frenneaux, M. P. 2009b. What is treatment success in cardiac resynchronization therapy? ***Europace**, 11 Suppl 5* v58-65.

Foley, P. W., Patel, K., Irwin, N., et al. 2011b. Cardiac resynchronisation therapy in patients with heart failure and a normal QRS duration: the RESPOND study. ***Heart**, 97* (13): 1041-1047.

Foley, P. W., Stegemann, B., Smith, R. E., et al. 2009c. Cardiac resynchronization therapy in patients with mildly impaired left ventricular function. ***Pacing Clin Electrophysiol**, 32 Suppl 1* S186-189.

Forleo, G. B., Di Biase, L., Panattoni, G., et al. 2015. Improved implant and postoperative lead performance in CRT-D patients implanted with a quadripolar left ventricular lead. A 6-month follow-up analysis from a multicenter prospective comparative study. ***J Interv Card Electrophysiol**, 42* (1): 59-66.

Gasparini, M., Mantica, M., Galimberti, P., et al. 2003. Is the outcome of cardiac resynchronization therapy related to the underlying etiology? ***Pacing Clin Electrophysiol**, 26* (1 Pt 2): 175-180.

Gasparini, M., Regoli, F., Ceriotti, C., et al. 2008. Remission of left ventricular systolic dysfunction and of heart failure symptoms after cardiac resynchronization therapy: temporal pattern and clinical predictors. ***Am Heart J**, 155* (3): 507-514.

Gervais, R., Leclercq, C., Shankar, A., et al. 2009. Surface electrocardiogram to predict outcome in candidates for cardiac resynchronization therapy: a sub-analysis of the CARE-HF trial. ***Eur J Heart Fail**, 11* (7): 699-705.

Geyer, H., Caracciolo, G., Abe, H., et al. 2010. Assessment of myocardial mechanics using speckle tracking echocardiography: fundamentals and clinical applications. ***J Am Soc Echocardiogr**, 23* (4): 351-369; quiz 453-355.

Gibbons Kroeker, C. A., Ter Keurs, H. E., Knudtson, M. L., et al. 1993. An optical device to measure the dynamics of apex rotation of the left ventricle. ***Am J Physiol**, 265* (4 Pt 2): H1444-1449.

Gjesdal, O., Hopp, E., Vartdal, T., et al. 2007. Global longitudinal strain measured by two-dimensional speckle tracking echocardiography is closely related to myocardial infarct size in chronic ischaemic heart disease. ***Clin Sci**, 113* (6): 287-296.

Gold, M. R., Birgersdotter-Green, U., Singh, J. P., et al. 2011. The relationship between ventricular electrical delay and left ventricular remodelling with cardiac resynchronization therapy. ***Eur Heart J**, 32* (20): 2516-2524.

Gold, M. R., Feliciano, Z., Gottlieb, S. S., et al. 1995. Dual-chamber pacing with a short atrioventricular delay in congestive heart failure: a randomized study. ***J Am Coll Cardiol**, 26* (4): 967-973.

Goldenberg, I., Kutyifa, V., Klein, H. U., et al. 2014. Survival with cardiac-resynchronization therapy in mild heart failure. ***N Engl J Med**, 370* (18): 1694-1701.

Gorcsan, J., 3rd, Tanabe, M., Bleeker, G. B., et al. 2007. Combined longitudinal and radial dyssynchrony predicts ventricular response after resynchronization therapy. ***J Am Coll Cardiol**, 50* (15): 1476-1483.

Gorcsan, J., Oyenuga, O., Habib, P. J., et al. 2010. Relationship of Echocardiographic Dyssynchrony to Long-Term Survival After Cardiac Resynchronization Therapy. ***Circulation**, 122* (19): 1910-1918.

Gorman, J. H., 3rd, Gupta, K. B., Streicher, J. T., et al. 1996. Dynamic three-dimensional imaging of the mitral valve and left ventricle by rapid sonomicrometry array localization. ***J Thorac Cardiovasc Surg**, 112* (3): 712-726.

Gottlieb, I., Macedo, R., Bluemke, D., et al. 2006. Magnetic resonance imaging in the evaluation of non-ischemic cardiomyopathies: Current applications and future perspectives. ***Heart Fail Rev**, 11* (4): 313-323.

Granger, C. B., McMurray, J. J. V., Yusuf, S., et al. 2003. Effects of candesartan in patients with chronic heart failure and reduced left-ventricular systolic function intolerant to angiotensin-converting-enzyme inhibitors: the CHARM-Alternative trial. ***Lancet**, 362* (9386): 772-776.

Greenbaum, R., Ho, S. Y., Gibson, D. G., et al. 1981. Left ventricular fibre architecture in man. ***Br Heart J.**, 45* 248-263.

Grines, C. L., Bashore, T. M., Boudoulas, H., et al. 1989. Functional abnormalities in isolated left bundle branch block. The effect of interventricular asynchrony. ***Circulation**, 79* (4): 845-853.

Grothues, F., Smith, G. C., Moon, J. C., et al. 2002. Comparison of interstudy reproducibility of cardiovascular magnetic resonance with two-dimensional echocardiography in normal subjects and in patients with heart failure or left ventricular hypertrophy. ***Am J Cardiol**, 90* (1): 29-34.

Gulati, A., Jabbour, A., Ismail, T. F., et al. 2013. ASsociation of fibrosis with mortality and sudden cardiac death in patients with nonischemic dilated cardiomyopathy. ***JAMA**, 309* (9): 896-908.

Haghjoo, M., Bagherzadeh, A., Farahani, M. M., et al. 2008. Significance of QRS morphology in determining the prevalence of mechanical dyssynchrony in heart failure patients eligible for cardiac resynchronization: particular focus on patients with right bundle branch block with and without coexistent left-sided conduction defects. ***Europace**, 10* (5): 566-571.

Haghjoo, M., Bagherzadeh, A., Fazelifar, A., et al. 2007. Prevalence of mechanical dyssynchrony in heart failure patients with different QRS durations. ***Pacing Clin Electrophysiol**, 30* 616-622.

Hankiewicz, J. H., Goldspink, P. H., Buttrick, P. M., et al. 2008. Principal strain changes precede ventricular wall thinning during transition to heart failure in a mouse model of dilated cardiomyopathy. ***Am J Physiol Heart Circ Physiol**, 294* (1): H330-336.

Hansen, D. E., Daughters, G. T., 2nd, Alderman, E. L., et al. 1988. Torsional deformation of the left ventricular midwall in human hearts with intramyocardial markers: regional heterogeneity and sensitivity to the inotropic effects of abrupt rate changes. ***Circ Res**, 62* (5): 941-952.

Harrild, D. M., Han, Y., Geva, T., et al. 2012. Comparison of cardiac MRI tissue tracking and myocardial tagging for assessment of regional ventricular strain. ***Int J Cardiovasc Imaging**, 28* (8): 2009-2018.

Hawkins, N. M., Petrie, M. C., Burgess, M. I., et al. 2009. Selecting Patients for Cardiac Resynchronization Therapy: The Fallacy of Echocardiographic Dyssynchrony. ***J Am Coll Cardiol**, 53* (21): 1944-1959.

Hayes, D. L., Boehmer, J. P., Day, J. D., et al. 2011. Cardiac resynchronization therapy and the relationship of percent biventricular pacing to symptoms and survival. ***Heart Rhythm**, 8* (9): 1469-1475.

Helle-Valle, T., Crosby, J., Edvardsen, T., et al. 2005. New noninvasive method for assessment of left ventricular rotation: speckle tracking echocardiography. ***Circulation**, 112* (20): 3149-3156.

Helm, R. H., Leclercq, C., Faris, O. P., et al. 2005. Cardiac Dyssynchrony Analysis Using Circumferential Versus Longitudinal Strain: Implications for Assessing Cardiac Resynchronization. ***Circulation**, 111* (21): 2760-2767.

Henry, W. L., Gardin, J. M.,Ware, J. H. 1980. Echocardiographic measurements in normal subjects from infancy to old age. ***Circulation**, 62* (5): 1054-1061.

Hippisley-Cox, J., Coupland, C., Vinogradova, Y., et al. 2008. Predicting cardiovascular risk in England and Wales: prospective derivation and validation of QRISK2. ***BMJ**, 336* (7659): 1475-1482.

Hor, K. N., Baumann, R., Pedrizzetti, G., et al. 2011. Magnetic resonance derived myocardial strain assessment using feature tracking. ***J Vis Exp*** (48).

Hor, K. N., Gottliebson, W. M., Carson, C., et al. 2010. Comparison of Magnetic Resonance Feature Tracking for Strain Calculation With Harmonic Phase Imaging Analysis. ***J Am Coll Cardiol Img**, 3* (2): 144-151.

Hsia, H. H.,Marchlinski, F. E. 2002. Characterization of the electroanatomic substrate for monomorphic ventricular tachycardia in patients with nonischemic cardiomyopathy. ***Pacing Clin Electrophysiol**, 25* (7): 1114-1127.

Hurlburt, H. M., Aurigemma, G. P., Hill, J. C., et al. 2007. Direct ultrasound measurement of longitudinal, circumferential, and radial strain using 2-dimensional strain imaging in normal adults. ***Echocardiography**, 24* (7): 723-731.

HyLown Consulting. (2013). Calculate sample size needed to test time to event data: Cox PH, 2 sided equality. Retrieved 13.03.18, from http://powerandsamplesize.com/Calculators/Test-Time-To-Event-Data/Cox-PH-2-Sided-Equality).

Ibrahim, el-S. H. 2011. Myocardial tagging by cardiovascular magnetic resonance: evolution of techniques--pulse sequences, analysis algorithms, and applications. ***J Cardiovasc Magn Reson**, 13* 36.

Iles, L., Pfluger, H., Lefkovits, L., et al. 2011. Myocardial Fibrosis Predicts Appropriate Device Therapy in Patients With Implantable Cardioverter-Defibrillators for Primary Prevention of Sudden Cardiac Death. ***J Am Coll Cardiol**, 57* (7): 821-828.

Iles, L., Pfluger, H., Phrommintikul, A., et al. 2008. Evaluation of diffuse myocardial fibrosis in heart failure with cardiac magnetic resonance contrast-enhanced T1 mapping. ***J Am Coll Cardiol**, 52* (19): 1574-1580.

Ingels, N. B., Jr., Daughters, G. T., 2nd, Stinson, E. B., et al. 1980. Evaluation of methods for quantitating left ventricular segmental wall motion in man using myocardial markers as a standard. ***Circulation**, 61* (5): 966-972.

Ingels, N. B., Jr., Hansen, D. E., Daughters, G. T., 2nd, et al. 1989. Relation between longitudinal, circumferential, and oblique shortening and torsional deformation in the left ventricle of the transplanted human heart. ***Circ Res**, 64* (5): 915-927.

Jacobsson, J., Borgquist, R., Reitan, C., et al. 2016. Usefulness of the Sum Absolute QRST Integral to Predict Outcomes in Patients Receiving Cardiac Resynchronization Therapy. ***Am J Cardiol**, 118* (3): 389-395.

Jansen, A. H. M., Bracke, F., van Dantzig, J. m., et al. 2008. The influence of myocardial scar and dyssynchrony on reverse remodeling in cardiac resynchronization therapy. ***Eur J Echocardiogr**, 9* (4): 483-488.

Japp, A. G., Gulati, A., Cook, S. A., et al. 2016. The Diagnosis and Evaluation of Dilated Cardiomyopathy. ***J Am Coll Cardiol**, 67* (25): 2996-3010.

Juenger, J., Schellberg, D., Kraemer, S., et al. 2002. Health related quality of life in patients with congestive heart failure: comparison with other chronic diseases and relation to functional variables. ***Heart**, 87* (3): 235-241.

Jung, B., Markl, M., Foll, D., et al. 2006. Investigating myocardial motion by MRI using tissue phase mapping. ***Eur J Cardiothorac Surg**, 29 Suppl 1* S150-157.

Kane GC, Karon BL, Mahoney DW, et al. 2011. Progression of left ventricular diastolic dysfunction and risk of heart failure. ***JAMA**, 306* (8): 856-863.

Kane, S. P. (2016). ClinCalc.com. Retrieved 13.03.2018, from http://clincalc.com/Stats/Power.aspx

Kanzaki, H., Nakatani, S., Yamada, N., et al. 2006. Impaired systolic torsion in dilated cardiomyopathy: reversal of apical rotation at mid-systole characterized with magnetic resonance tagging method. ***Basic Res Cardiol**, 101* (6): 465-470.

Kapetanakis, S., Bhan, A., Murgatroyd, F., et al. 2011. Real-time 3D echo in patient selection for cardiac resynchronization therapy. ***JACC Cardiovasc Imaging**, 4* (1): 16-26.

Karaahmet, T., Tigen, K., Dundar, C., et al. 2010. The effect of cardiac fibrosis on left ventricular remodeling, diastolic function, and N-terminal pro-B-type natriuretic peptide levels in patients with nonischemic dilated cardiomyopathy. ***Echocardiography**, 27* (8): 954-960.

Khan, F. Z., Virdee, M. S., Palmer, C. R., et al. 2012a. Targeted Left Ventricular Lead Placement to Guide Cardiac Resynchronization Therapy: The TARGET Study: A Randomized, Controlled Trial. ***J Am Coll Cardiol**, 59* (17): 1509-1518.

Khan, F. Z., Virdee, M. S., Palmer, C. R., et al. 2012b. Targeted Left Ventricular Lead Placement to Guide Cardiac Resynchronization Therapy: The TARGET Study: A Randomized, Controlled Trial. ***J Am Coll Cardiol***.

Kim, R. J., Wu, E., Rafael, A., et al. 2000. The Use of Contrast-Enhanced Magnetic Resonance Imaging to Identify Reversible Myocardial Dysfunction. ***N Engl J Med**, 343* (20): 1445-1453.

Kleijn, S. A., Pandian, N. G., Thomas, J. D., et al. 2014. Normal reference values of left ventricular strain using three-dimensional speckle tracking echocardiography: results from a multicentre study. ***Eur Heart J Cardiovasc Imaging***.

Knaapen, P., Boellaard, R., Gotte, M. J., et al. 2004. Perfusable tissue index as a potential marker of fibrosis in patients with idiopathic dilated cardiomyopathy. ***J Nucl Med**, 45* (8): 1299-1304.

Knaapen, P., Gotte, M. J., Paulus, W. J., et al. 2006. Does myocardial fibrosis hinder contractile function and perfusion in idiopathic dilated cardiomyopathy? PET and MR imaging study. ***Radiology**, 240* (2): 380-388.

Konstam, M. A., Rousseau, M. F., Kronenberg, M. W., et al. 1992. Effects of the angiotensin converting enzyme inhibitor enalapril on the long-term progression of left ventricular dysfunction in patients with heart failure. SOLVD Investigators. ***Circulation**, 86* (2): 431-438.

Koos, R., Sinha, A. M., Markus, K., et al. 2004. Comparison of left ventricular lead placement via the coronary venous approach versus lateral thoracotomy in patients receiving cardiac resynchronization therapy. ***Am J Cardiol**, 94* (1): 59-63.

Kowallick, J. T., Morton, G., Lamata, P., et al. 2017. Quantitative assessment of left ventricular mechanical dyssynchrony using cine cardiovascular magnetic resonance imaging: Inter-study reproducibility. ***JRSM Cardiovasc Dis**, 6* 2048004017710142.

Kowallick, J. T., Morton, G., Lamata, P., et al. 2016. Inter-study reproducibility of left ventricular torsion and torsion rate quantification using MR myocardial feature tracking. ***J Magn Reson Imaging**, 43* (1): 128-137.

Kraitchman, D. L., Sampath, S., Castillo, E., et al. 2003. Quantitative Ischemia Detection During Cardiac Magnetic Resonance Stress Testing by Use of FastHARP. ***Circulation**, 107* (15): 2025-2030.

Kreuz, J., Horlbeck, F., Linhart, M., et al. 2012. Independent predictors of mortality in patients with advanced heart failure treated by cardiac resynchronization therapy. ***Europace**, 14* (11): 1596-1601.

Kroeker, C. A., Tyberg, J. V.,Beyar, R. 1995. Effects of ischemia on left ventricular apex rotation. An experimental study in anesthetized dogs. ***Circulation**, 92* (12): 3539-3548.

Kuetting, D. L., Sprinkart, A. M., Dabir, D., et al. 2016. Assessment of cardiac dyssynchrony by cardiac MR: A comparison of velocity encoding and feature tracking analysis. ***J Magn Reson Imaging**, 43* (4): 940-946.

Kuhl, H. P., Schreckenberg, M., Rulands, D., et al. 2004. High-resolution transthoracic real-time three-dimensional echocardiography: quantitation of cardiac volumes and function using semi-automatic border detection and comparison with cardiac magnetic resonance imaging. ***J Am Coll Cardiol**, 43* (11): 2083-2090.

Kutyifa, V., Kloppe, A., Zareba, W., et al. 2013. The Influence of Left Ventricular Ejection Fraction on the Effectiveness of Cardiac Resynchronization Therapy: MADIT-CRT (Multicenter Automatic Defibrillator Implantation Trial With Cardiac Resynchronization Therapy). ***J Am Coll Cardiol**, 61* (9): 936-944.

Kuznetsova, T., Herbots, L., Richart, T., et al. 2008. Left ventricular strain and strain rate in a general population. ***Eur Heart J**, 29* (16): 2014-2023.

Kwon, D. H., Halley, C. M., Carrigan, T. P., et al. 2009. Extent of Left Ventricular Scar Predicts Outcomes in Ischemic Cardiomyopathy Patients With Significantly Reduced Systolic Function: A Delayed Hyperenhancement Cardiac Magnetic Resonance Study. ***J Am Coll Cardiol Img**, 2* (1): 34-44.

Kwong, R. Y., Chan, A. K., Brown, K. A., et al. 2006. Impact of unrecognized myocardial scar detected by cardiac magnetic resonance imaging on event-free survival in patients presenting with signs or symptoms of coronary artery disease. ***Circulation**, 113* (23): 2733-2743.

Kydd, A. C., Khan, F. Z., O'Halloran, D., et al. 2013. Radial strain delay based on segmental timing and strain amplitude predicts left ventricular reverse remodeling and survival after cardiac resynchronization therapy. ***Circ Cardiovasc Imaging**, 6* (2): 177-184.

Lamia, B., Tanabe, M., Tanaka, H., et al. 2011. Left ventricular systolic torsion correlates global cardiac performance during dyssynchrony and cardiac resynchronization therapy. ***Am J Physiol Heart Circ Physiol**, 300* (3): H853-858.

Leclercq, C., Cazeau, S., Le Breton, H., et al. 1998a. Acute hemodynamic effects of biventricular DDD pacing in patients with end-stage heart failure. ***J Am Coll Cardiol**, 32* (7): 1825-1831.

Leclercq, C., Cazeau, S., Le Breton, H., et al. 1998b. Acute hemodynamic effects of biventricular DDD pacing in patients with end-stage heart failure. ***J Am Coll Cardiol**, 32* (7): 1825-1831.

Leclercq, C., Faris, O., Tunin, R., et al. 2002. Systolic Improvement and Mechanical Resynchronization Does Not Require Electrical Synchrony in the Dilated Failing Heart With Left Bundle-Branch Block. ***Circulation**, 106* (14): 1760-1763.

Leclercq, C., Gras, D., Le Helloco, A., et al. 1995. Hemodynamic importance of preserving the normal sequence of ventricular activation in permanent cardiac pacing. ***Am Heart J**, 129* (6): 1133-1141.

Leeson, P., Mitchell, A.,Becher, H. (2008). *Echocardiography (Oxford Specialist Handbooks in Cardiology)* (First ed.). Oxford: Oxford University Press.

Lehrke, S., Lossnitzer, D., Schob, M., et al. 2011. Use of cardiovascular magnetic resonance for risk stratification in chronic heart failure: prognostic value of late gadolinium enhancement in patients with non-ischaemic dilated cardiomyopathy. ***Heart**, 97* (9): 727-732.

Leong, D. P., Chakrabarty, A., Shipp, N., et al. 2012. Effects of myocardial fibrosis and ventricular dyssynchrony on response to therapy in new-presentation idiopathic dilated cardiomyopathy: insights from cardiovascular magnetic resonance and echocardiography. ***Eur Heart J,*** *33* (5): 640-648.

Leyva, F., Foley, P., Chalil, S., et al. 2011. Cardiac resynchronization therapy guided by late gadolinium-enhancement cardiovascular magnetic resonance. ***J Cardiovasc Magn Reson,*** *13* (1): 29-35.

Leyva, F., Foley, P. W. X., Stegemann, B., et al. 2009. Development and validation of a clinical index to predict survival after cardiac resynchronisation therapy. ***Heart,*** *95* (19): 1619-1625.

Leyva, F., Taylor, R. J., Foley, P. W. X., et al. 2012. Left Ventricular Midwall Fibrosis as a Predictor of Mortality and Morbidity After Cardiac Resynchronization Therapy in Patients With Nonischemic Cardiomyopathy. ***J Am Coll Cardiol,*** *60* (17): 1659-1667.

Lijnen, P.,Petrov, V. 2000. Induction of cardiac fibrosis by aldosterone. ***J Mol Cell Cardiol,*** *32* (6): 865-879.

Lim, P., Buakhamsri, A., Popovic, Z. B., et al. 2008. Longitudinal strain delay index by speckle tracking imaging: a new marker of response to cardiac resynchronization therapy. ***Circulation,*** *118* (11): 1130-1137.

Lim, P., Donal, E., Lafitte, S., et al. 2011. Multicentre study using strain delay index for predicting response to cardiac resynchronization therapy (MUSIC study). ***Eur J Heart Fail,*** *13* (9): 984-991.

Linde, C., Abraham, W. T., Gold, M. R., et al. 2010. Cardiac resynchronization therapy in asymptomatic or mildly symptomatic heart failure patients in relation to etiology: results from the REVERSE (REsynchronization reVErses Remodeling in Systolic Left vEntricular Dysfunction) study. ***J Am Coll Cardiol,*** *56* (22): 1826-1831.

Linde, C., Abraham, W. T., Gold, M. R., et al. 2008. Randomized Trial of Cardiac Resynchronization in Mildly Symptomatic Heart Failure Patients and in Asymptomatic Patients With Left Ventricular Dysfunction and Previous Heart Failure Symptoms. ***J Am Coll Cardiol,*** *52* (23): 1834-1843.

Linde, C., Curtis, A. B., Fonarow, G. C., et al. 2016. Cardiac resynchronization therapy in chronic heart failure with moderately reduced left ventricular ejection fraction: Lessons from the Multicenter InSync Randomized Clinical Evaluation MIRACLE EF study. ***Int J Cardiol,*** *202* 349-355.

Linde, C., Gadler, F., Edner, M., et al. 1995. Results of atrioventricular synchronous pacing with optimized delay in patients with severe congestive heart failure. ***Am J Cardiol,*** *75* (14): 919-923.

Linde, C., Gold, M. R., Abraham, W. T., et al. 2013. Long-term impact of cardiac resynchronization therapy in mild heart failure: 5-year results from the REsynchronization reVErses Remodeling in Systolic left vEntricular dysfunction (REVERSE) study. ***Eur Heart J,*** *34* (33): 2592-2599.

Lorenz, C. H., Pastorek, J. S.,Bundy, J. M. 2000. Delineation of normal human left ventricular twist throughout systole by tagged cine magnetic resonance imaging. ***J Cardiovasc Magn Reson,*** *2* (2): 97-108.

Lu, M. J., Zhong, W. H., Liu, Y. X., et al. 2016. Sample Size for Assessing Agreement between Two Methods of Measurement by Bland-Altman Method. ***Int J Biostat,*** *12* (2).

Lumens, J., Delhaas, T., Arts, T., et al. 2006. Impaired subendocardial contractile myofiber function in asymptomatic aged humans, as detected using MRI. ***Am J Physiol Heart Circ Physiol**, 291* (4): H1573-1579.

Lyseggen, E., Skulstad, H., Helle-Valle, T., et al. 2005. Myocardial strain analysis in acute coronary occlusion: a tool to assess myocardial viability and reperfusion. ***Circulation**, 112* (25): 3901-3910.

Maceira, A., Prasad, S., Khan, M., et al. 2006. Normalized Left Ventricular Systolic and Diastolic Function by Steady State Free Precession Cardiovascular Magnetic Resonance. ***J Cardiovasc Magn Reson*** (8): 417-426.

Maehashi, N., Yokota, Y., Takarada, A., et al. 1991. The role of myocarditis and myocardial fibrosis in dilated cardiomyopathy. Analysis of 28 necropsy cases. ***Jpn Heart J**, 32* (1): 1-15.

Mahrholdt, H., Goedecke, C., Wagner, A., et al. 2004. Cardiovascular magnetic resonance assessment of human myocarditis: a comparison to histology and molecular pathology. ***Circulation**, 109* (10): 1250-1258.

Malaty, A. N., Shah, D. J., Abdelkarim, A. R., et al. 2011. Relation of replacement fibrosis to left ventricular diastolic function in patients with dilated cardiomyopathy. ***J Am Soc Echocardiogr**, 24* (3): 333-338.

Marcassa, C., Campini, R., Verna, E., et al. 2007. Assessment of cardiac asynchrony by radionuclide phase analysis: correlation with ventricular function in patients with narrow or prolonged QRS interval. ***Eur J Heart Fail**, 9* 484-490.

Marcus, F. I., McKenna, W. J., Sherrill, D., et al. 2010. Diagnosis of arrhythmogenic right ventricular cardiomyopathy/dysplasia: proposed modification of the task force criteria. ***Circulation**, 121* (13): 1533-1541.

Marra, M. P., De Lazzari, M., Rizzo, S., et al. 2013. The prognostic value of myocardial fibrosis in nonischemic dilated cardiomyopathy: a study by endomyocardial biopsy and cardiac magnetic resonance. ***Eur Heart J**, 34* (suppl 1).

Marwick, T. H. 2006. Measurement of strain and strain rate by echocardiography: ready for prime time? ***J Am Coll Cardiol**, 47* (7): 1313-1327.

Marwick, T. H. 2008. Hype and Hope in the Use of Echocardiography for Selection for Cardiac Resynchronization Therapy: The Tower of Babel Revisited. ***Circulation**, 117* (20): 2573-2576.

Marwick, T. H., Leano, R. L., Brown, J., et al. 2009. Myocardial Strain Measurement With 2-Dimensional Speckle-Tracking Echocardiography: Definition of Normal Range. ***JACC Cardiovasc Imaging**, 2* (1): 80-84.

Masci, P. G., Schuurman, R., Andrea, B., et al. 2013. Myocardial Fibrosis as a Key Determinant of Left Ventricular Remodeling in Idiopathic Dilated Cardiomyopathy: A Contrast-Enhanced Cardiovascular Magnetic Study. ***Circulation: Cardiovascular Imaging**, 6* (5): 790-799.

Matsumoto, K., Tanaka, H., Tatsumi, K., et al. 2012. Left ventricular dyssynchrony using three-dimensional speckle-tracking imaging as a determinant of torsional mechanics in patients with idiopathic dilated cardiomyopathy. ***Am J Cardiol**, 109* (8): 1197-1205.

McCrohon, J. A., Moon, J. C. C., Prasad, S. K., et al. 2003. Differentiation of Heart Failure Related to Dilated Cardiomyopathy and Coronary Artery Disease Using Gadolinium-Enhanced Cardiovascular Magnetic Resonance. ***Circulation**, 108* (1): 54-59.

McMurray, J. J., Ostergren, J., Swedberg, K., et al. 2003. Effects of candesartan in patients with chronic heart failure and reduced left-ventricular systolic function taking angiotensin-converting-enzyme inhibitors: the CHARM-Added trial. ***Lancet**, 362* (9386): 767-771.

McMurray, J. J., Packer, M., Desai, A. S., et al. 2014. Angiotensin-neprilysin inhibition versus enalapril in heart failure. ***N Engl J Med**, 371* (11): 993-1004.

McNally, E. M., Golbus, J. R.,Puckelwartz, M. J. 2013. Genetic mutations and mechanisms in dilated cardiomyopathy. ***J Clin Invest**, 123* (1): 19-26.

Mele, D., Agricola, E., Galderisi, M., et al. 2009. Echocardiographic Myocardial Scar Burden Predicts Response to Cardiac Resynchronization Therapy in Ischemic Heart Failure. ***J Am Soc Echocardiogr**, 22* (6): 702-708.

MERIT-HF Study Group. 1999. Effect of metoprolol CR/XL in chronic heart failure: Metoprolol CR/XL Randomised Intervention Trial in-Congestive Heart Failure (MERIT-HF). ***Lancet**, 353* (9169): 2001-2007.

Messroghli, D. R., Greiser, A., Frohlich, M., et al. 2007. Optimization and validation of a fully-integrated pulse sequence for modified look-locker inversion-recovery (MOLLI) T1 mapping of the heart. ***J Magn Reson Imaging**, 26* (4): 1081-1086.

Metz, C. E. 1978. Basic principles of ROC analysis. ***Semin Nucl Med**, 8* (4): 283-298.

Mignot, A., Donal, E., Zaroui, A., et al. 2010. Global longitudinal strain as a major predictor of cardiac events in patients with depressed left ventricular function: a multicenter study. ***J Am Soc Echocardiogr**, 23* (10): 1019-1024.

Miyatake, K., Yamagishi, M., Tanaka, N., et al. 1995. New method for evaluating left ventricular wall motion by color-coded tissue doppler imaging: In vitro and in vivo studies. ***J Am Coll Cardiol**, 25* (3): 717-724.

Miyazaki, C., Redfield, M. M., Powell, B. D., et al. 2010. Dyssynchrony indices to predict response to cardiac resynchronization therapy: a comprehensive prospective single-center study. ***Circ Heart Fail**, 3* (5): 565-573.

Mizuno, R., Fujimoto, S., Saito, Y., et al. 2007. Non-invasive quantitation of myocardial fibrosis using combined tissue harmonic imaging and integrated backscatter analysis in dilated cardiomyopathy. ***Cardiology**, 108* (1): 11-17.

Molhoek, S. G., Bax, J. J., van Erven, L., et al. 2002. Effectiveness of resynchronization therapy in patients with end-stage heart failure. ***Am J Cardiol**, 90* (4): 379-383.

Moody, W. E., Ferro, C. J., Edwards, N. C., et al. 2016. Cardiovascular Effects of Unilateral Nephrectomy in Living Kidney Donors. ***Hypertension**, 67* (2): 368-377.

Moody, W. E., Taylor, R. J., Edwards, N. C., et al. 2015. Comparison of magnetic resonance feature tracking for systolic and diastolic strain and strain rate calculation with spatial modulation of magnetization imaging analysis. ***J Magn Reson Imaging**, 41* (4): 1000-1012.

Moody, W. E., Tomlinson, L. A., Ferro, C. J., et al. 2014. Effect of A Reduction in glomerular filtration rate after NEphrectomy on arterial STiffness and central hemodynamics: rationale and design of the EARNEST study. ***Am Heart J**, 167* (2): 141-149.e142.

Moon, M. R., Ingels, N. B., Jr., Daughters, G. T., 2nd, et al. 1994. Alterations in left ventricular twist mechanics with inotropic stimulation and volume loading in human subjects. ***Circulation**, 89* (1): 142-150.

Moore, C. C., Lugo-Olivieri, C. H., McVeigh, E. R., et al. 2000a. Three-dimensional Systolic Strain Patterns in the Normal Human Left Ventricle: Characterization with Tagged MR Imaging. ***Radiology**, 214* (2): 453-466.

Moore, C. C., McVeigh, E. R.,Zerhouni, E. A. 2000b. Quantitative tagged magnetic resonance imaging of the normal human left ventricle. ***Top Magn Reson Imaging**, 11* (6): 359-371.

Mor-Avi, V., Lang, R. M., Badano, L. P., et al. 2011. Current and evolving echocardiographic techniques for the quantitative evaluation of cardiac mechanics: ASE/EAE consensus statement on methodology and indications endorsed by the Japanese Society of Echocardiography. ***Eur J Echocardiogr**, 12* (3): 167-205.

Moreo, A., Ambrosio, G., De Chiara, B., et al. 2009. Influence of myocardial fibrosis on left ventricular diastolic function: noninvasive assessment by cardiac magnetic resonance and echo. ***Circ Cardiovasc Imaging**, 2* (6): 437-443.

Moreo, A., Ambrosio, G., De Chiara, B., et al. 2013. Influence of midwall fibrosis on diastolic dysfunction in non-ischemic cardiomyopathy. ***Int J Cardiol**, 163* (3): 342-344.

Morgan, J. M., Biffi, M., Geller, L., et al. 2016. ALternate Site Cardiac ResYNChronization (ALSYNC): a prospective and multicentre study of left ventricular endocardial pacing for cardiac resynchronization therapy. ***Eur Heart J**, 37* (27): 2118-2127.

Morton, G., Schuster, A., Jogiya, R., et al. 2012. Inter-study reproducibility of cardiovascular magnetic resonance myocardial feature tracking. ***J Cardiovasc Magn Reson**, 14* (1): 43.

Moss, A. J., Hall, W. J., Cannom, D. S., et al. 2009. Cardiac-Resynchronization Therapy for the Prevention of Heart-Failure Events. ***N Engl J Med**, 361* (14): 1329-1338.

Mosteller, R. 1987. Simplified Calculation of Body-Surface Area. ***N Engl J Med**, 317* (17): 1098-1098.

Murgatroyd, F., Linker, N. J., Cunningham, D., et al. (2016). *National audit of cardiac rhythm managment devices 2014-15* National institute for cardiovascular outcomes research (Ed.) Retrieved from http://www.ucl.ac.uk/nicor/audits/cardiacrhythm/documents/annual-reports/cardiac_rhythm_management_devices_public_report_2014_15

Murphy, R. T., Sigurdsson, G., Mulamalla, S., et al. 2006. Tissue synchronization imaging and optimal left ventricular pacing site in cardiac resynchronization therapy. ***Am J Cardiol**, 97* (11): 1615-1621.

Nagele, H., Schomburg, R., Petersen, B., et al. 2002. Dual chamber pacing in patients with severe heart failure on beta blocker and amiodarone treatment: preliminary results of a randomised study. ***Heart**, 87* (6): 566-567.

Nagueh, S. F., Bachinski, L. L., Meyer, D., et al. 2001. Tissue Doppler imaging consistently detects myocardial abnormalities in patients with hypertrophic cardiomyopathy and provides a novel means for an early diagnosis before and independently of hypertrophy. ***Circulation**, 104* (2): 128-130.

Nakatani, S. 2011. Left ventricular rotation and twist: why should we learn? ***J Cardiovasc Ultrasound**, 19* (1): 1-6.

Nanjo, S., Yoshikawa, K., Harada, M., et al. 2009. Correlation between left ventricular diastolic function and ejection fraction in dilated cardiomyopathy using magnetic resonance imaging with late gadolinium enhancement. ***Circ J**, 73* (10): 1939-1944.

NICE. (2010, 11.02.2014). Chronic heart failure: Management of chronic heart failure in adults in primary and secondary care., from https://www.nice.org.uk/guidance/Cg108

NICE. (2014). Implantable cardioverter defibrillators and cardiac resynchronisation therapy for arrhythmias and heart failure. Retrieved 21st December 2015, from https://www.nice.org.uk/guidance/ta314

Nishimura, R. A., Hayes, D. L., Holmes, D. R., Jr., et al. 1995. Mechanism of hemodynamic improvement by dual-chamber pacing for severe left ventricular dysfunction: an acute Doppler and catheterization hemodynamic study. ***J Am Coll Cardiol**, 25* (2): 281-288.

Nosir, Y. F., Fioretti, P. M., Vletter, W. B., et al. 1996. Accurate measurement of left ventricular ejection fraction by three-dimensional echocardiography. A comparison with radionuclide angiography. ***Circulation**, 94* (3): 460-466.

Notabartolo, D., Merlino, J. D., Smith, A. L., et al. 2004. Usefulness of the peak velocity difference by tissue Doppler imaging technique as an effective predictor of response to cardiac resynchronization therapy. ***Am J Cardiol**, 94* (6): 817-820.

Onishi, T., Saha, S. K., Ludwig, D. R., et al. 2013. Feature tracking measurement of dyssynchrony from cardiovascular magnetic resonance cine acquisitions: comparison with echocardiographic speckle tracking. ***J Cardiovasc Magn Reson**, 15* 95.

Packer, M., Fowler, M. B., Roecker, E. B., et al. 2002. Effect of carvedilol on the morbidity of patients with severe chronic heart failure: results of the carvedilol prospective randomized cumulative survival (COPERNICUS) study. ***Circulation**, 106* (17): 2194-2199.

Pappone, C., Calovic, Z., Cuko, A., et al. 2014a. O157 Multipoint left ventricular pacing provides similar acute hemodynamic improvement regardless of QRS duration or lead location in cardiac resynchronization therapy patients. ***Global Heart**, 9* (1): e43.

Pappone, C., Calovic, Z., Vicedomini, G., et al. 2015. Improving cardiac resynchronization therapy response with multipoint left ventricular pacing: Twelve-month follow-up study. ***Heart Rhythm**, 12* (6): 1250-1258.

Pappone, C., Calovic, Z., Vicedomini, G., et al. 2014b. Multipoint left ventricular pacing improves acute hemodynamic response assessed with pressure-volume loops in cardiac resynchronization therapy patients. ***Heart Rhythm**, 11* (3): 394-401.

Park, R. C., Little, W. C.,O'Rourke, R. A. 1985. Effect of alteration of left ventricular activation sequence on the left ventricular end-systolic pressure-volume relation in closed - chest dogs. ***Circ Res**, 57* 706-717.

Park, T. H., Nagueh, S. F., Khoury, D. S., et al. 2006. Impact of myocardial structure and function postinfarction on diastolic strain measurements: implications for assessment of myocardial viability. ***Am J Physiol Heart Circ Physiol**, 290* (2): H724-731.

Perkins, N. J.,Schisterman, E. F. 2006. The inconsistency of "optimal" cutpoints obtained using two criteria based on the receiver operating characteristic curve. ***Am J Epidemiol**, 163* (7): 670-675.

Petersen, S., Rayner, M.,Wolstenholme, J. (2002). *Coronary heart disease statistics: heart failure supplement.* (B. H. Foundation Ed.). London: British Heart Foundation

Picano, E., Pelosi, G., Marzilli, M., et al. 1990. In vivo quantitative ultrasonic evaluation of myocardial fibrosis in humans. ***Circulation**, 81* (1): 58-64.

Pitt, B., Remme, W., Zannad, F., et al. 2003. Eplerenone, a Selective Aldosterone Blocker, in Patients with Left Ventricular Dysfunction after Myocardial Infarction. ***N Engl J Med**, 348* (14): 1309-1321.

Pitt, B., Zannad, F., Remme, W. J., et al. 1999. The Effect of Spironolactone on Morbidity and Mortality in Patients with Severe Heart Failure. ***N Engl J Med**, 341* (10): 709-717.

Pitzalis, M. V., Iacoviello, M., Romito, R., et al. 2002. Cardiac resynchronization therapy tailored by echocardiographic evaluation of ventricular asynchrony. ***J Am Col Cardiol**, 40* 1615-1622.

Plana, J. C., Galderisi, M., Barac, A., et al. 2014. Expert consensus for multimodality imaging evaluation of adult patients during and after cancer therapy: a report from the American Society of Echocardiography and the European Association of Cardiovascular Imaging. ***Eur Heart J Cardiovasc Imaging**, 15* (10): 1063-1093.

Ponikowski, P., Voors, A. A., Anker, S. D., et al. 2016. 2016 ESC Guidelines for the diagnosis and treatment of acute and chronic heart failure: The Task Force for the diagnosis and treatment of acute and chronic heart failure of the European Society of Cardiology (ESC)Developed with the special contribution of the Heart Failure Association (HFA) of the ESC. ***Eur Heart J**, 37* (27): 2129-2200.

Popescu, B. A., Beladan, C. C., Calin, A., et al. 2009. Left ventricular remodelling and torsional dynamics in dilated cardiomyopathy: reversed apical rotation as a marker of disease severity. ***Eur J Heart Fail**, 11* (10): 945-951.

Popovic, Z. B., Benejam, C., Bian, J., et al. 2007. Speckle-tracking echocardiography correctly identifies segmental left ventricular dysfunction induced by scarring in a rat model of myocardial infarction. ***Am J Physiol Heart Circ Physiol**, 292* (6): H2809-2816.

Prati, G., Vitrella, G., Allocca, G., et al. 2015. Right Ventricular Strain and Dyssynchrony Assessment in Arrhythmogenic Right Ventricular Cardiomyopathy: Cardiac Magnetic Resonance Feature-Tracking Study. ***Circ Cardiovasc Imaging**, 8* (11): e003647; discussion e003647.

Prinzen, F. W., Augustijn, C. H., Arts, T., et al. 1990. Redistribution of myocardial fiber strain and blood flow by asynchronous activation. ***Am J Physiol**, 259* H300-H308.

QRISK®2. (2012). QRISK®2 calculator. Retrieved 10.12.2012, from http://qrisk.org

Quarta, C. C., Solomon, S. D., Uraizee, I., et al. 2014. Left ventricular structure and function in transthyretin-related versus light-chain cardiac amyloidosis. ***Circulation**, 129* (18): 1840-1849.

Quinones, M. A., Greenberg, B. H., Kopelen, H. A., et al. 2000. Echocardiographic predictors of clinical outcome in patients with left ventricular dysfunction enrolled in the SOLVD registry and trials: significance of left ventricular hypertrophy. Studies of Left Ventricular Dysfunction. ***J Am Coll Cardiol**, 35* (5): 1237-1244.

Rademakers, F. E., Buchalter, M. B., Rogers, W. J., et al. 1992. Dissociation between left ventricular untwisting and filling. Accentuation by catecholamines. ***Circulation**, 85* (4): 1572-1581.

Ramanathan, C., Jia, P., Ghanem, R., et al. 2006. Activation and repolarization of the normal human heart under complete physiological conditions. ***Proc Natl Acad Sci U S A**, 103* (16): 6309-6314.

Raphael, C., Briscoe, C., Davies, J., et al. 2007. Limitations of the New York Heart Association functional classification system and self-reported walking distances in chronic heart failure. ***Heart**, 93* (4): 476-482.

Redfield, M. M., Jacobsen, S. J., Burnett, J. C., Jr., et al. 2003. Burden of systolic and diastolic ventricular dysfunction in the community: appreciating the scope of the heart failure epidemic. ***JAMA**, 289* (2): 194-202.

Rockman, H. A., Juneau, C., Chatterjee, K., et al. 1989. Long-term predictors of sudden and low output death in chronic congestive heart failure secondary to coronary artery disease. ***Am J Cardiol**, 64* (19): 1344-1348.

Roque, C., Trevisi, N., Silberbauer, J., et al. 2014. Electrical storm induced by cardiac resynchronization therapy is determined by pacing on epicardial scar and can be successfully managed by catheter ablation. ***Circ Arrhythm Electrophysiol**, 7* (6): 1064-1069.

Roubicek, T., Wichterle, D., Kucera, P., et al. 2015. Left Ventricular Lead Electrical Delay Is a Predictor of Mortality in Patients With Cardiac Resynchronization Therapy. ***Circ Arrhythm Electrophysiol**, 8* (5): 1113-1121.

Ruschitzka, F., Abraham, W. T., Singh, J. P., et al. 2013. Cardiac-resynchronization therapy in heart failure with a narrow QRS complex. ***N Engl J Med**, 369* (15): 1395-1405.

Russel, I. K., Gotte, M. J., de Roest, G. J., et al. 2009. Loss of opposite left ventricular basal and apical rotation predicts acute response to cardiac resynchronization therapy and is associated with long-term reversed remodeling. ***J Card Fail**, 15* (8): 717-725.

Ruwald, M. H., Solomon, S. D., Foster, E., et al. 2014. Left ventricular ejection fraction normalization in cardiac resynchronization therapy and risk of ventricular arrhythmias and clinical outcomes: results from the Multicenter Automatic Defibrillator Implantation Trial With Cardiac Resynchronization Therapy (MADIT-CRT) trial. ***Circulation**, 130* (25): 2278-2286.

Saba, S., Marek, J., Schwartzman, D., et al. 2013. Echocardiography-guided left ventricular lead placement for cardiac resynchronization therapy: results of the Speckle Tracking Assisted Resynchronization Therapy for Electrode Region trial. ***Circ Heart Fail**, 6* (3): 427-434.

Sade, L. E., Demir, O., Atar, I., et al. 2008. Effect of mechanical dyssynchrony and cardiac resynchronization therapy on left ventricular rotational mechanics. ***Am J Cardiol**, 101* (8): 1163-1169.

Saffitz, J. E., Davis, L. M., Darrow, B. J., et al. 1995. The molecular basis of anisotropy: role of gap junctions. ***J Cardiovasc Electrophysiol**, 6* (6): 498-510.

Sanderson, J. E. 2014. HFNEF, HFpEF, HF-PEF, or DHF: what is in an acronym? ***JACC Heart Fail**, 2* (1): 93-94.

Sandler, H.,Dodge, H. T. 1963. Left ventricular tension and stress in man. ***Circ Res**, 13* (2): 91-104.

Sarnoff, S. J., Mitchell, J. H., Gilmore, J. P., et al. 1960. Homeometric autoregulation in the heart. ***Circ Res**, 8* 1077-1091.

Sassone, B., Gambetti, S., Bertini, M., et al. 2015. Relation of QRS duration to response to cardiac resynchronization therapy. ***Am J Cardiol**, 115* (2): 214-219.

Schiller, N. B., Shah, P. M., Crawford, M., et al. 1989. Recommendations for quantitation of the left ventricle by two-dimensional echocardiography. American Society of

Echocardiography Committee on Standards, Subcommittee on Quantitation of Two-Dimensional Echocardiograms. ***J Am Soc Echocardiogr**, 2* (5): 358-367.
Schuster, A., Kutty, S., Padiyath, A., et al. 2011. Cardiovascular magnetic resonance myocardial feature tracking detects quantitative wall motion during dobutamine stress. ***J Cardiovasc Magn Reson**, 13* (1): 58.
Schuster, A., Paul, M., Bettencourt, N., et al. Cardiovascular magnetic resonance myocardial feature tracking for quantitative viability assessment in ischemic cardiomyopathy. ***Int J Cardiol*** (0).
Schuster, A., Stahnke, V. C., Unterberg-Buchwald, C., et al. 2015. Cardiovascular magnetic resonance feature-tracking assessment of myocardial mechanics: Intervendor agreement and considerations regarding reproducibility. ***Clin Radiol**, 70* (9): 989-998.
Schwartzman, D., Chang, I., Michele, J. J., et al. 1999. Electrical Impedance Properties of Normal and Chronically Infarcted Left Ventricular Myocardium. ***J Interv Card Electrophysiol**, 3* (3): 213-224.
Selvanayagam, J. B., Kardos, A., Francis, J. M., et al. 2004. Value of Delayed-Enhancement Cardiovascular Magnetic Resonance Imaging in Predicting Myocardial Viability After Surgical Revascularization. ***Circulation**, 110* (12): 1535-1541.
Sengelov, M., Jorgensen, P. G., Jensen, J. S., et al. 2015. Global Longitudinal Strain Is a Superior Predictor of All-Cause Mortality in Heart Failure With Reduced Ejection Fraction. ***JACC Cardiovasc Imaging**, 8* (12): 1351-1359.
Sengupta, P. P., Khandheria, B. K., Korinek, J., et al. 2005. Biphasic tissue Doppler waveforms during isovolumic phases are associated with asynchronous deformation of subendocardial and subepicardial layers. ***J Appl Physiol**, 99* (3): 1104-1111.
Sengupta, P. P., Khandheria, B. K., Korinek, J., et al. 2006. Apex-to-base dispersion in regional timing of left ventricular shortening and lengthening. ***J Am Coll Cardiol**, 47* (1): 163-172.
Sengupta, P. P., Kramer, C. M.,Narula, J. 2013. Cardiac Resynchronization: The Flow of Activation Sequence. ***JACC Cardiovasc Imaging**, 6* (8): 924-926.
Setser, R. M., Kasper, J. M., Lieber, M. L., et al. 2003. Persistent abnormal left ventricular systolic torsion in dilated cardiomyopathy after partial left ventriculectomy. ***J Thorac Cardiovasc Surg**, 126* (1): 48-55.
Simonetti, O. P., Kim, R. J., Fieno, D. S., et al. 2001. An improved MR imaging technique for the visualization of myocardial infarction. ***Radiology**, 218* (1): 215-223.
Singh, J. P., Fan, D., Heist, E. K., et al. 2006. Left ventricular lead electrical delay predicts response to cardiac resynchronization therapy. ***Heart Rhythm**, 3* (11): 1285-1292.
Singh, J. P., Klein, H. U., Huang, D. T., et al. 2011. Left ventricular lead position and clinical outcome in the multicenter automatic defibrillator implantation trial-cardiac resynchronization therapy (MADIT-CRT) trial. ***Circulation**, 123* (11): 1159-1166.
Soejima, K., Stevenson, W. G., Sapp, J. L., et al. 2004. Endocardial and epicardial radiofrequency ablation of ventricular tachycardia associated with dilated cardiomyopathy: the importance of low-voltage scars. ***J Am Coll Cardiol**, 43* (10): 1834-1842.
Soejima, K., Suzuki, M., Maisel, W. H., et al. 2001. Catheter ablation in patients with multiple and unstable ventricular tachycardias after myocardial infarction: short ablation lines

guided by reentry circuit isthmuses and sinus rhythm mapping. ***Circulation**, 104* (6): 664-669.
Sohaib, S. M., Finegold, J. A., Nijjer, S. S., et al. 2015. Opportunity to increase life span in narrow QRS cardiac resynchronization therapy recipients by deactivating ventricular pacing: evidence from randomized controlled trials. ***JACC Heart Fail**, 3* (4): 327-336.
Solomon, S. D., Anavekar, N., Skali, H., et al. 2005. Influence of ejection fraction on cardiovascular outcomes in a broad spectrum of heart failure patients. ***Circulation**, 112* (24): 3738-3744.
Spencer, K. T., Bednarz, J., Rafter, P. G., et al. 1998. Use of harmonic imaging without echocardiographic contrast to improve two-dimensional image quality. ***Am J Cardiol**, 82* (6): 794-799.
Stanton, T., Leano, R.,Marwick, T. H. 2009. Prediction of all-cause mortality from global longitudinal speckle strain: comparison with ejection fraction and wall motion scoring. ***Circ Cardiovasc Imaging**, 2* (5): 356-364.
Stavrakis, S., Lazzara, R.,Thadani, U. 2012. The benefit of cardiac resynchronization therapy and QRS duration: a meta-analysis. ***J Cardiovasc Electrophysiol**, 23* (2): 163-168.
Steffel, J., Robertson, M., Singh, J. P., et al. 2015. The effect of QRS duration on cardiac resynchronization therapy in patients with a narrow QRS complex: a subgroup analysis of the EchoCRT trial. ***Eur Heart J**, 36* (30): 1983-1989.
Steine, K., Stugaard, M.,Smiseth, O. A. 1999. Mechanisms of retarded apical filling in acute ischemic left ventricular failure. ***Circulation**, 99* (15): 2048-2054.
Stellbrink, C., Breithardt, O. A., Franke, A., et al. 2001. Impact of cardiac resynchronization therapy using hemodynamically optimized pacing on left ventricular remodeling in patients with congestive heart failure and ventricular conduction disturbances. ***J Am Coll Cardiol**, 38* (7): 1957-1965.
Stewart, S., MacIntyre, K., Hole, D. J., et al. 2001. More 'malignant' than cancer? Five-year survival following a first admission for heart failure. ***Eur J Heart Fail**, 3* (3): 315-322.
Suffoletto, M. S., Dohi, K., Cannesson, M., et al. 2006. Novel speckle-tracking radial strain from routine black-and-white echocardiographic images to quantify dyssynchrony and predict response to cardiac resynchronization therapy. ***Circulation**, 113* (7): 960-968.
Sutherland, G. R., Stewart, M. J., Groundstroem, K. W., et al. 1994. Color Doppler myocardial imaging: a new technique for the assessment of myocardial function. ***J Am Soc Echocardiogr**, 7* (5): 441-458.
Sutton, M. G., Plappert, T., Hilpisch, K. E., et al. 2006. Sustained reverse left ventricular structural remodeling with cardiac resynchronization at one year is a function of etiology: quantitative Doppler echocardiographic evidence from the Multicenter InSync Randomized Clinical Evaluation (MIRACLE). ***Circulation**, 113* (2): 266-272.
Sweeney, M. O., Hellkamp, A. S., Ellenbogen, K. A., et al. 2003. Adverse Effect of Ventricular Pacing on Heart Failure and Atrial Fibrillation Among Patients With Normal Baseline QRS Duration in a Clinical Trial of Pacemaker Therapy for Sinus Node Dysfunction. ***Circulation**, 107* (23): 2932-2937.
Swoboda, P., Larghat, A., Greenwood, J., et al. 2011. Reproducibility of strain and twist measurements calculated using CSPAMM tagging. ***J Cardiovasc Magn Reson.**, 13(Suppl 1)* 52.

Taber, L. A., Yang, M.,Podszus, W. W. 1996. Mechanics of ventricular torsion. ***J Biomech**, 29* (6): 745-752.

Takemoto, Y., Hozumi, T., Sugioka, K., et al. 2007. Beta-blocker therapy induces ventricular resynchronization in dilated cardiomyopathy with narrow QRS complex. ***J Am Coll Cardiol**, 49* 778-783.

Tan, Y. T., Wenzelburger, F., Lee, E., et al. 2009. The pathophysiology of heart failure with normal ejection fraction: exercise echocardiography reveals complex abnormalities of both systolic and diastolic ventricular function involving torsion, untwist, and longitudinal motion. ***J Am Coll Cardiol**, 54* (1): 36-46.

Tanaka, H., Nesser, H.-J., Buck, T., et al. 2010. Dyssynchrony by speckle-tracking echocardiography and response to cardiac resynchronization therapy: results of the Speckle Tracking and Resynchronization (STAR) study. ***Eur Heart J**, 31* (14): 1690-1700.

Tang, A. S., Wells, G. A., Talajic, M., et al. 2010. Cardiac-resynchronization therapy for mild-to-moderate heart failure. ***N Engl J Med**, 363* (25): 2385-2395.

Tatsumi, K., Tanaka, H., Yamawaki, K., et al. 2011. Utility of comprehensive assessment of strain dyssynchrony index by speckle tracking imaging for predicting response to cardiac resynchronization therapy. ***Am J Cardiol**, 107* (3): 439-446.

Taylor, R. J., Moody, W. E., Umar, F., et al. 2015. Myocardial strain measurement with feature-tracking cardiovascular magnetic resonance: normal values. ***Eur Heart J Cardiovasc Imaging**, 16(8)* 871-881.

Taylor, R. J., Umar, F., Moody, W. E., et al. 2014. Feature-tracking cardiovascular magnetic resonance as a novel technique for the assessment of mechanical dyssynchrony. ***Int J Cardiol**, 175(1)* 120-125.

Tedrow, U., Maisel, W. H., Epstein, L. M., et al. 2004. Feasibility of adjusting paced left ventricular activation by manipulating stimulus strength. ***J Am Coll Cardiol**, 44* (11): 2249-2252.

Tereshchenko, L. G., Cheng, A., Fetics, B. J., et al. 2011. A new electrocardiogram marker to identify patients at low risk for ventricular tachyarrhythmias: sum magnitude of the absolute QRST integral. ***J Electrocardiol**, 44* (2): 208-216.

Tereshchenko, L. G., Cheng, A., Park, J., et al. 2015a. Novel measure of electrical dyssynchrony predicts response in cardiac resynchronization therapy: Results from the SMART-AV Trial. ***Heart Rhythm**, 12* (12): 2402-2410.

Tereshchenko, L. G., Ghafoori, E., Kabir, M. M., et al. 2015b. Electrical Dyssynchrony on Noninvasive Electrocardiographic Mapping correlates with SAI QRST on surface ECG. ***Comput Cardiol (2010)**, 42* 69-72.

Thavendiranathan, P., Grant, A. D., Negishi, T., et al. 2013. Reproducibility of echocardiographic techniques for sequential assessment of left ventricular ejection fraction and volumes: application to patients undergoing cancer chemotherapy. ***J Am Coll Cardiol**, 61* (1): 77-84.

Thavendiranathan, P., Poulin, F., Lim, K. D., et al. 2014. Use of myocardial strain imaging by echocardiography for the early detection of cardiotoxicity in patients during and after cancer chemotherapy: a systematic review. ***J Am Coll Cardiol**, 63* (25 Pt A): 2751-2768.

The Consensus Trial Study Group. 1987. Effects of Enalapril on Mortality in Severe Congestive Heart Failure. ***N Engl J Med**, 316* (23): 1429-1435.

The SOLVD Investigators. 1991. Effect of Enalapril on Survival in Patients with Reduced Left Ventricular Ejection Fractions and Congestive Heart Failure. ***N Engl J Med**, 325* (5): 293-302.

Thibault, B., Harel, F., Ducharme, A., et al. 2013. Cardiac resynchronization therapy in patients with heart failure and a QRS complex <120 milliseconds: the Evaluation of Resynchronization Therapy for Heart Failure (LESSER-EARTH) trial. ***Circulation**, 127* (8): 873-881.

Thomson, H. L., Basmadjian, A. J., Rainbird, A. J., et al. 2001. Contrast echocardiography improves the accuracy and reproducibility of left ventricular remodeling measurements: a prospective, randomly assigned, blinded study. ***J Am Coll Cardiol**, 38* (3): 867-875.

Townsend N, Williams J, Bhatnagar P, et al. (2014). *Cardiovascular Disease Statistics 2014*. London: British Heart Foundation.

Tracy, C. M., Epstein, A. E., Darbar, D., et al. 2012. 2012 ACCF/AHA/HRS Focused Update of the 2008 Guidelines for Device-Based Therapy of Cardiac Rhythm AbnormalitiesA Report of the American College of Cardiology Foundation/American Heart Association Task Force on Practice Guidelines. ***J Am Coll Cardiol**, 60* (14): 1297-1313.

U.S. Department of Health and Human Services: Food and Drug Administration. (2015). *Expedited Access for Premarket Approval and De Novo Medical Devices Intended for Unmet Medical Need for Life Threatening or Irreversibly Debilitating Diseases or Conditions* Retrieved from http://www.fda.gov/downloads/MedicalDevices/DeviceRegulationandGuidance/GuidanceDocuments/UCM393978.pdf

Upadhyay, G. A., Choudhry, N. K., Auricchio, A., et al. 2008. Cardiac resynchronization in patients with atrial fibrillation: a meta-analysis of prospective cohort studies. ***J Am Coll Cardiol**, 52* (15): 1239-1246.

van Dalen, B. M., Kauer, F., Soliman, O. I., et al. 2009. Influence of the pattern of hypertrophy on left ventricular twist in hypertrophic cardiomyopathy. ***Heart**, 95* (8): 657-661.

van Dalen, B. M., Kauer, F., Vletter, W. B., et al. 2010. Influence of cardiac shape on left ventricular twist. ***J Appl Physiol**, 108* (1): 146-151.

Voigt, J. U., Lindenmeier, G., Exner, B., et al. 2003. Incidence and characteristics of segmental postsystolic longitudinal shortening in normal, acutely ischemic, and scarred myocardium. ***J Am Soc Echocardiogr**, 16* (5): 415-423.

Wagner, A., Mahrholdt, H., Holly, T. A., et al. 2003. Contrast-enhanced MRI and routine single photon emission computed tomography (SPECT) perfusion imaging for detection of subendocardial myocardial infarcts: an imaging study. ***Lancet**, 361* (9355): 374-379.

Weidemann, F., Jamal, F., Sutherland, G. R., et al. 2002. Myocardial function defined by strain rate and strain during alterations in inotropic states and heart rate. ***Am J Physiol Heart Circ Physiol**, 283* (2): H792-799.

White, J. A., Yee, R., Yuan, X., et al. 2006. Delayed Enhancement Magnetic Resonance Imaging Predicts Response to Cardiac Resynchronization Therapy in Patients With Intraventricular Dyssynchrony. ***J Am Coll Cardiol**, 48* (10): 1953-1960.

Wikstrom, G., Blomstrom-Lundqvist, C., Andren, B., et al. 2009. The effects of aetiology on outcome in patients treated with cardiac resynchronization therapy in the CARE-HF trial. ***Eur Heart J,*** *30* (7): 782-788.

Wilkoff, B., Cook, J., Epstein, A., et al. 2002. Dual-chamber pacing or ventricular backup pacing in patients with an implantable defibrillator: The dual chamber and vvi implantable defibrillator (david) trial. ***JAMA,*** *288* (24): 3115-3123.

Wong, M., Staszewsky, L., Latini, R., et al. 2004. Severity of left ventricular remodeling defines outcomes and response to therapy in heart failure: Valsartan heart failure trial (Val-HeFT) echocardiographic data. ***J Am Coll Cardiol,*** *43* (11): 2022-2027.

Wood, P. W., Choy, J. B., Nanda, N. C., et al. 2014. Left ventricular ejection fraction and volumes: it depends on the imaging method. ***Echocardiography,*** *31* (1): 87-100.

Wu, E. X., Wu, Y., Tang, H., et al. 2007. Study of myocardial fiber pathway using magnetic resonance diffusion tensor imaging. ***Magn Reson Imaging,*** *25* (7): 1048-1057.

Wu, K. C., Weiss, R. G., Thiemann, D. R., et al. 2008. Late gadolinium enhancement by cardiovascular magnetic resonance heralds an adverse prognosis in nonischemic cardiomyopathy. ***J Am Coll Cardiol,*** *51* (25): 2414-2421.

Wu, L., Germans, T., Guclu, A., et al. 2014. Feature tracking compared with tissue tagging measurements of segmental strain by cardiovascular magnetic resonance. ***J Cardiovasc Magn Reson,*** *16* (1): 10.

Wu, T. J., Ong, J. J., Hwang, C., et al. 1998. Characteristics of wave fronts during ventricular fibrillation in human hearts with dilated cardiomyopathy: role of increased fibrosis in the generation of reentry. ***J Am Coll Cardiol,*** *32* (1): 187-196.

Wu, Y.,Kovacs, S. J. 2006. Frequency-based analysis of the early rapid filling pressure-flow relation elucidates diastolic efficiency mechanisms. ***Am J Physiol Heart Circ Physiol,*** *291* (6): H2942-2949.

Yingchoncharoen, T., Agarwal, S., Popovic, Z. B., et al. 2013. Normal ranges of left ventricular strain: a meta-analysis. ***J Am Soc Echocardiogr,*** *26* (2): 185-191.

Yingchoncharoen, T., Gibby, C., Rodriguez, L. L., et al. 2012. Association of myocardial deformation with outcome in asymptomatic aortic stenosis with normal ejection fraction. ***Circ Cardiovasc Imaging,*** *5* (6): 719-725.

Yoneyama, K., Gjesdal, O., Choi, E.-Y., et al. 2012. Age, Sex, and Hypertension-Related Remodeling Influences Left Ventricular Torsion Assessed by Tagged Cardiac Magnetic Resonance in Asymptomatic Individuals: The Multi-Ethnic Study of Atherosclerosis. ***Circulation,*** *126* (21): 2481-2490.

Yong, Y., Wu, D., Fernandes, V., et al. 2002. Diagnostic accuracy and cost-effectiveness of contrast echocardiography on evaluation of cardiac function in technically very difficult patients in the intensive care unit. ***Am J Cardiol,*** *89* (6): 711-718.

Youden, W. J. 1950. Index for rating diagnostic tests. ***Cancer,*** *3* (1): 32-35.

Young, A. A., Kramer, C. M., Ferrari, V. A., et al. 1994. Three-dimensional left ventricular deformation in hypertrophic cardiomyopathy. ***Circulation,*** *90* (2): 854-867.

Ypenburg, C., Schalij, M. J., Bleeker, G. B., et al. 2007. Impact of viability and scar tissue on response to cardiac resynchronization therapy in ischaemic heart failure patients. ***Eur Heart J,*** *28* (1): 33-41.

Ypenburg, C., van Bommel, R. J., Borleffs, C. J., et al. 2009. Long-term prognosis after cardiac resynchronization therapy is related to the extent of left ventricular reverse remodeling at midterm follow-up. ***J Am Coll Cardiol**, 53* (6): 483-490.

Ypenburg, C., van Bommel, R. J., Delgado, V., et al. 2008. Optimal left ventricular lead position predicts reverse remodeling and survival after cardiac resynchronization therapy. ***J Am Coll Cardiol**, 52* (17): 1402-1409.

Yu, C.-M., Bleeker, G. B., Fung, J. W.-H., et al. 2005. Left Ventricular Reverse Remodeling but Not Clinical Improvement Predicts Long-Term Survival After Cardiac Resynchronization Therapy. ***Circulation**, 112* (11): 1580-1586.

Yu, C.-M., Chau, E., Sanderson, J. E., et al. 2002. Tissue Doppler echocardiographic evidence of reverse remodeling and improved synchronicity by simultaneously delaying regional contraction after biventricular pacing therapy in heart failure. ***Circulation**, 105* (4): 438-445.

Yu, C.-M., Fung, J. W.-H., Zhang, Q., et al. 2004. Tissue Doppler Imaging Is Superior to Strain Rate Imaging and Postsystolic Shortening on the Prediction of Reverse Remodeling in Both Ischemic and Nonischemic Heart Failure After Cardiac Resynchronization Therapy. ***Circulation**, 110* (1): 66-73.

Yu, C.-M., Lin, H., Zhang, Q., et al. 2003a. High prevalence of left ventricular systolic and diastolic asynchrony in patients with congestive heart failure and normal QRS duration. ***Heart**, 89* (1): 54-60.

Yu, C., Chan, Y., Zhang, Q., et al. 2006. Benefits of cardiac resynchronization therapy for heart failure patients with narrow QRS complexes and coexisting systolic asynchrony by echocardiography. ***J Am Col Cardiol**, 48* (11): 2251-2257.

Yu, C. M., Fung, W. H., Lin, H., et al. 2003b. Predictors of left ventricular reverse remodeling after cardiac resynchronization therapy for heart failure secondary to idiopathic dilated or ischemic cardiomyopathy. ***Am J Cardiol**, 91* (6): 684-688.

Yu, W., Li, S. N., Chan, G. C., et al. 2013. Transmural strain and rotation gradient in survivors of childhood cancers. ***Eur Heart J Cardiovasc Imaging**, 14* (2): 175-182.

Zannad, F., McMurray, J. J., Krum, H., et al. 2011. Eplerenone in patients with systolic heart failure and mild symptoms. ***N Engl J Med**, 364* (1): 11-21.

Zareba, W., Klein, H., Cygankiewicz, I., et al. 2011. Effectiveness of Cardiac Resynchronization Therapy by QRS Morphology in the Multicenter Automatic Defibrillator Implantation Trial-Cardiac Resynchronization Therapy (MADIT-CRT). ***Circulation**, 123* (10): 1061-1072.

Zhang, J. 2002. Myocardial energetics in cardiac hypertrophy. ***Clin Exp Pharmacol Physiol**, 29* (4): 351-359.